Probing the In Vivo Economy of Amyloid Beta-Protein during the Development of Alzheimer's Disease-Type Pathology

Dissertation Advisor: Professor Dennis Selkoe Soyon Hong

Probing the *in vivo* economy of amyloid beta-protein during the development of Alzheimer's disease-type pathology

Despite intense therapeutic and diagnostic focus on dyshomeostasis of amyloid β-peptide (Aβ) in Alzheimer's disease (AD), we still lack insight into the *in vivo* economy of Aβ in the normal and diseased brain. Thus, my thesis research focused on understanding the dynamics of Aβ in the living brain during the development of AD-type pathology. Using *in vivo* microdialysis, I showed that the steady-state level of Aβ that remains diffusible in the hippocampal interstitial fluid (ISF) of awake, behaving hAPP transgenic mice falls as Aβ steadily accumulates in the brain parenchyma. In accord, I observed distinct dispositions of microinjected radiolabeled Aβ in plaque-rich versus plaque-free mice, suggesting that cerebral amyloid deposits rapidly sequester newly released Aβ. This provides the first *in vivo* evidence from controlled animal experiments for the hypothesis that soluble $A\beta_{42}$ in human cerebrospinal fluid (CSF) falls in AD because it is sequestered into insoluble parenchymal deposits as the disease develops. My data further show that the association of Aβ with insoluble parenchymal deposits is not irreversible, as acute inhibition of γ-secretase in plaque-rich mice failed to lower ISF $A\beta_{42}$, whereas it did in plaque-free mice. Hence, the ISF in plaque-rich mice seems to be a reservoir for both newly

produced Aβ and Aβ that diffuse off of cell membrane- and plaque-bound deposits.

Finally, I showed that Aβ dimers, which are known to be potent synaptic neurotoxins, are undetectable in the aqueous compartments of the central nervous system, i.e., the brain ISF and CSF, in hAPP transgenic mice. Acute injection of Aβ dimers into living wild-type mice showed a rapid sequestration of the dimers away from the hippocampal ISF pool and a higher recovery in the membrane-bound pool than in the cytosolic pool of the brain homogenates. Interestingly, I found that the Aβ recovered in the membrane-bound pool was tightly associated with endogenous GM1 ganglioside. Taken together, my results suggest that Aβ dimers, and probably higher oligomers, are rapidly sequestered away from the ISF and bind to GM1 ganglioside-enriched lipid membranes, such as raft-like microdomains of secreted vesicles or on the plasma membranes of neurons and other cells.

I dedicate this dissertation to my mother, Young Ae Shim, who has truly exemplified the humble and unconditional love of Christ.

Table of Contents

Table of Figures

Appendix 3 Figures

Appendix 4 Figures

Acknowledgements

I can't believe it has been over five years since my first day in Boston as a Ph.D. candidate: I landed in Boston with two gargantuan bags and an equally mountainous level of excitement for the embarking of the next journey of my life. That was September 4, 2006. Looking back at the last five and a half years in Boston as a Ph.D. candidate, I realize that this particular step of my life has indeed been a life-molding process on multiple levels and one enabled by numerous people who have provided strong and sacrificial emotional support.

First of all, I would like to thank God for guiding me onto the path of biomedical research. Over these years, I grew to admire science, in particular for its mysterious wonder. As I learned more of the wonderful complexity of science, I came to be humbled again and again as I glimpsed, a minute fraction-worth, into His astonishing brilliance. Moreover, I feel so grateful and honored that I have come to be in a position where I can be one of the first people to unravel the marvelous mysteries and learn how He created this earth. I hope that I will continue to grow as a scientist.

I am truly indebted to my mentor, Dr. Dennis Selkoe, in whom I witnessed the inspirational heart of a faithful but disciplined lover of science – his keen enthusiasm for biomedical research is clearly fueled by a firm motivation to not only expand human knowledge but ultimately help better our lives through developing potential cure for devastating diseases. Dennis is such a gentle and

devoted teacher and someone I have come to tremendously respect. He has, on countless occasions, shown me grace, kindness and patience, and often provided much needed encouragement, especially during the most difficult times of my research. From Dennis, I also learned the crucial asset of critical thinking. Moreover, Dennis' adept ability to deconstruct complex problems into simple, key questions is something I hope to adopt as my own as I continue to grow as a scientist. I sincerely wish that I will one day simulate some of Dennis' outstanding qualities as a scientist and a mentor.

I am also grateful to Beth Ostaszewski, whom I have had the honor of working with for the past few years. Not only was it a lot of fun doing science with her, but I have also learned so much from her, for Beth is one of the most talented scientists I have met. I am also indebted to John Cirrito, who very graciously, generously and enthusiastically taught me the technique of *in vivo* microdialysis, which proved to be an invaluable tool I utilized for my doctoral research. I would also like to thank both the previous and current members of the Selkoe lab, from whom I have learned so much, primarily, the appreciation for quality science and clever methods to maintain such rigor in one's research studies. In particular, I would like to thank the brilliant scientists in the Selkoe lab whom I am also blessed to call as friends: Allen Chen, Heather Rice, Ting Yang, Oliver Holmes, Tracy Young-Pearse, Ulf Dettmer, Matt Hemming, and Eric Luth. I am also much obliged to my many wonderful friends who provided cheerful support throughout the different phases of my Ph.D. years, including Pastor

Ohm, BK, Amy, Shan, Yilei, Hyewon, Carol, Irene, Jessica and Eun Young. In particular, I would like to thank Cindy Lu, Julie Hong and Michelle Kim who provided much emotional support during the early stages of my Ph.D. studies.

Most importantly, I would like to thank my dear family, who throughout my life has displayed to me the marvelous meaning of sacrificial love and has been the cornerstone of every emotional and physical milestone. From my sister, Sung Yon, I learned the value of persistence, resilience and faithfulness. She is one of strongest people I know and respect the most, and I have often looked onto her persevering spirit, especially during the many challenging times of my Ph.D. studies. She has been my most loyal friend throughout the years and I am sincerely grateful to her for her deep and sacrificial love she has poured onto me since my birth. Dennis is not family, but I have to thank him here again for his unintentional stunt as a matchmaker. In Dennis' lab, I met the love of my life, Tim, whom in less than three weeks, I'll be married to! In particular for these last two years, I am so grateful to Tim for being such a strong and indispensible emotional and physical support and for always being by my side with an amazingly patient, gentle and understanding heart. His faithful and compassionate love truly humbles me everyday. I am much grateful to my father who never discouraged me from pursuing my interests but quietly supported me through all these years. It was actually because of my father, who excelled as an agronomist, that I had considered science and math as really cool subjects to study from a young age. My naïve interest in the subjects then that I knew my

father had loved has now turned into my own exciting pursuit and one that I believe will continue to be my lifelong passion.

Finally, I thank my mother, who not only gave me the most precious gift of all, which is faith in God, but also provided the strongest support and the most truthful words of advice. She is the wisest person I know and one of the smartest women whose remarkable inner strength and stunning beauty I have been so blessed to witness all my life. I know I owe everything to her, for her sacrificial and unconditional love for me, which included countless hours of prayer and tears. To my mother, who has truly exemplified the humble and unconditional love of Christ, I dedicate my dissertation.

Chapter 1

Introduction

Alzheimer's disease: brief introduction

On November 3 1906, Alois Alzheimer presented a talk at the 37th Meeting of the Southwest German Psychiatrists in Tübingen, Germany, entitled "Über eine eigenartige Erkrankung der Hirnrinde", which when translated into English is "On a peculiar disease process of the cerebral cortex". In this seminal talk (which was surmised shortly thereafter into a three-page report (Alzheimer, 1907)), Alzheimer described his first encounter in 1901 with a then-51-year old patient, Auguste Deter, who displayed clinical characteristics of memory and cognitive disturbances and whose brain, which upon her death in 1906 Alzheimer performed an autopsy on, showed the neuropathological features of dense neurofibrils (later identified to be tangles) and minute miliary foci (later identified as senile plaques), along with glial inflammation in cerebral cortical areas (Alzheimer, 1907; Graeber et al., 1998) (Figure 1.1 shows Auguste Deter's brain tissue sections, taken from Graeber and Mehraein, 1999).

First designated Alzheimer's disease (AD) by Emil Kraeplin (Alzheimer's mentor) in 1910 (Möller and Graeber, 1998), AD is a progressive neurological disorder of which the earliest clinical symptoms involve impaired declarative (particularly episodic) memory and general cognitive impairment, such as impaired judgment, decision-making, and orientation (Selkoe, 2002; Blennow et al., 2006). AD is recognized today as the most prevalent neurodegenerative disease and the most common form of dementia. The prevalence of AD worldwide is projected to quadruple from the estimated 26.6 million afflicted in

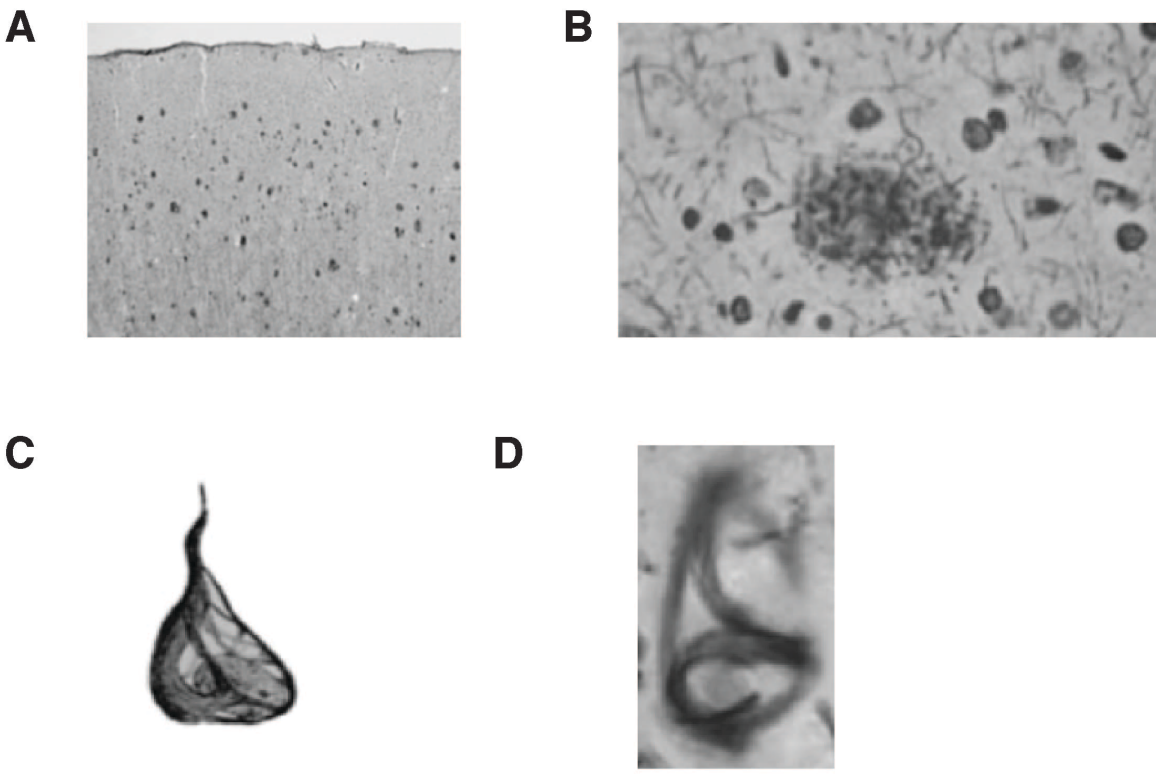

Figure 1.1. Auguste Deter's brain tissue sections show typical amyloid plaque deposition (A and B) and neurofibrillary tangles (C and D). (A-C) Bielschowsky silver impregnation; (D) a drawing of a tangle by Alzheimer in 1907. Figure modified from Graeber and Mehraein, 1999.

2006 to 106.23 million by 2050 (Brookmeyer et al., 2007). Brookmeyer et al. (2007) further stated that “If interventions could delay both disease onset and progression by a modest 1 year, there would be nearly 9.2 million fewer cases of the disease in 2050, with nearly the entire decline attributable to decreases in persons needing a high level of care”. However, today, there remains the unfulfilled need for some effective treatment, let alone a cure. This worrisome outlook is due to a belated clinical diagnosis of the disease, well after pathogenesis has progressed for years, and hence a considerable delay in the effort to intervene (Golde et al., 2011; Selkoe, 2011; Sperling et al., 2011).

Until recently, a definitive diagnosis of AD required tissue samples of the medial temporal lobe and cortical areas of the brain (which is acquired at autopsy, or much less commonly, during biopsy) to ensure the presence of the two pathological hallmarks of AD: neuritic (“senile”) plaques, in which the β-amyloid protein (Aβ) is the primary extracellular component (Glenner and Wong, 1984b; Masters et al., 1985; Selkoe et al., 1986) and the intraneuronal tangles, which are non-membrane bound masses of paired helical filaments composed primarily of hyperphosphorylated tau (Grundke-Iqbal et al., 1986; Kosik et al., 1986; Nukina and Ihara, 1986). It is important to note that neurofibrillary tangles are not unique to AD but found in a range of neurodegenerative diseases (Joachim et al., 1987).

With continuing advances in biomedical research, there has been a remarkable progress in the development of biomarkers for AD, which not only enhances the hope of detecting AD earlier, but also has helped confirm the

previous histopathological studies and, importantly, advanced our understanding of the pathogenesis. A prime example is the use of magnetic resonance imaging (MRI) and positron emission tomography (PET), where the findings have nicely complemented earlier histopathological evidence that the first structural and functional changes occur in the medial temporal lobe (for e.g., Braak et al., 1999; Blennow et al., 2006) (Figure 1.2, taken from Blennow et al., 2006), shows representative MRI and PET scans of Pittsburg compound B (PIB) and fluorodeoxyglucose (FDG) of an AD patient compared to those of a non-AD human control). Furthermore, recent work using functional MRI has linked function (hippocampal hyperactivation and impaired default network deactivation) with structural changes (amyloid deposition and cortical thinning in the inferior temporal gyrus and areas of the medial and lateral parietal cortices) (Sperling et al., 2009; Putcha et al., 2011).

AD: a disease of the synapse

Enhanced synapse loss in the temporal and frontal cortices is one of the histopathological alterations that differentiate AD from normal brain aging (West et al., 1994). The statistical correlation between cognitive decline and synapse loss in the hippocampus and association cortices is far stronger than the correlations between cognitive impairment and counts of amyloid plaques or neurofibrillary tangles (DeKosky and Scheff, 1990; Terry et al., 1991; Coleman and Yao, 2003). Furthermore, in some amyloid precursor protein (APP)

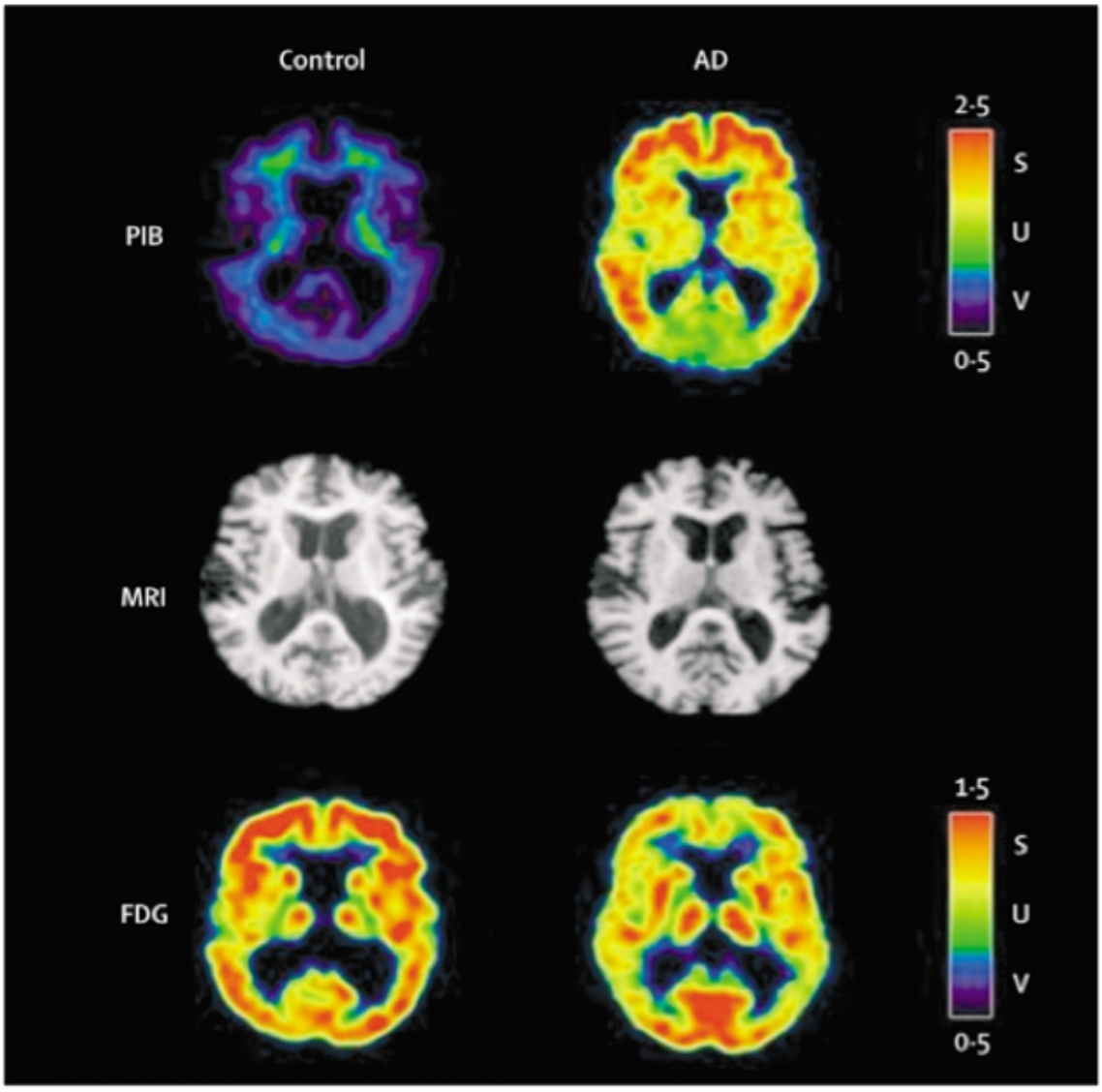

Figure 1.2. PIB, MRI, and FDG-PET images from a Control (a 69-year old cognitively normal with an MMSE score of 30) and an AD (a 71-year old with mild Alzheimer's disease with an MMSE score of 21). For AD, there is a marked PIB retention in conjunction with an FDG scan with temporoparietal and frontal hypometabolism. Scale bars: standardized uptake values (SUV) for PIB and FDG. Figure directly taken from Blennow et al., 2006.

transgenic mouse lines, the numbers of synaptophysin-positive presynaptic terminals and microtubule-associated protein (MAP2)-positive neurons are significantly less than in non-transgenic controls already at a very young age (~3 mo in the J9 line and ~8 mo in the J20 line), well before these mice develop amyloid plaques (Hsia et al., 1999; Mucke et al., 2000; Palop et al., 2003; Shankar et al., 2009). Importantly, the physical degeneration of synapses in the hippocampus appears to precede neuronal death (Walsh and Selkoe, 2004). Several quantitative studies using electron microscopy and immunohistochemical staining for synaptic markers (Terry et al., 1991; Masliah et al., 2001) as well as microarray studies of brain tissues from AD cases and APP transgenic mice (Yao et al., 2003) all provide strong evidence that AD is primarily, and at least initially, a disorder of synaptic function.

Dyshomeostasis of Aβ

One of the earliest biomarker changes indicative of AD in humans, even before clinical symptoms emerge, is thought to be low levels of the $A\beta_{42}$ peptide in cerebrospinal fluid (CSF) of subjects who have begun developing cerebral amyloid deposition. (Figure 1.3A (taken from Fagan et al., 2009) shows a negative correlation between levels of $A\beta_{42}$ in CSF of cognitively normal elderly and their cortical PIB binding potential.) Importantly, the decline of $A\beta_{42}$ peptide precedes the rise of the levels of tau and phosphorylated tau in the CSF

(reviewed in Craig-Schapiro et al., 2009; Golde et al., 2011). (Figure 1.3B (taken from Snider et al., 2009) shows that the rate of cognitive decline (by the clinical demential rating, CDR) in a period of 7 years is greatest in humans with steady state levels of $A\beta_{42} < 319$ pg/ml in their CSF.) Dyshomeostasis of $A\beta_{42}$, therefore, is currently thought to mark the earliest events in AD pathogenesis.

Although factors other than Aβ dyshomeostasis are likely to contribute importantly to the pathogenesis of AD (Pimplikar et al., 2010), evidence for Aβ dyshomeostasis being the principal driving force in AD comes from multiple levels, including genetics. That individuals with trisomy 21 (Down's syndrome) invariably develop diffuse plaques and vascular deposits (Olson and Shaw, 1969), in which Aβ is the principal component (Glenner and Wong, 1984a), led to the cloning of the gene that encodes Aβ, *APP* (amyloid precursor protein) (Kang et al., 1987). Subsequently, several missense mutations within the *APP* gene were identified in families with hereditary AD or the closely related hereditary cerebral hemorrhage with amyloidosis (HCHWA)-Dutch syndrome; the first two mutations identified were the E693Q ("Dutch") (Levy et al., 1990; Van Broeckhoven et al., 1990) and the V717I ("London") (Goate et al., 1991). These findings helped support the Aβ cascade hypothesis, which stated that an imbalance between production and clearance of the Aβ peptide leads to its gradual accumulation and the forming of plaques, initiating the AD pathological cascade (Selkoe, 1991; Hardy and Higgins, 1992; Hardy and Selkoe, 2002). One recent version of the amyloid hypothesis of AD is detailed in Figure 1.4 (taken from Haass, 2010).

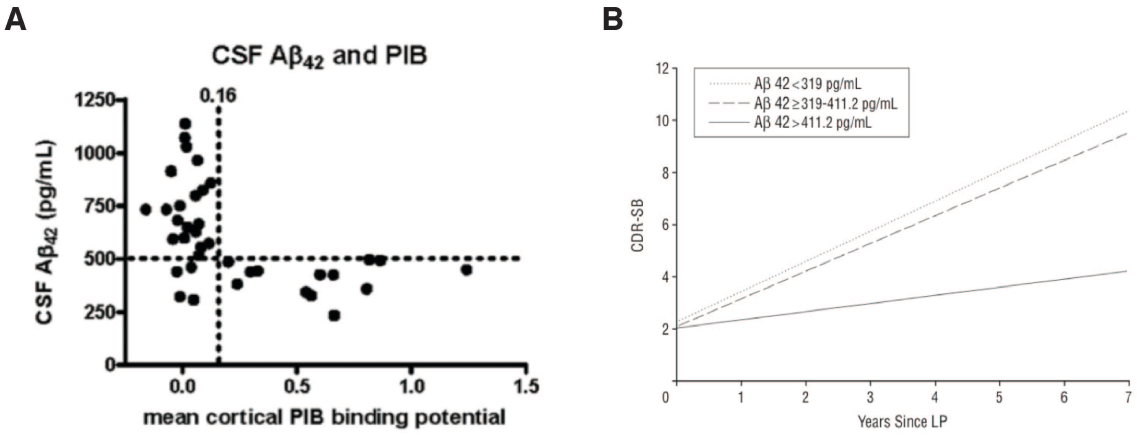

Figure 1.3. (A) All cognitively normal adults (i.e., CDR = 0) with cortical amyloid (i.e., mean cortical PIB binding potential ≥ 0.16) had low amounts of $A\beta_{42}$ in their CSF (i.e., < 500 pg/ml). Figure taken directly from Fagan et al., 2009. (B) Rate of cognitive decline (by CDR) in a period of 7 years is greatest in humans with steady state levels of $A\beta_{42}$ < 319 pg/ml in their CSF. Figure taken directly from Snider et al., 2009.

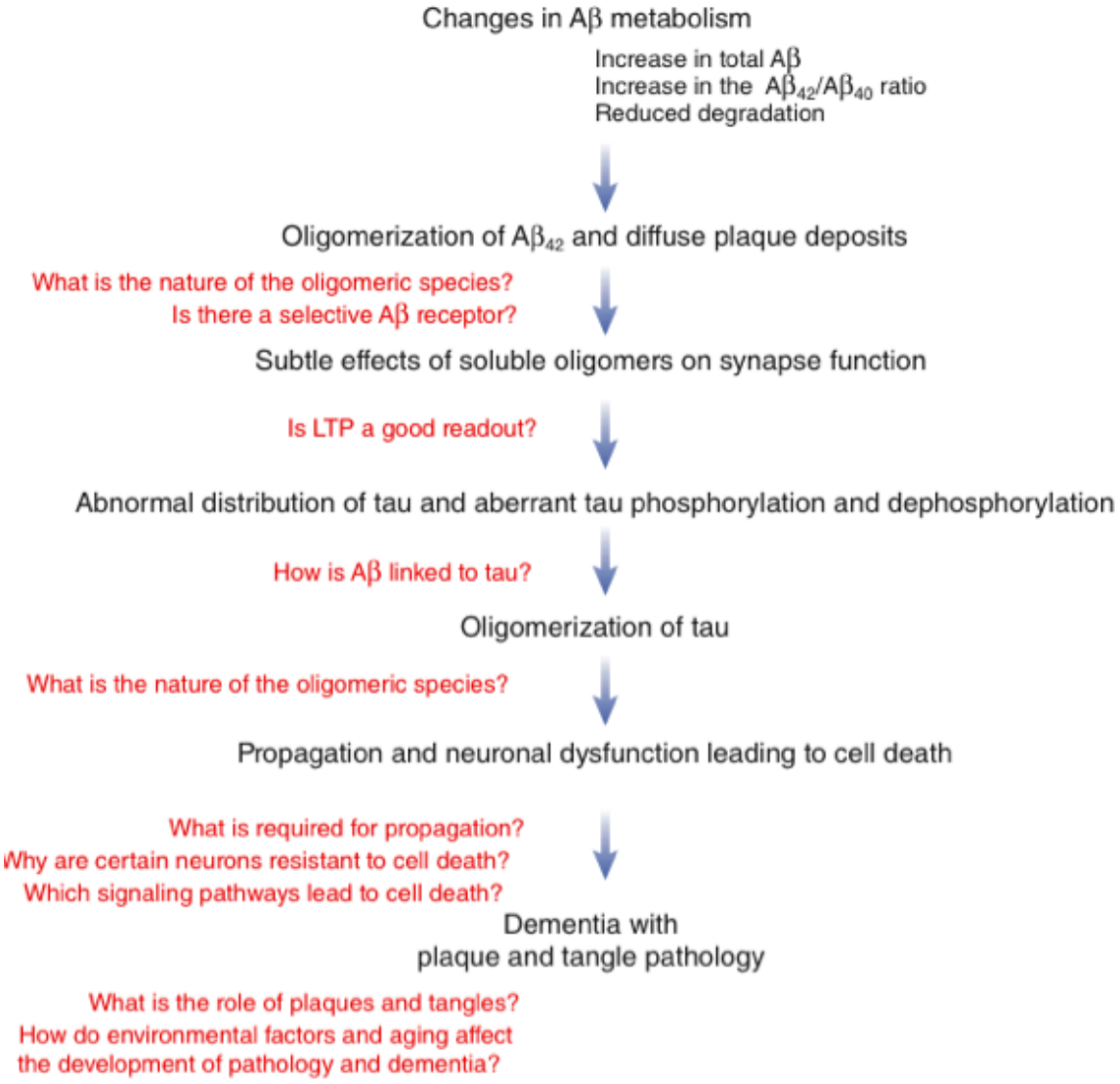

Figure 1.4. One recent version of the amyloid cascade hypothesis, which states that an imbalance between production and clearance of the Aβ peptide leads to its gradual accumulation and the forming of plaques, initiating the AD pathological cascade (originally put forth by Selkoe and Hardy (Selkoe, 1991; Hardy and Higgins, 1992; Hardy and Selkoe, 2002)). Here, the author annotated unattended questions in red. Figure taken directly from Haass, 2010.

Shortly after the discovery of the *APP* gene and some of its AD-causing mutations, Aβ was found to be normally secreted from cells (Haass et al., 1992; Shoji et al., 1992) and to be present in CSF and plasma of non-AD humans (Seubert et al., 1992). These findings led to the revelation of the proteolytic mechanism for APP (and other single transmembrane substrates): the concept of regulated intramembrane proteolysis (RIP), whereby type 1 membrane proteins (such as APP) first undergo regulated shedding of their ectodomains by membrane-anchored proteases (mostly ADAMs), after which the membrane-retained stubs are cleaved within their transmembrane domains (TMDs) to release small hydrophobic peptides (such as Aβ) into the extracellular space. In the APP amyloidogenic pathway, the holoprotein is first processed by β-site APP-cleaving enzyme (BACE) and then by the γ-secretase complex (Haass and Selkoe, 2007), which is a 4-member complex composed of presenilin-1 (or -2), Aph1, Pen2, and nicastrin (De Strooper, 2003). The second cleavage liberates the APP intracellular domain (AICD) (cut at the intramembranous "ε-site" within the β-CTF of APP) into the cytoplasm and Aβ peptides (cut at the "γ-site" in the TMD of the β-CTF) and released into vesicle lumens or the extracellular space). The variable γ-cutting site is of great pathogenic importance: the longer the Aβ peptide (i.e., the more C-terminal within the β-CTF TMD γ-secretase cleaves), the greater its hydrophobicity and propensity to oligomerize (Haass and Selkoe, 2007). Current evidence suggests that soluble low-*n* Aβ oligomers (e.g., Aβ dimers, trimers, dodecamers, etc.), but not Aβ monomers, mediate

synaptotoxicity (Walsh and Selkoe, 2007).

To date, all AD-causing mutations in APP occur either within or immediately flanking the Aβ region (Haass and Selkoe, 2007). The only other two dominantly transmitted AD-causing genes are *PSEN1* (*Presenilin 1*) and *PSEN2* (*Presenilin 2*) (reviewed in De Strooper et al., 2012), and these have turned out to be the catalytic center of γ-secretase (Wolfe et al., 1999). Missense mutations in either presenilin gene lead to increased $A\beta_{42}/A\beta_{40}$ ratios and in at least some examples, increased $A\beta_{43}/A\beta_{40}$ ratios (Saito et al., 2011). On the other hand, altered clearance (as opposed to production) of Aβ can promote Aβ accrual and plaque deposition: for e.g., loss of neprilysin, an Aβ-degrading protease, in mice increased the half-life of Aβ in the extracellular space and accelerated plaque deposition (Farris et al., 2007). Overexpression of low-density lipoprotein receptor, which facilitates Aβ transport across the blood brain barrier (Nazer et al., 2008), can lessen amyloid deposition in mice (Kim and Tsai, 2009). Importantly, by far the most significant genetic risk factor for AD, *APOE4*, is thought to play a central role in the dyshomeostasis of Aβ by impairing Aβ clearance from the interstitial fluid (ISF) and brain and thus promoting Aβ accumulation and plaque deposition (DeMattos et al., 2004; Castellano et al., 2011; Cerf et al., 2011).

Despite the evidence for a key role of Aβ dyshomeostasis in AD pathogenesis, the *in vivo* economy of Aβ is poorly understood. Recent studies utilizing elegant *in vivo* techniques in both humans and APP transgenic mouse

models have enhanced our understanding of the dynamics of Aβ in the living brain, both as regards normal physiological activities such as sleep or neuronal activation (Cirrito et al., 2005; Bateman et al., 2006; Brody et al., 2008; Cirrito et al., 2008; Bero et al., 2011) and in pathological setting, its relationship with plaque deposition and synaptic density (Cirrito et al., 2003; Spires et al., 2005; Kang et al., 2007; Meyer-Luehmann et al., 2008; Koffie et al., 2009; Yan et al., 2009; Mawuenyega et al., 2010; Hong et al., 2011). The secretion of Aβ into the ISF upon APP proteolysis is thought to require clathrin-mediated endocytosis (Cirrito et al., 2008) and to be regulated by synaptic/neuronal acitivity (Cirrito et al., 2005; Bero et al., 2011), consciousness (Brody et al., 2008), stress (Kang et al., 2007), and the sleep-wake cycle (Kang et al., 2009). Using an intravenous infusion of stable $^{13}C_6$-leucine and its incorporation into APP and thus Aβ peptides in CSF, the dynamics of Aβ in non-AD normal humans and its dyshomeostasis in AD patients have been elegantly analyzed (Bateman et al., 2006). Here, the rates of new Aβ production in cognitively normal individuals and AD patients were found to be comparable, but the Aβ clearance rates were significantly different; clearance rates in cognitively normal humans were ~7.6% per hour for $Aβ_{42}$ and 8.3% per hour for $Aβ_{40}$, whereas in AD subjects, they were lower at ~5.3% per hour for $Aβ_{42}$ and 5.2% per hour for $Aβ_{40}$ (Mawuenyega et al., 2010).

The complex relationship between the secreted soluble Aβ species and the formation of insoluble amyloid plaques is also becoming better understood

through usage of the *in vivo* tools described above. Emerging evidence suggests that the insoluble amyloid fibrils that comprise plaques may not directly confer neurotoxicity but sequester small, diffusible assemblies of Aβ that have been shown to potently alter synaptic structure and function (Walsh and Selkoe, 2007). That plaques may be relatively inert sinks for small, synaptotoxic oligomeric species was shown nicely by using amyloid plaque cores isolated directly from AD human brain: plaque cores themselves failed to impair LTP, but upon solubilizing them with formic acid (Selkoe et al., 1986), the cores released Aβ dimers and other oligomers which then impaired LTP (Shankar et al., 2008). The "plaques as sinks" hypothesis was further validated *in vivo* during this thesis research by measuring the half-lives of radioiodiniated Aβ in ISF of mice with or without plaque deposition (Hong et al., 2011). However, the plaques may not act solely as inert sinks; they also seem to act as a local contributor of potentially synaptotoxic Aβ oligomers (Cirrito et al., 2003; Spires et al., 2005; Koffie et al., 2009; Hong et al., 2011). Array tomography studies have shown that there is a halo of Aβ peptides intimately surrounding a plaque, and their relative levels have a strong negative correlation with local synaptic density (Koffie et al., 2009). The complexity of the *in vivo* dynamics of Aβ before, during, and after plaque formation has been particularly well shown using *in vivo* microdialysis in APP transgenic mouse models (Cirrito et al., 2003; Hong et al., 2011). In addition, the rate of plaque formation and growth has been studied in living mouse brains using *in vivo* multi-photon imaging, albeit with sometimes conflicting results. For

example, in Yan et al. (2009), plaques grew over a period of weeks before reaching a mature size, whereas in Meyer-Luehmann et al. (2008), the growth of plaques stabilized within 24 hours of their first appearance.

Finally, the recent *in vivo* studies have also revealed an intricate relationship among neuronal activity, levels of Aβ production, and degree of plaque deposition, a relationship that perhaps can account for the region-specific vulnerability observed in AD. Areas of the human brain that develop the most Aβ deposits may also have among the highest basal rates of metabolic and neural activity (Buckner, 2005; Sperling et al., 2009). The hippocampus is a unique region that has high neuronal activity and synaptic plasticity in the adult central nervous system (Nicoll and Malenka, 1999). Neuronal activity has been shown to directly modulate the production of Aβ (Kamenetz et al., 2003 (in slices); Cirrito et al., 2005 (in ISF)). Furthermore, a recent study showed that regions with higher levels of plaque deposition (such as the hippocampus and the piriform cortex) had higher levels of steady-state ISF Aβ, compared to regions with lower amounts of plaques (such as the striatum and barrel cortex) (Bero et al., 2011). Aβ may in turn impact neuronal activity, either as a negative regulator (i.e., by inhibiting long-term potentiation (LTP) and facilitating long-term depression (LTD) (for e.g., Li et al., 2009) or as a positive driver to induce aberrant excitatory neuronal activity (Palop et al., 2006; Palop et al., 2007). In particular, soluble assemblies of Aβ have been shown to inhibit the induction of LTP and alter dendritic spine density through a pathway that requires NMDA-type glutamate

receptors (NMDARs), calcineurin and cofilin, and such synaptic dysfunction and loss can be specifically prevented by antibodies to Aβ and by a small molecule inhibitor of Aβ aggregation (Townsend et al., 2006; Shankar et al., 2007). These signaling elements are part of a well-described pathway leading from synaptic activity to the induction of LTD (Mulkey et al., 1994; Cummings et al., 1996; Nagerl et al., 2004).

Soluble Aβ oligomers as the prime synaptotoxic offenders

Extensive research during the last 15 years has suggested that specific forms of Aβ may contribute importantly to the onset of a subtle, intermittent impairment of hippocampal neuronal function (Lambert et al., 1998; Walsh et al., 2002; Kamenetz et al., 2003; Lesné et al., 2006). In particular, evidence using Aβ directly isolated from human AD cortex shows that soluble dimers may act as the smallest oligomeric unit capable of exerting synaptotoxicity (McLean et al., 1999; Klyubin et al., 2008; Shankar et al., 2008; Li et al., 2009; Mc Donald et al., 2010; O'Nuallain et al., 2010; Li et al., 2011) and tau-altering effects (Jin et al., 2011). Such Aβ dimers may then quickly form metastable protofibrils that remain synaptotoxic (O'Nuallain et al., 2010). Although the precise biochemical nature of an array of potentially neurotoxic oligomers – dimers, trimers, Aβ*56, Aβ-derived diffusible ligands (ADDLs), annular complexes and large protofibrils – is still under debate (Haass and Selkoe, 2007; Roychaudhuri et al., 2008; Benilova et

al., 2012), there is a growing consensus that the Aβ forms which exert such synaptotoxic effects are the species that remain pre-fibrillar and soluble in the extracellular space (reviewed in Walsh and Selkoe, 2007). Importantly, an AD-causing APP mutation that was recently discovered in certain AD families leads to the production of Aβ species lacking residue E22 within the Aβ region of APP, and this results in rapid formation (and apparent stabilization) of Aβ oligomers (Tomiyama et al., 2008); in accord, a mouse model carrying this mutation led to synaptic and neuronal loss in the complete absence of amyloid plaques (Tomiyama et al., 2010). In an *in vitro* study comparing multiple synthetic $A\beta_{42}/A\beta_{40}$ ratios, the ratio which was the most effective at inhibiting synaptic activity and affecting neuronal viability was the ratio at which amyloid fibril formation was delayed and smaller oligomeric species stabilized (Kuperstein et al., 2010). Interestingly, amyloid fibrils could be reverted to a heterogeneous mixture of soluble, oligomeric intermediate species upon incubation with lipids (brain total extracts, sphingolipids, or GM1 ganglioside) and the previously inert fibrils now induced altered tau phosphorylation and memory impairment in mice (Martins et al., 2008). By SEC, the oligomeric species released upon fibril incubation with lipids eluted as ~9 kDa globular protein fractions, but by other biophysical methods, such as the 18-angles static light scattering, the species was considered to be a heterogeneous mixture of ~80-500 kDa assemblies (Martins et al., 2008).

Where and how these synaptotoxic low *n* Aβ assemblies are generated

and regulated and whether they are bound to other proteins are important questions that yet need to be answered in order to elucidate the exact steps behind the initiation of AD, with attendant therapeutic implications. The precise mechanism of how Aβ oligomers act as the principal synaptotoxic species is still under debate. As mentioned above, both the LTP-inhibiting and LTD-facilitating effects of Aβ are thought to be mediated in part through NMDA receptors (Wu et al., 1995; Molnar et al., 2004; Wang et al., 2004; Kelly and Ferreira, 2006; Li et al., 2009; Li et al., 2011). In particular, soluble Aβ oligomers were recently shown to disrupt neuronal glutamate uptake and thereby potentially overactivate extrasynaptic NR2B-containing NMDA receptors (Li et al., 2009; Li et al., 2011). The search for a particular receptor for Aβ oligomers has yielded a true "embarrassment of riches" (Selkoe, 2011); the candidate list is extensive, including α7-nicotinic acetylcholine receptor (Wang et al., 2000), insulin receptors (De Felice et al., 2009), NMDA receptors (De Felice et al., 2007) and AMPA receptors (Zhao et al., 2010). The newest member in this far-from-exclusive club is the cellular prion protein (PrP^c) (Laurén et al., 2009). Aβ has also been found to bind specifically to molecular chaperones present in extracellular fluids including CSF, i.e., apolipoprotein E (ApoE) (Strittmatter et al., 1993) and apolipoprotein J (ApoJ, also known as clusterin) (Ghiso et al., 1993).

The PrP^c/Aβ interaction has been a hotbed of controversy ever since Laurén et al. (2009) reported PrP^c as an apparent receptor for synthetic $Aβ_{42}$ oligomers, i.e., $Aβ_{42}$ peptides assembled into spherical particles of 5-6 nm

diameter that run at ~150 kDa on SDS-PAGE. This work did not find evidence that PrP^c acted as a receptor for "fresh Aβ monomers", i.e., Aβ that runs where monomers are expected to elute by non-denaturing SEC but on SDS-PAGE runs as monomers, trimers and tetramers. Using 30-200 nM synthetic $Aβ_{42}$ preparations, Laurén et al. (2009) reported that PrP^c mediates ~50% of the binding of these oligomers to hippocampal neurons, that residues 95-105 of PrP^c are the primary determinant of binding, and that PrP^c is required for Aβ's inhibition of LTP in hippocampal slices. Prior to this study, *PRNP*, the gene encoding human prion protein, has been found to be a potential AD susceptibility gene (Bertram et al., 2007), where the *PRNP* codon 129 polymorphism may act as a risk factor for AD (Dermaut et al., 2003; Riemenschneider et al., 2004). However, Laurén et al.'s findings were soon disputed by the Malinow laboratory, which showed that PrP^c was not required for synthetic Aβ's effect on dendritic spine loss or LTP inhibition (Kessels et al., 2010). Laurén et al. argued that the failure of Kessels et al. to repeat the PrP^c dependency of Aβ on LTP inhibition could be partially due to a dosage issue (1 μM was used in Kessels et al. vs. 30-100 nM was used in Lauren et al.). Similarly, two laboratories reported conflicting data when crossing an established transgenic mouse model of AD with a mouse model null for PrP^c (i.e., *PrnP -/-*). One group crossed APP/PS1 double transgenic mice with *PrnP -/-* mice and observed that whereas the levels of APP, Aβ and astrogliosis remain unchanged upon the loss of PrP^c, there was a rescue (to levels of wild-type mice) of axonal degeneration, loss of synaptic markers

(synaptophysin and PSD-95), and impairment of spatial learning and memory (by Morris water maze test) (Gimbel et al., 2010). On the contrary, another group that crossed hAPP transgenic mice (the J20 line) with *PrnP -/-* mice observed that abnormalities of learning and memory were retained in the absence of PrP^c, arguing that PrP^c does not play any role in Aβ-induced memory impairment (Cissé et al., 2011). Several other labs have joined in the controversy, reporting data either in support of (Chen et al., 2010; Chung et al., 2010; Barry et al., 2011; Freir et al., 2011; Resenberger et al., 2011; Kudo et al., 2012) or against (Balducci et al., 2010; Calella et al., 2010) a critical role of PrP^c for Aβ to suppress cognitive function. Other labs utilized a more natural source of Aβ, i.e., AD brain-derived Aβ low *n* oligomers, and found that these human AD brain-derived species were ineffective in inhibiting LTP in *PrnP -/-* hippocampal slices (Freir et al., 2011), and that pretreating rats with a Fab fragment binding to epitope 96-104 of PrP^c rescued the ability of AD brain-derived Aβ to inhibit LTP *in vivo* (Barry et al., 2011). Interestingly, treating plaque-rich APP/PS1 transgenic mice with an anti-PrP^c antibody (6D11) rescued behavioral deficits without ameliorating plaque burden (Chung et al., 2010). The binding *in vitro* of Aβ oligomers, but not monomers or fibrils, to the N-terminal region of PrP^c was verified using surface plasmon resonance (SPR) and site-directed spin labeling, and the apparent dissociation constant for the interaction was calculated to be ~70 nM Aβ (Chen et al., 2010). One laboratory reported Aβ to be co-immunoprecipitated with PrP^c in both hAPP transgenic mice and human AD

brains; however, key controls were missing in this study, so interpretation of their data should be taken with caution (Gao et al., 2010). Finally, an alternative, protective role of PrP^c has been suggested: transfection of PrP^c decreased Aβ and soluble APPβ fragments in SH-SY5Y cells; conversely, knockdown of endogenous PrP^c increased Aβ and soluble APPβ in mouse N2a cells and the authors suggested the regulation by PrP^c of APP processing was by its direct inhibition of BACE-1 through glycosylaminoglycans (Parkin et al., 2007).

Using an elaborate single-molecule imaging technique (Renner et al., 2008; Triller and Choquet, 2008), synthetic Aβ oligomers (sometimes called ADDLs) have been shown to induce aberrant clustering of metabotropic glutamate receptors (mGluR), thereby disrupting the normal dynamics of synaptic components (Renner et al., 2010). As Aβ oligomers have also been shown to increase localization of PrP^c to the cell surface (Caetano et al., 2011), it is possible that Aβ targets a specific protein receptor, such as the PrP^c or other synaptic components, and "overstabilizes" their presence on the cell membrane, thereby inducing "pathological signaling platforms" (Renner et al., 2010). Alternatively, the hydrophobic Aβ peptide may bind to certain lipids on plasma membranes, instead of a specific protein receptor, and exert subtle physicochemical properties of membranes (for e.g., by interfering with membrane fluidity, dynamics of membrane lipids and proteins, or ion permeability), which may in turn affect various proteins that are expressed on the membrane surface.

Soluble Aβ oligomers: their existence in vivo

The dazzling state of confusion in research regarding the mechanisms of Aβ oligomers can be blamed on the heterogeneity of Aβ sources used by different laboratories (e.g., synthetic versus natural) and to lack of clarity about the precise structural nature (e.g., dimers, trimers, dodecamers, ADDLs, etc), as noted above. To date, Aβ oligomers from natural sources (for e.g., cell culture media and AD brain homogenates) have been isolated using variable homogenization and/or concentration protocols, raising concerns whether they "really exist *in vivo*" (Haass, 2010), and thus the call for Aβ oligomers to be identified in biological fluids, primarily the CSF, has intensified in the past few years (Benilova et al., 2012). There has been a few reports on Aβ oligomers existing in CSF and plasma of humans developing AD (for e.g., Klyubin et al., 2008; Fukumoto et al., 2010; Gao et al., 2010; Villemagne et al., 2010); however, the interpretation of these various assays has been difficult due to vague definitions of the precise oligomeric unit the assays are detecting and whether one can really exclude the detection of Aβ monomers. In this regard, our lab has recently designed two ELISAs that specifically detect a range of soluble Aβ oligomers (from dimers to prefibrillar oligomers) but not Aβ monomers. These ELISAs sensitively detect low amounts of synthetic soluble Aβ oligomers (≤ 30 pg/ml) as well as natural, soluble Aβ oligomers isolated from AD brains. Utilizing these two oligomer-specific ELISAs (o-ELISAs), we failed to detect any soluble Aβ oligomers in CSF samples from 13 human individuals (Yang et al., *submitted*).

Furthermore, we failed to detect any low molecular weight Aβ oligomers, including dimers, in the ISF of APP transgenic mice, which has abundant Aβ, regardless of age or degree of plaque deposition (Hong et al., 2011). However, these results do not necessarily support critics' doubts as to whether low *n* Aβ oligomers exist *in vivo*; instead, they suggest that the low *n* Aβ oligomers may not exist in the aqueous biological fluids, but due to their substantial hydrophobicity, they may be sequestered away from the extracellular fluid onto membranes and/or existing aggregates (plaques) (I address this concept further in Chapter 4).

Aβ and lipids, particularly GM1 ganglioside

Hydrophobicity plays a crucial role in Aβ oligomerization. The most hydrophobic stretch of Aβ, aa 29-42, is thought to be helically wound in the lipid environment and changes in the aa 41 and 42 of Aβ induce changes in conformation that allow aberrant exposure of hydrophobic amino acids, thereby leading to increased propensity to aggregate. Aβ fibrils have β-sheet structure where the mid-region of Aβ, in particular aa 19-28, is buried. Mutations in *APP* and *PSEN* that increase the $A\beta_{42}/A\beta_{40}$ ratio are AD-causing (for e.g., *APP* V717F; *PSEN1* L166P) (Suzuki et al., 1994; Duff et al., 1996; Scheuner et al., 1996) and in both AD patients and transgenic mouse models of AD, $A\beta_{42}$ is the primary Aβ component in the senile amyloid plaques, despite the fact that $A\beta_{40}$ is produced at much higher levels. The additional isoleucine and alanine at the C-

terminus of $A\beta_{42}$ are considered to increase its hydrophobicity and thus its propensity to oligomerize to a much greater degree than $A\beta_{40}$. Indeed, the substitution of these two hydrophobic amino acids to hydrophilic residues greatly lessens the peptide's aggregation propensity (Kim and Hecht, 2005).

Given that hydrophobicity is a key feature of Aβ oligomers, there very well may not be a specific target protein receptor for Aβ. Instead, the hydrophobic Aβ oligomers, once released into the extracellular space, may quickly be sequestered to certain microdomain on plasma membranes of cells or to certain lipid vesicles. As the γ-secretase complex cleaves the APP C-terminal stub within the plasma membrane, Aβ may well retain some hyrophobic affinity for lipids. This could in turn explain why there seem to be so many candidate protein "receptors" for Aβ; as noted above, the hydrophobic Aβ peptide may "target" certain lipid molecules and exert subtle physicochemical properties on membranes, which may in turn affect various proteins that traverse the membrane or are anchored to it (e.g., PrP^c).

One appealing candidate for a lipid that could bind hydrophobic forms of Aβ is GM1 ganglioside. Gangliosides are glycosphingolipids composed of a hydrophilic sialic acid moiety exposed to the external environment and a hydrophobic membrane-embedded ceramide moiety (Fishman and Brady, 1976) (Figure 1.5 shows structure for GM1 ganglioside and proposed biosynthetic pathways for the major gangliosides in the mammalian brain (from Sheikh et al., 1999)). Gangliosides are particularly enriched in the nervous system, as

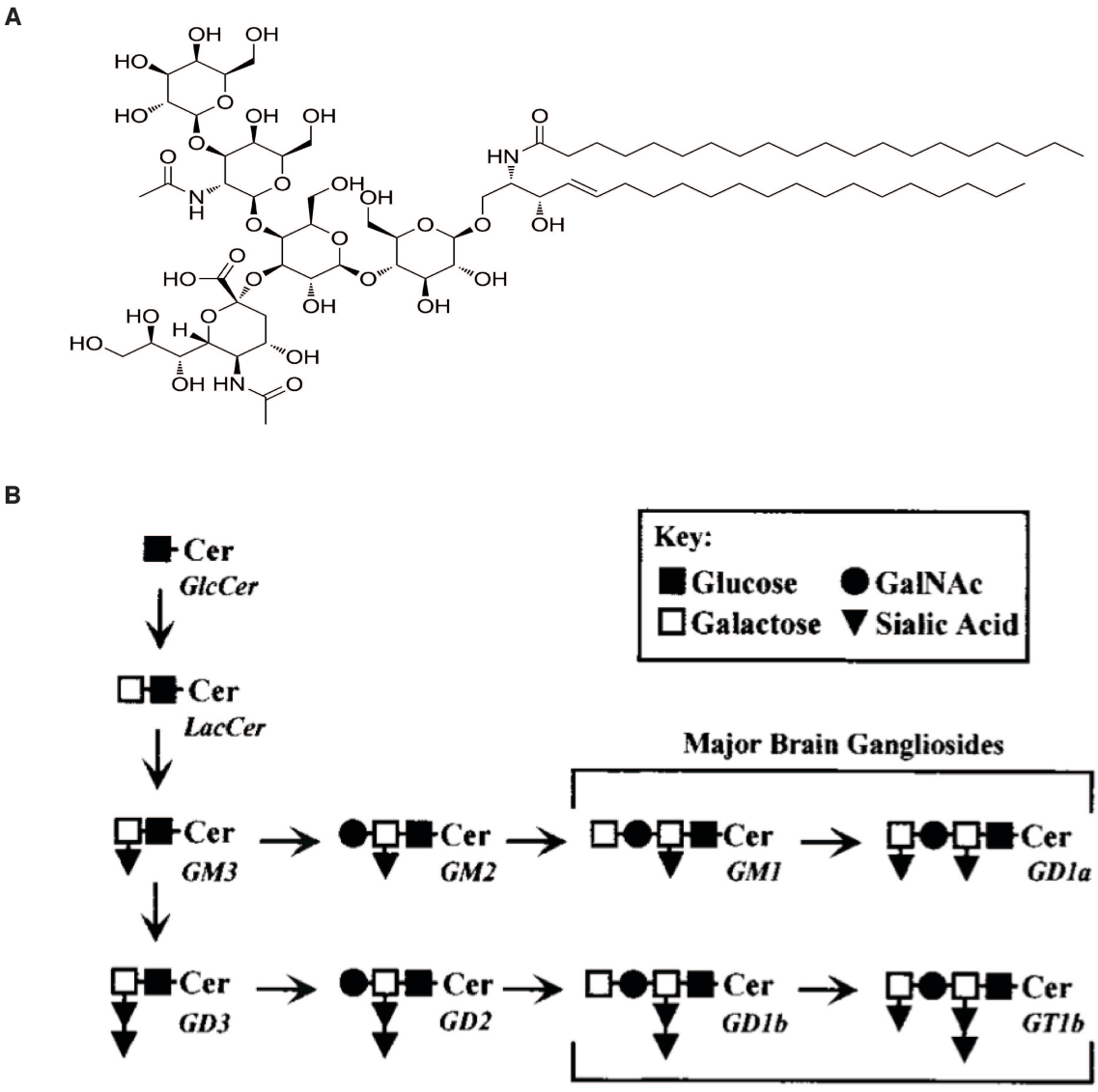

Figure 1.5. (A) Structure of GM1 ganglioside. (B) Proposed biosynthetic pathways for the major gangliosides in the mammalian brain; figure modified from Sheikh et al., 1999.

compared to other cellular membranes, and their composition changes during development (Svennerholm and Gottfries, 1994; Sonnino et al., 2007). In particular, using immunoelectron microscopy, the GM1 ganglioside was found to be localized onto the pre- and postsynaptic membranes of the external plexiform layer of rabbit retina and rat cerebral cortex (Hansson et al., 1977). The study of GM1 ganglioside was advanced when the B-subunit of cholera toxin was found to specifically bind to GM1 ganglioside but not other gangliosides such as Gd1b or GT1 (Holmgren et al., 1973; King and van Heyningen, 1973; van Heyningen, 1974).

Studies have shown that total methanol/chloroform-extractable gangliosides were significantly decreased in AD brain tissue (Svennerholm and Gottfries, 1994) and the concentration of GM1 (and to some extent, GM2) gangliosides were increased in the CSF of AD patients (Blennow et al., 1991). However, GM1 ganglioside achieved special attention in AD research when GM1-bound Aβ monomers were identified in membrane fractions of AD brains with diffuse plaques (Yanagisawa et al., 1995). Sucrose gradient fractions contained $A\beta_{1-42}$ species that migrated at ~5 kDa by denaturing PAGE, and delipidation brought the altered migration down to the usual 4 kDa monomer position. Furthermore, the Aβ antibody, 4G8, could not recognize the 5 kDa species (suggesting that this species had a masked epitope at aa 17-24), and treatment with methanol (but not with SDS, chloroform or acetone) revealed the epitope. Finally, the 5 kDa Aβ band was reactive with cholera toxin, which binds

specifically to GM1 ganglioside. As the 5 kDa species was observed only in brains that contained diffuse plaques, but not in typical AD brains that were rich with mature (fibrillar) amyloid plaques or in non-AD cortices, the authors speculated that the 5 kDa GM1 ganglioside-bound Aβ monomer could be a "seed" for amyloid fibril formation. Several biophysical studies that followed the Yanagisawa et al. (1995) paper supported the view that Aβ, upon binding to GM1 ganglioside on neuronal membranes, undergoes a conformational change that confers a higher propensity to aggregate, thus acting as an endogenous seed (reviewed in (Ariga et al., 2008; Yanagisawa, 2011)). Briefly, Aβ upon binding to GM1 ganglioside-containing lipid vesicles (but not to sphingomyelin or various anionic phospholipid vesicles) underwent a conformational change from random coil to β-sheet rich structure (McLaurin and Chakrabartty, 1996; Choo-Smith and Surewicz, 1997); upon binding, the ganglioside-containing vesicles greatly accelerated Aβ fibril formation *in vitro* (Choo-Smith et al., 1997; Hayashi et al., 2004). In particular, the sialic acid of GM1 seems to be a critical recognition site, and the other sugar groups in the ganglioside seem to help mediate the interaction (e.g., there is ~3-fold higher binding to GM1 than GM2, which lacks a galactose residue. The ranking of *in vitro* Aβ binding affinity (from high nM to low μM) was GD1a = GT1b > GM1 > GM2 (Choo-Smith et al., 1997). However, in vesicles that include sphingomyelin and cholesterol, i.e., liposomes of lipid raft-like composition, Aβ bound to GM1 gangliosides displayed the most rapid fibril formation compared to liposomes containing GT1b, GD1b or GD1a (Kakio et al.,

2002). Furthermore, the concentration of GM1, and to a lesser extent, GM2, was increased in detergent-resistant membranes isolated from the frontal cortices of early AD brains as compared to membranes from non-AD brains (Molander-Melin et al., 2005). Finally, a monoclonal antibody that was raised specifically against GM1 ganglioside-bound Aβ isolated from membrane fractions of human brains with diffuse plaques (i.e., the 4396C antibody) (Yanagisawa et al., 1997) immunostained the neuropil but not plaques and immunoprecipitated a cholera toxin- and Aβ-positive band from membrane fractions of brains of nonhuman primates (Hayashi et al., 2004). Taken together, these results suggest that GM1 ganglioside may act as a type of surface lipid "receptor" for Aβ. However, further studies are necessary to characterize the GM1 ganglioside-bound Aβ complex (some of which I address in Chapter 4).

References

Alzheimer A (1907) Ueber eine eigenartige Erkrankung der Hirnrinde. Centralblatt fur Nervenheilkunde und Psychiatrie 30:177-179.

Ariga T, McDonald MP, Yu RK (2008) Thematic Review Series: Sphingolipids. Role of ganglioside metabolism in the pathogenesis of Alzheimer's disease--a review. The Journal of Lipid Research 49:1157-1175.

Balducci C, Beeg M, Stravalaci M, Bastone A, Sclip A, Biasini E, Tapella L, Colombo L, Manzoni C, Borsello T, Chiesa R, Gobbi M, Salmona M, Forloni G (2010) Synthetic amyloid-beta oligomers impair long-term memory independently of cellular prion protein. Proc Natl Acad Sci USA 107:2295-2300.

Barry AE, Klyubin I, Mc Donald JM, Mably AJ, Farrell MA, Scott M, Walsh DM, Rowan MJ (2011) Alzheimer's disease brain-derived amyloid-β-mediated inhibition of LTP in vivo is prevented by immunotargeting cellular prion protein. Journal of Neuroscience 31:7259-7263.

Bateman RJ, Munsell LY, Morris JC, Swarm R, Yarasheski KE, Holtzman DM (2006) Human amyloid-beta synthesis and clearance rates as measured in cerebrospinal fluid in vivo. Nature Medicine 12:856-861.

Benilova I, Karran E, De Strooper B (2012) The toxic Aβ oligomer and Alzheimer's disease: an emperor in need of clothes. Nature Neuroscience 15:349-357.

Bero AW, Yan P, Roh JH, Cirrito JR, Stewart FR, Raichle ME, Lee J-M, Holtzman DM (2011) Neuronal activity regulates the regional vulnerability to amyloid-[beta] deposition. Nature Neuroscience.

Bertram L, McQueen MB, Mullin K, Blacker D, Tanzi RE (2007) Systematic meta-analyses of Alzheimer disease genetic association studies: the AlzGene database. Nature genetics 39:17-23.

Blennow K, de Leon MJ, Zetterberg H (2006) Alzheimer's disease. Lancet 368:387-403.

Blennow K, Davidsson P, Wallin A, Fredman P, Gottfries CG, Karlsson I, Mansson JE, Svennerholm L (1991) Gangliosides in cerebrospinal fluid in 'probable Alzheimer's disease'. Archives of Neurology 48:1032-1035.

Braak E, Griffing K, Arai K, Bohl J, Bratzke H, Braak H (1999) Neuropathology of Alzheimer's disease: what is new since A. Alzheimer? European archives of psychiatry and clinical neuroscience 249 Suppl 3:14-22.

Brody DL, Magnoni S, Schwetye KE, Spinner ML, Esparza TJ, Stocchetti N, Zipfel GJ, Holtzman DM (2008) Amyloid-beta dynamics correlate with neurological status in the injured human brain. Science 321:1221-1224.

Brookmeyer R, Johnson E, Ziegler-Graham K, Arrighi HM (2007) Forecasting the global burden of Alzheimer's disease. Alzheimers Dement 3:186-191.

Buckner RL (2005) Molecular, Structural, and Functional Characterization of Alzheimer's Disease: Evidence for a Relationship between Default Activity, Amyloid, and Memory. Journal of Neuroscience 25:7709-7717.

Caetano FA, Beraldo FH, Hajj GNM, Guimaraes AL, Jürgensen S, Wasilewska-Sampaio AP, Hirata PHF, Souza I, Machado CF, Wong DY-L, De Felice FG, Ferreira ST, Prado VF, Rylett RJ, Martins VR, Prado MAM (2011) Amyloid-beta oligomers increase the localization of prion protein at the cell surface. Journal of Neurochemistry 117:538-553.

Calella AM, Farinelli M, Nuvolone M, Mirante O, Moos R, Falsig J, Mansuy IM, Aguzzi A (2010) Prion protein and Abeta-related synaptic toxicity impairment. EMBO molecular medicine 2:306-314.

Castellano JM, Kim J, Stewart FR, Jiang H, DeMattos RB, Patterson BW, Fagan AM, Morris JC, Mawuenyega KG, Cruchaga C, Goate AM, Bales KR, Paul SM, Bateman RJ, Holtzman DM (2011) Human apoE isoforms differentially regulate brain amyloid-β peptide clearance. Science Translational Medicine 3:89ra57.

Cerf E, Gustot A, Goormaghtigh E, Ruysschaert JM, Raussens V (2011) High ability of apolipoprotein E4 to stabilize amyloid-beta peptide oligomers, the pathological entities responsible for Alzheimer's disease. FASEB J 25:1585-1595.

Chen S, Yadav SP, Surewicz WK (2010) Interaction between Human Prion Protein and Amyloid- (A) Oligomers: ROLE OF N-TERMINAL RESIDUES. Journal of Biological Chemistry 285:26377-26383.

Choo-Smith LP, Surewicz WK (1997) The interaction between Alzheimer amyloid beta(1-40) peptide and ganglioside GM1-containing membranes. FEBS Lett 402:95-98.

Choo-Smith LP, Garzon-Rodriguez W, Glabe CG, Surewicz WK (1997) Acceleration of amyloid fibril formation by specific binding of Abeta-(1-40) peptide to ganglioside-containing membrane vesicles. The Journal of biological chemistry 272:22987-22990.

Chung E, Ji Y, Sun Y, Kascsak RJ, Kascsak RB, Mehta PD, Strittmatter SM, Wisniewski T (2010) Anti-PrPC monoclonal antibody infusion as a novel

treatment for cognitive deficits in an Alzheimer's disease model mouse. BMC Neurosci 11:130.

Cirrito JR, Kang J-E, Lee J, Stewart FR, Verges DK, Silverio LM, Bu G, Mennerick S, Holtzman DM (2008) Endocytosis is required for synaptic activity-dependent release of amyloid-beta in vivo. Neuron 58:42-51.

Cirrito JR, Yamada KA, Finn MB, Sloviter RS, Bales KR, May PC, Schoepp DD, Paul SM, Mennerick S, Holtzman DM (2005) Synaptic activity regulates interstitial fluid amyloid-beta levels in vivo. Neuron 48:913-922.

Cirrito JR, May PC, O'Dell MA, Taylor JW, Parsadanian M, Cramer JW, Audia JE, Nissen JS, Bales KR, Paul SM, DeMattos RB, Holtzman DM (2003) In vivo assessment of brain interstitial fluid with microdialysis reveals plaque-associated changes in amyloid-beta metabolism and half-life. Journal of Neuroscience 23:8844-8853.

Cissé M, Sanchez PE, Kim DH, Ho K, Yu G-Q, Mucke L (2011) Ablation of cellular prion protein does not ameliorate abnormal neural network activity or cognitive dysfunction in the j20 line of human amyloid precursor protein transgenic mice. The Journal of neuroscience : the official journal of the Society for Neuroscience 31:10427-10431.

Coleman PD, Yao PJ (2003) Synaptic slaughter in Alzheimer's disease. Neurobiol Aging 24:1023-1027.

Craig-Schapiro R, Fagan AM, Holtzman DM (2009) Biomarkers of Alzheimer's disease. Neurobiol Dis 35:128-140.

Cummings BJ, Pike CJ, Shankle R, Cotman CW (1996) Beta-amyloid deposition and other measures of neuropathology predict cognitive status in Alzheimer's disease. Neurobiol Aging 17:921-933.

De Felice FG, Velasco PT, Lambert MP, Viola K, Fernandez SJ, Ferreira ST, Klein WL (2007) Abeta Oligomers Induce Neuronal Oxidative Stress through an N-Methyl-D-aspartate Receptor-dependent Mechanism That Is Blocked by the Alzheimer Drug Memantine. Journal of Biological Chemistry 282:11590-11601.

De Felice FG, Vieira MNN, Bomfim TR, Decker H, Velasco PT, Lambert MP, Viola KL, Zhao W-Q, Ferreira ST, Klein WL (2009) Protection of synapses against Alzheimer's-linked toxins: insulin signaling prevents the pathogenic binding of Abeta oligomers. Proc Natl Acad Sci U S A 106:1971-1976.

De Strooper B (2003) Aph-1, Pen-2, and Nicastrin with Presenilin generate an active gamma-Secretase complex. Neuron 38:9-12.

De Strooper B, Iwatsubo T, Wolfe MS (2012) Presenilins and gamma-Secretase: Structure, Function, and Role in Alzheimer Disease. Cold Spring Harb Perspect Med 2:a006304.

DeKosky ST, Scheff SW (1990) Synapse loss in frontal cortex biopsies in Alzheimer's disease: correlation with cognitive severity. Annals of Neurology 27:457-464.

DeMattos RB, Cirrito JR, Parsadanian M, May PC, O'Dell MA, Taylor JW, Harmony JA, Aronow BJ, Bales KR, Paul SM, Holtzman DM (2004) ApoE and Clusterin Cooperatively Suppress Abeta Levels and Deposition. Evidence that ApoE Regulates Extracellular Abeta Metabolism In Vivo. Neuron 41:193-202.

Dermaut B, Croes EA, Rademakers R, Van Den Broeck M, Cruts M, Hofman A, Van Duijn CM, Van Broeckhoven C (2003) PRNP Val129 homozygosity increases risk for early-onset Alzheimer's disease. Annals of Neurology 53:409-412.

Duff K, Eckman C, Zehr C, Yu X, Prada C-M, Perez-Tur J, Hutton M, Buee L, Harigaya Y, Yager D, Morgan D, Gordon MN, Holcomb L, Refolo L, Zenk B, Hardy J, Younkin S (1996) Increased amyloid-β42(43) in brains of mice expressing mutant presenilin 1. Nature 383:710-713.

Fagan AM, Head D, Shah AR, Marcus D, Mintun M, Morris JC, Holtzman DM (2009) Decreased cerebrospinal fluid Abeta(42) correlates with brain atrophy in cognitively normal elderly. Annals of Neurology 65:176-183.

Farris W, Schutz SG, Cirrito JR, Shankar GM, Sun X, George A, Leissring MA, Walsh DM, Qiu WQ, Holtzman DM, Selkoe DJ (2007) Loss of Neprilysin Function Promotes Amyloid Plaque Formation and Causes Cerebral Amyloid Angiopathy. American Journal Of Pathology 171:241-251.

Fishman PH, Brady RO (1976) Biosynthesis and function of gangliosides. Science (New York, NY) 194:906-915.

Freir DB, Nicoll AJ, Klyubin I, Panico S, Mc Donald JM, Risse E, Asante EA, Farrow MA, Sessions RB, Saibil HR, Clarke AR, Rowan MJ, Walsh DM, Collinge J (2011) Interaction between prion protein and toxic amyloid beta assemblies can be therapeutically targeted at multiple sites. Nat Commun 2:336.

Fukumoto H, Tokuda T, Kasai T, Ishigami N, Hidaka H, Kondo M, Allsop D, Nakagawa M (2010) High-molecular-weight beta-amyloid oligomers are elevated in cerebrospinal fluid of Alzheimer patients. The FASEB Journal 24:2716-2726.

Gao CM, Yam AY, Wang X, Magdangal E, Salisbury C, Peretz D, Zuckermann RN, Connolly MD, Hansson O, Minthon L, Zetterberg H, Blennow K, Fedynyshyn

JP, Allauzen S (2010) Aβ40 Oligomers Identified as a Potential Biomarker for the Diagnosis of Alzheimer's Disease. PLoS ONE 5:e15725.

Ghiso J, Matsubara E, Koudinov A, Choi-Miura NH, Tomita M, Wisniewski T, Frangione B (1993) The cerebrospinal-fluid soluble form of Alzheimer's amyloid beta is complexed to SP-40,40 (apolipoprotein J), an inhibitor of the complement membrane-attack complex. Biochemical Journal 293:27.

Gimbel DA, Nygaard HB, Coffey EE, Gunther EC, Laurén J, Gimbel ZA, Strittmatter SM (2010) Memory impairment in transgenic Alzheimer mice requires cellular prion protein. The Journal of neuroscience : the official journal of the Society for Neuroscience 30:6367-6374.

Glenner GG, Wong CW (1984a) Alzheimer's disease and Down's syndrome: Sharing of a unique cerebrovascular amyloid fibril protein. Biochem Biophys Res Commun 122:1131-1135.

Glenner GG, Wong CW (1984b) Alzheimer's disease: Initial report of the purification and characterization of a novel cerebrovascular amyloid protein. Biochem Biophys Res Commun 120:885-890.

Goate A, Chartier-Harlin MC, Mullan M, Brown J, Crawford F, Fidani L, Giuffra L, Haynes A, Irving N, James L, et al. (1991) Segregation of a missense mutation in the amyloid precursor protein gene with familial Alzheimer's disease. Nature 349:704-706.

Golde TE, Schneider LS, Koo EH (2011) Anti-aβ therapeutics in Alzheimer's disease: the need for a paradigm shift. Neuron 69:203-213.

Graeber MB, Mehraein P (1999) Reanalysis of the first case of Alzheimer's disease. Eur Arch Psychiatry Clin Neurosci 249 Suppl 3:10-13.

Graeber MB, Kosel S, Grasbon-Frodl E, Moller HJ, Mehraein P (1998) Histopathology and APOE genotype of the first Alzheimer disease patient, Auguste D. neurogenetics 1:223-228.

Grundke-Iqbal I, Iqbal K, Quinlan M, Tung Y-C, Zaidi MS, Wisniewski HM (1986) Microtubule-associated protein tau: a component of Alzheimer paired helical filaments. Journal of Biological Chemistry 261:6084-6089.

Haass C (2010) Initiation and propagation of neurodegeneration. Nature Medicine 16:1201-1204.

Haass C, Selkoe DJ (2007) Soluble protein oligomers in neurodegeneration: Lessons from the Alzheimer's amyloid ß-peptide. Nat Rev Mol Cell Biol 8:101-112.

Haass C, Schlossmacher M, Hung AY, Vigo-Pelfrey C, Mellon A, Ostaszewski B, Lieberburg I, Koo EH, Schenk D, Teplow D, Selkoe D (1992) Amyloid β-peptide is produced by cultured cells during normal metabolism. Nature 359:322-325.

Hansson HA, Holmgren J, Svennerholm L (1977) Ultrastructural localization of cell membrane GM1 ganglioside by cholera toxin. Proc Natl Acad Sci U S A 74:3782-3786.

Hardy J, Selkoe DJ (2002) The amyloid hypothesis of Alzheimer's disease: progress and problems on the road to therapeutics. Science 297:353-356.

Hardy JA, Higgins GA (1992) Alzheimer's disease: the amyloid cascade hypothesis. Science 256:184-185.

Hayashi H, Kimura N, Yamaguchi H, Hasegawa K, Yokoseki T, Shibata M, Yamamoto N, Michikawa M, Yoshikawa Y, Terao K, Matsuzaki K, Lemere CA, Selkoe DJ, Naiki H, Yanagisawa K (2004) A seed for Alzheimer amyloid in the brain. Journal of Neuroscience 24:4894-4902.

Holmgren J, Lonnroth I, Svennerh.L (1973) Tissue Receptor for Cholera Exotoxin - Postulated Structure from Studies with Gm1 Ganglioside and Related Glycolipids. Infection and Immunity 8:208-214.

Hong S, Quintero-Monzon O, Ostaszewski BL, Podlisny DR, Cavanaugh WT, Yang T, Holtzman DM, Cirrito JR, Selkoe DJ (2011) Dynamic Analysis of Amyloid β-Protein in Behaving Mice Reveals Opposing Changes in ISF versus Parenchymal Aβ during Age-Related Plaque Formation. Journal of Neuroscience 31:15861-15869.

Hsia AY, Masliah E, McConlogue L, Yu GQ, Tatsuno G, Hu K, Kholodenko D, Malenka RC, Nicoll RA, Mucke L (1999) Plaque-independent disruption of neural circuits in Alzheimer's disease mouse models. Proc Natl Acad Sci U S A 96:3228-3233.

Jin M, Shepardson N, Yang T, Chen G, Walsh D, Selkoe DJ (2011) Soluble amyloid beta-protein dimers isolated from Alzheimer cortex directly induce Tau hyperphosphorylation and neuritic degeneration. Proc Natl Acad Sci U S A 108:5819-5824.

Joachim CL, Morris JH, Kosik KS, Selkoe DJ (1987) Tau antisera recognize neurofibrillary tangles in a range of neurodegenerative disorders. Annals of Neurology 22:514-520.

Kakio A, Nishimoto S-i, Yanagisawa K, Kozutsumi Y, Matsuzaki K (2002) Interactions of Amyloid β-Protein with Various Gangliosides in Raft-Like

Membranes: Importance of GM1 Ganglioside-Bound Form as an Endogenous Seed for Alzheimer Amyloid †. Biochemistry 41:7385-7390.

Kamenetz F, Tomita T, Hsieh H, Seabrook G, Borchelt D, Iwatsubo T, Sisodia S, Malinow R (2003) APP processing and synaptic function. Neuron 37:925-937.

Kang J, Lemaire H-G, Unterbeck A, Salbaum JM, Masters CL, Grzeschik K-H, Multhaup G, Beyreuther K, Muller-Hill B (1987) The precursor of Alzheimer's disease amyloid A4 protein resembles a cell-surface receptor. Nature 325:733-736.

Kang J-E, Cirrito JR, Dong H, Csernansky JG, Holtzman DM (2007) Acute stress increases interstitial fluid amyloid-beta via corticotropin-releasing factor and neuronal activity. Proc Natl Acad Sci U S A 104:10673-10678.

Kang J-E, Lim MM, Bateman RJ, Lee JJ, Smyth LP, Cirrito JR, Fujiki N, Nishino S, Holtzman DM (2009) Amyloid-beta dynamics are regulated by orexin and the sleep-wake cycle. Science 326:1005-1007.

Kelly BL, Ferreira A (2006) beta-Amyloid-induced dynamin 1 degradation is mediated by N-methyl-D-aspartate receptors in hippocampal neurons. Journal of Biological Chemistry 281:28079-28089.

Kessels HW, Nguyen LN, Nabavi S, Malinow R (2010) The prion protein as a receptor for amyloid-β. Nature 466:E1-E1.

Kim D, Tsai L-H (2009) Bridging physiology and pathology in AD. Cell 137:997-1000.

Kim W, Hecht MH (2005) Sequence determinants of enhanced amyloidogenicity of Alzheimer A{beta}42 peptide relative to A{beta}40. The Journal of biological chemistry 280:35069-35076.

King CA, van Heyningen WE (1973) Deactivation of cholera toxin by a sialidase-resistant monosialosylganglioside. Journal of Infectious Diseases 127:639.

Klyubin I, Betts V, Welzel AT, Blennow K, Zetterberg H, Wallin A, Lemere CA, Cullen WK, Peng Y, Wisniewski T, Selkoe DJ, Anwyl R, Walsh DM, Rowan MJ (2008) Amyloid beta protein dimer-containing human CSF disrupts synaptic plasticity: prevention by systemic passive immunization. Journal of Neuroscience 28:4231-4237.

Koffie RM, Meyer-Luehmann M, Hashimoto T, Adams KW, Mielke ML, Garcia-Alloza M, Micheva KD, Smith SJ, Kim ML, Lee VM, Hyman BT, Spires-Jones TL (2009) Oligomeric amyloid beta associates with postsynaptic densities and

correlates with excitatory synapse loss near senile plaques. Proc Natl Acad Sci USA 106:4012-4017.

Kosik KS, Joachim CL, Selkoe DJ (1986) Microtubule-associated protein, tau, is a major antigenic component of paired helical filaments in Alzheimer's disease. Proc Natl Acad Sci USA 83:4044-4048.

Kudo W, Lee H-P, Zou W-Q, Wang X, Perry G, Zhu X, Smith MA, Petersen RB, Lee H-g (2012) Cellular prion protein is essential for oligomeric amyloid-β-induced neuronal cell death. Human molecular genetics 21:1138-1144.

Kuperstein I, Broersen K, Benilova I, Rozenski J, Jonckheere W, Debulpaep M, Vandersteen A, Segers-Nolten I, Van Der Werf K, Subramaniam V (2010) Neurotoxicity of Alzheimer's disease Aβ peptides is induced by small changes in the Aβ42 to Aβ40 ratio. The EMBO Journal 29:3408-3420.

Lambert MP, Barlow AK, Chromy BA, Edwards C, Freed R, iosatos M, Morgan TE, Rozovsky I, Trommer B, Viola KL, Wals P, Zhang C, Finch CE, Krafft GA, Klein WL (1998) Diffusible, nonfribrillar ligands derived from $Aß_{1-42}$ are potent central nervous system neurotoxins. Proc Natl Acad Sci USA 95:6448-6453.

Laurén J, Gimbel DA, Nygaard HB, Gilbert JW, Strittmatter SM (2009) Cellular prion protein mediates impairment of synaptic plasticity by amyloid-β oligomers. Nature 457:1128-1132.

Lesné S, Koh MT, Kotilinek L, Kayed R, Glabe CG, Yang A, Gallagher M, Ashe KH (2006) A specific amyloid-beta protein assembly in the brain impairs memory. Nature 440:352-357.

Levy E, Carman MD, Fernandez-Madrid IJ, Power MD, Lieberburg I, van Duinen SG, Bots GT, Luyendijk W, Frangione B (1990) Mutation of the Alzheimer's disease amyloid gene in hereditary cerebral hemorrhage, Dutch type. Science (New York, NY) 248:1124-1126.

Li S, Hong S, Shepardson NE, Walsh DM, Shankar GM, Selkoe D (2009) Soluble oligomers of amyloid Beta protein facilitate hippocampal long-term depression by disrupting neuronal glutamate uptake. Neuron 62:788-801.

Li S, Jin M, Koeglsperger T, Shepardson NE, Shankar GM, Selkoe DJ (2011) Soluble Aβ oligomers inhibit long-term potentiation through a mechanism involving excessive activation of extrasynaptic NR2B-containing NMDA receptors. Journal of Neuroscience 31:6627-6638.

Martins IC, Kuperstein I, Wilkinson H, Maes E, Vanbrabant M, Jonckheere W, Van Gelder P, Hartmann D, D'hooge R, De Strooper B, Schymkowitz J,

Rousseau F (2008) Lipids revert inert Aβ amyloid fibrils to neurotoxic protofibrils that affect learning in mice. Embo J 27:224-233.

Masliah E, Mallory M, Alford M, DeTeresa R, Hansen LA, McKeel DW, Jr., Morris JC (2001) Altered expression of synaptic proteins occurs early during progression of Alzheimer's disease. Neurology 56:127-129.

Masters CL, Simms G, Weinman NA, Multhaup G, McDonald BL, Beyreuther K (1985) Amyloid plaque core protein in Alzheimer disease and Down syndrome. Proc Natl Acad Sci USA 82:4245-4249.

Mawuenyega KG, Sigurdson W, Ovod V, Munsell L, Kasten T, Morris JC, Yarasheski KE, Bateman RJ (2010) Decreased Clearance of CNS -Amyloid in Alzheimer's Disease. Science 330:1774-1774.

Mc Donald JM, Savva GM, Brayne C, Welzel AT, Forster G, Shankar GM, Selkoe DJ, Ince PG, Walsh DM (2010) The presence of sodium dodecyl sulphate-stable A dimers is strongly associated with Alzheimer-type dementia. Brain 133:1328-1341.

McLaurin J, Chakrabartty A (1996) Membrane disruption by Alzheimer beta-amyloid peptides mediated through specific binding to either phospholipids or gangliosides. Implications for neurotoxicity. Journal of Biological Chemistry 271:26482-26489.

McLean C, Cherny R, Fraser F, Fuller S, Smith M, Vbeyreuther K, Bush A, Masters C (1999) Soluble pool of Aβ amyloid as a determinant of severity of neurodegeneration in Alzheimer's disease. Annals of Neurology 46:860-866.

Meyer-Luehmann M, Spires-Jones TL, Prada C, Garcia-Alloza M, De Calignon A, Rozkalne A, Koenigsknecht-Talboo J, Holtzman DM, Bacskai BJ, Hyman BT (2008) Rapid appearance and local toxicity of amyloid-β plaques in a mouse model of Alzheimer’s disease. Nature 451:720-724.

Molander-Melin M, Blennow K, Bogdanovic N, Dellheden B, Mansson J-E, Fredman P (2005) Structural membrane alterations in Alzheimer brains found to be associated with regional disease development; increased density of gangliosides GM1 and GM2 and loss of cholesterol in detergent-resistant membrane domains. Journal of Neurochemistry 92:171-182.

Möller HJ, Graeber MB (1998) The case described by Alois Alzheimer in 1911. Historical and conceptual perspectives based on the clinical record and neurohistological sections.

Molnar Z, Soos K, Lengyel I, Penke B, Szegedi V, Budai D (2004) Enhancement of NMDA responses by beta-amyloid peptides in the hippocampus in vivo. Neuroreport 15:1649-1652.

Mucke L, Masliah E, Yu GQ, Mallory M, Rockenstein EM, Tatsuno G, Hu K, Kholodenko D, Johnson-Wood K, McConlogue L (2000) High-level neuronal expression of abeta 1-42 in wild-type human amyloid protein precursor transgenic mice: synaptotoxicity without plaque formation. Journal of Neuroscience 20:4050-4058.

Mulkey RM, Endo S, Shenolikar S, Malenka RC (1994) Involvement of a calcineurin/inhibitor-1 phosphatase cascade in hippocampal long-term depression. Nature 369:486-488.

Nagerl UV, Eberhorn N, Cambridge SB, Bonhoeffer T (2004) Bidirectional activity-dependent morphological plasticity in hippocampal neurons. Neuron 44:759-767.

Nazer B, Hong S, Selkoe DJ (2008) LRP promotes endocytosis and degradation, but not transcytosis, of the amyloid-beta peptide in a blood-brain barrier in vitro model. Neurobiol Dis 30:94-102.

Nicoll RA, Malenka RC (1999) Expression mechanisms underlying NMDA receptor-dependent long-term potentiation. Anna 868:515-525.

Nukina N, Ihara Y (1986) One of the Antigenic Determinants of Paired Helical Filaments Is Related to Tau Protein. Journal of Biochemistry 99:1541-1544.

O'Nuallain B, Freir DB, Nicoll AJ, Risse E, Ferguson N, Herron CE, Collinge J, Walsh DM (2010) Amyloid beta-protein dimers rapidly form stable synaptotoxic protofibrils. Journal of Neuroscience 30:14411-14419.

Olson MI, Shaw CM (1969) Presenile dementia and Alzheimer's disease in mongolism. Brain 92:147-156.

Palop JJ, Chin J, Mucke L (2006) A network dysfunction perspective on neurodegenerative diseases. Nature 443:768-773.

Palop JJ, Jones B, Kekonius L, Chin J, Yu GQ, Raber J, Masliah E, Mucke L (2003) Neuronal depletion of calcium-dependent proteins in the dentate gyrus is tightly linked to Alzheimer's disease-related cognitive deficits. Proc Natl Acad Sci U S A 100:9572-9577.

Palop JJ, Chin J, Roberson ED, Wang J, Thwin MT, Bien-Ly N, Yoo J, Ho KO, Yu G-Q, Kreitzer A, Finkbeiner S, Noebels JL, Mucke L (2007) Aberrant excitatory neuronal activity and compensatory remodeling of inhibitory

hippocampal circuits in mouse models of Alzheimer's disease. Neuron 55:697-711.

Parkin ET, Watt NT, Hussain I, Eckman EA, Eckman CB, Manson JC, Baybutt HN, Turner AJ, Hooper NM (2007) Cellular prion protein regulates beta-secretase cleavage of the Alzheimer's amyloid precursor protein. Proc Natl Acad Sci U S A 104:11062-11067.

Pimplikar SW, Nixon RA, Robakis NK, Shen J, Tsai L-H (2010) Amyloid-independent mechanisms in Alzheimer's disease pathogenesis. J Neurosci 30:14946-14954.

Putcha D, Brickhouse M, O'Keefe K, Sullivan C, Rentz D, Marshall G, Dickerson B, Sperling R (2011) Hippocampal hyperactivation associated with cortical thinning in Alzheimer's disease signature regions in non-demented elderly adults. J Neurosci 31:17680-17688.

Renner M, Specht CG, Triller A (2008) Molecular dynamics of postsynaptic receptors and scaffold proteins. Current opinion in neurobiology 18:532-540.

Renner M, Lacor PN, Velasco PT, Xu J, Contractor A, Klein WL, Triller A (2010) Deleterious Effects of Amyloid β Oligomers Acting as an Extracellular Scaffold for mGluR5. Neuron 66:739-754.

Resenberger UK, Harmeier A, Woerner AC, Goodman JL, Müller V, Krishnan R, Vabulas RM, Kretzschmar HA, Lindquist S, Hartl FU, Multhaup G, Winklhofer KF, Tatzelt J (2011) The cellular prion protein mediates neurotoxic signalling of β-sheet-rich conformers independent of prion replication. The EMBO Journal 30:2057-2070.

Riemenschneider M, Klopp N, Xiang W, Wagenpfeil S, Vollmert C, Müller U, Förstl H, Illig T, Kretzschmar H, Kurz A (2004) Prion protein codon 129 polymorphism and risk of Alzheimer disease. Neurology 63:364-366.

Roychaudhuri R, Yang M, Hoshi MM, Teplow DB (2008) Amyloid -Protein Assembly and Alzheimer Disease. Journal of Biological Chemistry 284:4749-4753.

Saito T, Suemoto T, Brouwers N, Sleegers K, Funamoto S, Mihira N, Matsuba Y, Yamada K, Nilsson P, Takano J, Nishimura M, Iwata N, Van Broeckhoven C, Ihara Y, Saido TC (2011) Potent amyloidogenicity and pathogenicity of Aβ43. Nature Neuroscience 14:1023-1032.

Scheuner D et al. (1996) Secreted amyloid β-protein similar to that in the senile plaques of Alzheimer's disease is increased *in vivo* by the presenilin 1 and 2 and APP mutations linked to familial Alzheimer's disease. Nature Med 2:864-870.

Selkoe DJ (1991) The molecular pathology of Alzheimer's disease. Neuron 6:487-498.

Selkoe DJ (2002) Alzheimer's disease is a synaptic failure. Science 298:789-791.

Selkoe DJ (2011) Resolving controversies on the path to Alzheimer's therapeutics. Nature Medicine 17:1060-1065.

Selkoe DJ, Abraham CR, Podlisny MB, Duffy LK (1986) Isolation of low-molecular-weight proteins from amyloid plaque fibers in Alzheimer's disease. Journal of Neurochemistry 146:1820-1834.

Seubert P, Vigo-Pelfrey C, Esch F, Lee M, Dovey H, Davis D, Sinha S, Schiossmacher M, Whaley J, Swindlehurst C, McCormack R, Wolfert R, Selkoe D, Lieberburg I, Schenk D (1992) Isolation and quantification of soluble Alzheimer's β-peptide from biological fluids. Nature 359:325-327.

Shankar GM, Bloodgood BL, Townsend M, Walsh DM, Selkoe DJ, Sabatini BL (2007) Natural oligomers of the Alzheimer amyloid-beta protein induce reversible synapse loss by modulating an NMDA-type glutamate receptor-dependent signaling pathway. Journal of Neuroscience 27:2866-2875.

Shankar GM, Leissring MA, Adame A, Sun X, Spooner E, Masliah E, Selkoe DJ, Lemere CA, Walsh DM (2009) Biochemical and immunohistochemical analysis of an Alzheimer's disease mouse model reveals the presence of multiple cerebral Abeta assembly forms throughout life. Neurobiol Dis 36:293-302.

Shankar GM, Li S, Mehta TH, Garcia-Munoz A, Shepardson NE, Smith I, Brett FM, Farrell MA, Rowan MJ, Lemere CA, Regan CM, Walsh DM, Sabatini BL, Selkoe DJ (2008) Amyloid-l[beta]l protein dimers isolated directly from Alzheimer's brains impair synaptic plasticity and memory. Nature Medicine 14:837.

Sheikh KA, Sun J, Liu Y, Kawai H, Crawford TO, Proia RL, Griffin JW, Schnaar RL (1999) Mice lacking complex gangliosides develop Wallerian degeneration and myelination defects. Proc Natl Acad Sci U S A 96:7532-7537.

Shoji M, Golde TE, Ghiso J, Cheung TT, Estus S, Shaffer LM, Cai X, McKay DM, Tintner R, Frangione B, Younkin SG (1992) Production of the Alzheimer amyloid β protein by normal proteolytic processing. Science 258:126-129.

Snider B, Fagan A, Roe C, Shah A, Grant E, Xiong C, Morris J, Holtzman D (2009) Cerebrospinal Fluid Biomarkers and Rate of Cognitive Decline in Very Mild Dementia of the Alzheimer Type. Archives of Neurology 66:638.

Sonnino S, Mauri L, Chigorno V, Prinetti A (2007) Gangliosides as components of lipid membrane domains. Glycobiology 17:1R-13R.

Sperling RA, Laviolette PS, O'Keefe K, O'Brien J, Rentz DM, Pihlajamaki M, Marshall G, Hyman BT, Selkoe DJ, Hedden T, Buckner RL, Becker JA, Johnson KA (2009) Amyloid deposition is associated with impaired default network function in older persons without dementia. Neuron 63:178-188.

Sperling RA et al. (2011) Toward defining the preclinical stages of Alzheimer's disease: recommendations from the National Institute on Aging-Alzheimer's Association workgroups on diagnostic guidelines for Alzheimer's disease. Alzheimers Dement 7:280-292.

Spires TL, Meyer-Luehmann M, Stern EA, McLean PJ, Skoch J, Nguyen PT, Bacskai BJ, Hyman BT (2005) Dendritic spine abnormalities in amyloid precursor protein transgenic mice demonstrated by gene transfer and intravital multiphoton microscopy. Journal of Neuroscience 25:7278-7287.

Strittmatter WJ, Weisgraber KH, Huang DY, Dong LM, Salvesen GS, Pericak-Vance M, Schmechel D, Saunders AM, Goldgaber D, Roses AD (1993) Binding of human apolipoprotein E to synthetic amyloid beta peptide: isoform-specific effects and implications for late-onset Alzheimer disease. Proc Natl Acad Sci U S A 90:8098-8102.

Suzuki N, Cheung TT, Cai X-D, Odaka A, Otvos Jr L, Eckman C, Golde TE, Younkin SG (1994) An increased percentage of long amyloid β protein secreted by familial amyloid β protein precursor (βAPP717) mutants. Science 264:1336-1340.

Svennerholm L, Gottfries CG (1994) Membrane lipids, selectively diminished in Alzheimer brains, suggest synapse loss as a primary event in early-onset form (type I) and demyelination in late-onset form (type II). Journal of Neurochemistry 62:1039-1047.

Terry RD, Masliah E, Salmon DP, Butters N, DeTeresa R, Hill R, Hansen LA, Katzman R (1991) Physical basis of cognitive alterations in Alzheimer's disease: synapse loss is the major correlate of cognitive impairment. Annals of Neurology 30:572-580.

Tomiyama T, Matsuyama S, Iso H, Umeda T, Takuma H, Ohnishi K, Ishibashi K, Teraoka R, Sakama N, Yamashita T (2010) A Mouse Model of Amyloid {beta} Oligomers: Their Contribution to Synaptic Alteration, Abnormal Tau Phosphorylation, Glial Activation, and Neuronal Loss In Vivo. Journal of Neuroscience 30:4845.

Tomiyama T, Nagata T, Shimada H, Teraoka R, Fukushima A, Kanemitsu H, Takuma H, Kuwano R, Imagawa M, Ataka S, Wada Y, Yoshioka E, Nishizaki T, Watanabe Y, Mori H (2008) A new amyloid beta variant favoring oligomerization in Alzheimer's-type dementia. Annals of Neurology 63:377-387.

Townsend M, Shankar GM, Mehta T, Walsh DM, Selkoe DJ (2006) Effects of secreted oligomers of amyloid beta-protein on hippocampal synaptic plasticity: a potent role for trimers. Journal of Physiology 572:477-492.

Triller A, Choquet D (2008) New concepts in synaptic biology derived from single-molecule imaging. Neuron 59:359-374.

Van Broeckhoven C, Haan J, Bakker E, Hardy J, Van Hul W, Wehnert A, Vegter-Van der Vlis M, Roos R (1990) Amyloid beta protein precursor gene and hereditary cerebral hemorrhage with amyloidosis (Dutch). Science (New York, NY) 248:1120-1122.

van Heyningen S (1974) Cholera toxin: interaction of subunits with ganglioside GM1. Science (New York, NY) 183:656.

Villemagne VL, Perez KA, Pike KE, Kok WM, Rowe CC, White AR, Bourgeat P, Salvado O, Bedo J, Hutton CA, Faux NG, Masters CL, Barnham KJ (2010) Blood-Borne Amyloid- Dimer Correlates with Clinical Markers of Alzheimer's Disease. Journal of Neuroscience 30:6315-6322.

Walsh D, Klyubin I, Fadeeva J, William K. Cullen W, Anwyl R, Wolfe M, Rowan M, Selkoe D (2002) Naturally secreted oligomers of the Alzheimer amyloid ß-protein potently inhibit hippocampal long-term potentiation *in vivo*. Nature 416:535-539.

Walsh DM, Selkoe DJ (2004) Deciphering the molecular basis of memory failure in Alzheimer's disease. Neuron 44:181-193.

Walsh DM, Selkoe DJ (2007) A beta oligomers - a decade of discovery. Journal of Neurochemistry 101:1172-1184.

Wang HY, Lee DH, D'Andrea MR, Peterson PA, Shank RP, Reitz AB (2000) beta-Amyloid(1-42) binds to alpha7 nicotinic acetylcholine receptor with high affinity. Implications for Alzheimer's disease pathology. Journal of Biological Chemistry 275:5626-5632.

Wang Q, Rowan MJ, Anwyl R (2004) Beta-amyloid-mediated inhibition of NMDA receptor-dependent long-term potentiation induction involves activation of microglia and stimulation of inducible nitric oxide synthase and superoxide. Journal of Neuroscience 24:6049-6056.

West MJ, Coleman PD, Flood DG, Troncoso JC (1994) Differences in the pattern of hippocampal neuronal loss in normal ageing and Alzheimer's disease. Lancet 344:769-772.

Wolfe MS, Xia W, Ostaszewski BL, Diehl TS, Kimberly WT, Selkoe DJ (1999) Two transmembrane aspartates in presenilin-1 required for presenilin endoproteolysis and γ-secretase activity. Nature 398:513-517.

Wu J, Anwyl R, Rowan MJ (1995) beta-Amyloid selectively augments NMDA receptor-mediated synaptic transmission in rat hippocampus. Neuroreport 6:2409-2413.

Yan P, Bero A, Cirrito J, Xiao Q, Hu X, Wang Y, Gonzales E, Holtzman D, Lee J-M (2009) Characterizing the Appearance and Growth of Amyloid Plaques in APP/PS1 Mice. Journal of Neuroscience 29:10706.

Yanagisawa K (2011) Pathological significance of ganglioside clusters in Alzheimer's disease. Journal of Neurochemistry.

Yanagisawa K, Odaka A, Suzuki N, Ihara Y (1995) GM1 ganglioside-bound amyloid beta-protein (A beta): a possible form of preamyloid in Alzheimer's disease. Nature Medicine 1:1062-1066.

Yanagisawa K, McLaurin J, Michikawa M, Chakrabartty A, Ihara Y (1997) Amyloid beta-protein (A beta) associated with lipid molecules: immunoreactivity distinct from that of soluble A beta. FEBS Lett 420:43-46.

Yang T, Hong S, OMalley T, Farrell MA, Sperling RA, Walsh DM, Selkoe DJ (*submitted*) New ELISAs with high specificity for soluble oligomers of amyloid ß-protein reveal natural Aß oligomers in human brain but not CSF. In, pp 1-53: *Submitted*.

Yao PJ, Zhu M, Pyun EI, Brooks AI, Therianos S, Meyers VE, Coleman PD (2003) Defects in expression of genes related to synaptic vesicle trafficking in frontal cortex of Alzheimer's disease. Neurobiol Dis 12:97-109.

Zhao W-Q, Santini F, Breese R, Ross D, Zhang XD, Stone DJ, Ferrer M, Townsend M, Wolfe AL, Seager MA, Kinney GG, Shughrue PJ, Ray WJ (2010) Inhibition of calcineurin-mediated endocytosis and alpha-amino-3-hydroxy-5-methyl-4-isoxazolepropionic acid (AMPA) receptors prevents amyloid beta oligomer-induced synaptic disruption. Journal of Biological Chemistry 285:7619-7632.

Chapter 2

Dynamic analysis of amyloid β in behaving mice reveals opposing changes in interstitial fluid versus parenchymal amyloid β during age-related plaque formation

Contributions:

Experiments were designed by Soyon Hong and Dennis Selkoe. Bicine-urea/SDS PAGE experiments were performed by Omar Quintero-Monzon. Aβ ELISAs were performed by Beth Ostaszewski, Ting Yang, and Soyon Hong. All other experiments were performed by Soyon Hong.

Publication:

Parts of this chapter have been published in the *Journal of Neuroscience* **31**(44):15861-9.

Introduction

After decades of investigative focus on amyloid plaques in Alzheimer's disease (AD), recent findings have led to a conceptual shift. Emerging evidence suggests that the insoluble amyloid fibrils that comprise plaques may not directly confer neurotoxicity but sequester small, diffusible assemblies of amyloid β-peptide (Aβ) that have been shown to potently alter synaptic structure and function (Walsh and Selkoe, 2007). The recognition of Aβ oligomers as highly bioactive assemblies has furthered interest in detecting and analyzing soluble forms of the peptide for mechanistic, diagnostic and therapeutic purposes. Although factors other than Aβ dyshomeostasis contribute importantly to the pathogenesis of AD (Pimplikar et al., 2010), virtually all potentially disease-modifying treatments currently under development are focused on decreasing or neutralizing this neurotoxic peptide. Moreover, a reduced CSF level of $A\beta_{42}$ in subjects with incipient or very early AD is one of the most promising biomarkers. Despite this therapeutic and diagnostic focus, we still lack insight into the *in vivo* economy of the most soluble forms of Aβ in the brain during the development of AD-type pathology.

Interstitial fluid (ISF) is the extracellular fluid that bathes the cells within a specific tissue region. As soluble Aβ is released by neurons, the ISF represents the pool of Aβ that may best reflect the physiological secretion and fate of soluble Aβ species, giving insight to the functions of Aβ in the normal environment and also the earliest, subtle changes that occur in AD. Moreover, ISF is the main

"trade center" between plasma and brain. The production of water through oxidation of glucose within brain cells and movement of plasma water from the brain vasculature across the blood-brain-barrier (BBB) contributes to the formation of ISF, which finds its way into the ventricular and cranial subarachnoid cerebrospinal fluid (CSF) (Shen et al., 2004). Thus, CSF content is influenced to a significant extent by the composition of solutes entrained in the brain ISF.

The *in vivo* microdialysis technique is the only known method that allows the collection of ISF from the hippocampi of awake, behaving mice. Based on the principle of simple diffusion, soluble molecules within the extracellular fluid with molecular weights (MW) that are much smaller than the MW cutoff (MWCO) of the semi-permeable probe membrane will cross the microdialysis membrane into microdialysate. Using *in vivo* microdialysis, Cirrito et al. (2003) have shown that soluble Aβ can be collected directly from ISF of a mouse hippocampus on a dynamic time scale, exclusive from other CNS compartments. Moreover, this technique allows for delivery of anti-Aβ antibodies or other potential drugs via reverse microdialysis or through the injection cannula attached to the microdialysis probe without further manipulation of the tissue or handling of the animal. The advantages of this particular delivery are (1) tissue around the probe can be repaired before delivery begins; (2) it avoids the brain trauma caused as the solution is ejected from the injector tip; and (3) there is no net change in fluid.

Here, to gain insight into the *in vivo* economy of the most soluble forms of Aβ in the brain during the development of AD-type pathology, I used brain

microdialysis in awake and behaving hAPP transgenic mice to gain an understanding of Aβ dynamics before and during the process of Aβ plaque formation. Microdialysis in mouse models of AD and even human subjects is providing important insights into the dynamics of normal ISF Aβ economy (Brody et al., 2008; Cirrito et al., 2008; Kang et al., 2009) and may help identify the earliest, most subtle Aβ changes that occur as AD-type neuropathology begins. Given the power of this *in vivo* sampling method, I performed hippocampal microdialysis on > 40 freely moving J20 transgenic mice of increasing age as a model of cerebral Aβ accumulation, and we searched for changes in the quality and quantity of Aβ species as the brain accrues insoluble deposits and undergoes neuronal and glial injury. We systematically analyzed the nature of endogenous Aβ over time using sensitive sandwich ELISAs, immunoprecipitation (IP)-Western blotting (WB), native and denaturing polyacrylamide gel electrophoresis (PAGE), and size-exclusion chromatography (SEC). We then complemented these analyses by assessing the fate of radiolabeled Aβ microinjected at physiological concentrations as a surrogate of newly secreted Aβ, and the results help explain the fall of $A\beta_{42}$ in the CSF of humans with AD. Taken together, these experiments describe the *in vivo* dynamics of the most soluble pool of brain Aβ during the process of AD-type amyloid plaque formation.

Results

Biochemical analysis of Aβ peptides that remain soluble in the brains of young,

behaving hAPP transgenic mice

To examine the quality and quantity of Aβ that remains soluble and of low molecular weight in ISF *in vivo* (termed ISF Aβ herein), we used a microdialysis probe with a 35 kDa MWCO membrane in mice expressing familial AD-mutant human APP (expressing *APP* V717F/KM670/671/NL transgene) (Mucke et al., 2000). When we intraperitoneally injected Compound E, a potent and brain-penetrant γ-secretase inhibitor (Grimwood et al., 2005; Yan et al., 2009), total ISF Aβ captured in microdialysates fell rapidly ($t_{1/2}$ ~2 h) to baseline (Figure 2.1A), showing that most of the ISF Aβ we sample by microdialysis in young transgenic mice represents newly synthesized APP cleavage products. To capture the Aβ species that best reflect the physiological levels, we performed microdialysis at a slow perfusion rate of 0.2 µl/min for up to 72 hours, as this allows optimal exchange of free Aβ into the probe. ISF samples were immunoprecipitated with a polyclonal Aβ antiserum (AW8), and the precipitates were separated by denaturing PAGE and blotted with pooled monoclonal antibodies to the N-terminus (6E10) and mid-region (4G8) of Aβ. The ISF Aβ was separated by conventional SDS-PAGE into two species: a 4 kDa monomer and a novel ~5 kDa species, which ran roughly half the time as a band (Figure 2.1B) and the other half as a smear (Figure 2.4A). We did not detect dimers (which run at ~6.5 kDa in these gels; Figure 2.1B) by IP/WB in the ISF of any of the > 40 mice we examined in this study, regardless of age. *In vitro* (test-tube) microdialysis of synthetic $Aβ_{40}$ showed that our 35 kDa MWCO membrane

Figure 2.1. ISF Aβ obtained by microdialysis from behaving 3 mo J20 hAPP transgenic mice.

(A) Rapid decline of ISF Aβ ($t_{1/2}$ ~2 h) upon acute γ-secretase inhibition *in vivo* in 3 mo transgenic (vs. wild-type littermate) mice. ISF sampled hourly at 1 µl/min; Compound E injected at time = 0 h. (B, C) ISF collected at 0.2 µl/min were IP'ed with AW8 Aβ antiserum and subjected to two types of SDS-PAGE: (B) Conventional SDS-PAGE separates ISF Aβ into a ~4 kDa (monomers) and a ~5 kDa Aβ-immunoreactive species (lane 3). No dimers were detected in ISF (but can be seen in the TBS-extract of a 24 mo transgenic (lane 2) or in synthetic Aβ (lane 1)). WB: 6E10+4G8. (C) Bicine/urea SDS-PAGE resolved ISF Aβ into 3 bands comigrating with synthetic $Aβ_{1-38}$, $Aβ_{1-40}$, and $Aβ_{1-42}$, plus a fourth faint band corresponding to $Aβ_{1-39}$. WB: 6E10. (D) Using 6E10 Aβ triplex ELISA, we quantified $Aβ_{x-38}$, $Aβ_{x-40}$ and $Aβ_{x-42}$ in ISF. Mean ± s.e.m.: 635 ± 70, 1937 ± 311 and 592 ± 58 pg/ml, respectively; N = 7 mice. (E) Interpolated zero flow method. Mean ± s.e.m.; N = 3-4 mice.

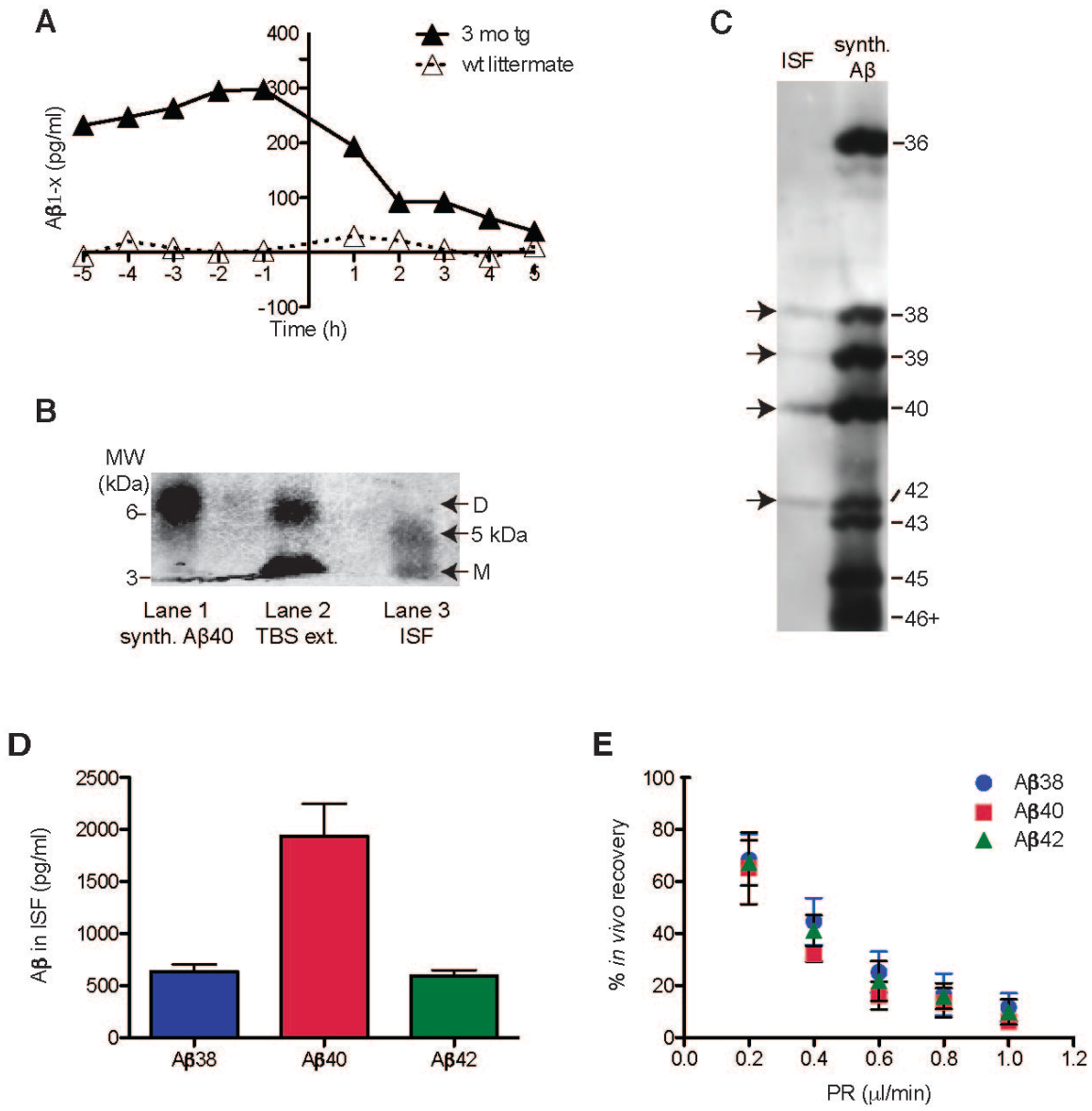

Figure 2.1 (Continued). ISF Aβ obtained by microdialysis from behaving 3 mo J20 hAPP transgenic mice.

allowed passage of dimers; however, their diffusion efficiency was low compared to that of monomers (Figure 4.1), suggesting that the lack of dimers in the ISF samples could be due to the detection limit of the technique. Next, we analyzed the mouse ISF by bicine/urea SDS-PAGE, which electrophoretically separates Aβ peptides of different lengths (Klafki et al., 1996). ISF Aβ was resolved into three principal bands comigrating with synthetic $Aβ_{1-38}$, $Aβ_{1-40}$, and $Aβ_{1-42}$, plus a fourth faint band comigrating with $Aβ_{1-39}$ (Figure 2.1C). Using a multiplex ELISA, we confirmed the bicine/urea gel result that $Aβ_{40}$ is the most abundant Aβ in ISF (Figure 2.1D). The $Aβ_{42}/Aβ_{40}$ ratio in the ISF of young, plaque-free J20 transgenic mice was calculated to be ~0.3. Using the interpolated zero flow method (Jacobson et al., 1985; Cirrito et al., 2003) (Figure 2.1E), we estimated the total soluble Aβ concentrations in hippocampal ISF of 3 mo transgenic to be ~1.2 nM.

ISF Aβ decreases with age as Aβ in brain parenchyma accrues

To elucidate how amyloid plaque development and maturation affect the steady-state levels of brain ISF Aβ, we sampled ISF from the hippocampi of living J20 transgenic mice at three ages: pre-plaque (~3 mo), early plaque deposition (~12 mo), and abundant and mature plaque deposition (~24 mo) (Figure 2.2A). The levels of holoAPP and its C-terminal fragments generated by β- and α-secretases were constant over the 3-24 mo ISF sampling period (Figure 2.2B), suggesting that Aβ production via APP proteolytic processing does not change

Figure 2.2. Amyloid plaques develop and mature with age in J20 APP transgenic mice, without significant changes in full-length APP or in its proteolytic processing by β- or α-secretases.

(A) Hippocampal sections from fixed J20 APP transgenic brains were paraffin-embedded, then stained for Aβ using R1282 polyclonal antibody. 3 mo sections were virtually plaque-free, whereas some plaques had formed by 12 mo. By 24 mo, abundant diffuse and dense-core plaques populated the hippocampus. (B) Representative blot of brain lysates of 3 mo transgenic, 24 mo transgenic and wild-type littermate loaded onto denaturing SDS-PAGE, then blotted for full-length APP (FL-APP) and its C-terminal fragments (CTFs) (WB: polyclonal C7) or to α-tubulin (WB: polyclonal tubulin-alpha). (C) Summary ratios of immunoreactive signals at 24 mo over 3 mo transgenic mice, for FL-APP and CTFs normalized to the α-tubulin signal. N = 3 mice per group; signal quantification by Licor Odyssey®.

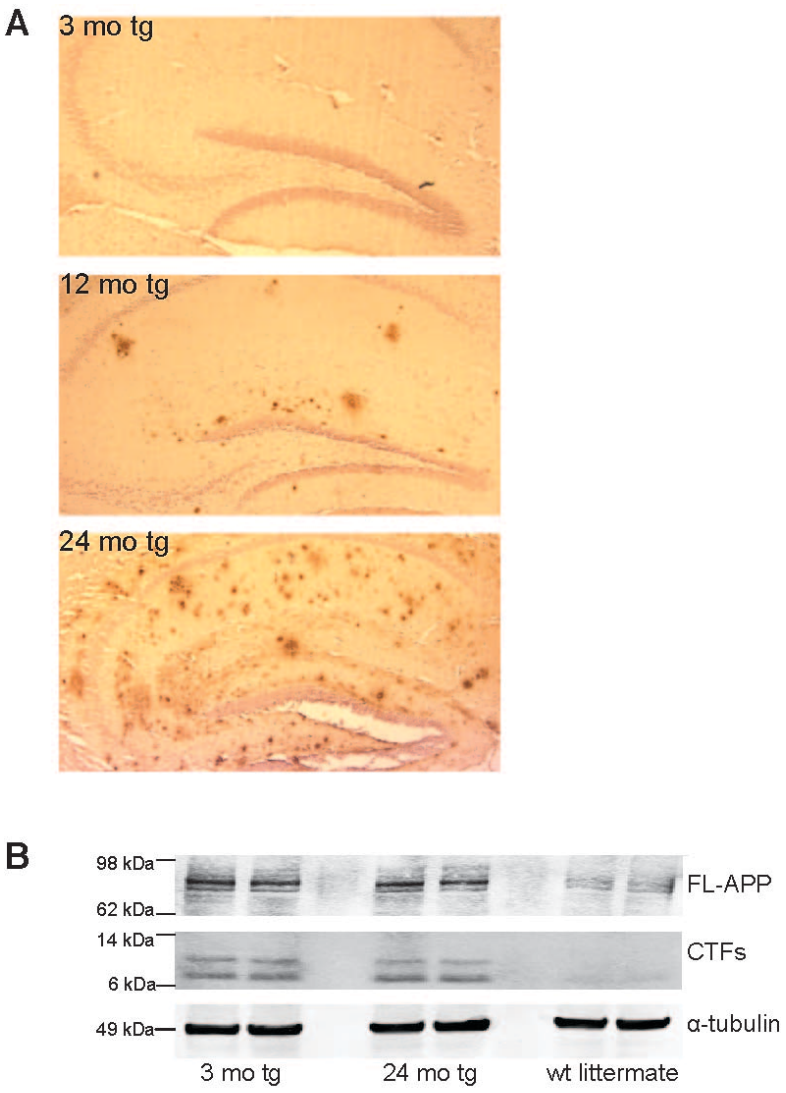

Figure 2.2 (Continued). Amyloid plaques develop and mature with age in J20 APP transgenic mice, without significant changes in full-length APP or in its proteolytic processing by β- or α-secretases.

appreciably over age.

As quantified by multiplex Aβ ELISA, all three Aβ peptides measured in ISF ($Aβ_{x-38}$, $Aβ_{x-40}$, and $Aβ_{x-42}$) decreased over time to levels that were significantly reduced by 24 mo (Figures 2.3A-C show absolute values; Figure 2.3D shows proportional levels). As the individual peptides fell to different degrees, the $Aβ_{42}/Aβ_{40}$ ratio in the ISF shifted from 0.3 at 3 mo transgenic mice to 0.13 at 24 mo transgenic mice.

We estimated that the total soluble Aβ concentrations in hippocampal ISF decreased from ~1.2 nM in 3 mo transgenic to ~0.5 nM in 24 mo transgenic (see Table 2.1 for concentrations of individual Aβ peptides in hippocampal ISF of 3 mo and 24 mo transgenic). The similar % recovery of microdialyzable Aβ at 3 and 24 mo (measured at 5 flow rates) indicates that the age-dependent decrease in ISF Aβ is not due to technical issues with the microdialysis system (Figure 2.3E). We measured analytes other than Aβ present in the ISF to see whether they are also altered with age, in particular, lactate, pyruvate, and glycerol. The ratio of lactate to pyruvate is an established marker of the redox state of cells; glycerol is an integral component of cellular membranes, and changes in its level can reflect degradation of membranes (Ungerstedt and Rostami, 2004). Neither the lactate-to-pyruvate ratio nor the level of glycerol in ISF changed significantly during our 3-24 mo sampling period (Figure 2.3F-G), suggesting that the decrease in Aβ is not associated with altered intermediary metabolism or perturbation of cell membrane integrity.

Figure 2.3. Levels of soluble ISF Aβ < 35 kDa in the brain fall with age.

(A-D) ISF was sampled from the hippocampi of 3 mo (pre-plaque), 12 mo (early plaque deposition), and 24 mo (abundant, mature plaques) J20 transgenic mice. Using Aβ triplex ELISAs, we found that $A\beta_{x\text{-}38}$ (A), $A\beta_{x\text{-}40}$ (B), and $A\beta_{x\text{-}42}$ (C) all decreased with age (means ± s.e.m.; N = 7, 4, 7 mice at 3, 12 and 24 mo, respectively). One-way ANOVA, followed by Bonferroni test: $^{*}P < 0.05$, $^{**}P < 0.01$ and $^{***}P < 0.001$ vs. 3 mo values; $^{\#}P < 0.05$ vs. 12 mo values. (D) Proportional levels of $A\beta_{38}$, $A\beta_{40}$ and $A\beta_{42}$, where each peptide was normalized to its level at 3 mo. $A\beta_{42}$ declined the most (80% by 24 mo vs. 3 mo). $^{***}P$ value < 0.0001 by two-way ANOVA with age as a variant. (E) At 0.2 µl/min, the perfusion rate used to collect all ISF samples in Figures 2.3 and 2.4, we obtained comparable % recoveries of microdialyzable Aβ in the two extreme ages (~63 ±3% in 3 mo transgenic and ~66 ±2% in 24 mo transgenic; means ± s.e.m.; N = 3-4 mice). (F-G) Ratios of lactate to pyruvate (F) and glycerol levels (G) in the ISF microdialysates were not altered with age (means ± s.e.m.; N = 3-8 mice).

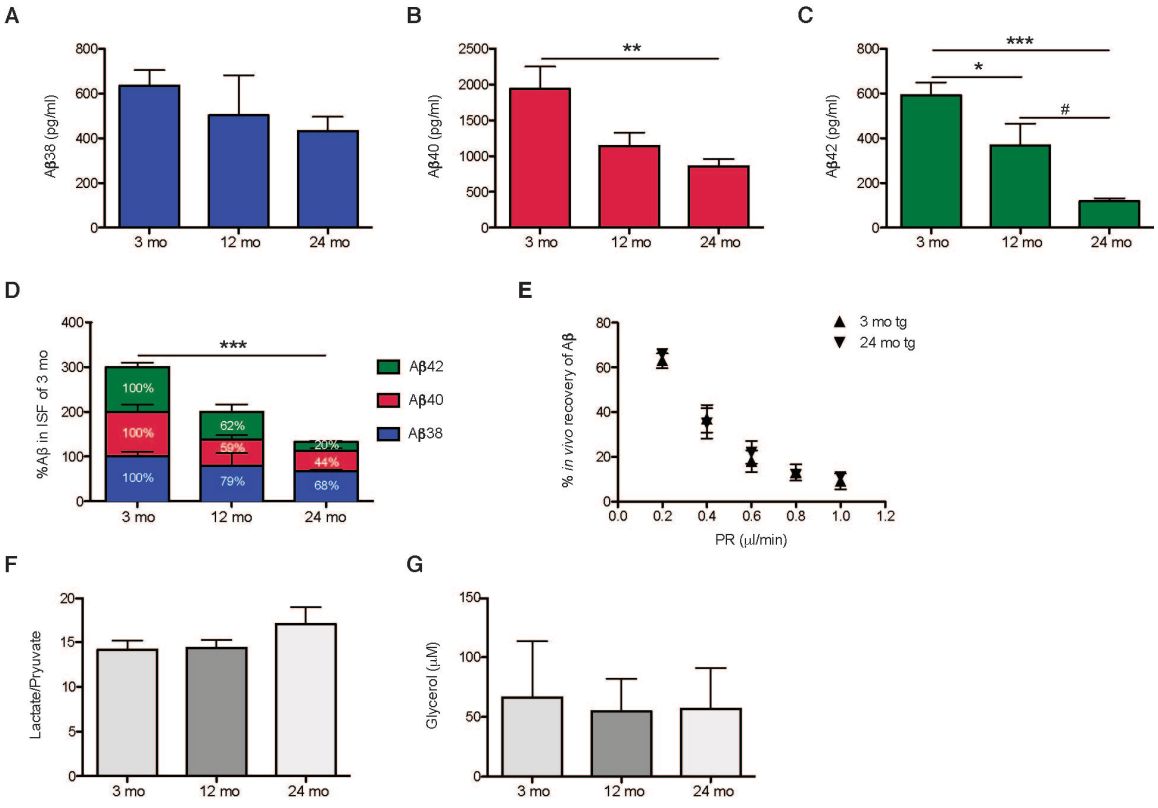

Figure 2.3 (Continued). Levels of soluble ISF Aβ < 35 kDa in the brain fall with age.

Table 2.1. Theoretical concentrations of microdialyzable ISF Aβ *in vivo* at zero flow rate.

	Aβ38 (pg/ml)		Aβ40 (pg/ml)		Aβ42 (pg/ml)		Aβ42:Aβ40	
	3 mo	24 mo	3 mo	24 mo	3 mo	24 mo	3 mo	24 mo
[ISF Aβ] of J20 transgenic mice	930	658	2975	1231	880	166	0.30	0.13

Concentrations of endogenous hippocampal ISF $A\beta_{38}$, $A\beta_{40}$, and $A\beta_{42}$ were calculated by extrapolating the curves generated from the interpolated zero-flow method to zero PR (see Figure 2.6). Ratios of $A\beta_{42}/A\beta_{40}$ in the ISF of 3 mo and 24 mo transgenic were calculated to be ~0.30 and 0.13, reflecting a higher drop of $A\beta_{42}$ vs. $A\beta_{40}$ in 24 mo transgenic mice.

Next, we sought to identify the pathophysiological relationship between ISF Aβ and the accrual of increasingly less soluble Aβ in brain parenchyma during the development of AD-type neuropathology. Using a sensitive IP-WB method (Walsh et al., 2002; Shankar et al., 2008), we compared the quantity and type of Aβ in ISF obtained *in vivo* with three pools of brain parenchymal Aβ isolated from the same mice right after the dialysis: Tris-buffered saline (TBS) extract (traditionally defined as the "soluble Aβ fraction"), detergent (SDS) extract (aggregated and membrane-associated Aβ), and formic acid (FA) extract (Aβ from highly insoluble deposits, including plaque cores (Masters et al., 1985; Selkoe et al., 1986)). As reported previously in the J20 line and other APP transgenic mice (Johnson-Wood et al., 1997; Hsia et al., 1999; Mucke et al.; Kawarabayashi et al., 2001; Shankar et al., 2009), we observed an age-dependent rise in levels of all three pools of parenchymal Aβ (Figure 2.4A). Both the SDS and FA extracts rose sharply with age (Figure 2.4A, D-E). Aβ in the TBS extract did not rise substantially until 24 mo, an age at which we regularly observed SDS-stable dimers in this fraction (Figure 2.4A, C). In contrast to these age-dependent rises in parenchymal Aβ, there was a decline in the ISF. We observed a 50% decrease in total absolute ISF Aβ levels between 3 and 12 mo (Figure 2.4B), before there was an appreciable rise in the TBS extract (Figure 2.4C). We next analyzed the values in each mouse to determine what portion of its TBS-soluble Aβ remains dialyzable *in vivo*, and observed a 5-fold decline in the ISF/TBS ratio between 3 and 12 mo (Figure 2.4F). When normalized to total

Figure 2.4. Aβ in all pools of brain parenchyma accrue with age while those that remain diffusible in the ISF declines.

(A) Representative IP-WB's of Aβ species in four pools: (1) ISF, and (2) TBS-extracted ("TBS ext"), (3) SDS-extracted ("SDS ext") and (4) FA-extracted ("FA ext") pools from brains of the same mice right after microdialysis. All pools (except the FA ext, which was lyophilized and straight-loaded onto the gel) were IP'ed with AW8 and blotted with 6E10 and 4G8. Synthetic Aβ run alongside for quantification. Perfusion buffer (PB) and Tris-buffered saline (TBS) were IP'ed as negative controls. (B-E) Quantification of IP-WB's from 21 mice shows (B) ~50% decrease in absolute values of ISF Aβ between 3 mo and 12 mo (NS by 1-way ANOVA followed by Bonferroni test) with a sharp (C-E) rise in TBS-, SDS-, and FA-extracted Aβ (pg per mg wet brain tissue). (F, G) Ratios of ISF to TBS-soluble Aβ (F) or to total parenchymal Aβ (G) calculated for each mouse and shown as mean ratio ± s.e.m.; N = 7 mice per group. Aβ quantified by Licor Odyssey® imaging and analyzed by 1-way ANOVA and Bonferroni test: $^{**}P < 0.01$ and $^{***}P < 0.001$ vs. 3 mo; $^{\#}P < 0.05$ and $^{\#\#}P < 0.01$ vs. 12 mo.

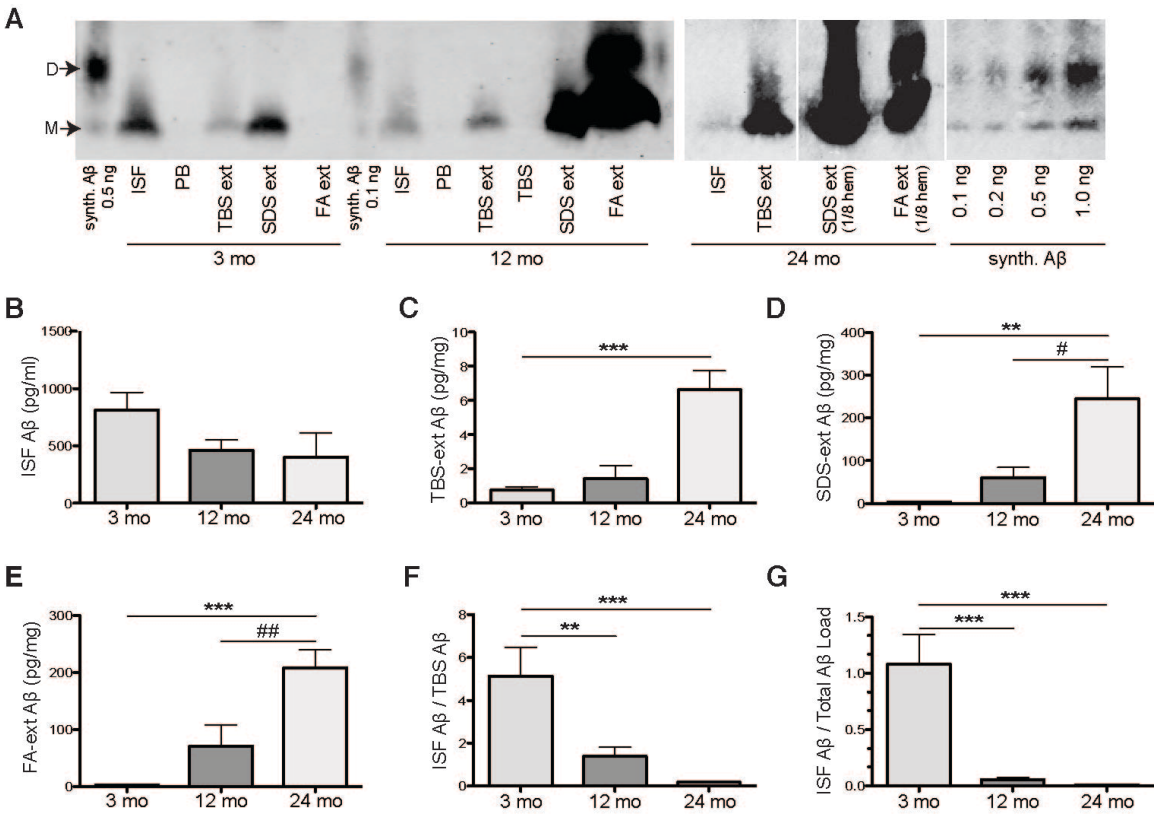

Figure 2.4 (Continued). Aβ in all pools of brain parenchyma accrue with age while those that remain diffusible in the ISF declines.

brain parenchymal Aβ, the relative ISF level declined even more (Figure 2.4G). Thus, all Aβ pools in brain parenchyma rise with age, while that which remains diffusible in ISF *in vivo* sharply declines. Furthermore, the bicine/urea SDS-PAGE showed the principal Aβ peptides present in ISF and TBS extracts from same mice from three age groups, 3 mo, 12 mo, and 24 mo and their relative levels in ISF and the corresponding TBS extract (Figure 2.5).

Altered dynamics of soluble Aβ in plaque-rich vs. plaque-free mice

Sampling the ISF at slower perfusion rates (which allows more efficient dialysis of ISF solutes) revealed age-dependent changes in ISF Aβ (Figure 2.6). In particular, this method revealed significantly decreased diffusion of endogenous $A\beta_{40}$ and $A\beta_{42}$ into the microdialysis probe in 24 mo than 3 mo transgenic mice. To better understand the basis for this marked decrease in recovery of diffusible ISF Aβ in the presence of abundant plaques, we approximated the fate of newly secreted Aβ molecules by exogenously administering radiolabeled soluble Aβ. We acutely injected soluble synthetic $[^{125}I]A\beta_{1-40}$ at a physiological concentration (1 nM) via a small cannula attached to the microdialysis probe into the hippocampal ISF of either age 3-7 mo (plaque-free) or age 24-27 mo (plaque-rich). We then measured the ability to recover the radiolabeled peptide from the ISF by microdialysis. From the ISF of the plaque-rich mice, we recovered only 45% of the injected peptide that was recovered from the ISF of plaque-free mice ($p < 0.0001$) (Figure 2.7A). The amounts of the

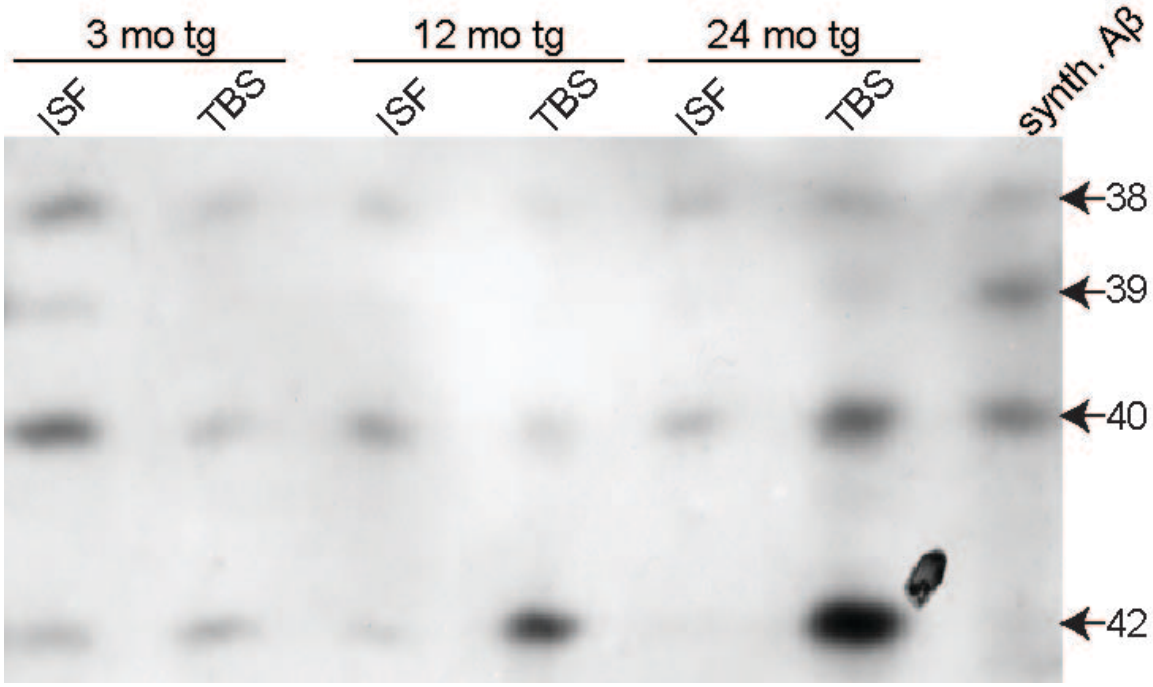

Figure 2.5. Aβ peptides that are microdialyzable in the ISF decline with age while the total Aβ in the brain homogenates that are extractable in saline increase.

Representative blot of bicine/urea SDS-PAGE in three age groups, 3 mo, 12 mo, and 24 mo, showing the principal Aβ peptides present and their relative expression levels in ISF and TBS extracts from the same transgenic mice. IP: AW8, WB: 6E10. Note the relative decrease of the individual Aβ peptides in ISF and their corresponding rise in the TBS extract.

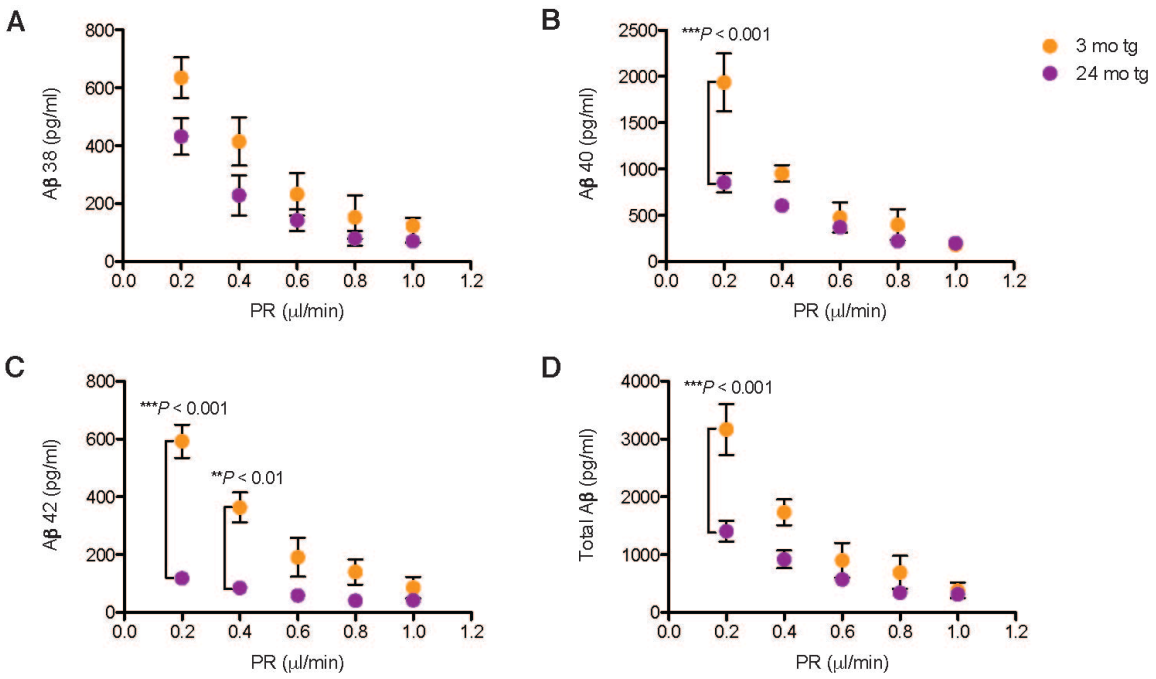

Figure 2.6. Microdialysis at slower perfusion rates reveals age-dependent changes in ISF Aβ.

ISF were collected from hippocampi of 3 mo (plaque-free) and 24 mo (plaque-rich) transgenic mice while varying the perfusion rate (PR). Samples were then quantified using 6E10 Aβ triplex ELISA. (A-C) At PR 1 μl/min, no age-dependent changes in all 3 peptides were detectable; however, at slow PRs (especially 0.2 μl/min), significant differences were noted, particularly in $Aβ_{40}$ and $Aβ_{42}$. (D) Sum of the three Aβ peptides measured (total Aβ). Values = means ± s.e.m., N = 3-7 mice; *P* values by 2-way ANOVA and Bonferroni test.

injected [^{125}I]Aβ that were recovered at the two ages correlated well with the respective endogenous Aβ concentrations in the ISF before injection: the [^{125}I]Aβ levels observed in the first hour and the endogenous Aβ levels just before injection were both high in young mice and both low in old mice (Figure 2.7B), indicating that the acutely injected radiopeptide achieves a similar equilibrium as the endogenous Aβ has at steady state. We hypothesized that in plaque-rich mice, the acutely administered monomer is more readily incorporated into their abundant Aβ deposits and thus is less recoverable in the ISF. To address this idea, we quantified the radioactivity retained in the TBS extracts of brain. We saw a substantially higher amount of the fresh, exogenous radiopeptide retained in the TBS extracts of the older mice (Figure 2.7C). In the short time frame we conducted these analyses (i.e., the first 90 minutes after administration), we did not detect significant levels of radioactivity in the SDS and FA fractions. Taken together, these results suggest that in plaque-burdened mice, newly generated soluble Aβ released into the ISF readily accrues onto parenchymal deposits, accounting for its lower steady-state level in the ISF.

The level of ISF $A\beta_{42}$ in plaque-rich mice is minimally affected by acute γ-secretase inhibition

To assess whether the ISF Aβ we measure in plaque-rich older transgenic mice also represents recent APP cleavage products, as we had determined in young plaque-free transgenic mice (Figure 2.1A), we acutely inhibited γ-

secretase *in vivo* with Compound E. There was a rapid decline of $A\beta_{38}$ and $A\beta_{40}$ (~60% fall in the first 3 h; $t_{1/2}$ ~1.9 h and ~2.3 h, respectively), whereas $A\beta_{42}$ declined significantly less (~20% fall) (Figure 2.7D-E). In contrast, all 3 peptides fell together in young plaque-free transgenic mice during the first 5 h after shutting down new production with Compound E (Figure 2.7F). As $A\beta_{42}$ is the species reported to accumulate much more into plaques than the other, more abundantly generated Aβ peptides in both AD patients and APP mice (Iwatsubo et al., 1994; Johnson-Wood et al., 1997), these results suggest that most of the soluble $A\beta_{42}$ peptide that populates the ISF pool in plaque-rich mice is not derived primarily from new Aβ biosynthesis but rather from the large reservoir of less soluble $A\beta_{42}$ in the brain parenchyma. The results also indicate that acute γ-secretase inhibition is less effective in lowering $A\beta_{42}$ in plaque-rich brains.

Discussion

Although factors other than Aβ dyshomeostasis contribute importantly to the pathogenesis of AD (Pimplikar et al., 2010), most potentially disease-modifying treatments currently under development are focused on decreasing or neutralizing this neurotoxic peptide. Moreover, a reduced CSF level of $A\beta_{42}$ in subjects with incipient or very early AD is one of the most promising biomarkers. Despite this therapeutic and diagnostic focus, we still lack insight into the *in vivo* economy of soluble Aβ in the brain as AD-type pathology forms. Here, we used the powerful method of brain microdialysis in awake, behaving hAPP transgenic

Figure 2.7. Dynamic shift in the *in vivo* economy of Aβ once plaques develop.

(A-C) Soluble synthetic [^{125}I]A$\beta_{1\text{-}40}$ at a physiological concentration (1 nM) was injected intra-hippocampally via a small cannula on the microdialysis probe in wake, behaving mice at 3-7 mo (plaque-free) or 24-27 mo (plaque-rich), and radioactivity was recovered in the ISF by microdialysis (A) and from the TBS extracts of the brains (B). Means normalized to amounts in the plaque-free mice (100%) ± s.e.m.; N = 3-4 mice per group; *P* values are 1-tailed *t* tests vs. 3-7 mo. (C) Amount of [^{125}I]Aβ recovered in the first hour of injection plotted versus the endogenous Aβ levels sampled from same mice before injection. (D-F) The level of ISF Aβ_{42} is minimally affected by Compound E in plaque-rich mice. (D) Representative graph of hourly ISF Aβ levels after Compound E injection (0 h) into 24 mo plaque-rich mice while collecting their brain ISF at 0.6 µl/min. Levels were normalized to levels of each Aβ species before injection. (E) Quantification of the individual ISF Aβ peptides in 24 mo plaque-rich mice for the first 5 hour post-injection (means ± s.e.m., N = 3 mice; *P* value is by 1-way ANOVA). (F) Hourly ISF Aβ levels after Compound E injection (0 h) in a 3 mo plaque-free transgenic mouse.

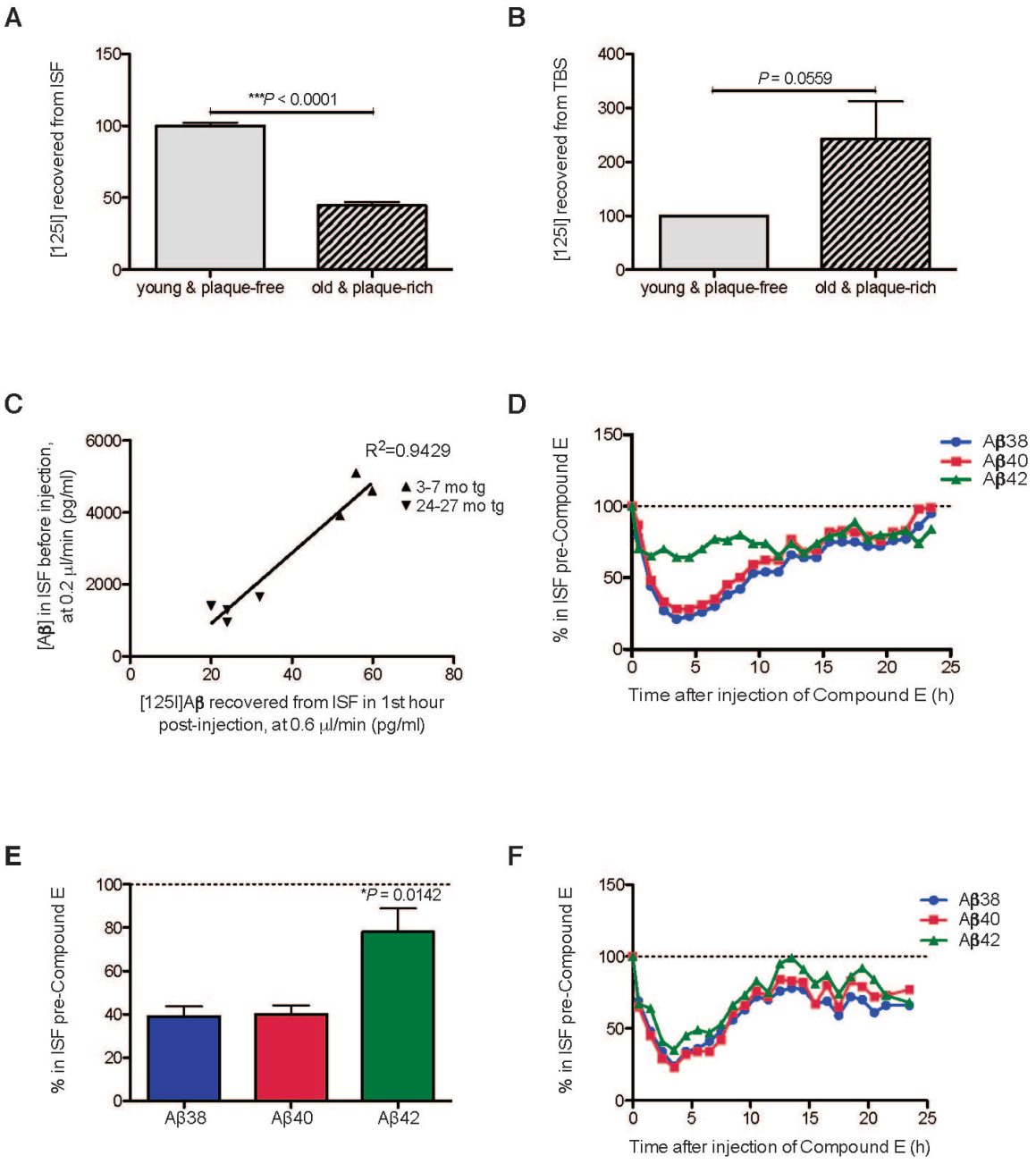

Figure 2.7 (Continued). Dynamic shift in the *in vivo* economy of Aβ once plaques develop.

mice to gain understanding of the dynamics of the most soluble forms of Aβ in the hippocampus before and during the process of Aβ plaque formation. Our results show that Aβ peptides which remain soluble and of low molecular weight in the interstitial fluid *in vivo* decrease significantly – both absolutely (Figures 2.3 and 2.4) and especially in relation to the soluble Aβ extractable from brain membranes (Figures 2.4D and 2.5) – as plaques accumulate. $A\beta_{42}$ decreases the most among the three major Aβ peptides in the ISF; in accord, $A\beta_{42}$ rises the most in the less soluble Aβ pools in the brain parenchyma (Figures 2.3 and 2.5), keeping with its documented primary role in oligomerization and plaque formation. (Figures 2.8A-C provide summaries of the temporal changes documented in this study.)

Of special clinical relevance is that our discovery of an age-dependent decrease in ISF $A\beta_{42}$ may be analogous to the widely-documented selective decrease in soluble $A\beta_{42}$ in human (AD) CSF (Motter et al., 1995). In humans, CSF levels of $A\beta_{42}$ appear to relate inversely to amyloid plaque burden, degree of brain atrophy and severity of cognitive deficits in humans (Motter et al., 1995; Fagan et al., 2009; Shaw et al., 2009). Our dynamic studies of the change in endogenous ISF Aβ and of the fate of radiolabeled Aβ before vs. after plaque initiation offer strong evidence from controlled animal experiments for the hypothesis that soluble $A\beta_{42}$ in humans falls in the CSF because it is sequestered into increasingly insoluble parenchymal deposits as AD develops.

What are the driving forces leading to the sharp decline of diffusible Aβ

Figure 2.8. Summary of the temporal changes in the four Aβ brain pools.

(A) Decreases with age in all three *in vivo* ISF Aβ peptides measured by 6E10 Aβ triplex sandwich ELISA (see Figure 2.3 for details). (B) The fold-decrease measured by ELISA (significant between 3 and 24 mo by two-way ANOVA; see Figure 2.2) is comparable to the fold-decrease measured by IP-WB (though the latter was not significant by one-way ANOVA; see Figure 2.4 for details). The total amount measured by IP-WB analysis method was only ~30% of the total amount measured by ELISA. (C) IP-WB analysis of Aβ in brain tissue. By ~24 mo, there was a steep increase in insoluble (SDS- and FA-extracted) Aβ. The TBS-extracted Aβ from the same mice did not rise until 24 mo and then only very slightly. Values = means ± s.e.m. from Figures 2.3 and 2.4.

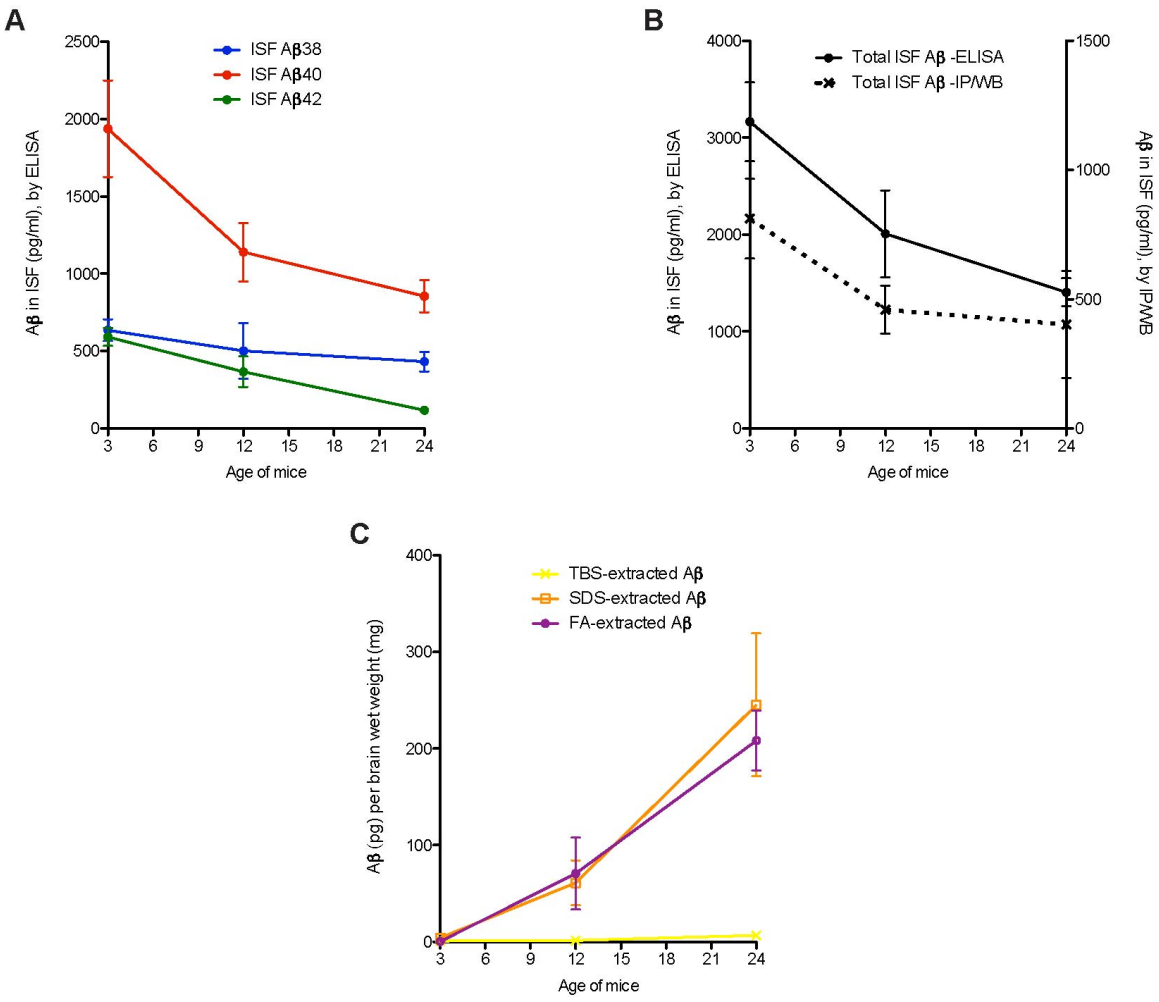

Figure 2.8 (Continued). Summary of the temporal changes in the four Aβ brain pools.

species as AD-like pathology progresses with age? The constant levels of both full-length APP and the CTFs generated by α- and β-secretases suggest that the fall we observe is not due to a decrease of cellular production of Aβ. We also saw no evidence for a perturbation of cell membrane integrity, a change in an indicator of intermediary metabolism, or altered spontaneous behavior (eating, exploring, grooming, etc.) in the mice, arguing against general cytotoxicity or cell death as an explanation for the drop. Thus, we obtained no evidence that decreased neuronal activity or decreased Aβ production explains the drop in soluble ISF Aβ as mice accrue amyloid deposits. Rather, the decrease in ISF Aβ occurred simultaneously with rises of insoluble Aβ in the SDS- and FA-extractable pools (Figures 2.3-2.4). Furthermore, the distinct dispositions of soluble radiolabeled Aβ injected at physiological concentrations directly into the ISF in plaque-free vs. plaque-rich animals provide insight into a shift in Aβ economy: in plaque-rich mice, Aβ becomes rapidly less diffusible and more associated with the loosely membrane-bound (TBS-extractable) pool (Figure 2.6). This dynamic shift leads us to hypothesize that once an Aβ peptide binds to membranes and/or plaques, it is sequestered there and becomes less diffusible, at least temporarily, leading to decreased recovery during microdialysis, consistent with a report of lengthened Aβ clearance time in old vs. young APP transgenic mice (Cirrito et al., 2003).

Indirect evidence for a converse pathway suggests that such membrane association is not irreversible. Our finding that upon acute γ-secretase inhibition

there was significantly less fall in ISF specifically of $A\beta_{42}$ (which is much more abundant in plaques) suggests that plaques contribute to a dynamic equilibrium between soluble and insoluble $A\beta_{42}$ pools in the brain and thus help regulate the steady state of ISF Aβ in aged mice (see Figure 2.9 for a model). This concept is consistent with evidence that amyloid plaques in APP transgenic mice appear to act as a local reservoir of "loosely-associated" Aβ that can diffuse from plaques and populate a halo of oligomeric and monomeric Aβ immediately surrounding the amyloid core (Spires et al., 2005; Koffie et al., 2009). It will be interesting to see whether acute alteration of one particular Aβ pool (e.g., via agents such as antibodies that can selectively bind aggregated Aβ or agents that only sequester the fully soluble ISF pool) will have transient or lasting effects on the equilibrium maintained among the Aβ pools.

Interestingly, we have not detected SDS-stable dimers in any of our ISF microdialysates to date, which could be due in part to the limits of detection. Using a test-tube model of our microdialysis technique, we found that synthetic Aβ dimers (~8 kDa) crossed over the 35 kDa MWCO membrane; however, the diffusion efficiency of dimers was poor in comparison to that of monomers (Figure 4.1). Therefore, we cannot exclude the existence of low levels of soluble dimers in the ISF of hAPP transgenic mice. On the other hand, our results may instead suggest that soluble dimers and other oligomers do not actually exist *per se* in the most diffusible brain pool (ISF); rather, newly formed oligomers (with their exposed hydrophobic amino acids) may distribute quickly onto hydrophobic

Figure 2.9. A hypothetical model of Aβ *in vivo* dynamics before vs. after plaque formation based on data in Chapter 2.

Several factors contribute to steady-state Aβ levels in brain ISF. There is a constant supply of Aβ in the ISF pool generated by new APP processing ($Aβ_{40}$ >> $Aβ_{38}$ = $Aβ_{42}$ > $Aβ_{39}$), and this generation appears to change little with age. ISF Aβ can be proteolytically degraded, cleared locally by glia and/or transported across the blood brain barrier (BBB). Soluble Aβ starts aggregating at an early age in brain parenchyma, as evidenced by the > 500 kDa TBS-extractable pool as well as an SDS-extractable pool in 3 mo, plaque-free mice. The most abundant pools in a plaque-free brain are the ISF pool and the SDS-extractable pool. In a plaque-rich brain, however, equilibrium between pools is greatly altered by the overwhelming amount of aggregated Aβ, which act as a sink, thereby diminishing the steady-state ISF pool. Plaques may also act as a contributor to the ISF pool, where Aβ42, the most abundant peptide in plaques (and also the most decreased in the ISF) diffuses back into the ISF.

In a plaque-free brain:

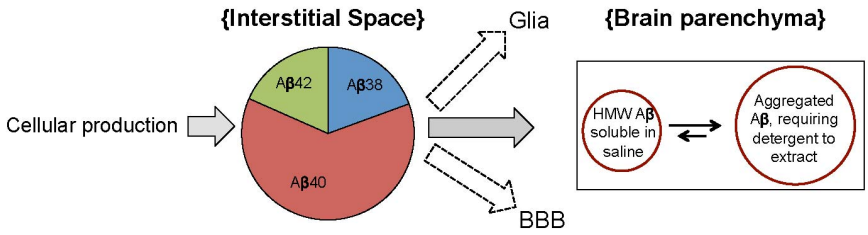

In a plaque-rich brain:

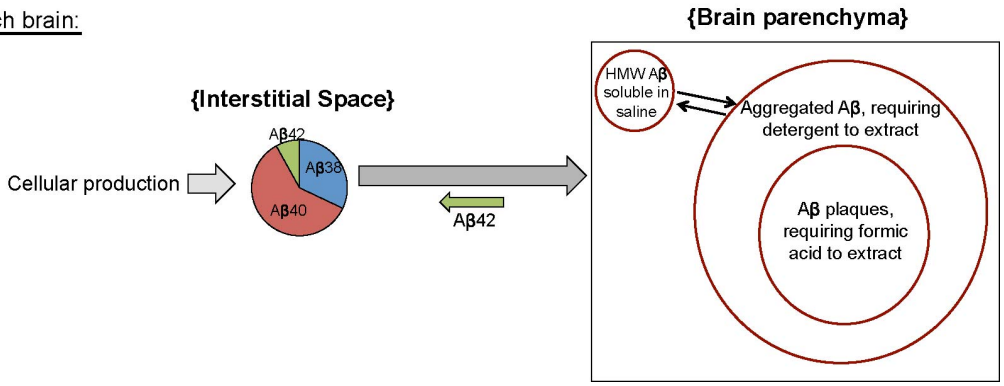

Figure 2.9 (Continued). A hypothetical model of Aβ *in vivo* dynamics before vs. after plaque formation based on data in Chapter 2.

surfaces (cell membranes and/or amyloid deposits). I address this question further in Chapter 4.

As regards the implications of our findings for the pathophysiology of AD, it will be important in future studies to attempt to detect any bioactivity of the ISF Aβ pool at the different plaque stages of APP transgenic mice. Whereas the ISF of young, plaque-free mice acts as a reservoir for mainly the acute cellular production of Aβ, ISF in plaque-rich mice seems to be a reservoir for both new Aβ production and Aβ that diffuses from membrane- and plaque-bound deposits (as evidenced by the finding that ISF $A\beta_{42}$ levels do not fall significantly upon acute inhibition of γ-secretase). Whether the $A\beta_{42}$ that comes off of parenchymal deposits into the ISF is pathogenically important (as compared to Aβ in the ISF of plaque-free brains) will be important to determine.

In conclusion, these dynamic analyses provide unique insights into the generation of first fully soluble and then increasingly less soluble Aβ species during age-related accrual of AD-type amyloid deposits in living animals. Based on the usefulness of these preclinical data, we suggest a provocative approach toward potentially extending such studies to humans. Patients with normal pressure hydrocephalus (NPH), which is typified by a clinical triad of subacutely developing dementia, incontinence and gait ataxia (Relkin et al., 2005; Shprecher et al., 2008), are frequently offered a neurosurgical procedure by which a ventriculoperitoneal shunt is inserted to chronically drain the excess ventricular CSF to the peritoneal cavity and thus potentially improve the patients' NPH

symptoms. Several studies of simultaneously obtained cortical biopsies have shown that some or many such shunted patients show amyloid plaques and neurofibrillary tangles indistinguishable from those in typical AD patients (Del Bigio et al., 1997; Bech et al., 1999; Golomb et al., 2000; Hamilton et al., 2010). This co-occurrence suggests that obtaining IRB approval to perform a brief (12-24 h) placement of a microdialysis probe at the time of an NPH shunt placement could enable *in vivo* analysis of ISF Aβ peptides in humans with varying degrees of Aβ deposition. We propose that such controlled clinical research studies in appropriate patients be considered in order to obtain direct information about the economy of the most soluble species of brain Aβ (those in ISF) as a function of the level of cerebral β-amyloidosis in humans.

Materials and Methods

Mice

J20 line carrying huAPP minigene with FAD mutations KM670/671NL and V717F was a kind gift of L. Mucke (Gladstone Institute, UCSF) and was maintained on a C57BL6 x DBA2 background (Mucke et al., 2000). All animal procedures were approved by the Harvard Medical School Institutional Animal Care and Use Committee. Mice of either sex were used in all experiments.

In vivo Aβ microdialysis

Microdialysis was performed as previously described (Cirrito et al., 2003): intracerebral guides were inserted following the coordinates for left hippocampal placement (bregma -3.1 mm, 2.5 mm lateral to midline, and 1.2 mm below dura at 12° angle). Perfusion buffer (1.5% bovine serum albumin (BSA) in artificial CSF (in mM: 1.3 $CaCl_2$, 1.2 $MgSO_4$, 3 KCl, 0.4 KH_2PO_4, 25 $NaHCO_3$, and 122 NaCl, pH 7.35)) was perfused using probes with 35 kDa MWCO membranes (BR-2, Bioanalytical Systems) at flow rates 0.2-1 µl/min with an infusion syringe pump (Stoelting). Microdialysates (ISF) were collected using a refrigerated fraction collector (Univentor). Mice were housed in a "Raturn" cage system (Bioanalytical Systems), which allows mice to resume normal activities, and were subjected to 12 h light/dark cycles.

Interpolated zero-flow method

The *in vivo* percent recovery was calculated as previously described (Cirrito et al., 2003). ISF was collected from 3 mo and 24 mo transgenic mice while varying the perfusion rates (PR): 1.0, 0.8, 0.6, 0.4, and 0.2 µl/min. Aβ levels were measured using the 6E10 Aβ Triplex ELISA (MesoScale Discovery) and the values obtained at each PR were plotted versus the PR. The 100% recovery (i.e. the theoretical maximal amount of exchangeable ISF Aβ species occurring at a zero PR) was calculated by extrapolating back the curve to a zero-flow rate. Then, for each PR, percent recovery was determined by calculating how much %Aβ was captured as compared to the theoretical [Aβ] at zero PR.

Aβ ELISA

For 6E10 Aβ Triplex ELISA, we used the MSD® 96-well MULTI-SPOT® Human (6E10) Abeta Triplex Assay (MesoScale Discovery) following the manufacturer's protocol. Briefly, ISF samples were loaded in duplicates onto MULTI-SPOT® microplates pre-coated with antibodies specific to the C-termini of $A\beta_{38}$, $A\beta_{40}$, and $A\beta_{42}$ and detected with SULFO-TAG^{TM}-labeled 6E10 antibody. Light emitted upon electrochemical stimulation was read using the SECTOR® Imager 2400A. For $A\beta_{1-x}$ ELISA, we followed a previously described protocol (Townsend et al., 2011). 96-well Nunc MaxiSorp plates were used with 4G8 (to $A\beta_{17-24}$, Covance) as capture and biotinylated 82E1 (to $A\beta_{1-16}$, IBL) as detection antibodies. Signals were amplified with AttoPhos (Promega) and measured by Victor2 fluorescent plate reader (PerkinElmer).

Lactate, pyruvate, and glycerol measurements

Levels were measured from ISF sampled at 0.2 µl/min using the CMA600 analyzer at the Yale Center for Clinical Investigation (YCCI) (sensitivities were: lactate 0.02 mM, pyruvate 2 µM, and glycerol 2 µM).

Mouse brain sample preparation for biochemical analyses

Brains were homogenized using a mechanical Dounce homogenizer with 20 strokes at 4000 rpm in ice-cold TBS (20 mM Tris-HCl, 150 mM NaCl, pH 7.4) and protease inhibitors at 4:1 TBS volume:brain wet weight. Homogenate was

centrifuged for 30 min at 175,000 g in a 4°C TLA100.2 rotor on Beckman TL 100 (resulting supernatant = "TBS extract"). Pellet was resuspended in 2% SDS using a 18-G needle, heated at 100°C for 10 min and spun at 21,130 g in an Eppendorf 5435 for 10 min (resulting supernatant = "SDS extract"). Pellet was washed twice more in SDS then incubated with 88% formic acid at RT for 2 h. Resulting supernatant ("FA extract") was diluted 10X with water and lyophilized.

Immunoprecipitation and Western blot for Aβ

ISF and brain extracts (except FA extract, which was lyophilized and directly reconstituted in LDS sample buffer prior to loading) were IP'ed with AW8 polyclonal antibody to Aβ (1:100, gift of D. Walsh, BWH) using Protein A (Sigma). For conventional SDS-PAGE, a previously described protocol (Shankar et al., 2008) was followed. Samples were electrophoresed using 12% Bis-Tris gel and MES SDS running buffer (Invitrogen), transferred onto 0.2-µm nitrocellulose, boiled, then blotted using monoclonal antibodies 6E10 (to $A\beta_{3-8}$, Covance) and 4G8, and visualized using the LiCor Odyssey Infrared Imaging System. For bicine/urea-based SDS PAGE, a previously described system (Klafki et al., 1996) was modified. Briefly, 11% T/2.6% C 8M urea separation gel was overlayered by 11% T/2.6% C 4M urea spacer gel and 4% T/3.3% C comb gel. Gels were run at 12 mA for 1 h, then 34 W for 3.8 h. Proteins were transferred to PVDF membranes, boiled then blotted with 6E10 with congo red and detected using HRP and ECL Plus WB Detection Reagent (GE Healthcare).

Immunohistochemistry of brain sections

J20 APP transgenic brains at ages 3 mo, 12 mo and 24 mo were fixed with 10% formalin, paraffin-embedded then sectioned at 8-µm thickness as previously described (Lemere et al., 2002). R1282 polyclonal antibody was used to stain Aβ and the immunoreactivity was visualized using the Vector Elite horseradish-peroxidase ABC kit (Vector Laboratories) with diaminobenzidine (Sigma) as the chromogen.

APP Western blotting

Mouse brains of 3 mo transgenic, 24 mo transgenic and wild-type littermate were homogenized in 1% (v/v) Nonidet P-40 (NP-40) STEN buffer (in mM: 150 NaCl, 50 Tris, 2 EDTA) using a Teflon® Dounce homogenizer. Brain lysates were loaded onto 4-12% Bis-Tris gel, electrophoresed with MES SDS running buffer, transferred onto 0.2-µm nitrocellulose, then blotted with polyclonal antibody C7 (to full-length APP and its C-terminal fragments) and anti-α-tubulin polyclonal antibody (Thermo Scientific).

Size-exclusion chromatography

TBS extracts (250 µl) or synthetic Aβ (2 ng) were eluted at 0.5 ml/min from a Superdex 200 10/300GL column (GE Healthcare) with 50 mM ammonium acetate, pH 8.5. Resulting 1-ml fractions were lyophilized, reconstituted in LDS sample buffer and heated at 65°C for 10 min. Samples were subjected to WB

using 3D6 (to $A\beta_{1-5}$, gift of Elan) and the LiCor Odyssey Infrared Imaging System or ECL Plus WB Detection Reagent (GE Healthcare).

Compound E treatment

Compound E (3 mg/kg, Axxora) was injected intraperitoneally to mice undergoing microdialysis. Half-lives were calculated according to Cirrito et al (Cirrito et al., 2003).

Radioactivity assay

For ISF experiments, 3 µl of 1 nM [^{125}I]-β-Amyloid(1-40) (PerkinElmer) was injected through a combination infusion cannula and microdialysis probe (IBR-2, Bioanalytical Systems) at 0.2 µl/min. ISF was collected hourly at 0.6 µl/min, paused during the injection, then restarted 1 min after injection. For TBS extractions, 5 µl [^{125}I]-β-Amyloid(1-40) was injected in paired mice (young and old). 1.5 h post injection, brains were harvested for TBS extract preparation. ^{125}I levels were counted using a LS6500 multipurpose scintillation counter (8-min counts).

Statistical analysis

Data was analyzed using PRISM (Graphpad Software) for one-way or two-way analysis of variance (ANOVA) followed by Bonferroni post-hoc test if means were significantly different by ANOVA, or Student's *t* test, as appropriate.

Footnotes

I sincerely thank John Cirrito (Washington University in St. Louis, MO) for teaching me the technique of *in vivo* microdialysis and also for his continued mentorship and friendship. I also thank David Holtzman (Washington University in St. Louis, MO) for his critical reading of the manuscript, Lennart Mucke (UCSF) for kindly providing J20 mice, Dominic M. Walsh (BWH) for AW8 antibody, Elan, plc (South San Francisco, CA) for 3D6, 2G3 and 21F12 antibodies, and Cynthia A. Lemere and Jeffrey L. Frost (BWH) for assistance with immunohistochemistry. I also thank William T. Cavanaugh (BWH) for assistance with maintenance of the J20 mouse colony. This work was supported by NIH grant AG027443 (D.J.S.), Harvard NeuroDiscovery Center Pre-doctoral Training Fellowship and James L. Rappaport Fellowship (S.H.), and AG017574-08S1 (O.Q.-M.).

References

Bech RA, Waldemar G, Gjerris F, Klinken L, Juhler M (1999) Shunting effects in patients with idiopathic normal pressure hydrocephalus; correlation with cerebral and leptomeningeal biopsy findings. Acta Neurochir (Wien) 141:633-639.

Brody DL, Magnoni S, Schwetye KE, Spinner ML, Esparza TJ, Stocchetti N, Zipfel GJ, Holtzman DM (2008) Amyloid-beta dynamics correlate with neurological status in the injured human brain. Science 321:1221-1224.

Cirrito JR, Kang J-E, Lee J, Stewart FR, Verges DK, Silverio LM, Bu G, Mennerick S, Holtzman DM (2008) Endocytosis is required for synaptic activity-dependent release of amyloid-beta in vivo. Neuron 58:42-51.

Cirrito JR, May PC, O'Dell MA, Taylor JW, Parsadanian M, Cramer JW, Audia JE, Nissen JS, Bales KR, Paul SM, DeMattos RB, Holtzman DM (2003) In vivo assessment of brain interstitial fluid with microdialysis reveals plaque-associated changes in amyloid-beta metabolism and half-life. Journal of Neuroscience 23:8844-8853.

Del Bigio MR, Cardoso ER, Halliday WC (1997) Neuropathological changes in chronic adult hydrocephalus: cortical biopsies and autopsy findings. Can J Neurol Sci 24:121-126.

Fagan AM, Head D, Shah AR, Marcus D, Mintun M, Morris JC, Holtzman DM (2009) Decreased cerebrospinal fluid Abeta(42) correlates with brain atrophy in cognitively normal elderly. Annals of Neurology 65:176-183.

Golomb J, Wisoff J, Miller DC, Boksay I, Kluger A, Weiner H, Salton J, Graves W (2000) Alzheimer's disease comorbidity in normal pressure hydrocephalus: prevalence and shunt response. J Neurol Neurosurg Psychiatry 68:778-781.

Grimwood S, Hogg J, Jay MT, Lad AM, Lee V, Murray F, Peachey J, Townend T, Vithlani M, Beher D, Shearman MS, Hutson PH (2005) Determination of guinea-pig cortical gamma-secretase activity ex vivo following the systemic administration of a gamma-secretase inhibitor. Neuropharmacology 48:1002-1011.

Hamilton R, Patel S, Lee EB, Jackson EM, Lopinto J, Arnold SE, Clark CM, Basil A, Shaw LM, Xie SX, Grady MS, Trojanowski JQ (2010) Lack of shunt response in suspected idiopathic normal pressure hydrocephalus with Alzheimer disease pathology. Ann Neurol 68:535-540.

Hsia AY, Masliah E, McConlogue L, Yu GQ, Tatsuno G, Hu K, Kholodenko D, Malenka RC, Nicoll RA, Mucke L (1999) Plaque-independent disruption of neural

circuits in Alzheimer's disease mouse models. Proc Natl Acad Sci U S A 96:3228-3233.

Iwatsubo T, Odaka A, Suzuki N, Mizusawa H, Nukina H, Ihara Y (1994) Visualization of A beta 42(43) and A beta 40 in senile plaques with end-specific A beta monoclonals: evidence that an initially deposited species is A beta 42(43). Neuron 13:45-53.

Jacobson I, Sandberg M, Hamberger A (1985) Mass transfer in brain dialysis devices—a new method for the estimation of extracellular amino acids concentration. Journal of Neuroscience Methods 15:263-268.

Johnson-Wood K, Lee M, Motter R, Hu K, Gordon G, Barbour R, Khan K, Gordon M, Tan H, Games D (1997) Amyloid precursor protein processing and Aβ42 deposition in a transgenic mouse model of Alzheimer disease. Proceedings of the National Academy of Sciences 94:1550.

Kang J-E, Lim MM, Bateman RJ, Lee JJ, Smyth LP, Cirrito JR, Fujiki N, Nishino S, Holtzman DM (2009) Amyloid-beta dynamics are regulated by orexin and the sleep-wake cycle. Science 326:1005-1007.

Kawarabayashi T, Younkin LH, Saido TC, Shoji M, Ashe KH, Younkin SG (2001) Age-dependent changes in brain, CSF, and plasma amyloid (beta) protein in the Tg2576 transgenic mouse model of Alzheimer's disease. J Neurosci 21:372-381.

Klafki HW, Wiltfang J, Staufenbiel M (1996) Electrophoretic separation of betaA4 peptides (1-40) and (1-42). Analytical Biochemistry 237:24-29.

Koffie RM, Meyer-Luehmann M, Hashimoto T, Adams KW, Mielke ML, Garcia-Alloza M, Micheva KD, Smith SJ, Kim ML, Lee VM, Hyman BT, Spires-Jones TL (2009) Oligomeric amyloid beta associates with postsynaptic densities and correlates with excitatory synapse loss near senile plaques. Proc Natl Acad Sci USA 106:4012-4017.

Lemere CA, Spooner ET, Leverone JF, Mori C, Clements JD (2002) Intranasal immunotherapy for the treatment of Alzheimer's disease: Escherichia coli LT and LT(R192G) as mucosal adjuvants. Neurobiology of Aging 23:991-1000.

Masters CL, Simms G, Weinman NA, Multhaup G, McDonald BL, Beyreuther K (1985) Amyloid plaque core protein in Alzheimer disease and Down syndrome. Proc Natl Acad Sci USA 82:4245-4249.

Motter R, Vigo-Pelfrey C, Kholodenko D, Barbour R, Johnson-Wood K, Galasko D, Chang L, Miller B, Clark C, Green R, et al (1995) Reduction of beta-amyloid peptide 42 in the cerebrospinal fluid of patients with Alzheimer's disease. Ann Neurol 38:643-648.

Mucke L, Masliah E, Yu G-Q, Mallory M, Rockenstein E, Tatsuno G, Hu K, Kholodenko D, Johnson-Wood K, Mcconlogue L (2000) High-Level Neuronal Expression of Abeta 1-42 in Wild-Type Human Amyloid Protein Precursor Transgenic Mice: Synaptotoxicity without Plaque Formation. Journal of Neuroscience 20:4050.

Pimplikar SW, Nixon RA, Robakis NK, Shen J, Tsai L-H (2010) Amyloid-independent mechanisms in Alzheimer's disease pathogenesis. J Neurosci 30:14946-14954.

Relkin N, Marmarou A, Klinge P, Bergsneider M, Black PM (2005) Diagnosing idiopathic normal-pressure hydrocephalus. Neurosurgery 57:S4-16; discussion ii-v.

Selkoe DJ, Abraham CR, Podlisny MB, Duffy LK (1986) Isolation of low-molecular-weight proteins from amyloid plaque fibers in Alzheimer's disease. Journal of Neurochemistry 146:1820-1834.

Shankar G, Leissring M, Adame A, Sun X, Spooner E, Masliah E, Selkoe D, Lemere C, Walsh D (2009) Biochemical and immunohistochemical analysis of an Alzheimer's disease mouse model reveals the presence of multiple cerebral Abeta assembly forms throughout life. Neurobiol Dis.

Shankar GM, Li S, Mehta TH, Garcia-Munoz A, Shepardson NE, Smith I, Brett FM, Farrell MA, Rowan MJ, Lemere CA, Regan CM, Walsh DM, Sabatini BL, Selkoe DJ (2008) Amyloid-β protein dimers isolated directly from Alzheimer's brains impair synaptic plasticity and memory. Nat Med 14:837-842.

Shaw LM, Vanderstichele H, Knapik-Czajka M, Clark CM, Aisen PS, Petersen RC, Blennow K, Soares H, Simon A, Lewczuk P, Dean R, Siemers E, Potter W, Lee VM-Y, Trojanowski JQ, Initiative AsDN (2009) Cerebrospinal fluid biomarker signature in Alzheimer's disease neuroimaging initiative subjects. Ann Neurol 65:403-413.

Shen D, Artru A, Adkison K (2004) Principles and applicability of CSF sampling for the assessment of CNS drug delivery and pharmacodynamics. Advanced drug delivery reviews 56:1825-1857.

Shprecher D, Schwalb J, Kurlan R (2008) Normal pressure hydrocephalus: diagnosis and treatment. Curr Neurol Neurosci Rep 8:371-376.

Spires TL, Meyer-Luehmann M, Stern EA, McLean PJ, Skoch J, Nguyen PT, Bacskai BJ, Hyman BT (2005) Dendritic spine abnormalities in amyloid precursor protein transgenic mice demonstrated by gene transfer and intravital multiphoton microscopy. Journal of Neuroscience 25:7278-7287.

Townsend MK, Okereke OI, Xia W, Yang T, Selkoe DJ, Grodstein F (2011) Relation Between Insulin, Insulin-related Factors, and Plasma Amyloid Beta Peptide Levels at Midlife in a Population-based Study. Alzheimer Dis Assoc Disord.

Ungerstedt U, Rostami E (2004) Microdialysis in neurointensive care. Curr Pharm Des 10:2145-2152.

Walsh DM, Selkoe DJ (2007) A beta oligomers - a decade of discovery. Journal of Neurochemistry 101:1172-1184.

Walsh DM, Klyubin I, Fadeeva JV, Cullen WK, Anwyl R, Wolfe MS, Rowan MJ, Selkoe DJ (2002) Naturally secreted oligomers of amyloid beta protein potently inhibit hippocampal long-term potentiation in vivo. Nature 416:535-539.

Yan P, Bero A, Cirrito J, Xiao Q, Hu X, Wang Y, Gonzales E, Holtzman D, Lee J-M (2009) Characterizing the Appearance and Growth of Amyloid Plaques in APP/PS1 Mice. Journal of Neuroscience 29:10706.

Chapter 3

Saline-extractable amyloid β of APP transgenic mouse brain has properties distinct from the truly soluble amyloid β species in interstitial fluid

Contributions:

Experiments were designed by Soyon Hong and Dennis Selkoe. Bicine-urea/SDS-PAGE experiments were performed by Omar Quintero-Monzon. Size-exclusion chromatography experiments were performed by Soyon Hong and Daniel Podlisny. All other experiments were performed by Soyon Hong.

Publication:

Parts of this chapter have been published in the *Journal of Neuroscience* **31**(44):15861-9.

Introduction

β-amyloid peptide (Aβ) in aqueous extracts of homogenized cerebral cortex has been termed by our group and others as the "soluble Aβ" pool and thought to be derived from interstitial fluid (ISF) and cytosol, not necessarily from particulates such as amyloid deposits (Gravina et al., 1995; Lue et al., 1999; McLean et al., 1999; Walsh and Selkoe, 2004; Shankar et al., 2009); the rise in this pool was thought to reflect a rise in diffusible Aβ *in vivo*. However, our bicine/urea SDS-PAGE results (Figure 2.5) indicate that the principal Aβ peptides in the saline extracts of brain homogenates markedly differed from the ISF collected from the same mice *in vivo*, even in the brains from young transgenic mice which are virtually devoid of plaques. Therefore, we questioned the established view in the field that the saline extracts of *post-mortem* brain homogenates truly reflect the *in vivo* soluble Aβ peptides that remain diffusible in the ISF. Here, we performed bicine/urea SDS-PAGE, non-denaturing size-exclusion chromatography (SEC), and native gels to examine the Aβ species in the aqueous extracts of Aβ.

Results

Bicine/urea SDS-PAGE gels showed that the Aβ peptide distribution differed between the ISF and Tris-buffered saline (TBS)-extracted pools at all ages in APP transgenic mice (Figure 2.5). Even at age 3 mo, when the brain has virtually no plaques (Figure 2.2), $A\beta_{40}$ was the primary Aβ species in ISF while in

the TBS-extracted pool, $A\beta_{42}$ was already the more abundant peptide at steady state, despite the fact that it is generated in much lower amounts than $A\beta_{40}$. Accordingly, the $A\beta_{42}/A\beta_{40}$ ratio differed markedly between the ISF (low ratio) and TBS extract (very high ratio) in the young transgenic mice (Figure 3.1A). This stark difference was enhanced in 24 mo transgenic mice, which had severe plaque deposition (Figure 3.1B). The pronounced difference of the Aβ peptide composition between ISF and TBS-extracted pools, particularly in plaque-free brains, led us to question the general assumption that the brain Aβ pool which comes into solution upon mechanical homognization in physiological buffers represents the truly soluble pool (McLean et al., 1999; Walsh and Selkoe, 2004; Shankar et al., 2009). We performed non-denaturing SEC on the TBS extract and subjected the resultant SEC fractions to SDS-PAGE for WB analysis. Surprisingly, most Aβ in the TBS extracts of plaque-free (3 mo transgenic) mice eluted in the void volume of a Superdex 200 SEC column (suggesting a molecular weight (MW) > 500 kDa), and this material ran principally as monomers when electrophoresed on a denaturing gel (Figure 3.2A, fractions 6-7). The SEC elution profiles of TBS extracts from 3 mo (Figure 3.2A) and 24 mo (Figure 3.2B) transgenic mice were similar and differed sharply from that of synthetic $A\beta_{40}$ peptide alone (Figure 3.2C). In accord, Aβ in TBS extracts from 24 mo transgenic ran as an aggregated, high MW complex on a clear-native PAGE gel, whereas synthetic $A\beta_{40}$ ran close to the dye front (Figure 3.3A). Excision of the > 300 kDa region and subsequent denaturation in LDS sample

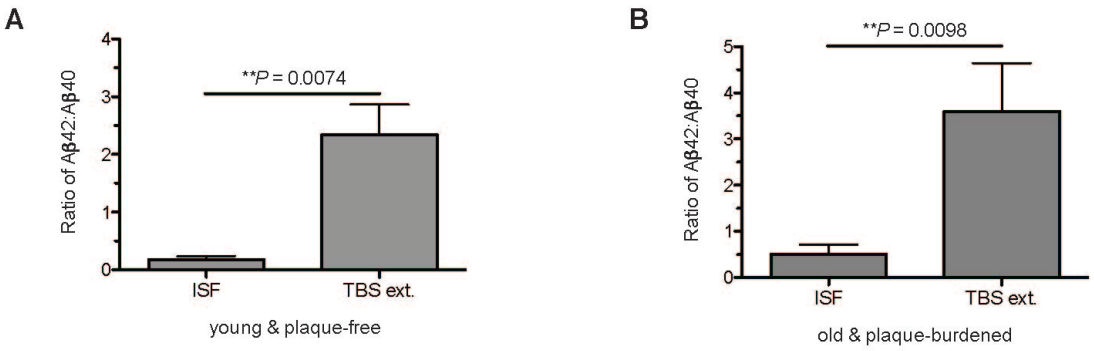

Figure 3.1. $A\beta_{42}/A\beta_{40}$ ratios differ markedly between the ISF and saline brain extracts of APP transgenic mice.

The principal Aβ peptides in the ISF and TBS extracts of 3 mo and 24 mo transgenic mice (Figure 2.5; bicine/urea SDS-PAGE, IP: AW8, WB: 6E10) were quantified by ImageJ software and the $A\beta_{42}/A\beta_{40}$ ratios were calculated. *P* value by 1-tailed *t* test; N = 3 each.

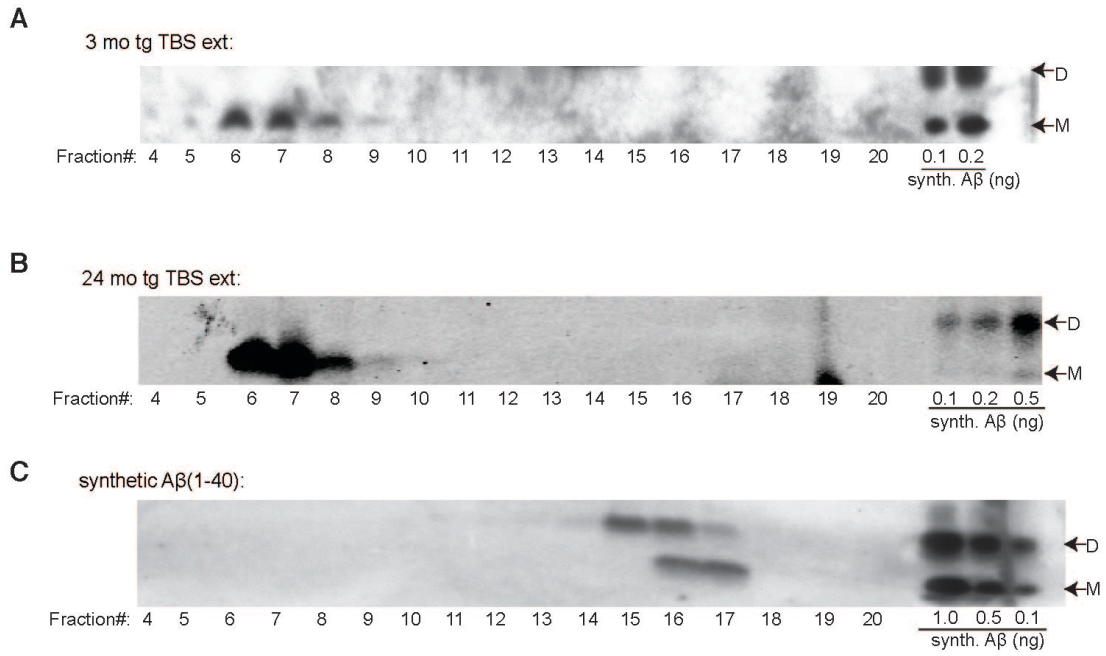

Figure 3.2. Saline-extractable Aβ of brain parenchyma in its native form appears to exist principally in assemblies > 500 kDa.

Non-denaturing SEC of TBS extracts of 3 mo transgenic (A) and 24 mo transgenic (B) was performed on a Superdex 200 SEC column followed by SDS-PAGE of each SEC fraction. Synthetic $A\beta_{40}$ was run on the same SEC column for comparison (C). WB: 3D6.

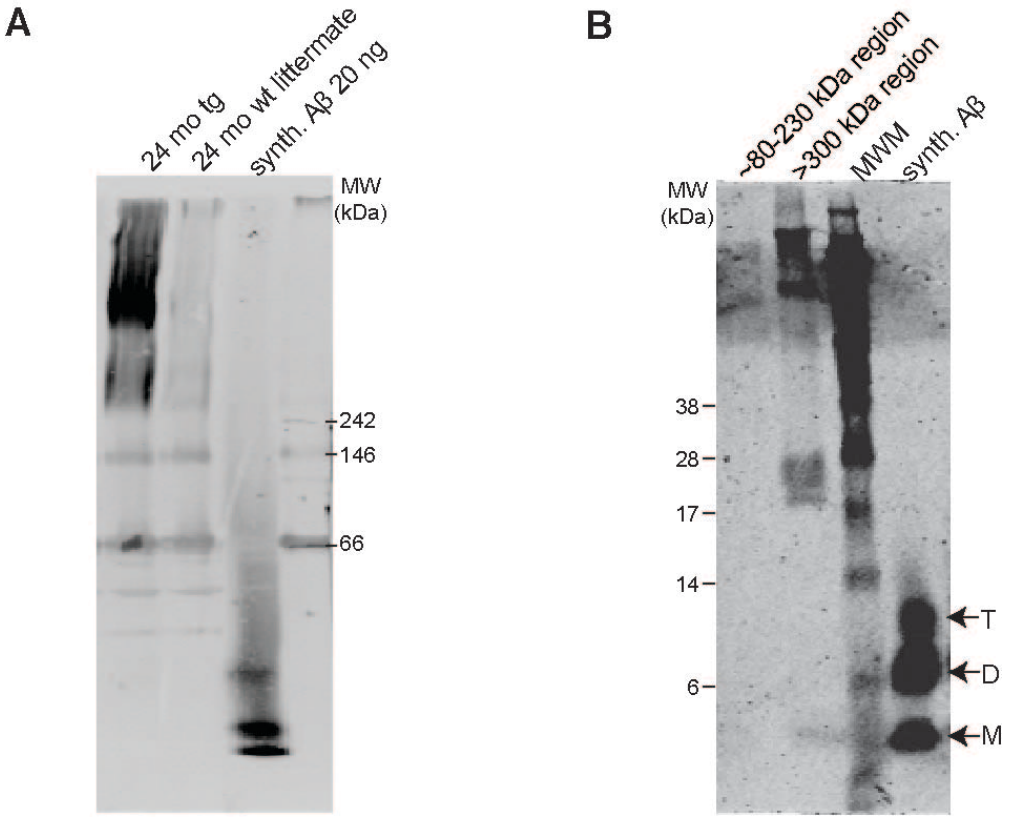

Figure 3.3. Most Aβ in the saline extracts of transgenic mice run natively as > 300 kDa.

(A) TBS extracts from 24 mo transgenic and its wt littermate subjected to clear-native PAGE and blotted for Aβ. WB: 2G3 and 21F12. (B) Excision of the > 300 kDa region and subsequent electrophoresis by denaturing SDS-PAGE showed that this high MW material is disassembled into low MW SDS-stable Aβ species. WB: 3D6.

buffer yielded lower MW Aβ species, including monomers (Figure 3.3B).

Next, we spiked synthetic Aβ into saline extracts of wild-type (wt) mice *ex vivo* and performed SEC. We used the S26C $A\beta_{1-40}$ oligomers, which stays as mostly dimers on SDS-PAGE. In TBS buffer alone, the S26C Aβ eluted mostly at the expected dimer position (corresponding to MW ~8 kDa) off the Superdex 75 SEC column (Figure 3.4A). However, when we spiked the S26C Aβ into the saline extracts of wt mice, we observed an immediate shift of its elution profile from the previous dimer fractions toward the void volume fractions of the SEC column (corresponding to MW > 70 kDa) (Figure 3.4).

Discussion

Here, we show that Aβ peptides in aqueous parenchymal extracts differ significantly in quality and quantity from those that remain of low MW in the ISF pool. Furthermore, using non-denaturing SEC and native gels, we show that much native Aβ in the TBS extracts of APP transgenic mouse brains, even at a pre-plaque age of 3 mo, exists in assemblies that size at > 500 kDa, extending similar data on the aqueous extracts of AD brains (Shankar et al., 2008). The findings in this Chapter, therefore, raise a concern for the current definition of Aβ in aqueous extracts of homogenized cerebral cortex as reflecting the soluble Aβ in ISF and cytosol (Gravina et al., 1995; Lue et al., 1999; McLean et al., 1999; Walsh and Selkoe, 2004; Shankar et al., 2009). Instead, the aqueous extracts of Aβ may principally reflect aggregated Aβ peptides bound to cell membranes (in

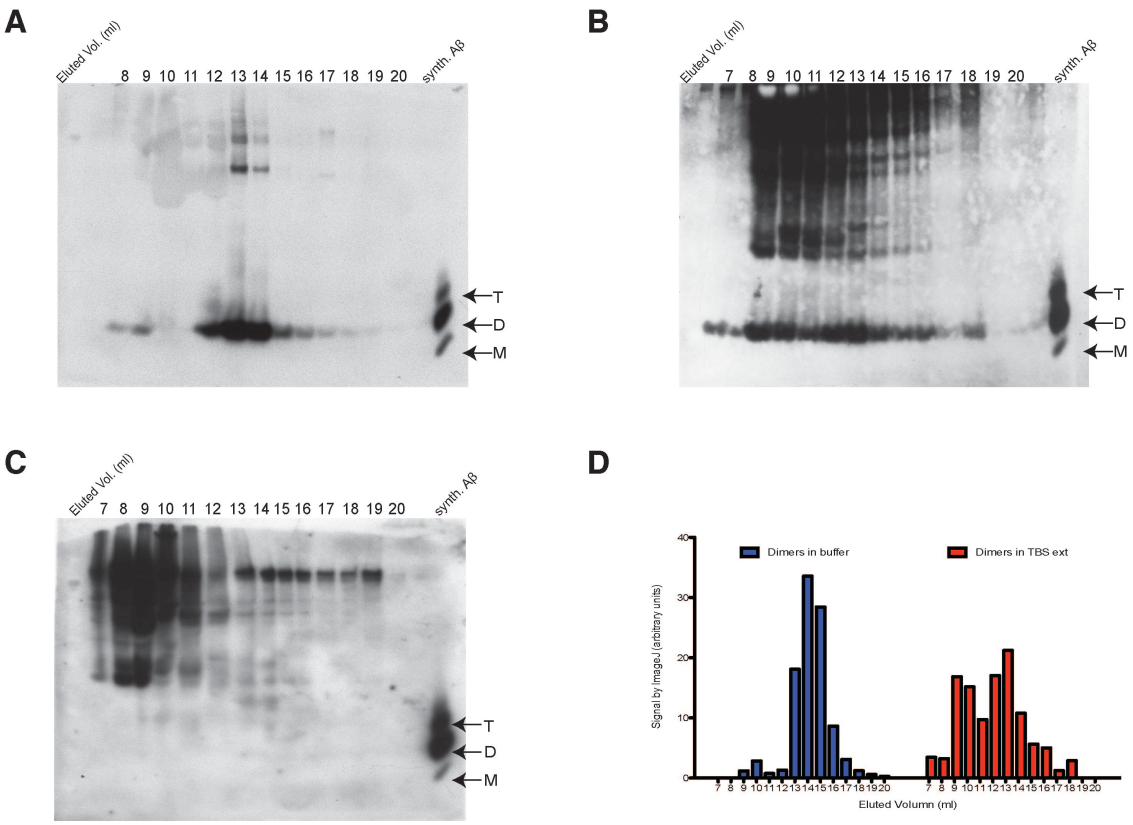

Figure 3.4. Subjection of Aβ dimers to saline extracts of non-transgenic mice immediately shifts the SEC elution profile of the Aβ dimers to the void volume of the column (> 70 kDa).

Non-denaturing SEC of S26C Aβ in TBS buffer alone (A), S26C Aβ spiked into wt TBS extract (B), and wt TBS extract alone (C) were performed with a Superdex 75 SEC column, followed by SDS-PAGE of each SEC fraction. WB: 3D6. (D) Elution profile of the S26C Aβ in buffer (in blue) and S26C Aβ in wt TBS extract (in red), as quantified by ImageJ software.

young mice) and to membranes and plaques (in older mice) but which remain water-extractable.

Given the new understanding that aqueous extracts of brain may not reflect the truly diffusible Aβ species *in vivo*, it will be important to examine the nature of synaptotoxicity in the different Aβ pools, including the ISF pool and the TBS-extracted pool, which is currently thought to principally contain the synaptotoxic oligomeric species. Interestingly, as noted in Chapter 2, we have not detected SDS-stable dimers in any of our ISF microdialysates to date. Although we cannot exclude the existence of very low levels of soluble dimers in the ISF of hAPP transgenic mice, our results here suggest that soluble dimers and other oligomers do not actually exist *per se* in the most diffusible brain pool (i.e., the ISF); rather, newly formed oligomers, with their exposed hydrophobic amino acids, may distribute quickly onto hydrophobic surfaces (cell membranes and/or amyloid deposits). The rapid shift of the spiked synthetic Aβ dimers to the void volume fractions upon exposure to the wt TBS extract (shown in Figure 3.4) provides suggestive data supporting this view. Most of the Aβ dimers in TBS buffer alone eluted at the expected dimer position (Figure 3.4A), arguing against mere aggregation of the Aβ. We have also failed to see a specific interaction (by co-immunoprecipitation studies) of candidate binding proteins, such as the apolipoprotein E and apolipoprotein J to Aβ (addressed in Appendix 2). Rather, we hypothesize that the hydrophobic Aβ oligomers may rapidly bind to lipid membranes, such as raft-like microdomains on lipid vesicles or plasma

membranes of neurons and glia. I address this further in the next Chapter (Chapter 4).

Materials and Methods

Mice

J20 line carrying hAPP minigene with FAD mutations KM670/671NL and V717F was a kind gift of L. Mucke (Gladstone Institute, UCSF) and was maintained on a C57BL6 x DBA2 background (Mucke et al., 2000). All animal procedures were approved by the Harvard Medical School Institutional Animal Care and Use Committee. Mice of either sex were used in all experiments.

In vivo Aβ microdialysis

Microdialysis was performed as previously described (Cirrito et al., 2003): intracerebral guides were inserted following the coordinates for left hippocampal placement (bregma -3.1 mm, 2.5 mm lateral to midline, and 1.2 mm below dura at 12° angle). Perfusion buffer (1.5% bovine serum albumin (BSA) in artificial CSF (in mM: 1.3 $CaCl_2$, 1.2 $MgSO_4$, 3 KCl, 0.4 KH_2PO_4, 25 $NaHCO_3$, and 122 NaCl, pH 7.35)) was perfused using probes with 35 kDa MWCO membranes (BR-2, Bioanalytical Systems) at flow rates 0.2-1 µl/min with an infusion syringe pump (Stoelting). Microdialysates (ISF) were collected using a refrigerated fraction collector (Univentor). Mice were housed in a "Raturn" cage system (Bioanalytical Systems), which allows mice to resume normal activities, and were

subjected to 12 h light/dark cycles.

Mouse brain sample preparation for biochemical analyses

Brains were homogenized using a mechanical Dounce homogenizer with 20 strokes at 4000 rpm in ice-cold TBS (20 mM Tris-HCl, 150 mM NaCl, pH 7.4) and protease inhibitors at 4:1 TBS volume:brain wet weight. Homogenate was centrifuged for 30 min at 175,000 g in a 4°C TLA100.2 rotor on Beckman TL 100 (resulting supernatant = "TBS extract").

Immunoprecipitation and Western blot for Aβ

ISF and brain extracts (except FA extract, which was lyophilized and directly reconstituted in LDS sample buffer prior to loading) were IP'ed with AW8 polyclonal antibody to Aβ (1:100, gift of D. Walsh, BWH) using Protein A (Sigma). For conventional SDS-PAGE, a previously described protocol (Shankar et al., 2008) was followed. Samples were electrophoresed using 12% Bis-Tris gel and MES SDS running buffer (Invitrogen), transferred onto 0.2-µm nitrocellulose, boiled, then blotted using monoclonal antibodies 6E10 (to $A\beta_{3-8}$, Covance) and 4G8, and visualized using the LiCor Odyssey Infrared Imaging System. For bicine/urea-based SDS-PAGE, a previously described system (Klafki et al., 1996) was modified. Briefly, 11% T/2.6% C 8M urea separation gel was overlayered by 11% T/2.6% C 4M urea spacer gel and 4% T/3.3% C comb gel. Gels were run at 12 mA for 1 h, then 34 W for 3.8 h. Proteins were transferred to PVDF

membranes, boiled then blotted with 6E10 with Congo red and detected using HRP and ECL Plus WB Detection Reagent (GE Healthcare).

Size-exclusion chromatography

TBS extracts (250 µl) or synthetic Aβ (2 ng) were eluted at 0.5 ml/min either from a Superdex 200 10/300GL column or a Superdex 75 10/30HR column (both from GE Healthcare) with 50 mM ammonium acetate, pH 8.5. Resulting 1-ml fractions were lyophilized, reconstituted in LDS sample buffer and heated at 65°C for 10 min. Samples were subjected to WB using 3D6 (to $A\beta_{1-5}$, gift of Elan) and the LiCor Odyssey Infrared Imaging System or ECL Plus WB Detection Reagent (GE Healthcare).

Clear-native PAGE and subsequent denaturation for SDS-PAGE

TBS extracts were prepared from homogenized brains of 24 mo transgenic and wt littermate, then subjected to non-denaturing clear-native PAGE, which separates proteins with pI < 7 based on their intrinsic charge (Wittig and Schagger, 2005). Briefly, samples were electrophoresed using Native PAGE 4-16% Bis-Tris gel (Invitrogen) with Bis-Tris-HCl, pH 7.0 as anode and Tricine Bis-Tris, pH 7.0 as cathode buffers. Proteins were then transferred onto 0.2-µm PVDF (Millipore), boiled and blotted for Aβ using monoclonal antibodies 2G3 and 21F12 (to $A\beta_{33-40}$ and $A\beta_{33-42}$, respectively, gifts of Elan). For subsequent denaturation, we excised two regions of the native PAGE gel following

electrophoresis: the > 300 kDa and the 80-230 kDa (based on NativeMark™ Unstained Protein Standard (Invitrogen)). The diced gels were heated at 100°C in denaturing LDS sample buffer and supernatants were electrophoresed using 12% Bis-Tris gel and MES SDS running buffer (Invitrogen) for Western-blotting using monoclonal antibody 3D6 (to $A\beta_{1-5}$, gift of Elan). Proteins were visualized using the LiCor Odyssey Infrared Imaging System.

Statistical analysis

Data was analyzed by Student's *t* test using PRISM (Graphpad Software).

References

Cirrito JR, May PC, O'Dell MA, Taylor JW, Parsadanian M, Cramer JW, Audia JE, Nissen JS, Bales KR, Paul SM, DeMattos RB, Holtzman DM (2003) In vivo assessment of brain interstitial fluid with microdialysis reveals plaque-associated changes in amyloid-beta metabolism and half-life. Journal of Neuroscience 23:8844-8853.

Gravina SA, Ho L, Eckman CB, Long KE, Otvos LJ, Younkin LH, Suzuki N, Younkin SG (1995) Amyloid ß protein (Aß) in Alzheimer's disease brain. J Biol Chem 270:7013-7016.

Klafki HW, Wiltfang J, Staufenbiel M (1996) Electrophoretic separation of betaA4 peptides (1-40) and (1-42). Analytical Biochemistry 237:24-29.

Lue LF, Kuo YM, Roher AE, Brachova L, Shen Y, Sue L, Beach T, Kurth JH, Rydel RE, Rogers J (1999) Soluble amyloid beta peptide concentration as a predictor of synaptic change in Alzheimer's disease. Am J Pathol 155:853-862.

McLean C, Cherny R, Fraser F, Fuller S, Smith M, Vbeyreuther K, Bush A, Masters C (1999) Soluble pool of Aβ amyloid as a determinant of severity of neurodegeneration in Alzheimer's disease. Annals of Neurology 46:860-866.

Mucke L, Masliah E, Yu G-Q, Mallory M, Rockenstein E, Tatsuno G, Hu K, Kholodenko D, Johnson-Wood K, Mcconlogue L (2000) High-Level Neuronal Expression of Abeta 1-42 in Wild-Type Human Amyloid Protein Precursor Transgenic Mice: Synaptotoxicity without Plaque Formation. Journal of Neuroscience 20:4050.

Shankar GM, Leissring MA, Adame A, Sun X, Spooner E, Masliah E, Selkoe DJ, Lemere CA, Walsh DM (2009) Biochemical and immunohistochemical analysis of an Alzheimer's disease mouse model reveals the presence of multiple cerebral Abeta assembly forms throughout life. Neurobiol Dis 36:293-302.

Shankar GM, Li S, Mehta TH, Garcia-Munoz A, Shepardson NE, Smith I, Brett FM, Farrell MA, Rowan MJ, Lemere CA, Regan CM, Walsh DM, Sabatini BL, Selkoe DJ (2008) Amyloid-β protein dimers isolated directly from Alzheimer's brains impair synaptic plasticity and memory. Nat Med 14:837-842.

Walsh DM, Selkoe DJ (2004) Deciphering the molecular basis of memory failure in Alzheimer's disease. Neuron 44:181-193.

Wittig I, Schagger H (2005) Advantages and limitations of clear-native PAGE. Proteomics 5:4338-4346.

Chapter 4

Amyloid β oligomers do not exist in the fluid compartments of the central nervous system but instead are rapidly sequestered away from the interstitial fluid to associate with GM1 ganglioside on lipid membranes

Contributions:

Experiments were designed by Soyon Hong, Beth Ostaszewski, and Dennis Selkoe. Mouse brain sample preparations and Western blots were performed by Beth Ostaszewski and Soyon Hong. In vitro microdalysis was performed by Daniel Podlisny and Soyon Hong. Ting Yang prepared the human brain extracts. All other experiments were performed by Soyon Hong.

Introduction

Using *in vivo* microdialysis in hAPP transgenic mice (the J20 line; Mucke et al., 2000), the steady state levels of amyloid β-protein (Aβ) species which are < 35 kDa and remain aqueously diffusible in brain interstitial fluid (ISF) fall steadily with age as Aβ accumulate in the brain parenchyma (Chapter 2) (Hong et al., 2011). In accord, we see distinct dispositions of microinjected Aβ peptide in plaque-rich versus plaque-free mice, suggesting that the cerebral amyloid deposits can rapidly sequester newly generated Aβ. The Aβ in the hippocampal ISF of these transgenic mice (as analyzed on bicine-urea gels) constitute a heterogeneous mixture of principally four Aβ peptides of relative abundance $A\beta_{40}$ >> $A\beta_{38}$ = $A\beta_{42}$ >> $A\beta_{39}$. ISF levels of all four Aβ peptides fall with increasing age. Furthermore, using denaturing SDS-PAGE, we fail to detect any low molecular weight (LMW) Aβ oligomers (e.g., dimers, trimers, etc.), but detected only monomers in the ISF from more than 25 awake, behaving hAPP transgenic mice, regardless of the age of the mice or their extent of amyloid plaque deposition (Chapter 2). Using an *in vitro* (test tube) version of microdialysis, we verified that Aβ dimers (~8 kDa MW) could cross over the microdialysis membrane with a MW cutoff (MWCO) of 35 kDa that we had used for the *in vivo* brain microdialysis (Figure 4.1). Hence, ISF, the most soluble compartment in the living brain of hAPP transgenic mice, appear to contain solely Aβ monomers, regardless of the extent of plaque deposition. This finding is significant because soluble Aβ dimers and other LMW oligomers (trimers, dodecamers, etc.), but not

monomers, have been widely reported to exert synaptotoxic and other adverse neural effects (Selkoe, 2011).

Therefore, here, we explored whether LMW Aβ oligomers, particularly Aβ dimers, do or do not exist as free, soluble species in ISF. We reasoned that due to their increased hydrophobicity, dimers may bind to cell membranes, pre-existing aggregates (e.g., plaques) or other hydrophobic surfaces much more rapidly than monomers do. If so, this could help clarify why dimers, not monomers, act as the smallest Aβ unit that exerts synaptotoxic (McLean et al., 1999; Klyubin et al., 2008; Shankar et al., 2008; Li et al., 2009; Mc Donald et al., 2010; O'Nuallain et al., 2010; Li et al., 2011), tau-altering (Jin et al., 2011) and other pathogenic neuronal effects.

Results

Aβ oligomers are undetectable in aqueous brain compartments of APP transgenic mice

We first asked whether Aβ oligomers are indeed undetectable in aqueous compartments. Hippocampal ISF was microdialyzed at a slow rate (0.2-0.4 µl/min) in awake, behaving transgenic mice, a rate low enough to allow recovery of ample amounts of soluble Aβ species (see Chapter 2; Hong et al., 2011). To ensure that the apparent lack of oligomers in ISF samples was not simply due to ineffective passage of the ~8 kDa dimers and any other LMW oligomers across our 35 kDa MWCO membrane, we also collected cerebrospinal fluid (CSF) from

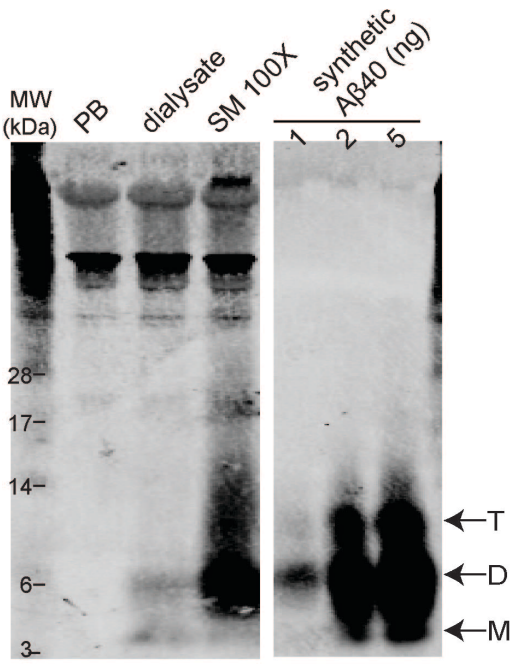

Figure 4.1. Aβ dimers can cross over the 35 kDa MWCO microdialysis membrane, but their crossover efficiency is poor in comparison to that of monomers.

In vitro (test tube) microdialysis was performed with synthetic $A\beta_{40}$ spiked into human CSF (251 nM) at 0.2 µl/min perfusion rate for 700 min, then dialysate was subjected to IP-WB. PB (Perfusion buffer) was IP'ed as negative control; SM 100X, starting material, was diluted 100-fold prior to IP; synthetic $A\beta_{40}$ was run alongside as WB control. IP: AW8 polyclonal antibody, WB: 6E10 (against $A\beta_{5-9}$) and 2G3 (against $A\beta_{31-40}$) Aβ monoclonal antibodies.

the cisterna magna of anesthetized transgenic mice (DeMattos et al., 2002). Using SDS-PAGE and Western blotting (WB), the Aβ in both the ISF and CSF from transgenic mice separated into monomers (4 kDa) and a ~5 kDa species, but we failed to see Aβ dimers (which runs ~6.5 kDa in these gels) in the ISF or the CSF samples (Figure 4.2A). The apparent lack of Aβ dimers was not due to the inability of the polyclonal AW8 Aβ antiserum to immunoprecipitate (IP) dimers, as the AW8 antibody IP'ed both the endogenous Aβ dimers in the saline extracts of older transgenic mouse brains (Figure 4.2A) and the synthetic Aβ dimers (Figure 4.2B). Next, we used another Aβ antiserum, the R1282 antibody (Podlisny et al., 1998), to IP Aβ from ISF and CSF and again detected no Aβ species larger than monomers in the samples (Figure 4.2C).

To verify this apparent lack of LMW Aβ oligomers in ISF and CSF, we used two additional methods besides IP-WB to look for oligomers in the aqueous compartments: (1) an oligomer-specific ELISA (o-ELISA) that uses the Aβ-N-terminal monoclonal 3D6 (against $Aβ_{1-5}$, gift of Elan, plc.) as both the capture and (biotinylated) detection antibodies (Yang et al., *submitted*); and (2) non-denaturing size-exclusion chromatography (SEC) and assay of the resultant fractions with an ELISA that sensitively detect $Aβ_{38}$, $Aβ_{40}$, and $Aβ_{42}$. Our o-ELISA specifically recognizes Aβ oligomers of a wide range of sizes including dimers, but not monomers, and it documents the rising levels of endogenous Aβ oligomers in brain tissues of APP transgenic mice (Yang et al., *submitted*) (Figure 4.3A). The o-ELISA failed to detect any signals in all ISF and CSF samples we

Figure 4.2. Low molecular weight Aβ oligomers are not recovered in the ISF or CSF of young J20 transgenic mice by IP-WB technique.

Buffer (1.5% BSA in artificial CSF), ISF collected at 0.2 µl/min from the hippocampi of living 3 mo transgenic mice, CSF collected from the cisterna magna of anesthetized 3 mo transgenic mice, and TBS extracts from 24 mo transgenic mice were IP'ed with either AW8 (A) or R1282 (C) Aβ antibodies, and subjected to SDS-PAGE. (A) Aβ from ISF and CSF IP'ed with AW8 Aβ antibody were separated into 4 kDa monomers and a ~5 kDa Aβ-immunoreactive species. On the other hand, Aβ from TBS extract of a 24 mo transgenic were separated into monomers and dimers. WB: 3D6, 2G3, and 21F12 (against $Aβ_{1-5}$, $Aβ_{31-40}$, and $Aβ_{33-42}$, respectively). (B) Both the synthetic Aβ monomers and dimers were IP'ed by the AW8 Aβ antibody. Start: 2 ng synthetic wt $Aβ_{1-40}$. WB: 3D6 and 6E10. (C) Aβ from ISF, CSF and TBS extracts IP'ed with R1282 Aβ antibody were separated into ~4 kDa monomers only. Dimers were not detected in ISF, CSF or synthetic wt Aβ monomers. The IP-WB method successfully brought down both the endogenous Aβ dimers in the TBS extract of 24 mo transgenic and the synthetic S26C Aβ dimers. WB: 3D6 and 6E10.

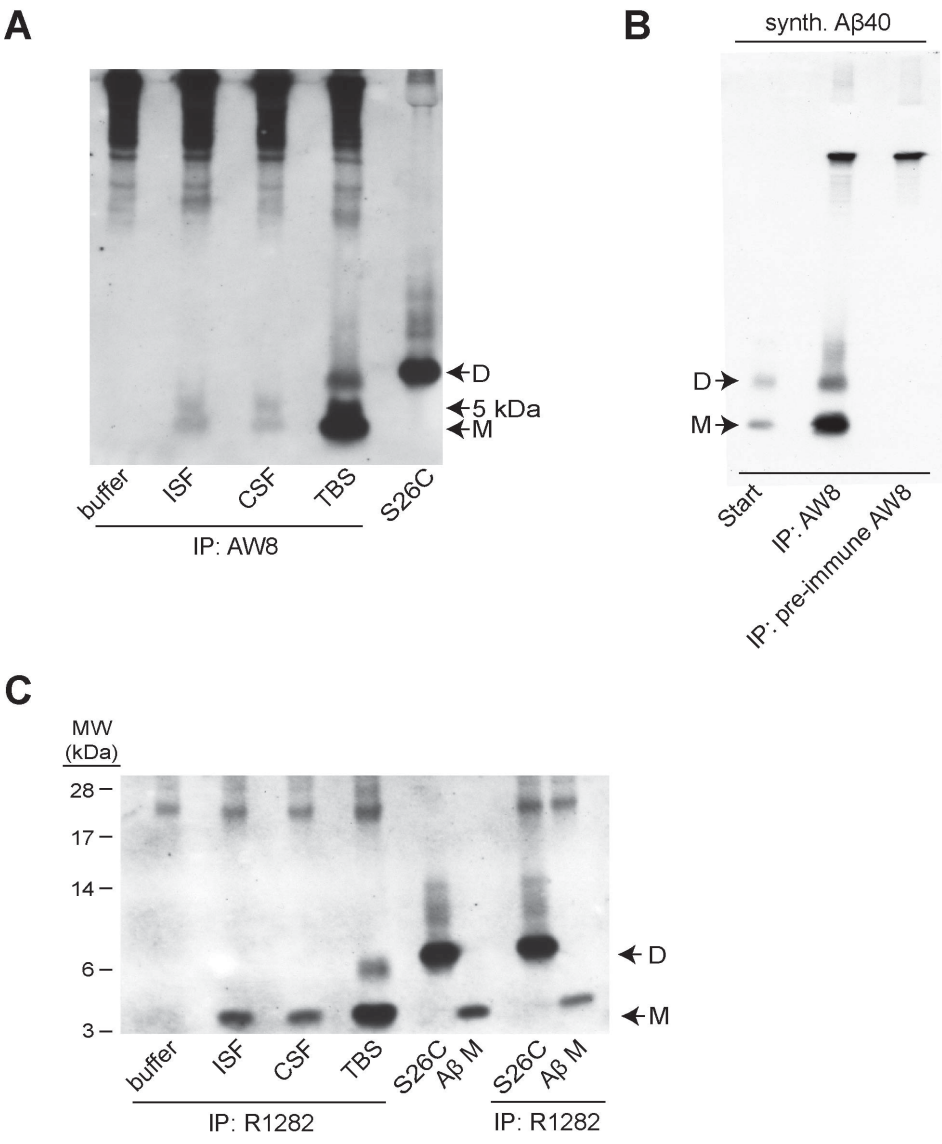

Figure 4.2 (Continued). Low molecular weight Aβ oligomers are not recovered in the ISF or CSF of young J20 transgenic mice by IP-WB technique.

tested, regardless of the age of the transgenic mice (Figure 4.3B). Using a conventional ELISA which uses 266 (against $A\beta_{16-23}$, gift of Elan) as the capture antibody and biotinylated 3D6 as the detection antibody and hence recognizes all $A\beta_{1-x}$ species including the monomers (the $A\beta_{1-x}$ ELISA), we confirmed that both the ISF and CSF samples, which failed to give any signal in the o-ELISA, did in fact contain ample amounts of Aβ (Figure 4.3C). As a control for the specificity of these signals, we saw about half as much $A\beta_{1-x}$ signal in the ISF collected at a flow rate of 0.4 µl/min than the ISF collected at 0.2 µl/min (Figure 4.3C), as expected with microdialysis. Furthermore, we spiked the ISF and CSF samples with low amounts of synthetic Aβ dimers and got signals at the expected range, thereby excluding the possibility that molecules in ISF or CSF interfere with the o-ELISA signal (Figure 4.3B).

Next, we combined two non-denaturing methods to further probe Aβ in the ISF. We chromatographed the microdialysates on a Superdex 75 SEC column and subjected the resultant fractions to a multiplex ELISA that simultaneously and sensitively recognizes low concentrations of endogenous $A\beta_{38}$, $A\beta_{40}$, and $A\beta_{42}$ peptides (the 6E10 Aβ triplex ELISA; MesoScale Discovery). Whereas SEC fractions in which Aβ monomers elute gave abundant signals for all three peptides, fractions corresponding to where dimers should elute yielded no detectable signals from both 3 mo (pre-plaque) and 24 mo (plaque-rich) transgenic mice (Figures 4.4A and B). Using a batch of synthetic Aβ containing both dimers and monomers of Aβ, we confirmed that the 6E10 Aβ triplex ELISA

Figure 4.3. Aβ oligomers are not detected in either ISF or CSF of J20 mice by the Aβ oligomer-specific ELISA.

(A) The o-ELISA did not detect synthetic Aβ monomers, even at a high concentration of 10 ng/ml, but it recognized rising levels of endogenous Aβ oligomers in TBS extracts of the J20 transgenic mice from 3 mo to 24 mo. The Aβ signals were abolished upon Aβ immunodepletion of the TBS extracts using the 3D6 Aβ antibody. (B) The o-ELISA failed to give any detectable Aβ signal for the ISF collected from the hippocampi of living 3 mo transgenic (N=4 mice) or 24 mo transgenic (N=7 mice). The o-ELISA also did not yield any signal for the CSF collected from the cisterna magna of anesthetized 3 mo transgenic (N=7 mice). In contrast, it detected low amounts of synthetic Aβ dimers that were spiked into the ISF and CSF samples. (C) When tested in parallel with a conventional $A\beta_{1-x}$ ELISA, the samples that failed to yield any detectable signals in the o-ELISA indeed gave ample signal (N=4 for ISF collected at PR 0.2 µl/min; N=10 for ISF collected at PR 0.4 µl/min; and N=7 for CSF samples).

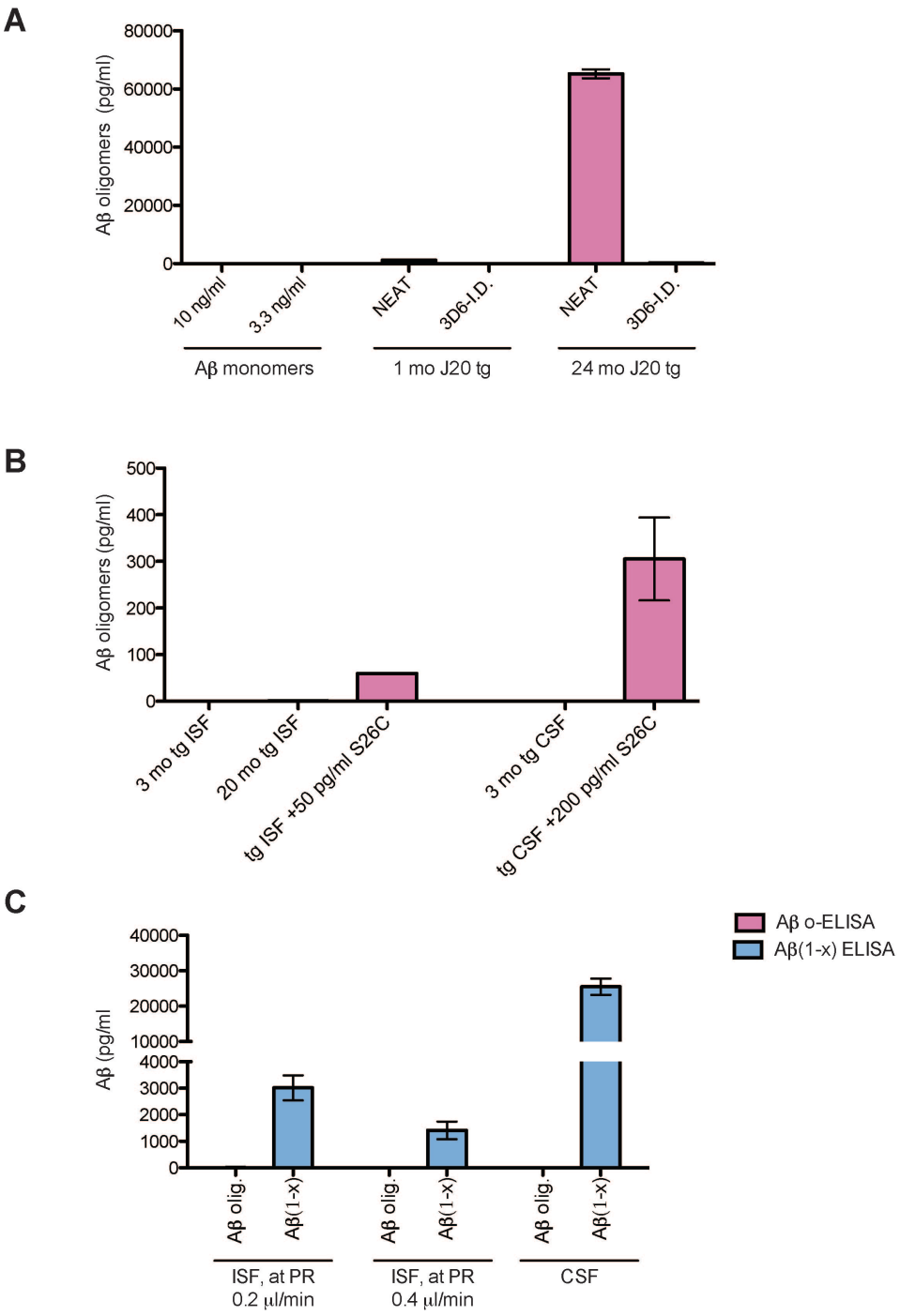

Figure 4.3 (Continued). Aβ oligomers are not detected in either ISF or CSF of J20 mice by the Aβ oligomer-specific ELISA.

indeed detects dimers and monomers to commensurate degrees (Figure 4.4C-E; signals of the SEC fractions by WB (Figure 4.4C) and by 6E10 Aβ triplex ELISA (Figure 4.4D) are directly compared in Figure 4.4E). These results indicate that the lack of detectable signals in fractions corresponding to dimers is not due to an inability of the 6E10 Aβ triplex ELISA to detect dimers.

Taken together, the results from three biochemical methods – IP-WB, o-ELISA, and SEC fractionation – suggest that Aβ dimers do not exist in hippocampal ISF and CSF of hAPP J20 transgenic mice at the levels of detection of these assays.

Aβ dimers are rapidly sequestered away from the hippocampal ISF pool in vivo and principally recovered in a membrane-associated brain pool

We next examined the half-life of Aβ dimers and monomers in ISF by administering low (8-40 nM) concentrations of synthetic Aβ directly into the hippocampal ISF of behaving wild-type (wt) mice. Because Aβ dimers cross over the microdialysis membrane with 35 kDa MWCO less readily than Aβ monomers do (Figure 4.1), we first sought experimental conditions at which one achieves similar crossover efficiency between monomeric and dimeric species. As the monomer source, we used synthetic wt $A\beta_{1-40}$ monomers (MesoScale Discovery) (Figure 4.5A) and as the dimer-enriched source, we used synthetic S26C $A\beta_{1-40}$ S26C oligomers (gift of D. Walsh, BWH), which were mostly dimeric and contained trace amounts of trimers (Figure 4.5B). Hence, the Aβ monomers from

Figure 4.4. $A\beta_{38}$, $A\beta_{40}$, and $A\beta_{42}$ peptides in the ISF of both 3 mo pre-plaque and 24 mo plaque-rich transgenic mice are eluted as Aβ monomers by size-exclusion chromatography.

(A-B) Non-denaturing SEC of hippocampal ISF from the hippocampi of 3 mo pre-plaque (A) and 24 mo plaque-rich (B) transgenic mice were performed with a Superdex 75 SEC column, followed by analysis of each SEC fraction by 6E10 Aβ triplex ELISA. (C-D) Non-denaturing SEC of synthetic wt $A\beta_{1-40}$ that contained dimers and monomers were performed with the same Superdex 75 SEC column, followed by analysis of the SEC fractions by WB on SDS-PAGE (C) and 6E10 Aβ triplex ELISA (D). WB: 3D6 and 6E10. (E) Elution profiles of the SEC fractions of the synthetic $A\beta_{1-40}$ as analyzed by 6E10 Aβ triplex ELISA (bold line) or WB (dotted line).

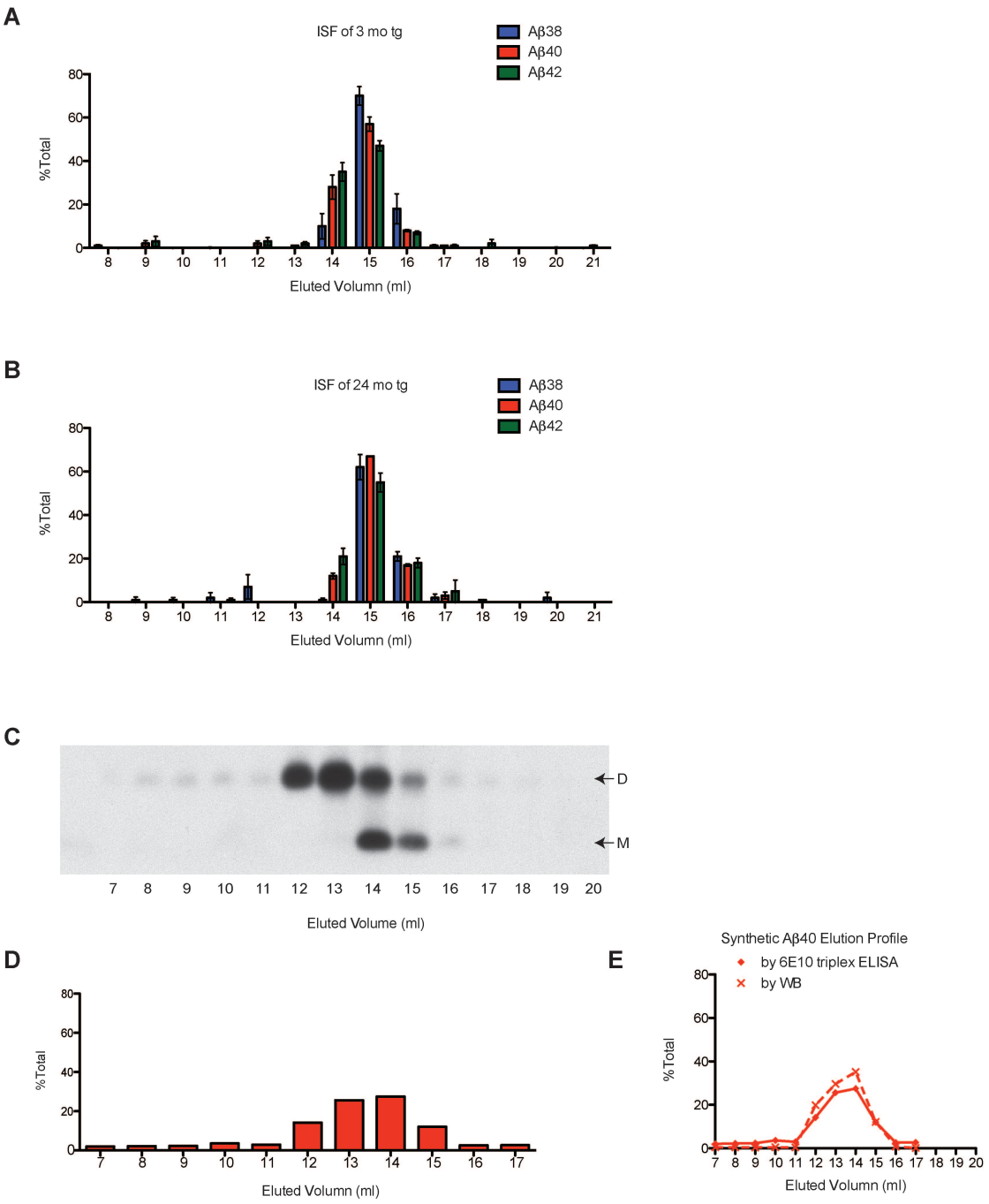

Figure 4.4 (Continued). $A\beta_{38}$, $A\beta_{40}$, and $A\beta_{42}$ peptides in the ISF of both 3 mo pre-plaque and 24 mo plaque-rich transgenic mice are eluted as Aβ monomers by size-exclusion chromatography.

MesoScale Discovery are termed herein as “Aβ monomers” and the S26C $Aβ_{1-40}$ oligomers as “Aβ dimers”. To keep the Aβ mostly in their original monomeric and dimeric forms, we avoided multiple freeze-thaw cycles (O'Nuallain et al., 2010). We confirmed that the Aβ that crossed over the microdialysis probe indeed reflected their starting material, i.e., the microdialysate of a monomer-enriched sample contained mostly monomers (Figure 4.5A) and the microdialysate of a dimer-rich sample contained mostly dimers (Figure 4.5B), and the Aβ monomers and dimers in the microdialysates stayed as such throughout the time of our analysis. We then performed *in vitro* microdialysis using a range of Aβ concentrations and measured the resultant amount of Aβ in the dialysates with the $Aβ_{1-x}$ ELISA. We found that at concentrations 8 nM for Aβ monomers and 40 nM for Aβ dimers, comparable crossover efficiencies were achieved between the monomers and the dimers at all three perfusion rates we tested (Figure 4.5C). Furthermore, using the interpolated zero flow microdialysis method (see Chapter 2) (Hong et al., 2011), we verified that comparable amounts of microdialyzable Aβ were captured for both Aβ monomer-rich and dimer-rich materials at all perfusion rates (Figure 4.5D). Therefore, we chose to pursue the *in vivo* microdialysis studies using Aβ monomers at 8 nM and S26C Aβ dimers at 40 nM and at perfusion rate of 0.4 µl/min, as such slow perfusion rates allow a more accurate reflection of the theoretical zero-flow rate (see Chapter 2) (Hong et al., 2011); moreover, the 0.4 µl/min perfusion rate allow for a time resolution by the hour.

Figure 4.5. Aβ monomers at 8 nM and Aβ dimers at 40 nM have comparable crossover efficiencies *in vitro*.

(A-B) The Aβ in the microdialysates reflected their respective starting materials (A: Aβ monomers; B: Aβ dimers) throughout the 24-36 h of the analysis. IP: R1282, WB: 3D6. (C) Comparable crossover efficiencies were achieved using 8 nM Aβ monomers (wt) and 40 nM Aβ dimers (S26C) at all three perfusion rates tested using *in vitro* (test tube) microdialysis. (D) Comparable percentages of microdialyzable Aβ were captured for both Aβ monomers and dimers at all perfusion rates as analyzed by the interpolated zero flow microdialysis method (N=3 sets, where the wt Aβ monomers and the S26C Aβ dimers were microdialyzed in pairs side by side).

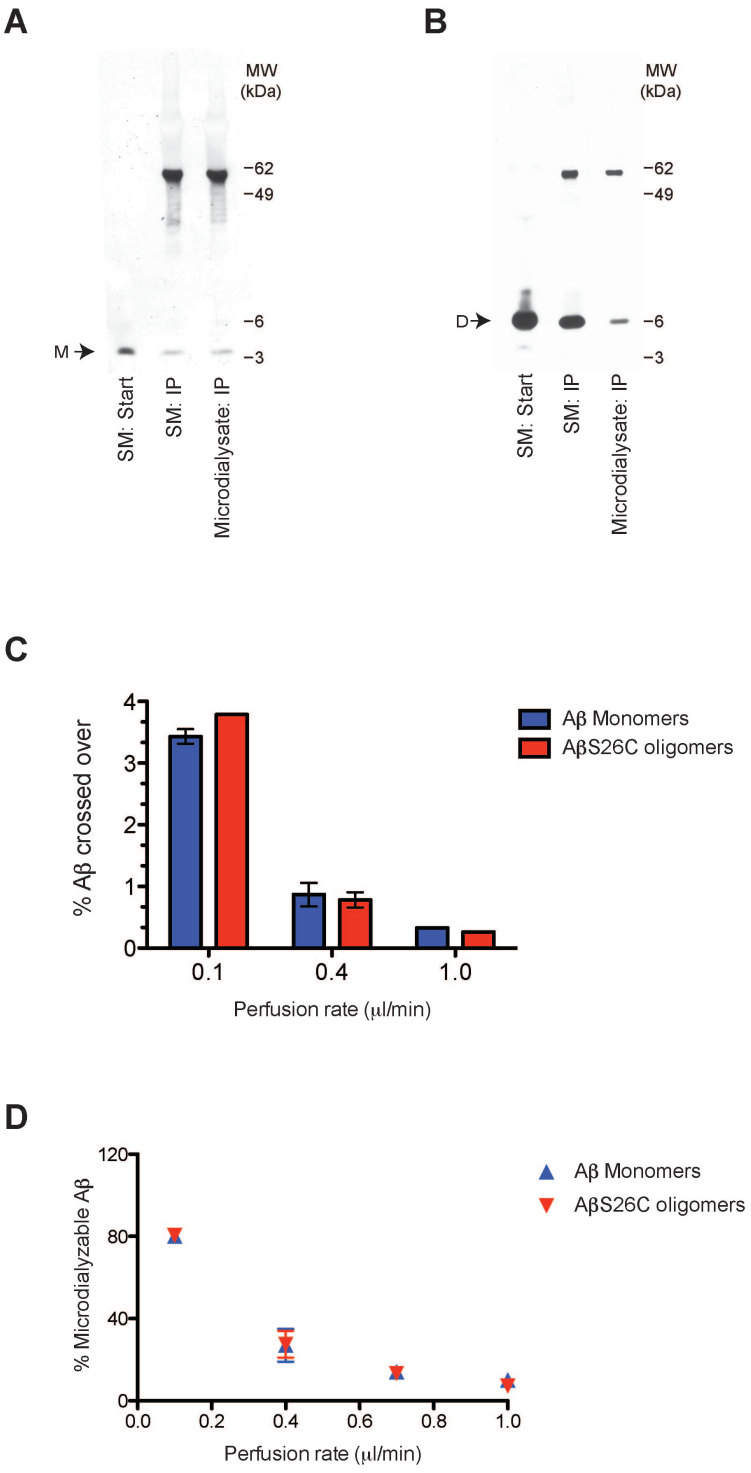

Figure 4.5 (Continued). Aβ monomers at 8 nM and Aβ dimers at 40 nM have comparable crossover efficiencies *in vitro*.

Once we established conditions at which we observed comparable percent Aβ crossing over the membrane *in vitro*, we acutely administered exogenous dimers (at 40 nM) or monomers (at 8 nM) into mouse brain ISF *in vivo* via a cannula attached to the microdialysis probe. To distinguish between the acutely administered Aβ and the endogenously secreted Aβ, we injected synthetic Aβ of human sequence into the ISF of wt mice and quantified the recovery of the injected human Aβ in the microdialysates using the $A\beta_{1-x}$ ELISA (which selectively recognizes human Aβ). We found that in the first hour post-injection, a much lower percentage of the injected Aβ dimers was recovered in the ISF than for the injected Aβ monomers (Figure 4.6A). In contrast to our *in vitro* test tube experiments where comparable percentages of Aβ dimers and monomers were recovered, the *in vivo* recovery of injected dimers was less than 10% of that of injected monomers, and the difference between *in vitro* and *in vivo* recoveries was highly significant ($p < 0.0001$) (Figure 4.6B). The loss from the ISF of the injected Aβ dimers happened rapidly (Figure 4.6C: hourly monitoring of ISF Aβ pre- and post-injection; inset shows values using a finer y-scale). The reduced recovery of Aβ dimers vs. monomers does not seem to be due to a general limit on *in vivo* diffusion, as ISF levels of urea (frequently used as an endogenous reference compound in microdialysis experiments (Ronne-Engström et al., 2001; Brody et al., 2008) did not change with Aβ injection (Figure 4.6D). We also showed that at the low nanomolar concentrations of Aβ we injected (3 µl injections, corresponding to 96-960 pg Aβ), neither the ratio of lactate/pyruvate

Figure 4.6. Aβ dimers are much more rapidly sequestered away from the ISF pool than the Aβ monomers.

(A) In first hour post-injection, a much lower percentage of the injected Aβ dimers was recovered from the ISF than was recovered for the injected Aβ monomers. N=6 mice for the monomer-injected, N=5 mice for the dimer-injected. $P = 0.0126$ by two-tailed Student's *t* test. (B) The *in vivo* recovery of injected dimers was 8.85 ± 2.81% of that of injected monomers (N=5 pairs), in contrast to the *in vitro* recovery, 102 ± 11.4% (N=3 pairs) (average ± S.E.M.s). $P < 0.0001$ between the *in vitro* and *in vivo* recoveries by two-tailed Student's *t* test. (C) Representative hourly monitoring of the injected Aβ monomers (blue triangle) or Aβ dimers (red circle) in the ISF of the wt mice before and after injection. Inset shows values using a finer y-scale. (D-F) Hourly monitoring of urea (D), ratio of lactate over pyruvate (E), and glucose (F) in the ISF of wt mice pre- and post-injection of the Aβ monomers (blue triangle) or Aβ dimers (red circle). N=2-4 pairs.

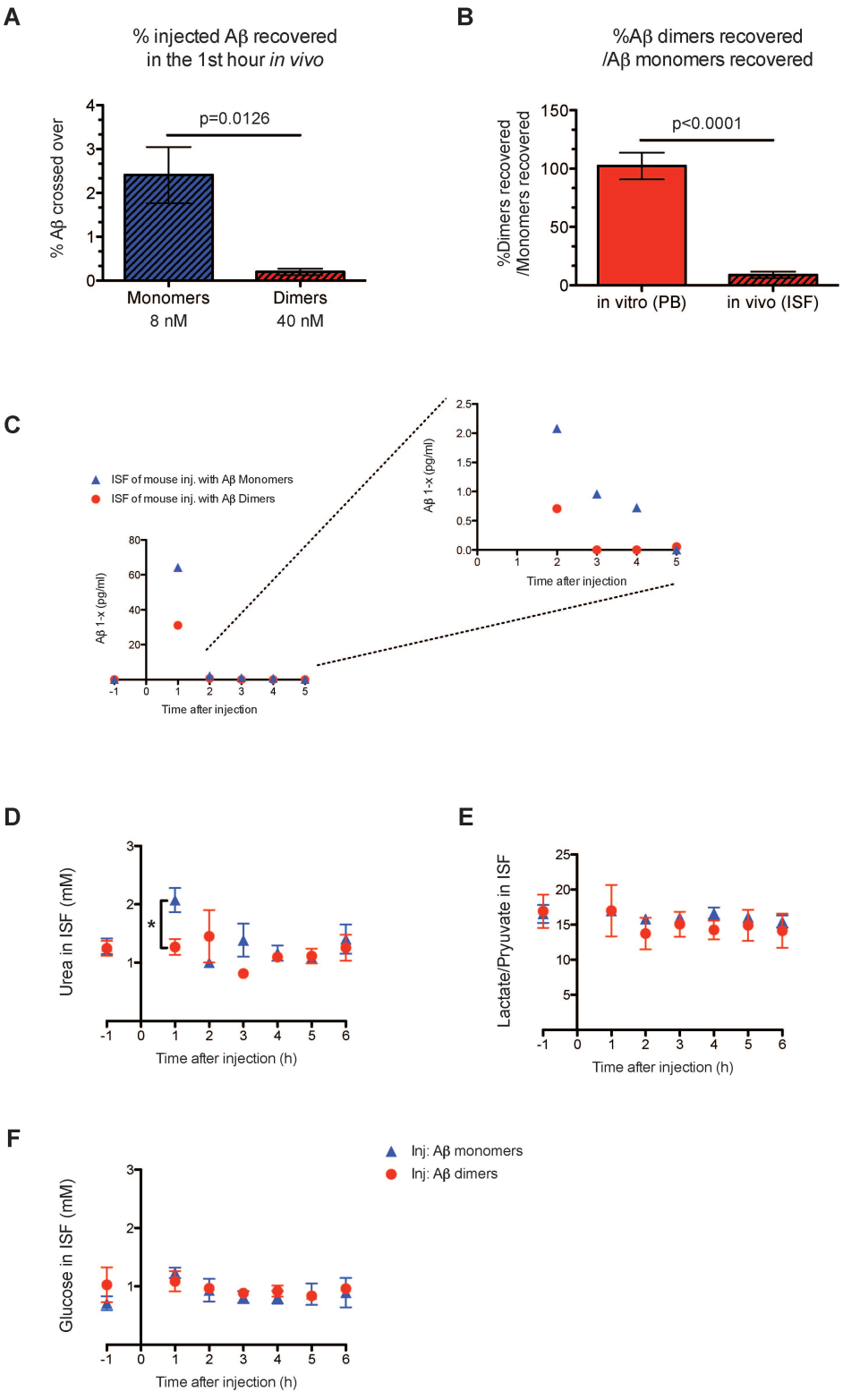

Figure 4.6 (Continued). Aβ dimers are much more rapidly sequestered away from the ISF pool than the Aβ monomers.

(Figure 4.6E) nor the level of glucose (Figure 4.6F) in the ISF was altered.

At just one hour post-injection, Aβ dimers showed ~8.5-fold less recovery when injected into the ISF than did Aβ monomers (Figure 4.6). When we spiked the S26C Aβ oligomers into saline extracts of wt mice *ex vivo* and performed SEC, we observed an immediate shift of its elution profile on a Superdex 75 SEC column from the dimer fractions (corresponding to MW ~8 kDa) to the void volume fractions (corresponding to MW > 70 kDa) (see Figure 3.4). These results led us to ask what could mediate a rapid shift of the S26C dimers to the void volume fractions. Most of the synthetic Aβ dimers spiked into TBS buffer alone eluted at the expected dimer position (Figure 3.4A), arguing against mere aggregation of the Aβ. Rather, we hypothesized that the Aβ could be binding to lipid membranes and that the dimers have a higher affinity for them than do monomers.

We then examined the corresponding brain homogenates to see in which pool of brain parenchyma we could recover the injected Aβ. We found that the injected Aβ was recovered in both the TBS-soluble extracts (TBS) and the membrane-bound extracts (TBS with 1% Triton-X: TBS-Tx) (Figure 4.7A). The proportion of Aβ recovered in the membrane-bound extract after the injection of Aβ dimers was much higher than that of the monomers, whereas the amount of Aβ recovered in the saline extracts was comparable (Figure 4.7B). These results suggest that Aβ dimers quickly bind to membranes.

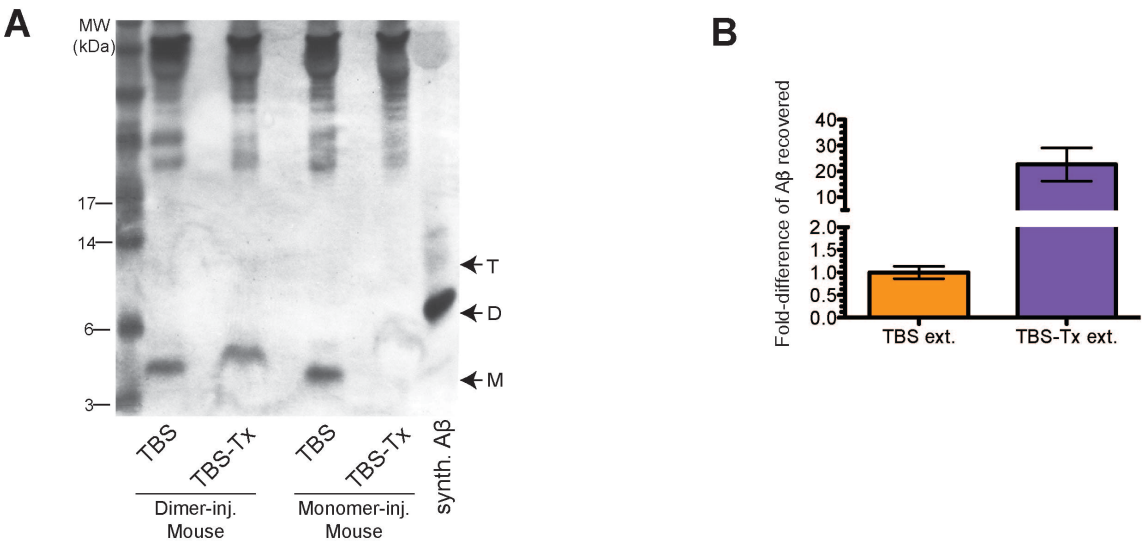

Figure 4.7. A higher proportion of the injected Aβ dimers are recovered from the membrane-bound extracts of the brain homogenates as compared to the injected Aβ monomers.

(A) Aβ monomers or dimers that were injected into the hippocampi of wt mice were recovered in the TBS and the TBS-Tx extracts. IP: R1282, WB: 3D6 and 6E10. (B) The proportion of Aβ recovered in the TBS-Tx extracts after the injection of Aβ dimers was 23 ± 6.4 fold than that of the Aβ monomers, whereas the amount of Aβ recovered in the TBS extracts was comparable (1.00 ± 0.136 fold; average ± S.E.M., N=4 pairs). WB quantification by ImageJ of N=8 mice injected side-by-side with either wt monomers or S26C Aβ dimers.

In vivo injection of soluble Aβ dimers (both synthetic and natural (Aβ isolated from human AD cortex)) led to their recovery from the membrane-associated brain fractions bound to GM1 ganglioside and Prion protein

Interestingly, synthetic Aβ dimers injected into wt mouse hippocampal ISF were not retained as dimers as judged by WB of subsequent saline extracts but rather as a 4 kDa Aβ monomer in the TBS-soluble fraction and as a ~5 kDa Aβ species in the membrane (TBS-Tx) fraction (Figure 4.7A). We also found that, in contrast to the *in vitro* setting where synthetic dimers were stable (Figure 4.5B), the Aβ dimers injected *in vivo* into the ISF pool did not retain their dimeric state, as measured by the o-ELISA, but were apparently reduced to monomers, as evidenced by positive signals in the $A\beta_{1-x}$ ELISA (Figure 4.8A). As the synthetic Aβ S26C dimers are disulfide cross-linked, their reduction to monomers when injected *in vivo* can be explained by the brain providing a reducing environment. We next injected into the ISF of wt mice *in vivo* a natural form of Aβ: dimers isolated from the cerebral cortex of typical AD patients (Shankar et al., 2008). Even the natural dimers were recovered as monomers from the mouse brain homogenates (Figure 4.8B). The injected natural Aβ was not recovered in the TBS-Tx pellet dissolved in 88% formic acid (Figure 4.8C shows the WB of the formic acid-treated samples; Figure 4.8D shows that the same method yielded ample amount of Aβ of both monomers and dimers from the TBS-Tx pellet of old transgenic brain, which has an abundant Aβ monomers and dimers). This suggested that all of the injected material in the wt brain were recovered in TBS

Figure 4.8. The Aβ dimers injected *in vivo* into the ISF are promptly reduced to monomers.

(A) The ISF sampled in the first hour from wt mice that were injected with the synthetic Aβ S26C dimers failed to yield any detectable signals in the o-ELISA, but gave positive signals in the $A\beta_{1-x}$ ELISA. Both ELISAs can detect low (< 80 pg/ml) amount of Aβ dimers, but o-ELISA cannot detect Aβ monomers, even at a high (70 ng/ml) concentration. (B) Soluble Aβ dimers derived from human AD TBS extract that were injected into the wt mice were recovered as monomers from the brain homogenates. IP: R1282, WB: 3D6 and 6E10. SM: Starting material that was injected into the brain, which contained mostly dimers and some monomers. Synthetic Aβ dimers or monomers were loaded as controls. Representative blot of N=5 mice. (C-D) WB of TBS-Tx pellets after treatment with 88% formic acid. WB: 3D6 and 6E10. (C) There was no detectable Aβ present in the TBS-Tx pellets of wt brains injected with either natural or synthetic Aβ. Entire 2 hemispheres loaded per lane. (D) Ample amounts of Aβ of both monomers and dimers from the TBS-Tx pellet of 19 mo transgenic were eluted using the formic acid treatment (<1/16 hemisphere loaded).

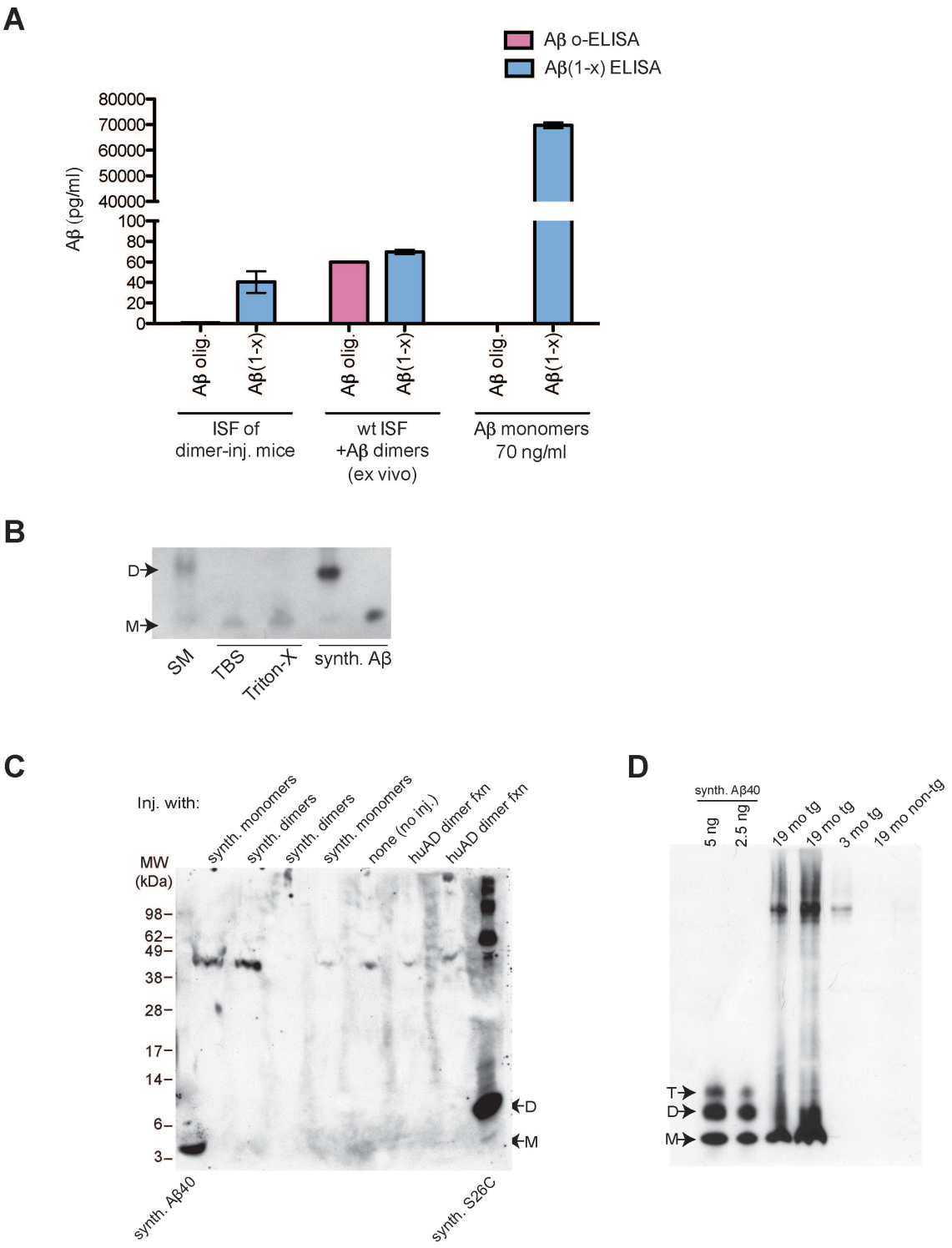

Figure 4.8 (Continued). The Aβ dimers injected *in vivo* into the ISF are promptly reduced to monomers.

and TBS-Tx extracts.

To search for endogenous molecules that the *in vivo* injected Aβ might have bound to, we IP'ed the brain extracts for Aβ and blotted for two previously reported ligands of human Aβ: GM1 ganglioside (Yanagisawa et al., 1995; Choo-Smith et al., 1997; Hayashi et al., 2004; Williams et al., 2011) and the cellular prior protein (PrP^c) (Laurén et al., 2009; Freir et al., 2011; Kudo et al., 2012). Both the injected AD brain-derived Aβ dimers (Figures 4.8B and 4.9A) and the synthetic S26C Aβ dimers (Figures 4.7A and 4.9D) which were recovered in the membrane-associated brain fraction (TBS-Tx) and migrated as a 5 kDa monomeric species were reactive with cholera toxin, which specifically binds to GM1 ganglioside (van Heyningen, 1974) (Figure 4.9B: mouse injected with AD brain-derived Aβ dimers; Figure 4.9E: mouse injected with synthetic S26C Aβ dimers). Furthermore, we found that the recovered Aβ from the TBS-Tx fraction, but not the Aβ from the TBS fraction, was associated with PrP^c (Figure 4.9C: mouse injected with AD brain-derived Aβ dimers; Figure 4.9F: mouse injected with synthetic S26C Aβ dimers). We did not observe any co-IP of GM1 ganglioside or PrP^c with Aβ in brains of wt mice that did not receive Aβ injection (Figures 4.9G-I), arguing that the pull-down of the GM1 ganglioside and PrP^c with Aβ was not due to non-specific immunoprecipitation. Importantly, the binding of Aβ monomers to GM1 ganglioside (and hence their altered migration at 5 kDa on SDS-PAGE) and their association with PrP^c could not be seen when we spiked synthetic S26C Aβ dimers *ex vivo* into *post-mortem* wt brain homogenates

Figure 4.9. The injected Aβ are recovered from the membrane-associated fraction as bound to GM1 ganglioside and Prion protein.

(A-C) Human AD brain-derived Aβ dimers were injected *in vivo* to anesthetized wt mice or spiked *ex vivo*, then the brain extracts were IP'ed for Aβ using the R1282 Aβ antibody. (D-E) Synthetic S26C Aβ dimers were injected *in vivo* to anesthetized wt mice, then the brain extracts or S26C Aβ in buffer alone were IP'ed for Aβ using R1282. (F-I) Brain extracts with or without spiking of the synthetic S26C Aβ dimers were IP'ed for Aβ using R1282. (A, D and G) WB for Aβ using 3D6 and 6E10 mouse monoclonal antibodies (against $Aβ_{1-5}$ and $Aβ_{5-9}$, respectively). (B, E and H) WB for GM1 ganglioside using cholera toxin. (C, F and I) WB for Prion protein using a mouse monoclonal anti-PrP antibody (the ICSM 35 antibody, against aa 93-102 of PrP).

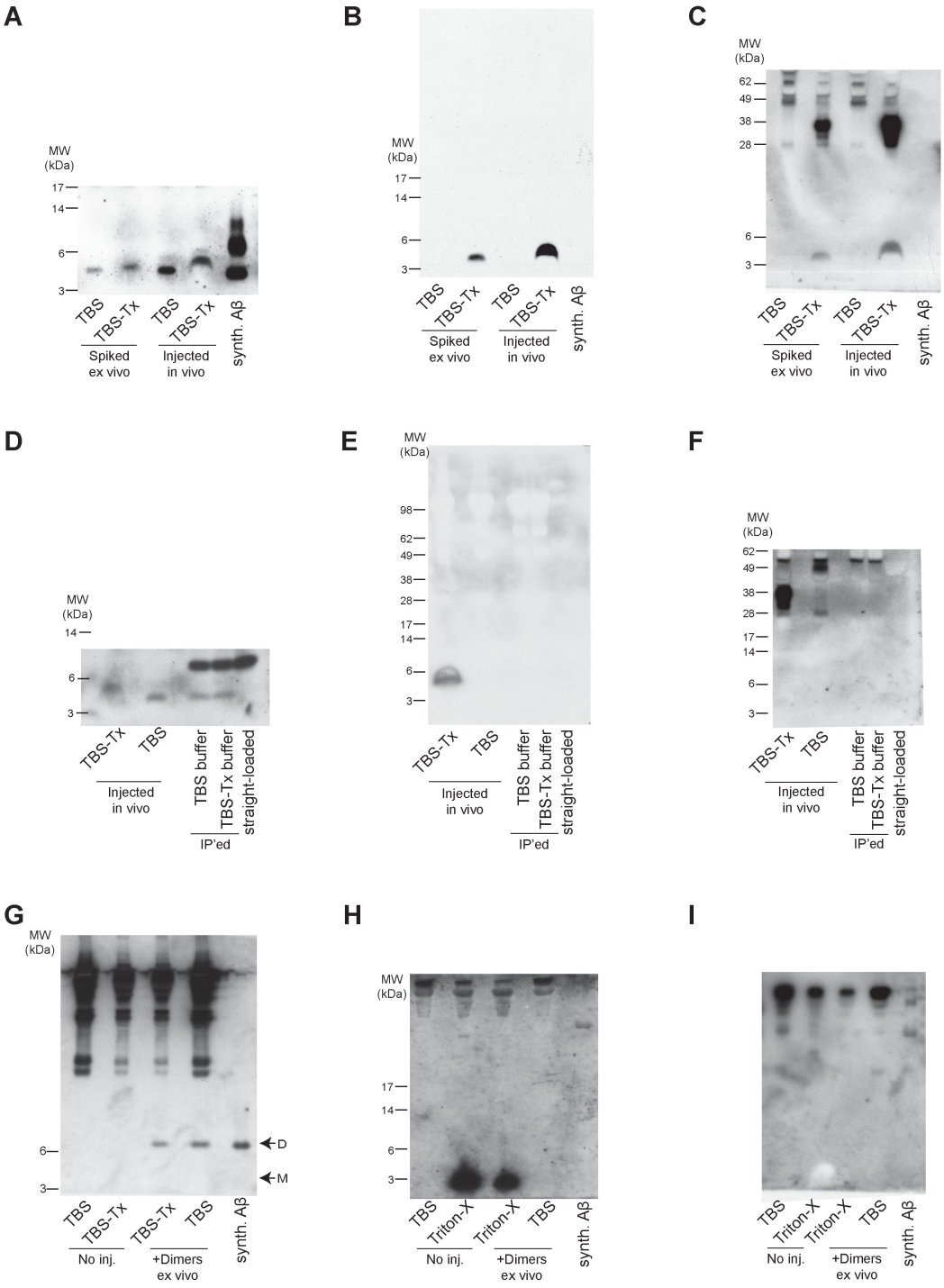

Figure 4.9 (Continued). The injected Aβ are recovered from the membrane-associated fraction as bound to GM1 ganglioside and Prion protein.

(Figures 4.9G-I), suggesting that the binding of Aβ to endogenous GM1 ganglioside and PrP^c requires an environment that the intact, living brain provides.

The membrane-bound fractions in hAPP transgenic mice contain GM1 ganglioside- and Prion protein-bound Aβ

We're currently investigating whether we can recover the Aβ-GM1 ganglioside complex, which may also be associated with PrP^c, in the membrane-bound fractions of hAPP transgenic mice. Preliminary results indicate that such a complex exists in young, pre-plaque J20 transgenic mice: Aβ in the TBS-Tx fraction of a 3 mo transgenic mouse which was pulled down by the R1282 Aβ antibody was also reactive for GM1 ganglioside; however, Aβ in the TBS-Tx fractions of a 24 mo transgenic mouse which was pulled down by the R1282 Aβ was not as reactive for GM1 ganglioside despite having much more Aβ present (Figures 4.10A and B). The endogenous Aβ in the TBS-Tx extract of the 3 mo transgenic was also associated with more PrP^c than Aβ in the TBS-Tx extracts of the 24 mo transgenic or non-transgenic littermate control (Figure 4.10C). Furthermore, a monoclonal antibody that was raised against GM1 ganglioside-bound Aβ isolated from membrane fractions of human brains with diffuse plaques (i.e., the 4396C antibody) (Yanagisawa et al., 1997; Hayashi et al., 2004) specifically pulled out an Aβ-immunoreactive band from the 3 mo pre-plaque

Figure 4.10. Aβ from the membrane-bound fractions of young hAPP transgenic mice are associated with GM1 ganglioside and PrP^c.

(A-C) TBS-Tx extracts of 3 mo transgenic, 20 mo transgenic and 20 mo non-transgenic littermate control were subjected to IP with the R1282 Aβ antibody. The immunoprecipitates were then subjected to SDS-PAGE and blotted for Aβ using 3D6 and 6E10 mouse monoclonal antibodies (A), GM1 ganglioside using cholera toxin (B), and PrP^c using 6D11 mouse monoclonal antibody (against aa 93-109 of PrP) (C).

(D-F) TBS-Tx extracts of 3 mo transgenic, 20 mo transgenic and 20 mo non-transgenic littermate control were subjected to IP with the 4396C antibody (raised against GM1 ganglioside-bound human Aβ), then the subsequent 4396C-immunodepleted supernatant was IP'ed with R1282. The 4396C and the R1282 immunoprecipitates were then subjected to SDS-PAGE and blotted for Aβ using 3D6 and 6E10 monoclonal antibodies (D), GM1 ganglioside using cholera toxin (E), and PrP^c using 6D11 monoclonal antibody (F).

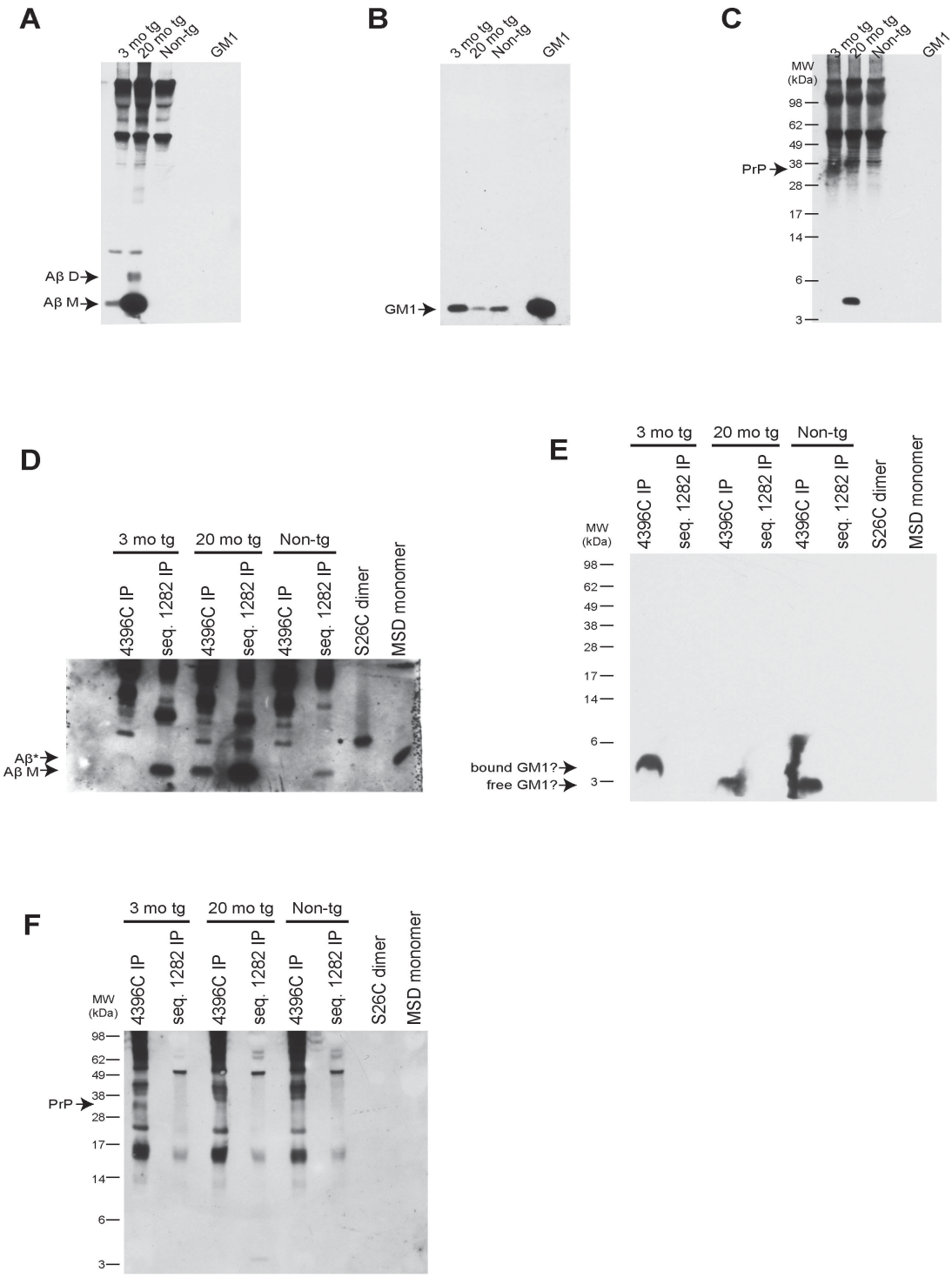

Figure 4.10 (Continued). Aβ from the membrane-bound fractions of young hAPP transgenic mice are associated with GM1 ganglioside and PrP^c.

transgenic mouse that migrated ~5 kDa and retained a cusp-like shape similar to the shape of the Aβ that was injected into wt mice and subsequently recovered from the membrane-bound fractions (Figures 4.9A and D) (Figure 4.10D). This 5 kDa Aβ-immunoreactive band was then positively stained for GM1 ganglioside (Figure 4.10E) and PrP^c (Figure 4.10F). When there was an absence of this cusp-like structure, as was the case for the plaque-rich old transgenic and the non-transgenic, there was no apparent Aβ-bound GM1 ganglioside that migrated above the 3 kDa MW marker (Figure 4.10E); accordingly, there was no PrP^c (between 28-38 kDa) that was pulled down with the 4396C (Figure 4.10F). Importantly, the subsequent R1282 immunoprecipitate of the 4396C-immuodepleted materials lacked any GM1 ganglioside, despite there still being an abundant amount of Aβ left in the material (Figures 4.10D and E), suggesting that the 4396C was effectively pulling down a specific GM1 ganglioside-bound and PrP^c-associated Aβ complex from the membrane-bound fractions of 3 mo transgenic mice.

Aβ dimers may have a higher affinity to lipid membranes

In a separate set of experiments, I am currently performing surface plasmon resonance (SPR) experiments to assess directly whether Aβ dimers and monomers have different binding affinities to lipid membranes. To ensure that I am using predominantly the dimeric form of Aβ, I perform non-denaturing SEC with S26C Aβ oligomers using the Superdex 75 SEC column < 24 h before

running the SPR experiments and use the fractions where the Aβ dimers are eluted; I also avoid multiple freeze-thaw cycles to decrease the likelihood of *in vitro* aggregation (O'Nuallain et al., 2010). To obtain Aβ monomers, I treat the Aβ S26C dimers with 3% β-mercaptoethanol (βME) for 10 min at RT, which reduces most of the Aβ S26C dimers to monomers (Figure 4.11A). The monomers are treated shortly before they are used and handled in buffer containing 0.1% βME to ensure they are kept in a reduced state. I coat the SPR chips with freshly prepared small unilamellar vesicles of brain total lipid extracts in regular buffer (50 mM ammonium acetate, pH 8.5) or buffer containing 0.1% βME. First, I confirm uniform lipid coating of the chips by subsequently injecting BSA as a control (data not shown). I then perfuse the oxidized S26C dimers (in regular buffer) or the reduced S26C monomers (in buffer containing 0.1% βME). Preliminary results indicate that the non-reduced Aβ S26C dimers yielded a 3-fold enhanced SPR signal (Figure 4.11B) over the reduced Aβ monomers (Figure 4.11C). When I perfused the chips with melittin in either buffer as a positive control, I observed no significant changes in the response signal (Figures 4.11D and E). The preliminary findings thus suggest that Aβ dimers have an enhanced affinity for lipid bilayer membranes than the Aβ monomers do. Given the recent findings of a potential GM1 ganglioside- and PrP^c-bound Aβ complex, it will be imperative to test by SPR the role of these two molecules the binding of Aβ to the lipid membranes, i.e., to determine whether one or both of these two molecules mediate the binding of Aβ to the lipid membrane.

Figure 4.11. Aβ dimers may have a ~3-fold enhanced affinity to lipid membranes.

(A) The SEC fraction containing mostly SDS-stable S26C Aβ dimers was treated with 3% βME at RT for 5, 10, 15, and 20 min. WB: 3D6. (B-E) SPR response units, corresponding to the binding of the injected molecules (B-C: S26C Aβ dimers at different concentrations; D-E: Melittin at 3 ng/ml). (B) Dose-dependent increase in the binding of the S26C Aβ dimers to the lipid bilayer membrane. (C) A much reduced binding response seen with the reduced Aβ S26C monomers (in 0.1% βME) to the lipid bilayer membrane. (D-E) There are no significant changes in the response signal with melittin between the non-reduced (no βME) and reduced (with 0.1% βME) conditions.

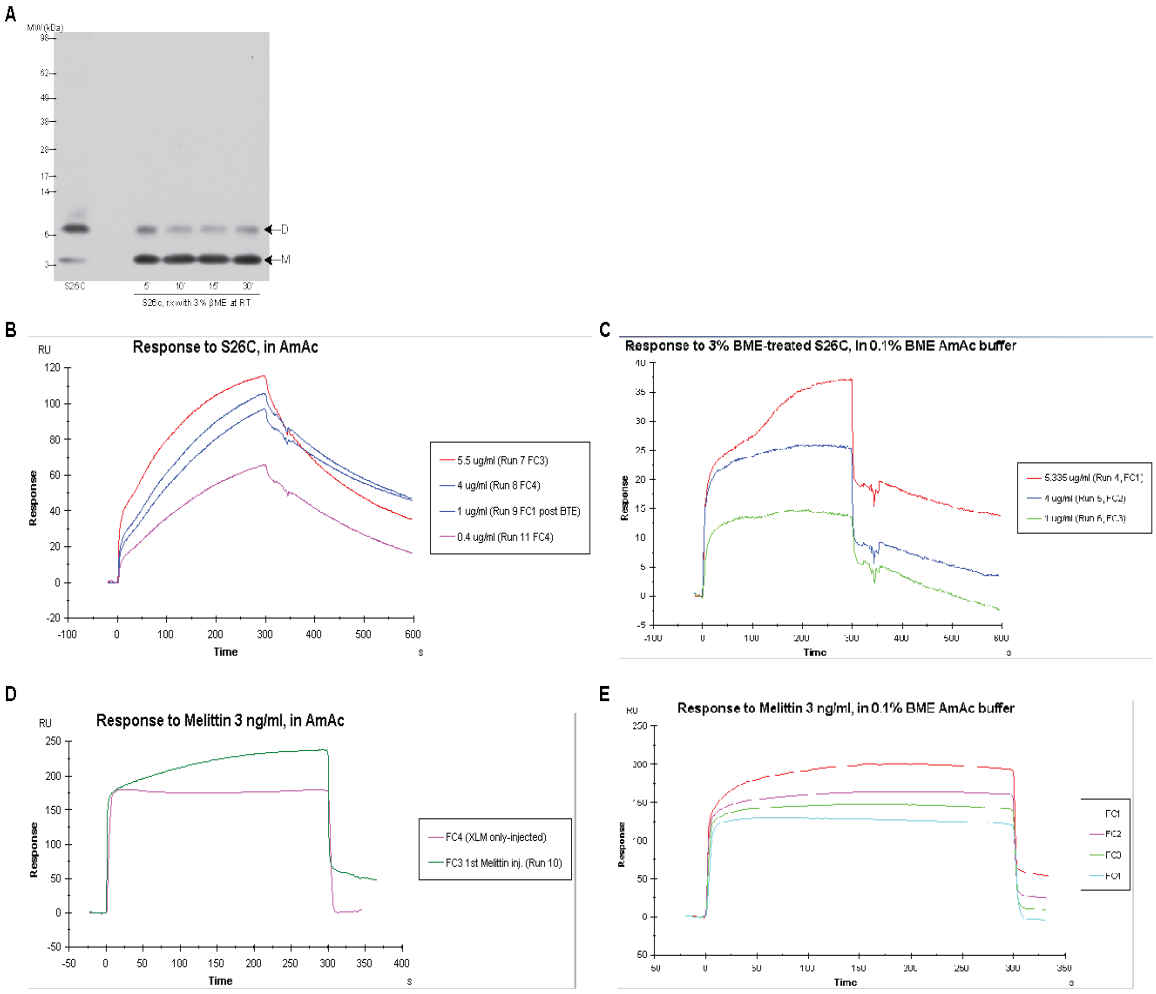

Figure 4.11 (Continued). Aβ dimers may have a ~3-fold enhanced affinity to lipid membranes.

Discussion

Using three biochemical methods – IP-WB, ELISA specific for Aβ oligomers (o-ELISA), and non-denaturing size-exclusion chromatography (SEC) – we failed to detect any low-molecular weight (LMW) Aβ oligomers in the hippocampal ISF or CSF of the J20 hAPP transgenic mice, regardless of their age or plaque deposition. Using two polyclonal Aβ antibodies that can pull down Aβ dimers, if they are present, only Aβ monomers were recovered from the ISF and CSF (Figure 4.2). The o-ELISA also failed to detect any signal for Aβ oligomers in all ISF and CSF samples we tested, despite there being ample amounts of Aβ present in both samples (Figure 4.3). Finally, using a combination of two non-denaturing methods, the SEC and a sensitive ELISA for $A\beta_{38}$, $A\beta_{40}$ and $A\beta_{42}$ that detects Aβ dimers and monomers to a comparable degree, we failed to gain any evidence that there exist $A\beta_{38}$, $A\beta_{40}$, or $A\beta_{42}$ LMW oligomers in the ISF (Figure 4.4). Hence, we report that there does not exist any LMW Aβ oligomers in the aqueous compartments of the brain, i.e., the CSF and the ISF, of the hAPP transgenic mice; if a LMW oligomeric unit may exist in the fluid compartment, we calculate it to be of a negligible amount (< 0.004% of total Aβ present).

This data reinforces our recent finding using two Aβ o-ELISAs (whose specificity for oligomers was extensively validated) that in all 13 human CSF samples tested (among which 4 were CSF from individuals clinically diagnosed to have AD), we failed to detect any Aβ oligomers (Yang et al., *submitted*).

Although there has been a few reports on Aβ oligomers existing in CSF and plasma of humans developing AD (for e.g., (Klyubin et al., 2008; Fukumoto et al., 2010; Gao et al., 2010; Villemagne et al., 2010), the interpretation of these various assays has been difficult due to vague definitions of the precise oligomeric unit the assays are detecting and whether one can really exclude the detection of Aβ monomers. However, our results do not necessarily support critics' doubts as to whether LMW Aβ oligomers really exist *in vivo* (Haass, 2010; Benilova et al., 2012); instead, they suggest that the Aβ oligomers may not exist in the aqueous biological fluids, but due to their substantial hydrophobicity, they may be sequestered away from the extracellular fluid onto membranes and/or existing aggregates (plaques).

To determine whether LMW Aβ oligomers in fact have a shortened half-life in the aqueous compartment, we acutely injected exogenous Aβ into brains naïve of plaques (i.e., the wt mouse hippocampi) and observed a rapid sequestration of the Aβ dimers away from the hippocampal ISF pool: in just one hour, Aβ dimers showed ~8.5-fold less recovery when injected into the ISF than did Aβ monomers (Figure 4.6). This was in stark contrast to the *in vitro* test tube setting, where comparable percentages of the starting Aβ monomers and dimers were recovered in the microdialysates (Figure 4.5). This suggested that *in vivo*, Aβ dimers are much more rapidly sequestered away from the aqueous compartment because they have an enhanced affinity for a binding platform. Accordingly, the injected Aβ dimers were recovered at a much higher proportion in the

membrane-bound pool than in the cytosolic pool (Figure 4.7), suggesting that Aβ dimers, compared to monomers, much more quickly bind membranes. The sequestration of the Aβ dimers from the brain ISF happened pretty rapidly (< 1 h) in a plaque-naïve brain, arguing against mere aggregation of the Aβ. We suspected whether Aβ dimers, being much more hydrophobic than the monomers, could be binding to lipid membranes, and whether the dimers have a higher affinity for them. To this end, we recently began surface plasmon resonance to directly measure the affinity of Aβ dimers or monomers to lipid bilayer membrane; preliminary results indicate that Aβ dimers may in fact have an enhanced affinity to the lipid membrane than do the monomers (Figure 4.11).

Interestingly, the injected Aβ materials (both the synthetic cross-linked dimers and the natural Aβ dimers from human AD cortical tissue) that were recovered from the membrane-bound fractions migrated as 5 kDa monomers, and the 5 kDa Aβ band was reactive for GM1 ganglioside. Furthermore, the GM1-bound Aβ was found to be associated with PrP^c (Figure 4.9). Using two antibodies – a polyclonal antibody that recognizes all forms of Aβ (the R1282) and a monoclonal antibody specifically raised against human GM1-associated Aβ (the 4396C) – we also recovered this apparent Aβ/GM1/PrP^c tri-complex from the membrane-bound fractions of pre-plaque 3 mo transgenic mice (Figure 4.10).

The abnormally migrating Aβ monomers on SDS-PAGE (i.e., migrating ~5 kDa instead of the usual 4 kDa) was reported once earlier: it was found to be GM1 ganglioside-bound Aβ monomers (mostly $Aβ_{42}$) detected in early sucrose

gradient fractions of AD brains with diffuse plaques (Yanagisawa et al., 1995). As the GM1 ganglioside-bound Aβ monomer was observed only in brains that contained diffuse plaques, but not in AD brains that were rich with fibrillar amyloid plaques or in non-AD cortices, the authors hypothesized that the GM1 ganglioside-bound Aβ could be a "seed" for amyloid fibril formation. Several *in vitro* biophysical studies that followed the Yanagisawa et al. (1995) paper supported the view that Aβ, upon binding to GM1 ganglioside on neuronal membranes, undergoes a conformational change that confers a higher propensity to aggregate, thus acting as an endogenous seed (reviewed in Ariga et al., 2008; Yanagisawa, 2011); however, to date, no other group has reported seeing such species *in vivo* from transgenic mouse brain homogenates or human AD brains. Furthermore, we have shown (in Chapters 3 and 4) that the hippocampal ISF and CSF of APP transgenic carried an abundant amount (~40% of total ISF Aβ) of a 5 kDa Aβ species that was immunoprecipitable by a polyclonal Aβ antibody (the AW8); however, we have not been able to determine its molecular identity or whether the 5 kDa Aβ species found endogenously in these fluid compartments is of similar molecular identity (i.e., GM1 ganglioside-bound) to that recovered from the membrane-bound brain fractions.

The PrP^c/Aβ interaction on the other hand has been a recent hotbed of controversy ever since Laurén et al. (2009) reported PrP^c as an apparent receptor for the synaptotoxic synthetic $Aβ_{42}$ oligomers (where residues 95-105 of PrP^c were mapped out as the primary determinant of binding). However, Laurén

et al.'s findings were soon disputed (Kessels et al., 2010), and since, a series of papers have reported data either in support of (Chen et al., 2010; Chung et al., 2010; Gimbel et al., 2010; Barry et al., 2011; Freir et al., 2011; Resenberger et al., 2011; Kudo et al., 2012) or against (Balducci et al., 2010; Calella et al., 2010; Kessels et al., 2010; Cissé et al., 2011) a critical role of PrP^c for Aβ to suppress cognitive function.

As Aβ oligomers have also been suggested to increase localization of PrP^c to the cell surface (Caetano et al., 2011), it is possible that Aβ targets a specific protein receptor, such as the PrP^c or other synaptic components, and "overstabilizes" their presence on the cell membrane, thereby inducing "pathological signaling platforms" (Renner et al., 2010). Alternatively, given that hydrophobicity is a key feature of Aβ oligomers (Haass and Selkoe, 2007), there very well may not be a specific target protein receptor for Aβ. The hydrophobic Aβ oligomers, once released into the extracellular space, may quickly be sequestered to certain microdomains on plasma membranes of cells or to certain lipid vesicles and exert subtle physicochemical properties of membranes (for e.g., by interfering with membrane fluidity, dynamics of membrane lipids and proteins, or ion permeability), which may in turn affect various proteins that are expressed on the membrane surface.

In particular, Aβ has been found to bind preferentially to GM1 ganglioside-containing liposomes that also include sphingomyelin and cholesterol, and upon binding, to display rapid fibril formation (McLaurin and Chakrabartty, 1996; Choo-

Smith and Surewicz, 1997; Kakio et al., 2002; Hayashi et al., 2004). Gangliosides are particularly enriched in the nervous system, as compared to other cellular membranes, and their localization is thought to be on specific raft-like domains that are also enriched in cholesterol and sphingomyelin on pre- and postsynaptic membranes or on certain lipid vesicles, such as the exosomes (where PrP^c is also highly localized) (Hansson et al., 1977; Svennerholm and Gottfries, 1994; Sonnino et al., 2007; Théry et al., 2009). Furthermore, GM1 ganglioside has recently been found to bind to the C-termini of PrP^c and to be a necessary ligand for PrP^c to be anchored on lipid rafts (Sanghera et al., 2011). Hence, the physical proximity of GM1 ganglioside and PrP^c on specific raft-like domains may explain the association of Aβ to both GM1 and PrP^c in the membrane-bound fractions.

Whether it is the PrP^c or the GM1 ganglioside that acts as the primary binding site for Aβ has yet to be investigated. To this end, we are planning to obtain some *PrnP* null mice to see whether we can still recover the Aβ/GM1/PrP^c tri-complex upon Aβ injection. Mice that lack GM1 gangliosides in their central nervous system do exist (mice with disrupted GM2/GD2 synthase); however, the amount of GM3 increases accordingly and hence the readout may not be as straightforward (Takamiya et al., 1996; Sheikh et al., 1999; Oikawa et al., 2009). On the other hand, Aβ's binding site could require both GM1 ganglioside and PrP^c to be in a specific complex. When we spiked Aβ dimers *ex vivo* into *post-mortem* wt brain extracts, we did not see a binding of the spiked Aβ to either

GM1 ganglioside or PrP^c (Figure 4.9), which suggests that the Aβ does not bind to any free endogenous GM1 ganglioside or PrP^c, but to a specific complex that requires an environment that the intact, living brain provides. Changing the pH (from 7.4 to 6.0, which has been reported to facilitate binding of Aβ to GM1 ganglioside (McLaurin and Chakrabartty, 1996)), temperature, or incubation times did not allow for a complete recapitulation of the binding of injected Aβ to endogenous GM1 and PrP^c such as those shown in the *in vivo* setting (data not shown). Furthermore, preliminary results suggest that the altered migration of acutely injected Aβ as a GM1-associated 5 kDa molecule may be time-dependent, i.e., the longer we wait to sacrifice the mouse after injecting the Aβ, the less of an altered migration we observe.

Interestingly, both the Aβ IP-WBs on the injected mouse brain homogenates and the Aβ ELISAs on the ISF samples indicated that the synthetic Aβ dimers injected into the ISF no longer existed as a dimer-unit, i.e., they were promptly reduced to monomers (Figure 4.8). This was in contrast to the *in vitro* test tube setting, where the molecular unit of the Aβ dimers and monomers remained unperturbed even after 36 h at RT, i.e., Aβ recovered in the microdialysate from a starting material that contained mostly monomers stayed as monomers, and those from a dimer-containing material stayed as dimers (Figure 4.5). As the synthetic Aβ dimers were disulfide cross-linked, the reduction of these dimers to monomers when injected *in vivo* could be explained by the brain providing a reducing environment. However, we also found that the

non-cross-linked Aβ dimers isolated directly from human AD cortical tissue were recovered as monomers in the mouse brain homogenates (Figure 4.8). When Aβ dimers were applied onto rat hippocampal neuronal cultures, the Aβ dimers (both synthetic and human brain-derived) remained as dimers up to 3 days at 37 °C (Jin et al., 2011). One possible explanation for the rapid depolymerization of the injected Aβ dimers we observed here could be that in the wt brain, local microglia are able to rapidly degrade the injected Aβ dimers into monomers. We are unsure whether the reduction of Aβ dimers to monomers happens first or the binding to GM1 ganglioside and/or PrP^c occurs first. Our current thought is that the depolymerization to monomers occurs first, then the monomers bind to GM1 ganglioside/PrP^c. Regardless of the exact order of events, the depolymerization to monomers and the binding of Aβ to GM1 and PrP^c seem to be a concurrent phenomenon, i.e., if we fail to see the spiked Aβ dimers reduced to monomers (as was the case for most of the *ex vivo* spiking experiments (Figures 4.9G-I)), we also do not see binding of Aβ to GM1 or PrP^c.

As to the recovery of the Aβ/GM1/PrP^c tri-complex in young (pre-plaque) J20 transgenic mice but not in the old (plaque-rich) transgenic, despite there being a substantially higher amount of total Aβ recoverable in the membrane-bound fraction in the old transgenic, we speculate that a specific pool of Aβ, i.e., the Aβ in the extracellular space (the ISF Aβ), binds to the GM1 ganglioside and/or PrP^c available on the surface of neuronal membranes and hence form the Aβ/GM1/PrP^c tri-complex. The amount of ISF Aβ in young, pre-plaque transgenic

is considerably higher than in old, plaque-rich transgenic: ISF Aβ falls significantly (especially the $A\beta_{42}$) as mice accrue plaques (Chapter 2; Hong et al., 2011). The substantial level of steady-state ISF Aβ in the pre-plaque brain, where Aβ mostly represents recent products of APP processing ($t_{1/2}$ ~2 h) (see Chapter 2) may therefore lead to a higher amount of Aβ/GM1/PrP^c tri-complex as seen in the young, pre-plaque transgenic mice. In contrast, a plaque-rich brain, which contains minimal levels of ISF Aβ, especially the $A\beta_{42}$, has less amount of Aβ available to bind to GM1 and PrP^c, as the Aβ is rapidly sequestered onto existing plaques. The injected Aβ (at the low concentrations of 8-40 nM we used here) may in essence mimic the ISF Aβ of young transgenic mice. This may support the hypothesis that GM1 ganglioside-bound Aβ could be a "seed" for amyloid fibril formation (Yanagisawa, 2011) and that this formation initially occurs on the surface of neuronal membranes (Selkoe, 2011). (Note, in plaque-rich brains, the Aβ recovered in the TBS-Tx fraction may represent not only the membrane-bound Aβ, but also the Aβ associated with extracellular plaques that were eluted off with the TBS-Tx buffer.)

In summary, I report in this Chapter three major findings: first, Aβ oligomers were undetectable in aqueous brain compartments (i.e., the ISF and CSF) of the J20 hAPP transgenic mice; second, the Aβ dimers were rapidly sequestered away from the hippocampal ISF pool *in vivo* and principally recovered as 5 kDa Aβ monomers in membrane-associated brain pool; and third, both the injected Aβ in wt mice and the endogenous Aβ in young hAPP

transgenic mice were recovered from the membrane-associated fraction as bound to GM1 ganglioside and Prion protein (PrP^c). Taken together, these results suggest that LMW Aβ oligomers are rapidly sequestered away from the ISF and bind to GM1 ganglioside- and PrP^c-enriched lipid membranes, such as raft-like microdomains on secreted vesicles or on plasma membranes of cells.

Materials and Methods

Mice

J20 line carrying hAPP minigene with FAD mutations KM670/671NL and V717F was a kind gift of L. Mucke (Gladstone Institute, UCSF) and was maintained on a C57BL6 x DBA2 background (Mucke et al., 2000). All animal procedures were approved by the Harvard Medical School Institutional Animal Care and Use Committee. Mice of either sex were used in all experiments.

In vivo Aβ microdialysis

Microdialysis was performed as previously described (Cirrito et al., 2003): intracerebral guides were inserted following the coordinates for left hippocampal placement (bregma -3.1 mm, 2.5 mm lateral to midline, and 1.2 mm below dura at 12° angle). Perfusion buffer (1.5% bovine serum albumin (BSA) in artificial CSF (in mM: 1.3 $CaCl_2$, 1.2 $MgSO_4$, 3 KCl, 0.4 KH_2PO_4, 25 $NaHCO_3$, and 122 NaCl, pH 7.35)) was perfused using probes with 35 kDa MWCO membranes (BR-2, Bioanalytical Systems) at flow rates 0.2-1 µl/min with an infusion syringe

pump (Stoelting). Microdialysates (ISF) were collected using a refrigerated fraction collector (Univentor). Mice were housed in a "Raturn" cage system (Bioanalytical Systems), which allows mice to resume normal activities, and were subjected to 12 h light/dark cycles.

Mouse brain sample preparation for biochemical analyses

Brains were homogenized using a mechanical Dounce homogenizer with 20 strokes at 4000 rpm in ice-cold TBS (20 mM Tris-HCl, 150 mM NaCl, pH 7.4) and protease inhibitors at 4:1 TBS volume:brain wet weight. Homogenate was centrifuged for 30 min at 175,000 g in a 4°C TLA100.2 rotor on Beckman TL 100 (resulting supernatant = "TBS extract"). Pellet was homogenized in ice-cold TBS with 1% Triton-X (TBS-Tx) and protease inhibitors at 4:1 TBS-Tx volume:brain wet weight and centrifuged for 30 min at 175,000 g in a 4°C TLA100.2 rotor on Beckman TL 100 (resulting supernatant = "TBS-Tx extract"). The pellet was then incubated with 88% formic acid at RT for 2 h. Resulting supernatant ("FA extract") was diluted 10X with water and lyophilized.

CSF collection from cisterna magna

CSF was collected from cisterna magna compartment from anesthetized mice as previously described (DeMattos et al., 2002). Briefly, mouse was deeply anesthetized with 100 mg/kg ketamine and 10 mg/kg xylazine administered intraperitoneally. Midline incision was made from the top of the skull to the dorsal

thorax, followed by a series of excision of muscles and excess tissue from the base of the skull to the first vertebrae for proper exposure of the cisterna magna. Any residual blood or ISF were rid using cotton swabs. A puncture to the arachnoid membrane covering the cistern was made using the very tip of a 29 G ½" needle, then very quickly, a gel loading pipet tip was gently applied to collect CSF as it exited the compartment.

Immunoprecipitation and Western blot for Aβ

Buffer alone, synthetic Aβ, ISF, CSF or brain extracts were first pre-cleared using Protein A (Sigma) alone, then IP'ed using either AW8 Aβ antiserum (1:100, gift of D. Walsh, BWH) or R1282 Aβ antiserum (1:75) and Protein A. Alternatively, the brain extracts were pre-cleared with Protein G (GE Healthcare) alone, then IP'ed using the 4396C monoclonal antibody (gift of K. Yanagisawa, NILS, Japan) and Protein G. For conventional SDS-PAGE, a previously described protocol (Walsh et al., 2000) was followed. Samples were electrophoresed using 12% Bis-Tris gel and MES SDS running buffer (Invitrogen), transferred onto 0.2-µm nitrocellulose, boiled, then blotted to Aβ using a combination of Aβ antibodies as fitting (for e.g., for specific recognition of human Aβ, we used a combination of 3D6 (against $A\beta_{1-5}$, gift of Elan) and 6E10 (against $A\beta_{5-9}$, Covance) mouse monoclonal antibodies), to GM1 ganglioside using HRP-conjugated cholera toxin (Sigma), or to Prion protein using ICSM 35 (D-Gen) or 6D11 (Covance) mouse monoclonal antibodies, and detected using HRP and ECL Plus, Advanced or Prime WB Detection Reagent (GE Healthcare).

Aβ ELISA

All sandwich ELISAs for Aβ were performed using the MULTI-ARRAY® 96-well Plate platform (MesoScale Discovery) following the manufacturer's protocol and as described in (Yang et al., *submitted*). For Aβ o-ELISA, 3D6 monoclonal antibody (against $Aβ_{1-5}$, gift of Elan) was used as capture antibody at 3 μg/ml and the biotinylated 3D6 was used as detection antibody at 100 ng/ml with SULFO-TAG™ Streptavidin (MesoScale Discovery). For $Aβ_{1-x}$ ELISA, the 266 monoclonal antibody (against $Aβ_{16-23}$, gift of Elan) was used as capture antibody at 3 μg/ml and the biotinylated 3D6 was used as detection antibody at 100 ng/ml with SULFO-TAG™ Streptavidin (MesoScale Discovery). For 6E10 Aβ Triplex ELISA, we used the MSD® 96-well MULTI-SPOT® Human (6E10) Abeta Triplex Assay, following the manufacturer's protocol and as described in (Hong et al., 2011). The 6E10 Aβ Triplex ELISA uses MULTI-SPOT® microplates pre-coated with antibodies specific to the C-termini of $Aβ_{38}$, $Aβ_{40}$, and $Aβ_{42}$ and detected with SULFO-TAG™-labeled 6E10 antibody.

Size-exclusion chromatography

ISF sampled at 0.4 μl/min (250 μl), synthetic Aβ (2 ng) or 3D6 IP'ed material of TBS extract of human AD brain were eluted at 0.5 ml/min from a Superdex 75 10/300GL column (GE Healthcare) with 50 mM ammonium acetate, pH 8.5. Resulting 1-ml fractions were lyophilized, reconstituted in LDS sample buffer and heated at 65 °C for 10 min. Samples were subjected to WB using 3D6

(to $A\beta_{1-5}$, gift of Elan) and the ECL Plus WB Detection Reagent (GE Healthcare).

Preparation of Aβ isolated from AD cortex

Aβ from TBS extract of human AD cortical tissue was prepared as previously described (Shankar et al., 2008; Yang et al., *submitted*). Briefly, frozen temporal or frontal cortex samples were dissected then homogenized as described above for mouse brain sample preparation. The TBS extract was then IP'ed with 3D6 antibody and the Aβ immunoprecipitate was eluted off a Superdex 75 SEC column in 50 mM ammonium acetate, pH 8.5. The SEC elution profile for Aβ was verified by SDS-PAGE. The corresponding fractions where Aβ dimers were eluted were used for the injection studies.

Test tube model of microdialysis for crossover efficiency

For the initial test tube microdialysis (Figure 4.1), buffer (1.5% BSA in artificial CSF) was perfused at 0.2 µl/min through human CSF spiked with synthetic $A\beta_{40}$ (251 nM) using the BR-2 35 kDa MWCO microdialysis membrane. Samples were then IP'ed using AW8 polyclonal antibody to Aβ. Precipitates were subjected to SDS-PAGE and Western blotted using monoclonal antibodies 6E10 (to $A\beta_{3-8}$, Covance) and 2G3 (to $A\beta_{33-40}$, gift of Elan). For the crossover studies of dimers versus monomers (Figure 4.5), we first performed microdialysis at 0.4 µl/min with differing starting concentrations of either wt $A\beta_{1-40}$ monomers (MesoScale Discovery) or S26C $A\beta_{1-40}$ dimers (gift of D. Walsh, BWH). The

amount of Aβ recovered in the microdialysates was then assessed by $Aβ_{1-x}$ ELISA, then the % starting material that crossed over the microdialysis membrane was plotted against the respective starting concentrations. The crossover efficiency (i.e., the % Aβ that was in the test tube as the starting material now recovered in the microdialysates) increased in a non-linear fashion with increasing concentrations of the starting material. The crossover efficiency of the Aβ dimers was calculated to be comparable to that of the Aβ monomers when enhanced 5-fold, i.e., Aβ dimers at 40 nM and Aβ monomers at 8 nM. To test this, test tubes containing S26C dimers at 40 nM or wt monomers at 8 nM were microdialyzed side by side at 3 different rates, 0.1, 0.4 and 1.0 µl/min, and the resulting microdialysates were assessed for levels of Aβ using the $Aβ_{1-x}$ ELISA. The quality of the Aβ in the starting materials in the test tubes and their corresponding microdialysates were also checked by IP-WB.

Interpolated zero-flow method

The *in vitro* percent recovery was calculated as previously described (Cirrito et al., 2003; Hong et al., 2011). Microdialysis was performed from starting materials that contained either 8 nM $Aβ_{1-40}$ monomers or 40 nM $Aβ_{1-40}$ S26C dimers in perfusion buffer (1.5% BSA in artificial CSF), while varying the perfusion rates (PR): 1.0, 0.7, 0.4, and 0.1 µl/min. Aβ levels were measured using the $Aβ_{1-x}$ ELISA and the values obtained at each PR were plotted versus the PR. The 100% recovery (i.e., the theoretical maximal amount of

exchangeable ISF Aβ species occurring at a zero PR) was calculated by extrapolating back the curve to a zero-flow rate. Then, for each PR, percent recovery was determined by calculating how much % Aβ was captured as compared to the theoretical [Aβ] at zero PR.

Half-life studies of Aβ in ISF in vivo

3 µl of either 8 nM $A\beta_{1-40}$ monomers (MesoScale Discovery) or 40 nM $A\beta_{1-40}$ S26C dimers (gift of D. Walsh, BWH) was injected through a combination infusion cannula and microdialysis probe (IBR-2, Bioanalytical Systems) at 0.2 µl/min. ISF was collected hourly at 0.4 µl/min, paused during the injection, then restarted 1 min after injection. The resulting ISF microdialysates were then analyzed by $A\beta_{1-x}$ ELISA or sent to the Yale Center for Clinical Investigation for measurements of lactate, pyruvate, glycerol, and glucose.

Intracortical injection of Aβ

For intracortical injection, a previously described protocol (Spires et al., 2005) was modified. Briefly, anesthetized mouse was placed in a stereotaxic equipment and using the same coordinates as described above for the guide cannula placement into the left hippocampus, 320 pg Aβ (corresponding to 1-2 µl vol.) was injected at 0.5 µl/min via a Hamilton syringe. Immediately (< 1 min) upon injection, mice were sacrificed and brains were harvested for biochemical analysis.

Surface plasmon resonance

SPR was performed with modified protocols from (Bartels et al., 2011) and (Hou et al., 2010). Briefly, SPR was performed at 20 °C on a BIACORE 3000 apparatus using the L1 sensor chip (Biacore AB). The running buffer was 50 mM ammonium acetate, pH 8.5. SUVs were prepared by sonicating brain total lipid extract (chloroform:methanol extract from bovine brain tissue; Avanti) and 300 µl SUVs were applied onto the sensor chip surface at a flow rate of 10 µl/min until equilibrium was achieved (~1 h). For regeneration buffers, either 5% ethanol or 300 mM sodium chloride was used. All injections were performed at 10 µl/min with 50 µl sample volume.

Statistical analysis

Data was analyzed using PRISM (Graphpad Software) for one-way or two-way analysis of variance (ANOVA) followed by Bonferroni post-hoc test if means were significantly different by ANOVA, or Student's *t* test, as appropriate.

References

Ariga T, McDonald MP, Yu RK (2008) Thematic Review Series: Sphingolipids. Role of ganglioside metabolism in the pathogenesis of Alzheimer's disease--a review. The Journal of Lipid Research 49:1157-1175.

Balducci C, Beeg M, Stravalaci M, Bastone A, Sclip A, Biasini E, Tapella L, Colombo L, Manzoni C, Borsello T, Chiesa R, Gobbi M, Salmona M, Forloni G (2010) Synthetic amyloid-beta oligomers impair long-term memory independently of cellular prion protein. Proc Natl Acad Sci USA 107:2295-2300.

Barry AE, Klyubin I, Mc Donald JM, Mably AJ, Farrell MA, Scott M, Walsh DM, Rowan MJ (2011) Alzheimer's disease brain-derived amyloid-β-mediated inhibition of LTP in vivo is prevented by immunotargeting cellular prion protein. Journal of Neuroscience 31:7259-7263.

Bartels T, Choi JG, Selkoe DJ (2011) alpha-Synuclein occurs physiologically as a helically folded tetramer that resists aggregation. Nature 477:107-110.

Benilova I, Karran E, De Strooper B (2012) The toxic Aβ oligomer and Alzheimer's disease: an emperor in need of clothes. Nature Neuroscience 15:349-357.

Brody DL, Magnoni S, Schwetye KE, Spinner ML, Esparza TJ, Stocchetti N, Zipfel GJ, Holtzman DM (2008) Amyloid-beta dynamics correlate with neurological status in the injured human brain. Science 321:1221-1224.

Caetano FA, Beraldo FH, Hajj GNM, Guimaraes AL, Jürgensen S, Wasilewska-Sampaio AP, Hirata PHF, Souza I, Machado CF, Wong DY-L, De Felice FG, Ferreira ST, Prado VF, Rylett RJ, Martins VR, Prado MAM (2011) Amyloid-beta oligomers increase the localization of prion protein at the cell surface. Journal of Neurochemistry 117:538-553.

Calella AM, Farinelli M, Nuvolone M, Mirante O, Moos R, Falsig J, Mansuy IM, Aguzzi A (2010) Prion protein and Abeta-related synaptic toxicity impairment. EMBO molecular medicine 2:306-314.

Chen S, Yadav SP, Surewicz WK (2010) Interaction between Human Prion Protein and Amyloid- (A) Oligomers: ROLE OF N-TERMINAL RESIDUES. Journal of Biological Chemistry 285:26377-26383.

Choo-Smith LP, Surewicz WK (1997) The interaction between Alzheimer amyloid beta(1-40) peptide and ganglioside GM1-containing membranes. FEBS Lett 402:95-98.

Choo-Smith LP, Garzon-Rodriguez W, Glabe CG, Surewicz WK (1997) Acceleration of amyloid fibril formation by specific binding of Abeta-(1-40) peptide to ganglioside-containing membrane vesicles. The Journal of biological chemistry 272:22987-22990.

Chung E, Ji Y, Sun Y, Kascsak RJ, Kascsak RB, Mehta PD, Strittmatter SM, Wisniewski T (2010) Anti-PrPC monoclonal antibody infusion as a novel treatment for cognitive deficits in an Alzheimer's disease model mouse. BMC Neurosci 11:130.

Cirrito JR, May PC, O'Dell MA, Taylor JW, Parsadanian M, Cramer JW, Audia JE, Nissen JS, Bales KR, Paul SM, DeMattos RB, Holtzman DM (2003) In vivo assessment of brain interstitial fluid with microdialysis reveals plaque-associated changes in amyloid-beta metabolism and half-life. Journal of Neuroscience 23:8844-8853.

Cissé M, Sanchez PE, Kim DH, Ho K, Yu G-Q, Mucke L (2011) Ablation of cellular prion protein does not ameliorate abnormal neural network activity or cognitive dysfunction in the j20 line of human amyloid precursor protein transgenic mice. The Journal of neuroscience : the official journal of the Society for Neuroscience 31:10427-10431.

DeMattos RB, Bales KR, Parsadanian M, O'Dell MA, Foss EM, Paul SM, Holtzman DM (2002) Plaque-associated disruption of CSF and plasma amyloid-beta (Abeta) equilibrium in a mouse model of Alzheimer's disease. J Neurochem 81:229-236.

Freir DB, Nicoll AJ, Klyubin I, Panico S, Mc Donald JM, Risse E, Asante EA, Farrow MA, Sessions RB, Saibil HR, Clarke AR, Rowan MJ, Walsh DM, Collinge J (2011) Interaction between prion protein and toxic amyloid beta assemblies can be therapeutically targeted at multiple sites. Nat Commun 2:336.

Fukumoto H, Tokuda T, Kasai T, Ishigami N, Hidaka H, Kondo M, Allsop D, Nakagawa M (2010) High-molecular-weight beta-amyloid oligomers are elevated in cerebrospinal fluid of Alzheimer patients. The FASEB Journal 24:2716-2726.

Gao CM, Yam AY, Wang X, Magdangal E, Salisbury C, Peretz D, Zuckermann RN, Connolly MD, Hansson O, Minthon L, Zetterberg H, Blennow K, Fedynyshyn JP, Allauzen S (2010) Aβ40 Oligomers Identified as a Potential Biomarker for the Diagnosis of Alzheimer's Disease. PLoS ONE 5:e15725.

Gimbel DA, Nygaard HB, Coffey EE, Gunther EC, Lauren J, Gimbel ZA, Strittmatter SM (2010) Memory Impairment in Transgenic Alzheimer Mice Requires Cellular Prion Protein. Journal of Neuroscience 30:6367-6374.

Haass C (2010) Initiation and propagation of neurodegeneration. Nature Medicine 16:1201-1204.

Haass C, Selkoe DJ (2007) Soluble protein oligomers in neurodegeneration: Lessons from the Alzheimer's amyloid ß-peptide. Nat Rev Mol Cell Biol 8:101-112.

Hansson HA, Holmgren J, Svennerholm L (1977) Ultrastructural localization of cell membrane GM1 ganglioside by cholera toxin. Proc Natl Acad Sci U S A 74:3782-3786.

Hayashi H, Kimura N, Yamaguchi H, Hasegawa K, Yokoseki T, Shibata M, Yamamoto N, Michikawa M, Yoshikawa Y, Terao K, Matsuzaki K, Lemere CA, Selkoe DJ, Naiki H, Yanagisawa K (2004) A seed for Alzheimer amyloid in the brain. Journal of Neuroscience 24:4894-4902.

Hong S, Quintero-Monzon O, Ostaszewski BL, Podlisny DR, Cavanaugh WT, Yang T, Holtzman DM, Cirrito JR, Selkoe DJ (2011) Dynamic Analysis of Amyloid β-Protein in Behaving Mice Reveals Opposing Changes in ISF versus Parenchymal Aβ during Age-Related Plaque Formation. Journal of Neuroscience 31:15861-15869.

Hou X, Small DH, Aguilar M-I (2010) Surface plasmon resonance spectroscopy in determination of the interactions between amyloid beta proteins (Abeta) and lipid membranes. Methods in molecular biology (Clifton, NJ) 627:225-235.

Jin M, Shepardson N, Yang T, Chen G, Walsh D, Selkoe DJ (2011) Soluble amyloid beta-protein dimers isolated from Alzheimer cortex directly induce Tau hyperphosphorylation and neuritic degeneration. Proc Natl Acad Sci U S A 108:5819-5824.

Kakio A, Nishimoto S-i, Yanagisawa K, Kozutsumi Y, Matsuzaki K (2002) Interactions of Amyloid β-Protein with Various Gangliosides in Raft-Like Membranes: Importance of GM1 Ganglioside-Bound Form as an Endogenous Seed for Alzheimer Amyloid †. Biochemistry 41:7385-7390.

Kessels HW, Nguyen LN, Nabavi S, Malinow R (2010) The prion protein as a receptor for amyloid-β. Nature 466:E1-E1.

Klyubin I, Betts V, Welzel AT, Blennow K, Zetterberg H, Wallin A, Lemere CA, Cullen WK, Peng Y, Wisniewski T, Selkoe DJ, Anwyl R, Walsh DM, Rowan MJ (2008) Amyloid beta protein dimer-containing human CSF disrupts synaptic plasticity: prevention by systemic passive immunization. Journal of Neuroscience 28:4231-4237.

Kudo W, Lee H-P, Zou W-Q, Wang X, Perry G, Zhu X, Smith MA, Petersen RB, Lee H-g (2012) Cellular prion protein is essential for oligomeric amyloid-β-induced neuronal cell death. Human molecular genetics 21:1138-1144.

Laurén J, Gimbel DA, Nygaard HB, Gilbert JW, Strittmatter SM (2009) Cellular prion protein mediates impairment of synaptic plasticity by amyloid-β oligomers. Nature 457:1128-1132.

Li S, Hong S, Shepardson NE, Walsh DM, Shankar GM, Selkoe D (2009) Soluble oligomers of amyloid Beta protein facilitate hippocampal long-term depression by disrupting neuronal glutamate uptake. Neuron 62:788-801.

Li S, Jin M, Koeglsperger T, Shepardson NE, Shankar GM, Selkoe DJ (2011) Soluble Aβ oligomers inhibit long-term potentiation through a mechanism involving excessive activation of extrasynaptic NR2B-containing NMDA receptors. Journal of Neuroscience 31:6627-6638.

Mc Donald JM, Savva GM, Brayne C, Welzel AT, Forster G, Shankar GM, Selkoe DJ, Ince PG, Walsh DM (2010) The presence of sodium dodecyl sulphate-stable A dimers is strongly associated with Alzheimer-type dementia. Brain 133:1328-1341.

McLaurin J, Chakrabartty A (1996) Membrane disruption by Alzheimer beta-amyloid peptides mediated through specific binding to either phospholipids or gangliosides. Implications for neurotoxicity. Journal of Biological Chemistry 271:26482-26489.

McLean CA, Cherny RA, Fraser FW, Fuller SJ, Smith MJ, Beyreuther K, Bush AI, Masters CL (1999) Soluble pool of Abeta amyloid as a determinant of severity of neurodegeneration in Alzheimer's disease. Ann Neurol 46:860-866.

Mucke L, Masliah E, Yu G-Q, Mallory M, Rockenstein E, Tatsuno G, Hu K, Kholodenko D, Johnson-Wood K, Mcconlogue L (2000) High-Level Neuronal Expression of Abeta 1-42 in Wild-Type Human Amyloid Protein Precursor Transgenic Mice: Synaptotoxicity without Plaque Formation. Journal of Neuroscience 20:4050.

O'Nuallain B, Freir DB, Nicoll AJ, Risse E, Ferguson N, Herron CE, Collinge J, Walsh DM (2010) Amyloid beta-protein dimers rapidly form stable synaptotoxic protofibrils. Journal of Neuroscience 30:14411-14419.

Oikawa N, Yamaguchi H, Ogino K, Taki T, Yuyama K, Yamamoto N, Shin R-W, Furukawa K, Yanagisawa K (2009) Gangliosides determine the amyloid pathology of Alzheimer's disease. Neuroreport 20:1043-1046.

Podlisny MB, Walsh DM, Amarante P, Ostaszewski BL, Stimson ER, Maggio JE, Teplow DB, Selkoe DJ (1998) Oligomerization of Endogenous and Synthetic Amyloid β-Protein at Nanomolar Levels in Cell Culture and Stabilization of Monomer by Congo Red †. Biochemistry 37:3602-3611.

Renner M, Lacor PN, Velasco PT, Xu J, Contractor A, Klein WL, Triller A (2010) Deleterious Effects of Amyloid β Oligomers Acting as an Extracellular Scaffold for mGluR5. Neuron 66:739-754.

Resenberger UK, Harmeier A, Woerner AC, Goodman JL, Müller V, Krishnan R, Vabulas RM, Kretzschmar HA, Lindquist S, Hartl FU, Multhaup G, Winklhofer KF, Tatzelt J (2011) The cellular prion protein mediates neurotoxic signalling of β-sheet-rich conformers independent of prion replication. The EMBO Journal 30:2057-2070.

Ronne-Engström E, Cesarini KG, Enblad P, Hesselager G, Marklund N, Nilsson P, Salci K, Persson L, Hillered L (2001) Intracerebral microdialysis in neurointensive care: the use of urea as an endogenous reference compound. J Neurosurg 94:397-402.

Sanghera N, Correia BE, Correia JR, Ludwig C, Agarwal S, Nakamura HK, Kuwata K, Samain E, Gill AC, Bonev BB, Pinheiro TJ (2011) Deciphering the molecular details for the binding of the prion protein to main ganglioside GM1 of neuronal membranes. Chem Biol 18:1422-1431.

Selkoe DJ (2011) Resolving controversies on the path to Alzheimer's therapeutics. Nature Medicine 17:1060-1065.

Shankar GM, Li S, Mehta TH, Garcia-Munoz A, Shepardson NE, Smith I, Brett FM, Farrell MA, Rowan MJ, Lemere CA, Regan CM, Walsh DM, Sabatini BL, Selkoe DJ (2008) Amyloid-l[beta]l protein dimers isolated directly from Alzheimer's brains impair synaptic plasticity and memory. Nature Medicine 14:837.

Sheikh KA, Sun J, Liu Y, Kawai H, Crawford TO, Proia RL, Griffin JW, Schnaar RL (1999) Mice lacking complex gangliosides develop Wallerian degeneration and myelination defects. Proc Natl Acad Sci U S A 96:7532-7537.

Sonnino S, Mauri L, Chigorno V, Prinetti A (2007) Gangliosides as components of lipid membrane domains. Glycobiology 17:1R-13R.

Spires TL, Meyer-Luehmann M, Stern EA, McLean PJ, Skoch J, Nguyen PT, Bacskai BJ, Hyman BT (2005) Dendritic spine abnormalities in amyloid precursor protein transgenic mice demonstrated by gene transfer and intravital multiphoton microscopy. Journal of Neuroscience 25:7278-7287.

Svennerholm L, Gottfries CG (1994) Membrane lipids, selectively diminished in Alzheimer brains, suggest synapse loss as a primary event in early-onset form (type I) and demyelination in late-onset form (type II). Journal of Neurochemistry 62:1039-1047.

Takamiya K, Yamamoto A, Furukawa K, Yamashiro S, Shin M, Okada M, Fukumoto S, Haraguchi M, Takeda N, Fujimura K, Sakae M, Kishikawa M, Shiku H, Furukawa K, Aizawa S (1996) Mice with disrupted GM2/GD2 synthase gene lack complex gangliosides but exhibit only subtle defects in their nervous system. Proc Natl Acad Sci U S A 93:10662-10667.

Théry C, Ostrowski M, Segura E (2009) Membrane vesicles as conveyors of immune responses. Nature reviews Immunology 9:581-593.

van Heyningen S (1974) Cholera toxin: interaction of subunits with ganglioside GM1. Science (New York, NY) 183:656.

Villemagne VL, Perez KA, Pike KE, Kok WM, Rowe CC, White AR, Bourgeat P, Salvado O, Bedo J, Hutton CA, Faux NG, Masters CL, Barnham KJ (2010) Blood-Borne Amyloid- Dimer Correlates with Clinical Markers of Alzheimer's Disease. Journal of Neuroscience 30:6315-6322.

Walsh DM, Tseng BP, Rydel RE, Podlisny MB, Selkoe DJ (2000) Detection of intracellular oligomers of amyloid ß-protein in cells derived from human brain. Biochemistry 39:10831-10839.

Williams TL, Johnson BRG, Urbanc B, Jenkins ATA, Connell SDA, Serpell LC (2011) Aβ42 oligomers, but not fibrils, simultaneously bind to and cause damage to ganglioside-containing lipid membranes. The Biochemical journal 439:67-77.

Yanagisawa K (2011) Pathological significance of ganglioside clusters in Alzheimer's disease. Journal of Neurochemistry.

Yanagisawa K, Odaka A, Suzuki N, Ihara Y (1995) GM1 ganglioside-bound amyloid beta-protein (A beta): a possible form of preamyloid in Alzheimer's disease. Nature Medicine 1:1062-1066.

Yanagisawa K, McLaurin J, Michikawa M, Chakrabartty A, Ihara Y (1997) Amyloid beta-protein (A beta) associated with lipid molecules: immunoreactivity distinct from that of soluble A beta. FEBS Lett 420:43-46.

Yang T, Hong S, OMalley T, Farrell MA, Sperling RA, Walsh DM, Selkoe DJ (*submitted*) New ELISAs with high specificity for soluble oligomers of amyloid ß-protein reveal natural Aß oligomers in human brain but not CSF. In, pp 1-53: *Submitted*.

Chapter 5

Conclusion

After decades of investigative focus on amyloid plaques, a hallmark of Alzheimer's disease (AD), findings in the past ten years have led to a conceptual shift. Accumulating evidence suggests that the insoluble amyloid fibrils that comprise plaques may not directly confer neurotoxicity, but that they sequester the soluble oligomeric forms of the amyloid β-peptide (Aβ) that potently alter synaptic structure and function. Recognition of Aβ oligomers as highly bioactive assemblies has furthered interest in detecting and analyzing soluble forms of the peptide for mechanistic, diagnostic and therapeutic purposes. Currently, virtually all treatments under development are focused on decreasing or neutralizing Aβ. Moreover, a reduced CSF level of $A\beta_{42}$ in subjects with incipient or very early AD is one of the most promising biomarkers. However, despite the therapeutic and diagnostic focus on the dyshomeostasis of Aβ, we still lack insight into the *in vivo* economy of Aβ in the brain. Thus, my thesis work focused on understanding the dynamics of Aβ in a living brain during the development of AD-type pathology. The first half of my thesis aimed at gaining insight into the dyhomeostasis of Aβ as plaques accrue in brain parenchyma. The second half of my thesis focused on deciphering the fate of Aβ once it is released into the extracellular space.

In order to gain insight into the dynamics of Aβ that remains diffusible in the extracellular space *in vivo*, I sampled by microdialysis the hippocampal interstitial fluid (ISF) of awake and behaving hAPP transgenic mice. *First*, I found that the Aβ species that remained soluble, diffusible, and of < 35 kDa molecular weight (MW) in the ISF *in vivo* (termed ISF Aβ herein) were composed of $A\beta_{38}$,

$A\beta_{39}$, $A\beta_{40}$, and $A\beta_{42}$ (relative abundance: $A\beta_{40}$ >> $A\beta_{38}$, $A\beta_{42}$ >> $A\beta_{39}$). Interestingly, the ISF Aβ contained species of two distinct MWs: 4 kDa (corresponding to the MW of Aβ monomers; ~60% of ISF Aβ) and a novel 5 kDa species (~40% of ISF Aβ). Acute inhibition of γ-secretase in young transgenic mice led to a rapid fall of the ISF Aβ captured in microdialysates ($t_{1/2}$ of fall ~2 h), showing that most of the ISF Aβ sampled by microdialysis represented newly synthesized APP cleavage products.

Second, in order to understand the dyshomeostasis of Aβ during development of AD-type pathology, I sampled ISF of hAPP transgenic mice from three age groups: before (3 mo), during (12 mo), and after (24 mo) plaque deposition. I found that Aβ levels in the most soluble compartment (the ISF) declined significantly as mice underwent progressive parenchymal deposition of Aβ (from 1.2 nM [ISF Aβ] in pre-plaque 3 mo to 0.5 nM [ISF Aβ] in plaque-rich 24 mo). Among the ISF Aβ peptides measured, $A\beta_{42}$ decreased the most; in accord, $A\beta_{42}$ rose the most in the brain parenchyma, in keeping with its documented primary role in oligomerization and plaque formation. Using the interpolated zero-flow method of microdialysis, I observed similar % recovery of microdialyzable Aβ at both 3 mo and 24 mo transgenic, which indicated that the age-dependent decrease in ISF Aβ was not due to technical issues with the microdialysis system. Furthermore, neither the lactate-to-pyruvate ratio (an established marker of the redox state of cells) nor the level of glycerol (an integral component of cellular membranes for which changes in ISF levels may reflect

degradation of membranes) in the ISF changed significantly between 3 mo and 24 mo in the APP transgenic mice, suggesting that the decrease in ISF Aβ was not associated with altered intermediary metabolism or perturbation of cell membrane integrity. The levels of full-length APP and their C-terminal fragments generated by α- and β-secretases were constant between 3 mo and 24 mo, indicating that the fall in ISF Aβ was not likely due to a decrease of cellular production of Aβ. Hence, I obtained no evidence that decreased neuronal activity, decreased Aβ production, or altered spontaneous behavior (eating, exploring, grooming, etc.) in the mice explains the drop in soluble ISF Aβ as mice accrue amyloid deposits.

Rather, the decrease in steady-state ISF Aβ occurred simultaneously with rises of insoluble Aβ in the brain parenchyma (i.e., Aβ obtained in the SDS- and formic acid-extractable pools of brain homogenates). In order to mimic new Aβ production and monitor its fate, I administered soluble radiolabeled Aβ at physiological concentrations directly into the ISF. In plaque-rich (24-27 mo transgenic) mice, the acutely injected radiolabeled Aβ became rapidly less diffusible and more associated with the loosely membrane-bound (i.e., saline-extractable) pool, as compared to the radiolabeled Aβ injected into the ISF of plaque-free (3-7 mo transgenic) mice. The distinct disposition of the radiolabeled Aβ in plaque-rich vs. plaque-free mice suggested that in plaque-rich mice, cerebral amyloid deposits rapidly sequester newly released Aβ, thereby accounting for the lower steady-state level of Aβ in the ISF. Taken together, the

studies of the steady-state ISF Aβ and the fate of radiolabeled Aβ before vs. after plaque initiation provide, for the first time, *in vivo* evidence from controlled animal experiments for the hypothesis that soluble $A\beta_{42}$ in human CSF falls because it is sequestered into insoluble parenchymal deposits as AD develops.

The association of Aβ with the insoluble deposits may not be irreversible, however, because when I acutely inhibited γ-secretase *in vivo* in plaque-rich mice, this failed to lower ISF $A\beta_{42}$ (whereas ISF $A\beta_{38}$ and $A\beta_{40}$ fell rapidly ($t_{1/2}$ ~1.9 h and ~2.3 h, respectively)). As $A\beta_{42}$ is the species reported to accumulate much more into insoluble plaques than $A\beta_{38}$ and $A\beta_{40}$ in both AD patients and APP transgenic mice, this result suggests that most of the soluble $A\beta_{42}$ peptide that populates the ISF in plaque-rich mice is not derived primarily from new Aβ biosynthesis but rather from the large reservoir of $A\beta_{42}$ deposited in the brain parenchyma. This concept is consistent with earlier reports that amyloid plaques in APP transgenic mice appear to act as a local reservoir of "loosely-associated" Aβ that can diffuse from plaques. Hence, whereas the ISF of young, plaque-free mice acts as a reservoir for mainly the acute cellular production of Aβ, ISF in plaque-rich mice seems to be a reservoir for both new Aβ production and Aβ that diffuses off of membrane- and plaque-bound deposits.

The above results (along with some biochemical characterization of saline-extractable brain Aβ suggesting that aqueous extracts do not contain the truly diffusible Aβ species *in vivo* as thought heretofore) were published in the *Journal of Neuroscience* on November 2, 2011.

Finally, I showed that Aβ dimers, which are known to be potent synaptic neurotoxins, are undetectable in the aqueous compartments of the central nervous system, i.e., the brain ISF and the cerebrospinal fluid (CSF), as they are rapidly sequestered away from the aqueous pool to lipid membranes, where they bind to GM1 ganglioside and/or Prion protein. One interesting observation made in my earlier work was that in ISF from more than 25 hAPP transgenic mice, Aβ dimers were not detected by the immunoprecipitation (IP)-Western blotting (WB) technique, regardless of the age of mice or their extent of plaque deposition (i.e., even when dimers can be found in the saline extracts of their brain homogenates). I found this particularly interesting, as Aβ dimers are currently thought to be the earliest oligomeric assembly that exerts synaptotoxic effects. Using a test tube version of microdialysis, I verified that Aβ dimers (~8 kDa MW) indeed crossed over the 35 kDa MW cutoff membrane that I use for *in vivo* brain microdialysis. Therefore, I wanted to explore whether Aβ dimers cannot exist as free entities in the ISF; rather, due to their increased hydrophobicity, the dimers bind to membranes, pre-existing aggregates or other potential binding partners much more rapidly than monomers do. This could explain why dimers, but not monomers, are thought to be the earliest synaptotoxic assembly forms of Aβ.

I first confirmed that Aβ dimers were indeed undetectable in the brain fluid compartments using young hAPP transgenic mice, which should contain abundant levels of soluble Aβ. To ensure that the apparent lack of oligomers in ISF samples was not simply due to ineffective passage of the ~8 kDa dimers and

any other LMW oligomers across the 35 kDa MWCO membrane, I also collected CSF from the cisterna magna. Using three biochemical methods, IP-WB, an Aβ oligomer-specific ELISA, and a non-denaturing size-exclusion chromatography (SEC), I failed to observe any Aβ oligomers in the hippocampal ISF or CSF from hAPP transgenic mice.

Next, I used *in vitro* (test tube) microdialysis to establish conditions in which dimers and monomers have similar % crossover efficiency. I found that at a five-fold higher concentration as that of monomers, dimers crossed over the microdialysis membrane with similar efficiency as the monomers. I verified that the Aβ recovered in the microdialysates indeed reflected their starting material throughout the time of my analysis; i.e., the microdialysate recovered from starting material that contained mostly dimers was in fact principally dimers and stayed as such, and those recovered from monomer-containing material stayed as monomers. Having established conditions where comparable % Aβ crossover efficiencies could be achieved *in vitro*, I next examined the half-life of acutely administered synthetic dimers vs. monomers in hippocampal ISF *in vivo*. I injected synthetic Aβ of human sequence into the ISF of wild-type (wt) mice to distinguish between the acutely administered human Aβ and endogenously secreted mouse Aβ. I found that acutely administered dimers were much more rapidly sequestered away from the hippocampal ISF pool *in vivo*: in just one hour, Aβ dimers showed ~8.5-fold less recovery when injected into the ISF than did Aβ monomers. Accordingly, the injected Aβ dimers were recovered at higher

proportions in the membrane-bound pool than in the cytosolic pool, suggesting that Aβ dimers (versus monomers) quickly bind membranes. When I spiked the dimers into TBS extracts of wt mice *ex vivo* and performed SEC using a Superdex 75 SEC column, I observed an immediate shift of its elution profile from the dimer (~ 8 kDa) fractions to the void volume fractions (i.e., > 70 kDa). Dimers spiked into buffer alone eluted at the expected dimer position, arguing against mere aggregation of the Aβ. Thus, I suspected whether Aβ could be binding to lipid membranes, and whether the dimers have a higher affinity for them. As a direct *in vitro* measurement of binding affinities, I recently began surface plasmon resonance experiments on chips coated with lipid bilayer membranes. Preliminary results indicate that Aβ dimers may in fact have an enhanced affinity to the lipid membrane than do the monomers; however, the experiments need to be repeated.

Interestingly, the injected Aβ (both the synthetic Aβ dimers and the natural Aβ dimers isolated from human AD cortical tissue) were now recovered as monomers. Furthermore, the Aβ recovered in the membrane-bound fractions were found to be tightly associated to endogenous GM1 ganglioside (and hence migrating ~5 kDa) and Prion protein. I found that the endogenous Aβ in the membrane-bound fractions of young hAPP transgenic mice were also tightly bound to GM1 ganglioside and that these GM1 ganglioside-bound Aβ were associated with Prion protein. Further experiments will be necessary to determine which of these two molecules, the GM1 ganglioside and Prion protein,

acts the primary binding site that mediates Aβ's notorious synaptotoxic offense and which may be the accomplice.

In summary, my studies show that upon plaque accumulation, the dynamics of Aβ are altered, and that Aβ dimers, and probably higher oligomers, do not exist in the aqueous brain compartments but instead are rapidly sequestered away from the ISF and bind to GM1 ganglioside- and Prion protein-enriched lipid membranes.

Appendix 1

Disrupting the *in vivo* economy of amyloid β in an intact living brain of APP transgenic mouse using antibodies against the amyloid β-peptide

Contributions to this Appendix:

Experiments were designed by Soyon Hong and Dennis Selkoe. ELISAs and Western blotting experiments were performed by Beth Ostaszewski and Soyon Hong. All other experiments were performed by Soyon Hong.

Introduction

A project I have started but suspended at this time relates to the question of how two antibodies against β-amyloid (Aβ) that are currently in Phase 3 clinical trials alter Aβ equilibrium in an intact living brain. One antibody is against the free N-terminus of Aβ (the 3D6 antibody) and the second antibody is against the mid-region of Aβ (the 266 antibody); both are delivered to patients with Alzheimer's disease (AD) by passive intravenous infusion. Initially, I injected intraperitoneally each of these antibodies into pre-plaque (3 mo) or plaque-rich (24 mo) APP transgenic (tg) mice and asked whether the quantity and quality of the most soluble Aβ species in the interstitial fluid (ISF) (sampled by microdialysis) changed before vs. after the antibody injection.

Currently, there are more than 13 active clinical immunotherapy trials in patients with mild to moderate AD aimed at lowering the total Aβ burden in the central nervous system (CNS) (Lemere and Masliah, 2010). Multiple passive immunotherapy studies using mouse models of AD have successfully shown that anti-Aβ antibodies promote plaque clearance in the CNS and subsequent neuronal and behavioral rescue (for e.g., Schenk et al., 1999; Bard et al., 2000; DeMattos et al., 2001; Dodart et al., 2002; Brendza et al., 2005). There are three proposed mechanisms behind passive immunization: direct resolution, microglial-cell mediated, and peripheral sink hypothesis (Solomon et al., 1996; Bard et al., 2000; Dematttos et al., 2002; Weiner and Frenkel, 2006). 3D6 (directed against 1-5 of Aβ) is among the most effective antibodies studied, especially in binding

and triggering the clearance of plaques (Bard et al., 2003). Fc-mediated microglial phagocytosis of Aβ, together with the direct resolution against the Aβ fibrils, has been suggested as the primary mechanism for the 3D6 antibody-mediated plaque clearance. The 266 antibody (directed against 16-23 of Aβ) has been found to effectively induce behavioral improvements in 11 mo to 24 mo PDAPP tg mice, but without lowering the Aβ plaque burden in the brain. Interestingly, a single dose of 266 antibody effectively reversed learning impairments in the 12 mo PDAPP mice in a time period as short as 24 h (Dodart et al., 2002). As Aβ-266 antibody complexes were found in both CSF and plasma but the total Aβ plaque burden seemed unperturbed (even in the subchronic weekly treated mice for up to 6 months), the primary mechanism suggested for the 266 antibody was the peripheral sink, i.e., the 266 antibody sequestered the free Aβ in the plasma and thereby shifted the Aβ equilibrium, continuously pulling the Aβ from the CNS (Demattos et al., 2002; Dodart et al., 2002).

Here, we hypothesize that the 3D6 antibody primarily binds aggregated Aβ, i.e., Aβ deposited onto the brain parenchyma, and works to dissolve the plaques, ultimately leading to an altered dynamics in the CNS. We therefore hypothesize to observe a short initial fall in the ISF Aβ levels (as the 3D6 antibody may at first directly sequester the available $A\beta_{1-x}$ species in the ISF pool), then a prolonged rise (as over time, the 3D6 antibody may directly resolve the aggregated Aβ fibrils, hence releasing more Aβ into the ISF). On the other hand, the 266

antibody may only sequester the immediately available soluble pool, i.e., the ISF, but may not be able to dissolve the plaques directly (as the epitope for 266, the mid-region of Aβ, may be hidden in fibrils).

The specific questions we aim to address here are: (1) what are the acute effects that an anti-Aβ antibody administration has on steady-state brain ISF Aβ? To this end, we aim to monitor pre- and post-injection ISF Aβ levels and measure other non-Aβ analytes present in the ISF; (2) how does the presence of plaques influence such effects? To this end, we will use two ages of the J20 tg mice: ~3 mo which are virtually free of plaques, and ~24 mo which are plaque-rich (see Chapter 2); (3) how specific are the effects to the 3D6 or 266 antibody? To this end, we will administer mice with vehicle alone or IgG isotype control. In addition, we may use a different monoclonal anti-Aβ antibody that recognizes a distinct epitope from 3D6 and 266 (for e.g., antibodies directed against the C-termini of Aβ, the 2G3 (against $Aβ_{31-40}$) or 21F12 (against $Aβ_{33-42}$)); and (4) can we gain insight into the main mechanism(s) at play? To understand whether the increase or decrease of ISF Aβ is due to an alternate source other than manipulation of the acute APP processing process (i.e., Aβ production), we will treat mice with Compound E, a potent γ-secretase inhibitor which decreases ISF Aβ levels with $t_{t/2}$ ~2 h (see Chapter 2). To see whether direct resolution is at play, we could attempt *in vitro* microdialysis using different brain pools (TBS or SDS extracts). We will also perform immunohistochemistry against CD-45, Iba-1, or GFAP to see the effect a single dose injection may have on microglial and astrocytic

activation. Finally, we can also measure Aβ levels in blood before and after injection to see to what extent Aβ levels in plasma are altered and how these levels correlate with the brain ISF Aβ levels.

Results and Discussion

Levels of ISF Aβ were monitored for 72 hours before injection of the antibody. It took ~12 hours for the levels of ISF Aβ to stabilize after initiation of microdialysis, but then ISF Aβ stayed stable (Figure A1.1). Therefore, in all experiments, we waited 36-48 hours after microdialysis was initiated in the mice and confirmed that their ISF levels were stable for at least 24 hours before injecting the antibodies.

Next, pre-plaque (3-4 mo tg) mice were given intraperitoneal injections of the 3D6 antibody at 5 mg/kg and their Aβ levels in ISF were monitored until day 8 post injection using the 6E10 Aβ triplex ELISA. Within 48 hours of injection (injection performed at day 0), the levels of all three peptides, i.e., $A\beta_{38}$, $A\beta_{40}$ and $A\beta_{42}$, rose rapidly to a two-fold and continued to slightly increase until day 4 post injection, upon which the enhanced levels seemed to stabilize (Figure A1.2A). Interestingly, the degree to which Aβ levels rose was the least for $A\beta_{42}$, as compared to $A\beta_{38}$ and $A\beta_{40}$. To see whether these effects were distinct in the presence of plaques, the 3D6 antibody was administered to plaque-rich (26-28 mo tg) mice and their ISF levels were collected before and after the 3D6 injection. Similar to the observation made in pre-plaque mice, the levels of $A\beta_{38}$ and $A\beta_{40}$

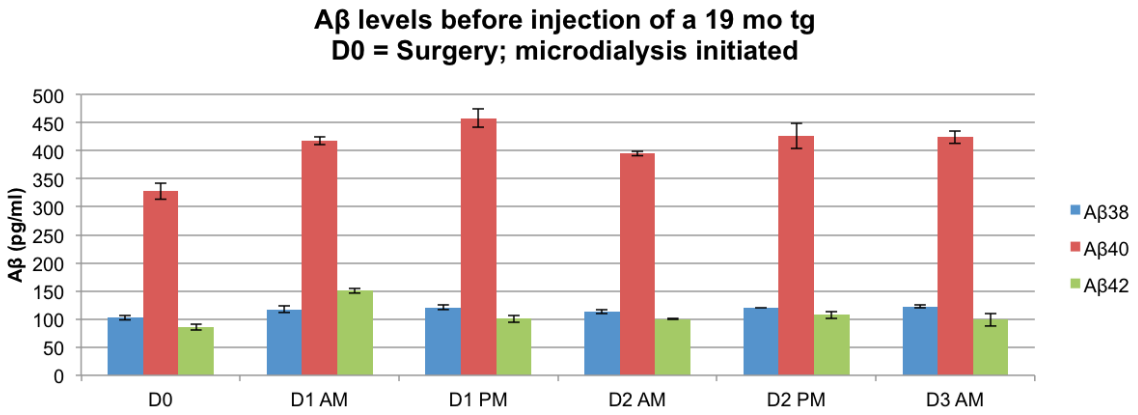

Figure A1.1. There is little fluctuation in the levels of ISF Aβ from 12th hour onwards after microdialysis is initiated.

A representative figure showing the levels of ISF Aβ immediately following microdialysis, as measured by the 6E10 Aβ triplex ELISA.

rose steadily until day 4 post injection, albeit more slowly than the rate at which these two peptides rose in the pre-plaque brain (Figure A1.2B). The peptides then seemed to either stabilize or rise slightly. Interestingly, $A\beta_{42}$ peptide behaved exceptionally in the plaque-rich mice: $A\beta_{42}$ barely rose until day 8 following the 3D6 administration (Figure A1.2B). We measured the ISF Aβ levels with another ELISA, which uses antibodies that recognize different epitopes of Aβ (the 266/3D6B or more commonly known as the $A\beta_{1\text{-}x}$ ELISA), and confirmed that the readout by the $A\beta_{1\text{-}x}$ ELISA was comparable to the readout given by the 6E10 Aβ triplex ELISA (Figure A1.3). By IP-WB, we did not see any significant changes in the molecular composition of ISF Aβ collected between days 4 and 5 of 3D6 administration, i.e., the ISF Aβ seemed to have similar degrees of both 4 and 5 kDa Aβ-immunoreactive species (as pulled out by the AW8 Aβ antisera) (Figure A1.4) as the ISF Aβ from mice that did not receive an antibody injection (see Chapter 2). Likewise, we saw similar levels of increase in $A\beta_{38}$, $A\beta_{40}$ and $A\beta_{42}$ in SEC fractions that correspond to monomers and the 5 kDa species (data not shown). The rise of ISF Aβ we observed in the microdialysates was not due to IgG interfering with the ELISA itself, as (1) IgGs are not expected to cross over the 35 kDa MWCO membrane and therefore will be absent in the microdialysates; and (2) even if they may cross over into the microdialysate, the IgG may interfere with the ELISA by reducing the total Aβ reading (and not by increasing it) (Figure A1.5A). To determine whether the increase of ISF Aβ was due to increased APP processing (i.e., increased Aβ production), we

A

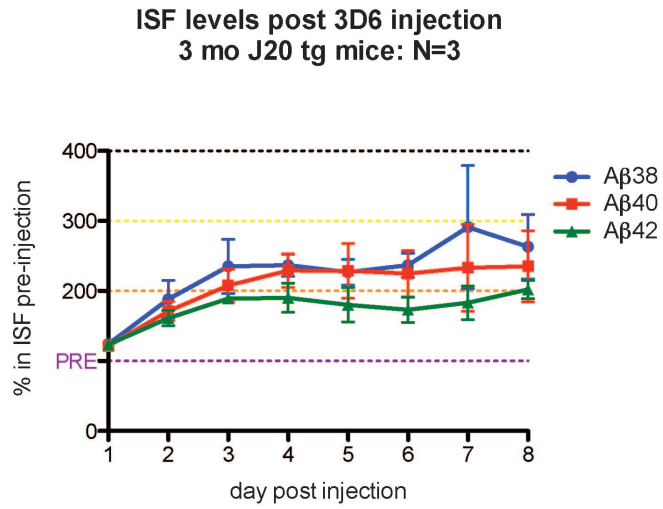

B

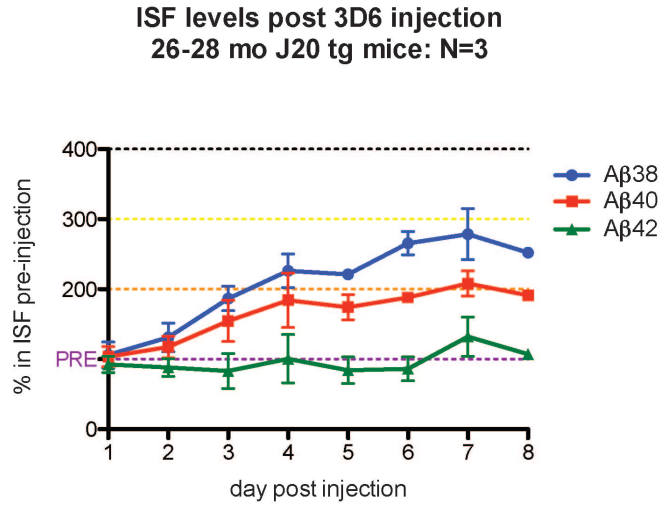

Figure A1.2. A single injection of the 3D6 antibody leads to prolonged increased levels of ISF Aβ in both plaque-free (3 mo) and plaque-rich (26-28 mo) J20 tg mice, with exception for $A\beta_{42}$ in the plaque-rich mice.

ISF Aβ levels in (A) pre-plaque 3-4 mo tg (N=3 mice) and (B) plaque-rich 26-28 mo tg (N=3 mice) before and after 3D6 intraperitoneal administration.

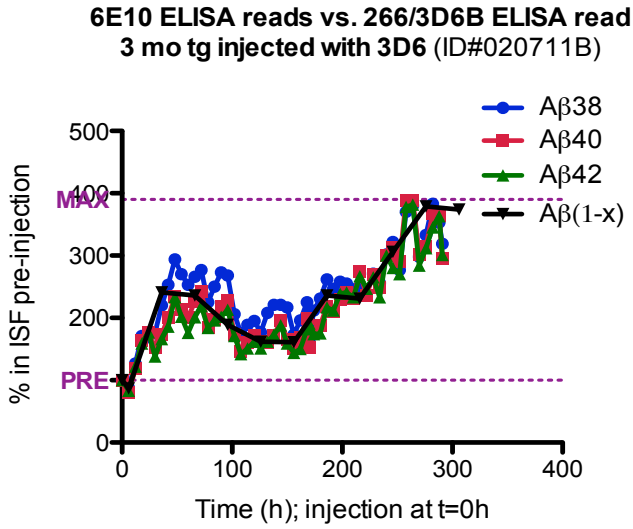

Figure A1.3. Levels of $A\beta_{1-x}$ rise in the ISF of mice injected with the 3D6 antibody.

A representative figure showing the ISF Aβ levels in a 3 mo tg after 3D6 antibody injection. Black line: $A\beta_{1-x}$ levels, as read by the 266/3D6B ELISA; blue, red and green lines: $A\beta_{x-38}$, $A\beta_{x-40}$ and $A\beta_{x-42}$ levels, respectively, as read by the 6E10 Aβ triplex ELISA.

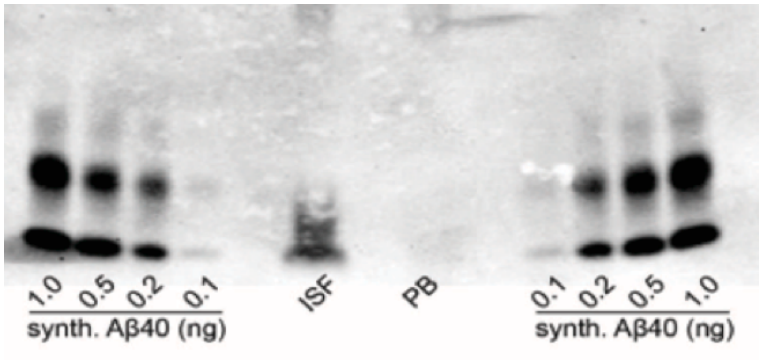

Figure A1.4. ISF Aβ is separated to 4 kDa and 5 kDa species by SDS-PAGE.

500 µl of perfusion buffer (PB) and 500 µl of ISF collected on days 4 and 5 post-3D6 injection were IP'ed with AW8 (1:100) and subjected to denaturing SDS-PAGE. Synthetic $A\beta_{40}$ were loaded as control. WB: 6E10, 2G3 and 21F12.

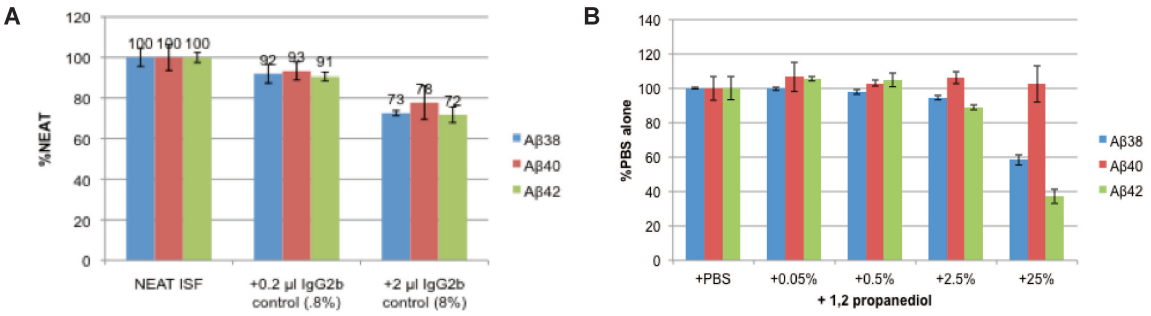

Figure A1.5. IgGs and 1,2-propanediol may interfere with the 6E10 Aβ triplex ELISA.

Different amounts of (A) IgG_{2b} or (B) 1,2-propanediol were spiked directly into the ELISA wells to determine whether they interfere with the ELISA antibodies and induce an artifactual increase in the Aβ levels obtained by the ELISA.

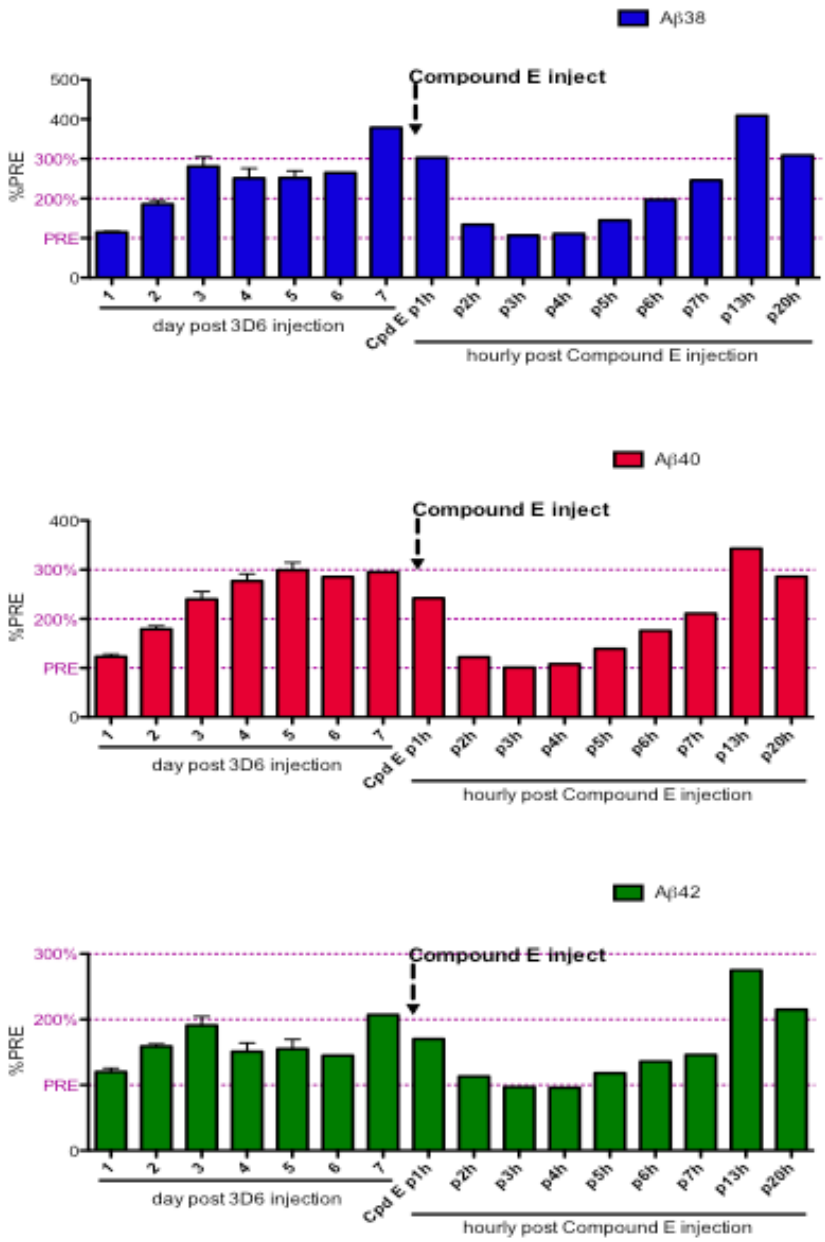

Figure A1.6. Compound E injection fails to bring the ISF Aβ levels completely down.

ISF levels from a 3 mo J20 tg, as measured by the 6E10 Aβ triplex ELISA. Day 0: 3D6 injection (5 mg/kg). Day 7: Compound E injection (10 mg/kg).

intraperitoneally injected Compound E (5-10 mg/kg) into the 3D6-injected mice. We saw that the Compound E injection decreased the ISF Aβ levels to only ~50% (Figure A1.6) (instead of the nearly complete (> 80%) decrease observed in non-3D6-injected young tg mice (see Chapter 2)), which implies that the increased levels of ISF Aβ post 3D6 administration is not due to increased Aβ production by cells, but rather due to a manipulation of an alternative source (decreased degradation of Aβ and/or dissolution of pre-existing Aβ aggregates). There seemed to have been a reset in the equilibrium between the Aβ pools that exist in ISF and brain parenchyma to give rise to an altered steady-state level.

To see whether the rise in the ISF Aβ levels were mediated by the antibody, we injected vehicle alone (which was 1,2-propanediol, a vehicle also used for the Compound E injection studies) and observed a rise in all three Aβ peptides in the ISF of both pre-plaque (Figure A1.7A) and plaque-rich (Figure A1.7B) mice; this rise was even more substantial than the rise from ISF of mice injected with 3D6 antibody (Figure A1.7: bold line). Although the vehicle injection experiment was done only in N=1 mouse each for pre-plaque and plaque-rich group, and the rise of the ISF Aβ levels upon antibody injection did not seem to be an artifact of 1,2-propanediol (as high amounts of 1,2-propanediol may lead to an artifactual decrease in Aβ ELISA values, not to an increase) (Figure A1.5B), it was clear that vehicle alone mediated a rise similar to what we observed with the 3D6 antibody. This result therefore called into question whether the rise in ISF Aβ we had upon 3D6 antibody administration was indeed mediated by the

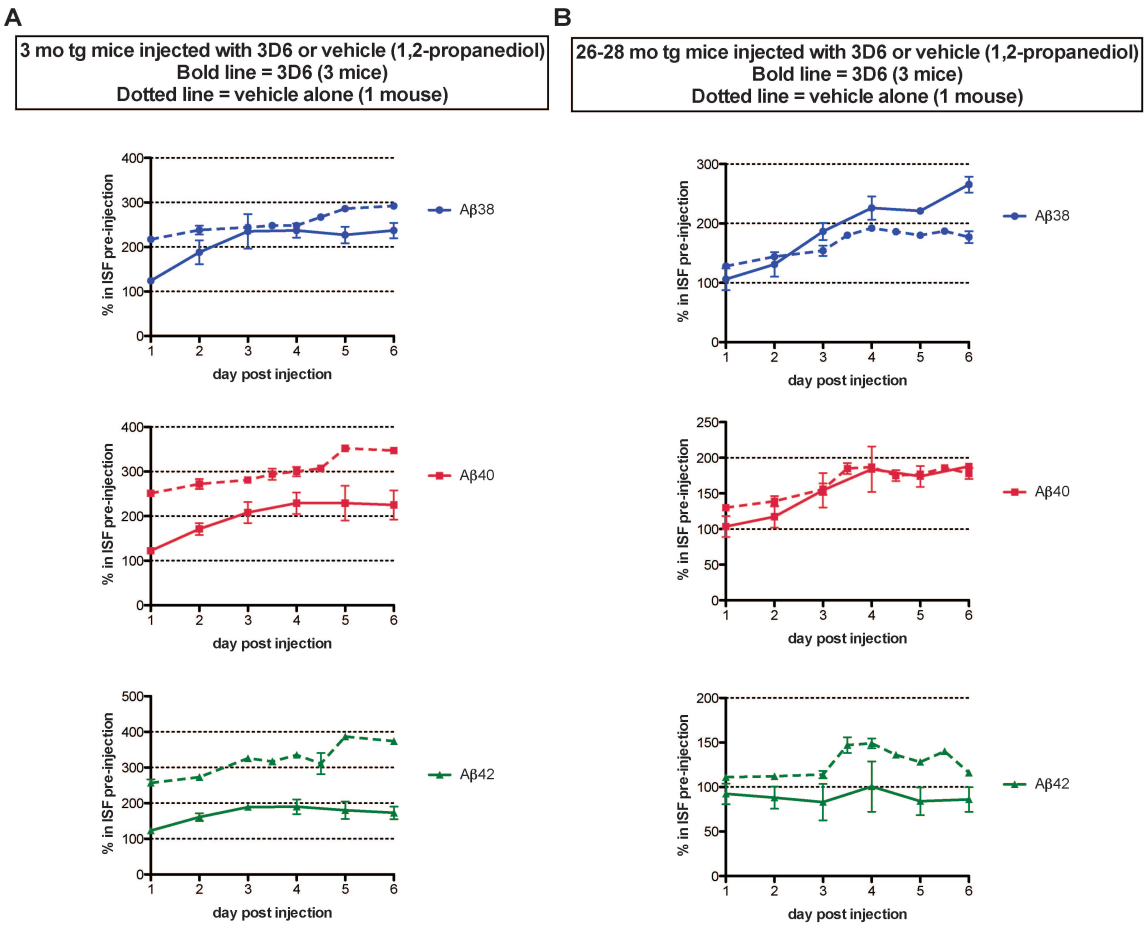

Figure A1.7. Vehicle alone (1,2-propanediol) induces an enhanced rise in levels of ISF Aβ in both pre-plaque and plaque-rich mice.

ISF levels from a 3 mo and a 26 mo J20 tg were monitored for 6 days post injection of vehicle at day 0 (1,2-propanediol:PBS 1:1). Vehicle alone induced a rise in the levels of all three $A\beta_{38}$, $A\beta_{40}$ and $A\beta_{42}$ peptides in the 3 mo tg and $A\beta_{38}$ and $A\beta_{40}$ in the 24 mo tg (and to some degree, $A\beta_{42}$).

antibody.

Next, we repeated the 3D6 antibody injection with PBS as vehicle, and compared the effects of the 3D6 on ISF Aβ with mock (no injection) or vehicle (PBS) injection (Figure A1.8A shows results in young tg (pre-plaque) and Figure A1.8B shows results in old tg (plaque-rich)). Although there was N=1 mouse for each group, it was evident that it would be challenging to distinguish antibody-mediated results above PBS injection or mock alone. We therefore determined that the current experimental paradigm would not allow for a clear interpretation of results, especially as only a single injection was given per mouse and it has been reported that a minute fraction (~0.4%) of the antibody crosses over the blood brain barrier (BBB) into the CNS. In previous Aβ antibody infusion studies with 3D6 antibody where effective plaque clearance in the brain parenchyma was noted, the hAPP tg mice received weekly treatments for at least 6 weeks to 6 months. Therefore, a single intraperitoneal administration of the antibody may not be sufficient to observe a significant change in the CNS Aβ equilibrium. Hence, I want to restart this project by directly injecting the antibodies into the hippocampal ISF through the injection cannula attached to the microdialysis probe, mimicking antibody that has already crossed the BBB. I also want to utilize a larger (100 kDa) MW cutoff microdialysis membrane. The question I will be asking then will thus be a more straightforward one: how does the Aβ antibody affect the Aβ equilibrium in an intact living brain either devoid of (3 mo tg) or enriched with (24 mo tg) amyloid plaques? Monitoring the ISF Aβ in this

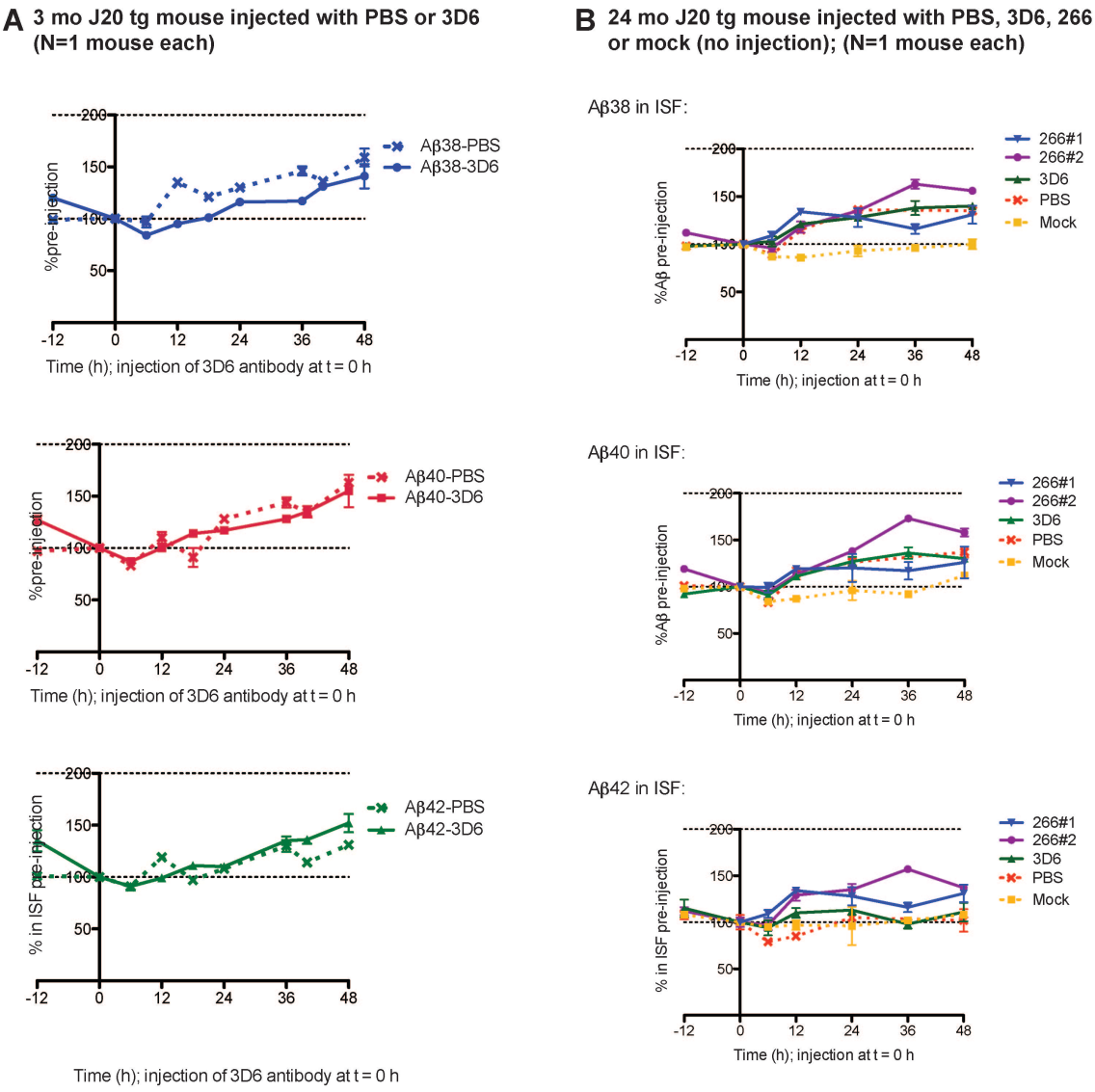

Figure A1.8. ISF Aβ levels upon PBS, mock, or antibody injection.

ISF Aβ levels were monitored up to 48 hours after PBS or 3D6 in pre-plaque young mice (A) or after PBS, 3D6, 266 or mock (no) injection in plaque-rich old mice (N=1 mouse per group).

way may give insight into the overall equilibrium maintained between the different Aβ pools in the brain and how the antibodies may alter this; e.g., by dissolution of amyloid fibrils or by direct sequestration of the soluble species. The results may help clarify the underlying mechanism of the current passive anti-Aβ immunotherapy on trials.

Materials and Methods

Two age groups of J20 tg mice, pre-plaque (3-4 mo) and plaque-rich (20-28 mo), were used in this study. The APP genotype was verified twice by PCR of genomic DNA. ISF was sampled at 0.4 µl/min with perfusate composed of 1.5% BSA in artificial cerebrospinal fluid (see Chapter 2 for composition and details in material and methods). Microdialysis was initiated in the tg mice at least 36 hours before the Aβ antibody was injected. The basal steady-state levels of Aβ in the ISF were verified using the 6E10 Aβ triplex ELISA, which captures Aβ according to their C-termini (i.e., $A\beta_{38}$, $A\beta_{40}$ and $A\beta_{42}$) and detects using the 6E10 antibody (directed against $A\beta_{5-9}$) (MesoScale Discovery). 36-48 hours after surgery and initiation of microdialysis, 3D6 antibody (IgG_{2b}; gift of Elan), 266 antibody (IgG_1; gift of Elan), 21F12 antibody (IgG_{2a}; gift of Elan), or IgG isotype control (from R&D Systems and Abcam) was administered once to the tg mice by intraperitoneal injection. The ISF microdialysates were collected hourly before and after antibody injection and the levels of Aβ were measured using the 6E10 triplex Aβ ELISA. The ISF were also analyzed for Aβ by immunoprecipitation

(IP)-Western blotting (WB), where Aβ antisera (AW8, gift of D. Walsh, BWH) was used for IP and the 6E10, 2G3 and 21F12 anti-Aβ antibodies were used for WB. Some ISF microdialysates were pooled, run on a size-exclusion chromatography (SEC) Superdex 75 HR 10/30 column, and were eluted at 0.4 ml/min in 50 mM ammonium acetate, pH 8.5. The subsequent 1-ml fractions were promptly lyophilized, then assayed for Aβ38, Aβ40 and Aβ42 using the 6E10 Aβ triplex ELISA.

References

Bard F et al. (2003) Epitope and isotype specificities of antibodies to beta -amyloid peptide for protection against Alzheimer's disease-like neuropathology. Proc Natl Acad Sci U S A 100:2023-2028.

Bard F et al. (2000) Peripherally administered antibodies against amyloid beta-peptide enter the central nervous system and reduce pathology in a mouse model of Alzheimer disease. Nat Med 6:916-919.

Brendza RP, Bacskai BJ, Cirrito JR, Simmons KA, Skoch JM, Klunk WE, Mathis CA, Bales KR, Paul SM, Hyman BT, Holtzman DM (2005) Anti-Abeta antibody treatment promotes the rapid recovery of amyloid-associated neuritic dystrophy in PDAPP transgenic mice. J Clin Invest 115:428-433.

Demattos R, Bales K, Cummins D, Paul S, Holtzman D (2002) Brain to Plasma Amyloid-beta Efflux: a Measure of Brain Amyloid Burden in a Mouse Model of Alzheimer's Disease. Science 295:2264.

DeMattos RB, Bales KR, Cummins DJ, Dodart JC, Paul SM, Holtzman DM (2001) Peripheral anti-A beta antibody alters CNS and plasma A beta clearance and decreases brain A beta burden in a mouse model of Alzheimer's disease. Proc Natl Acad Sci U S A 98:8850-8855.

Dodart J-C, Bales KR, Gannon KS, Greene SJ, DeMattos RB, Mathis C, Delong CA, Wu S, Wu X, Holtzman DM, Paul SM (2002) Immunization reverses memory deficits without reducing brain Abeta burden in Alzheimer's disease model. Nat Neurosci 5:452-457.

Lemere CA, Masliah E (2010) Can Alzheimer disease be prevented by amyloid-beta immunotherapy? Nat Rev Neurol 6:108-119.

Schenk D et al. (1999) Immunization with amyloid-beta attenuates Alzheimer-disease-like pathology in the PDAPP mouse. Nature 400:173-177.

Solomon B, Koppel R, Hanan E, Katzav T (1996) Monoclonal antibodies inhibit in vitro fibrillar aggregation of the Alzheimer beta-amyloid peptide. Proc Natl Acad Sci USA 93:452-455.

Weiner HL, Frenkel D (2006) Immunology and immunotherapy of Alzheimer's disease. Nat Rev Immunol 6:404-416.

Appendix 2

Co-immunoprecipitation studies using saline extracts of Alzheimer's disease human brains do not show a specific binding of Aβ to apolipoprotein E or apolipoprotein J over GAPDH or β-tubulin

Contributions to this Appendix:

Experiments were designed by Soyon Hong and Dennis Selkoe. Western blotting was performed by Beth Ostaszewski and Daniel Podlisny. Size-exclusion chromatography was performed by Daniel Podlisny and Soyon Hong.

Introduction

The β-amyloid peptide (Aβ) in saline (TBS) extracts of human brains of Alzheimer's disease (huAD) and hAPP transgenic (J20) mice appears to be a > 500 kDa complex in non-denaturing conditions (see Chapter 3) (Shankar et al., 2008; Hong et al., 2011). We wondered whether the Aβ is in a complex with specific proteins. We decided to take a candidate-based approach: we wanted to see whether the two proteins that have been shown to bind Aβ, the Apolipoprotein E (ApoE) (Näslund et al., 1995) and Apolipoprotein J (ApoJ), which is also known as clusterin (Ghiso et al., 1993), are solely responsible for mediating the Aβ to run as a > 500 kDa. First, we checked whether endogenous ApoE and ApoJ from huAD TBS extract are co-eluted in the void volume fractions where the soluble Aβ is eluted. Next, we used co-immuoprecipitation (co-IP) methods to verify whether Aβ in the huAD TBS extract is specifically bound to ApoE and ApoJ.

Results and Discussion

First, we performed non-denaturing size-exclusion chromatography (SEC) by loading the TBS extract from huAD brain homogenate onto a Superdex 200 SEC column. Fractions were eluted at 0.5 ml/min in 50 mM ammonium acetate, pH 8.5. The fractions that correspond to the void volume fractions (> 500 kDa) were immediately lyophilized upon elution. The fractions were then straight-

loaded onto denaturing SDS-PAGE, and subsequently Western blotted for Aβ, ApoE, and ApoJ (Figure A2.1). Figure A2.1A shows the SEC elution profile of synthetic Aβ off the column and Figure A2.1B shows the elution profile of soluble Aβ from huAD TBS extract. The SEC elution profile of the human AD brain-derived soluble Aβ is distinct from the elution profile of the synthetic Aβ (red arrows indicate the fractions where synthetic Aβ were eluted using this column). Next, we blotted the fractions for ApoE (Figure A2.1C: red arrow indicates where the ApoE is expected to run; boxed areas are where Aβ immunoreactivity was the strongest on this blot) and ApoJ (Figure A2.1D; red arrow indicates where the ApoJ is expected to run). Therefore, endogenous ApoE and ApoJ from huAD brain TBS extracts were co-eluted with Aβ in the void volume fractions of Superdex 200 SEC column.

Next, we performed co-IP experiments to see whether ApoE and ApoJ are specifically bound to Aβ. TBS extracts of huAD brain were IP'ed for Aβ using R1282 antiserum, then the immunoprecipitates were washed and loaded onto denaturing SDS-PAGE. The R1282 antibody brought down ApoE in a concentration-dependent manner, whereas the pre-immune sera failed to do so (Figures A2.2A and B). Furthermore, the R1282 antibody failed to pull down any ApoE in human brain extracts that had little or no Aβ (an AD brain that contained minute amount of Aβ and a non-AD control brain that carried undetectable levels of Aβ) (Figures A2.2C and D). ApoJ was also brought down with Aβ, in an apparent Aβ-specific and concentration-dependent manner (Figures A2.2E and

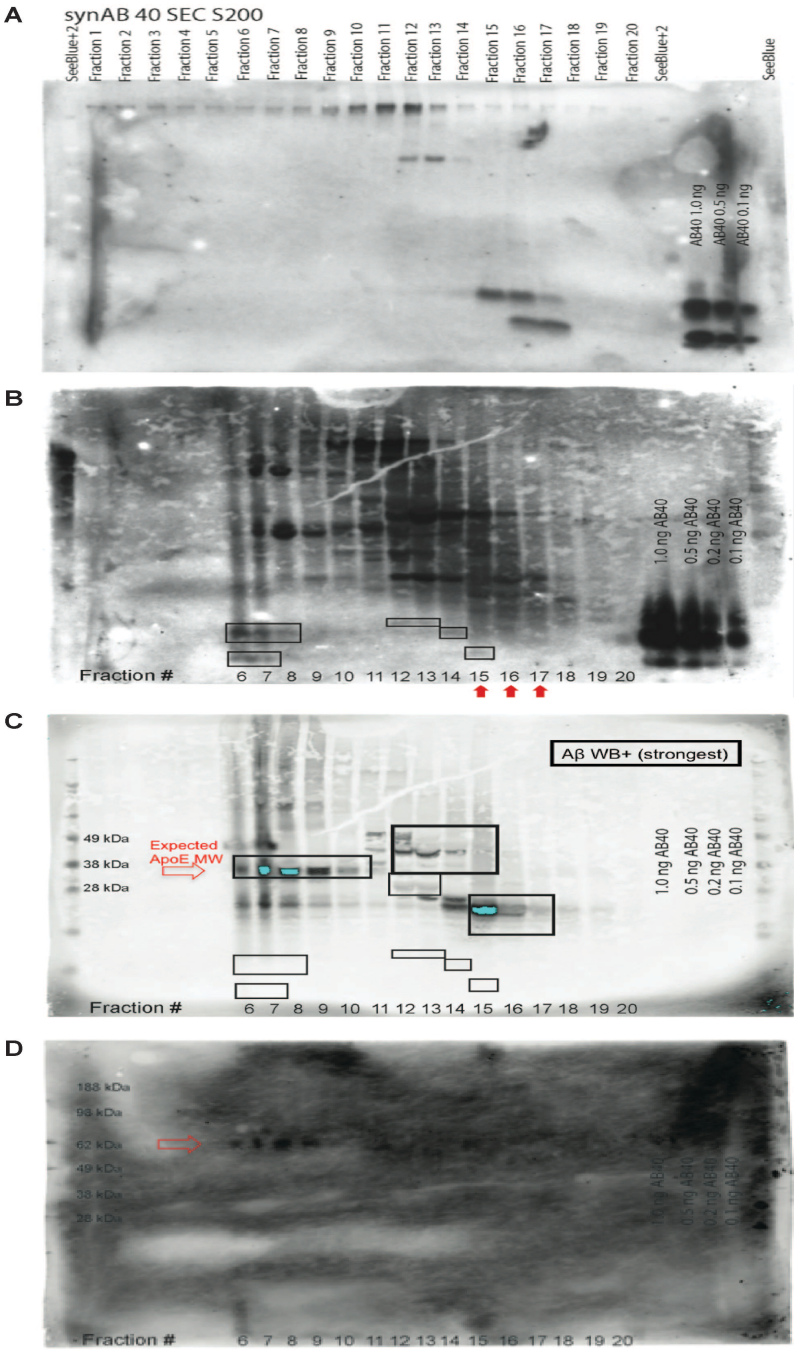

Figure A2.1. Endogenous ApoE and ApoJ in huAD TBS extracts are co-eluted with Aβ in the void volume fractions of Superdex 200 SEC column.

(A) SEC elution profile of synthetic Aβ. WB: 3D6. (B-D) SEC elution profiles of (B) Aβ (WB: 3D6), (C) ApoE, and (D) ApoJ from huAD brain TBS extract.

Figure A2.2. ApoE and ApoJ are co-immunoprecipitated with Aβ from the huAD TBS extracts.

(A-B) The R1282 Aβ antisera brought down ApoE, whereas the pre-immune sera failed to do so. (A) ApoE WB; (B) Aβ WB.

(C-D) The R1282 Aβ antisera pulled out little ApoE from TBS extacts of an AD brain that did not have much Aβ and a non-AD control human brain. (C) ApoE WB; (D) Aβ WB. Red arrows indicate ApoE-immunoreactive band and green arrows indicate Aβ-immunoreactive bands.

(E-F) Likewise, the R1282 Aβ antisera brought down ApoJ, whereas the pre-immune sera failed to do so. (E) ApoJ WB; (F) Aβ WB. Red arrows indicate ApoJ-immunoreactive band and green arrows indicate Aβ-immunoreactive bands.

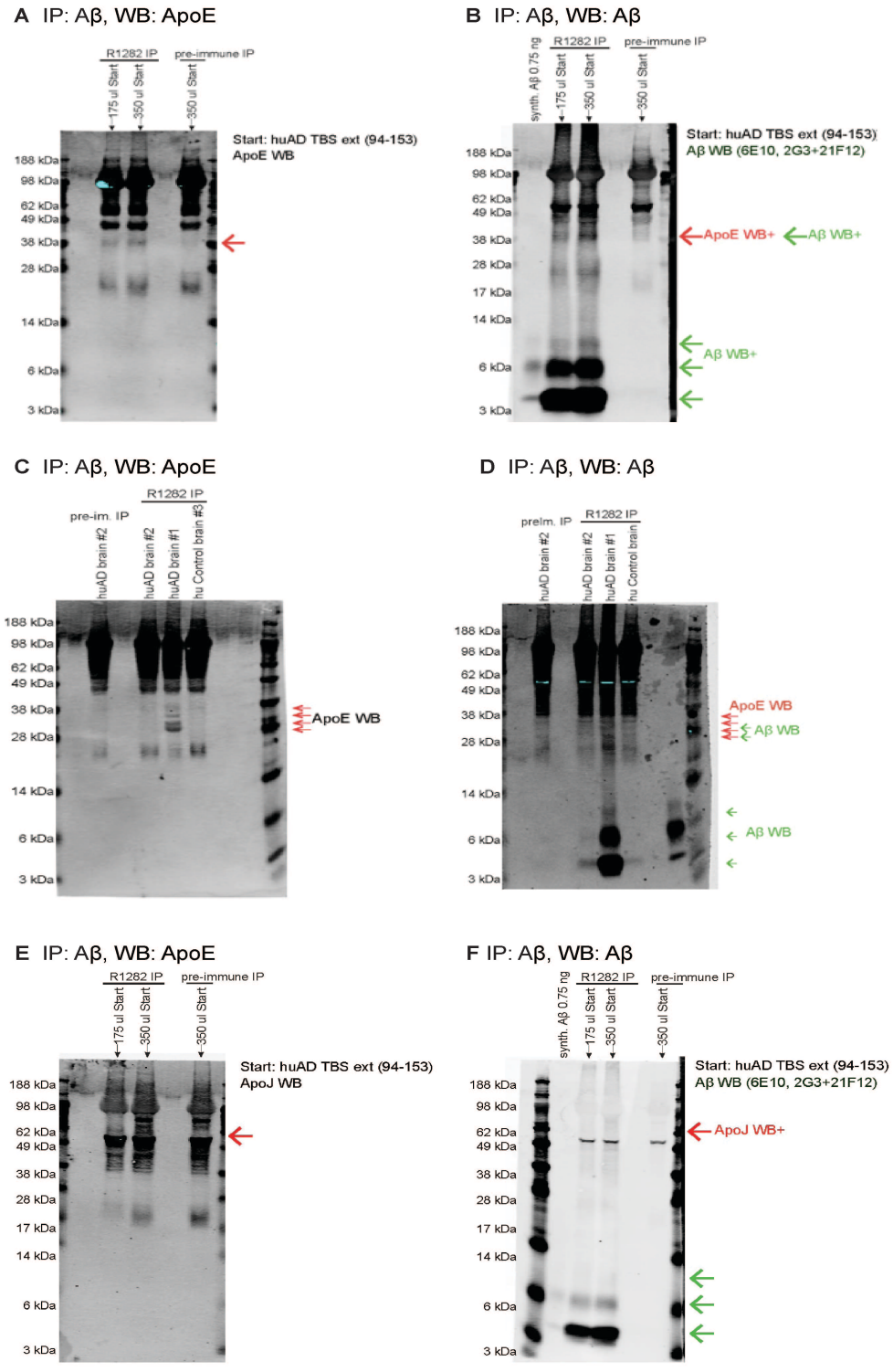

Figure A2.2 (Continued). ApoE and ApoJ are co-immunoprecipitated with Aβ from the huAD TBS extracts.

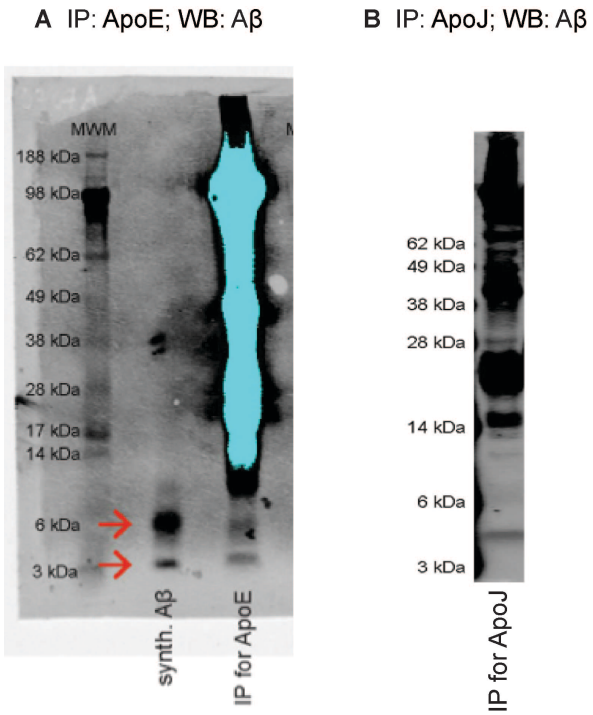

Figure A2.3. Pulling down for ApoE and ApoJ also brings down Aβ.

IP'ing huAD TBS extract for ApoE (A) or ApoJ (B) brought down Aβ. Synthetic Aβ loaded as control. Aβ WB (6E10, 2G3 and 21F12).

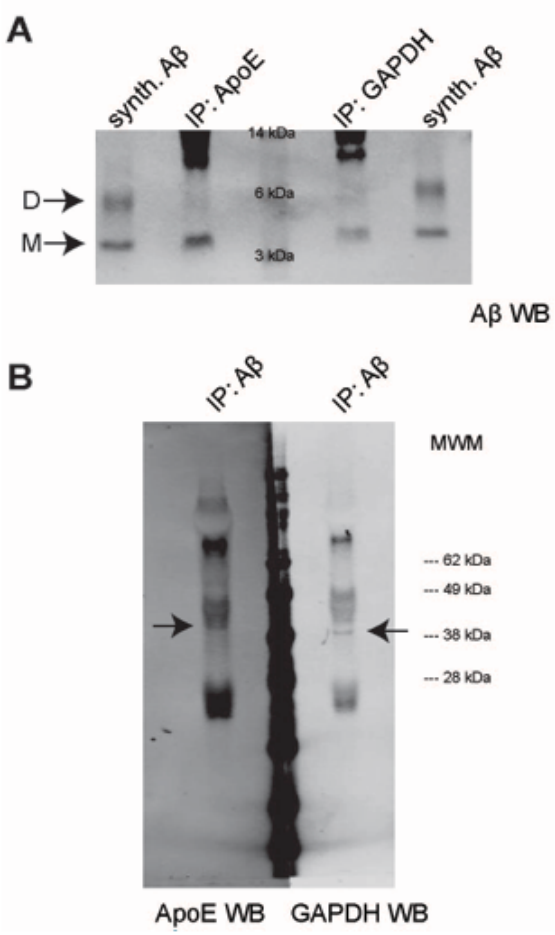

Figure A2.4. GAPDH is also co-immunoprecipitated with Aβ.

(A) IP'ing for GAPDH also brought down Aβ. Aβ WB (6E10, 2G3 and 21F12). D: Aβ dimers, M: Aβ monomers. (B) R1282 Aβ antisera pulled down GAPDH (right WB), albeit less efficiently than it did ApoE (left WB). Arrows point to ApoE and GAPDH.

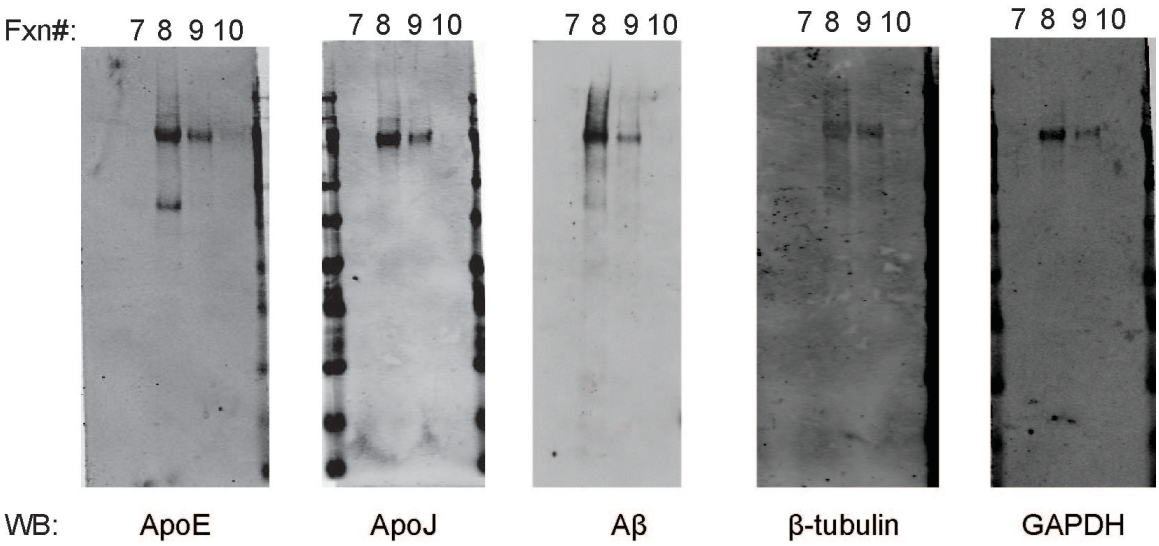

Figure A2.5. GAPDH and β-tubulin are also eluted together with ApoE, ApoJ and Aβ in the void volume fractions of the Superdex 75 SEC column.

The R1282 Aβ immunoprecipitate was eluted using Superdex 75 SEC column, and the void volume fractions (corresponding to fraction numbers 8-10 shown above) were blotted for ApoE, ApoJ, Aβ, β-tubulin, and GAPDH.

F). We performed reverse co-IP studies and confirmed that immunoprecipitating for ApoE or ApoJ also brought down Aβ (Figure A2.3).

To confirm whether the apparent interaction of ApoE and ApoJ with Aβ were specific for the two apolipoproteins, we pulled down for GAPDH in the huAD TBS extract and also checked for presence of GAPDH in the R1282 Aβ antisera pull-down. We saw that IP'ing for GAPDH in the huAD TBS extract also brought down Aβ; in accord, IP'ing for Aβ brought down GAPDH (Figure A2.4). Next, we attempted to clean the SEC fractions by first IP'ing the huAD TBS extract for Aβ, then loading the Aβ immunoprecipitate onto the SEC column (i.e., IP/SEC). We found that the Aβ, ApoE and ApoJ still co-eluted in the void volume IP/SEC fractions; however, so did GAPDH and β-tubulin (Figure A2.5).

Conclusion

We first obtained promising co-IP data that ApoE and ApoJ may exist in a complex with Aβ in the saline extract of huAD brain homogenate. However, we failed to see a significantly enhanced specificity in the apparent interaction between Aβ and the reported chaperon molecules, the ApoE and ApoJ, over what we considered to be negative control molecules, i.e., the GAPDH and β-tubulin. Instead, the saline-extractable Aβ may exist as a > 500 kDa molecule (Chapter 3) due to an artifactual globule formed during the homogenization process and/or unspecific hydrophobic binding to proteins or lipid molecules. In

conclusion, we found no evidence for a specific interaction of Aβ to ApoE and ApoJ in the saline extracts of human AD brain homogenate.

References

Ghiso J, Matsubara E, Koudinov A, Choi-Miura NH, Tomita M, Wisniewski T, Frangione B (1993) The cerebrospinal-fluid soluble form of Alzheimer's amyloid beta is complexed to SP-40,40 (apolipoprotein J), an inhibitor of the complement membrane-attack complex. Biochemical Journal 293:27.

Hong S, Quintero-Monzon O, Ostaszewski BL, Podlisny DR, Cavanaugh WT, Yang T, Holtzman DM, Cirrito JR, Selkoe DJ (2011) Dynamic Analysis of Amyloid β-Protein in Behaving Mice Reveals Opposing Changes in ISF versus Parenchymal Aβ during Age-Related Plaque Formation. Journal of Neuroscience 31:15861-15869.

Näslund J, Thyberg J, Tjernberg LO, Wernstedt C, Karlström AR, Bogdanovic N, Gandy SE, Lannfelt L, Terenius L, Nordstedt C (1995) Characterization of stable complexes involving apolipoprotein E and the amyloid beta peptide in Alzheimer's disease brain. Neuron 15:219-228.

Shankar GM, Li S, Mehta TH, Garcia-Munoz A, Shepardson NE, Smith I, Brett FM, Farrell MA, Rowan MJ, Lemere CA, Regan CM, Walsh DM, Sabatini BL, Selkoe DJ (2008) Amyloid-l[beta]l protein dimers isolated directly from Alzheimer's brains impair synaptic plasticity and memory. Nature Medicine 14:837.

Appendix 3

Soluble amyloid β oligomers and their potential on *in vitro* microglial activation

Contributions to this Appendix:

Experiments were designed by Soyon Hong and Dennis Selkoe. Cell treatments were performed by Beth Ostaszewski, Meghana Kamineni and Soyon Hong. Human brain extracts were prepared by Ting Yang. Size-exclusion chromatography was performed by Daniel Podlisny and Soyon Hong.

Introduction

Soluble Aβ dimers and trimers are currently thought to act as the smallest oligomeric unit to exert synapto- and neurotoxic effects, whereas the Aβ monomers are thought to be an innocuous species. Although there has been numerous studies in the past that helps us gain insight into the complex relationship between the β-amyloid protein (Aβ) and microglia, most of these studies have utilized synthetic source for Aβ, rather than natural sources (for e.g., Aβ from cell-culture media or Aβ isolated from human AD cortical tissue). Furthermore, how soluble low molecular weight (LMW) Aβ oligomers affect microglia and how this effect may differ from monomers still needs to be investigated. To gain insight into this, I used a cell culture line of microglia (the N9 cells) and soluble Aβ dimers and monomers isolated either from cell-culture media or from human AD cortical tissue.

Microglia

Microglia are the resident macrophages in the central nervous system (CNS) (Adames et al., 1995). Composing about 10% of the CNS population, the main function of microglia is to protect the CNS against various injuries (Streit and Kincaid-Colton, 1995). In the healthy adult brain, microglia are said to be "resting", characterized by a ramified and highly branched morphology, that is, a small cell body with fine, elaborated processes. Microglia in the resting state

have a very low surface antigenic profile (van Rossum and Hanisch, 2004), but display rapid dynamics of fine processes, constantly sampling the CNS environment (Chung et al., 1999; Davalos et al., 2005; Nimmerjahn et al., 2005). Upon CNS injury, microglia transform into an “activated” state, followed by the “phagocytic” state, where microglia clear cellular debris (Streit and Kincaid-Colton, 1995). The hallmarks of microglial activation are increased surface antigen expression, proliferation, migration to the site of injury, and release of various immuno- and neuromodulatory factors, chemokines, pro- and anti-inflammatory cytokines, and growth factors (Hanisch, 2002; van Rossum and Hanisch, 2004).

Microglial activation is considered a double-edged sword. There is the neuroprotective side: substances released from damaged tissue trigger microglial activation with an attempt to restore the CNS environment. Microglia release growth factors, anti-inflammatory molecules, and neuroprotective cytokines to restore tissue homeostasis (Hanisch, 2002; Streit, 2002). However, sustained microglial activation can turn around to exacerbate the situation. Microglia release proinflammatory cytokines, such as TNF-α, and other cytotoxic and neurotoxic substances such as nitric oxide, glutamate and proteases. Thus, the neurotoxicity mediated by activated microglia may lead to a “secondary CNS injury” (Wyss-Coray et al., 2002; van Rossum and Hanisch, 2004). These detrimental consequences of chronic microglial activation have posed microglia as a principal culprit in the pathogenesis of many acute and chronic neurological diseases (Carson, 2002; Wyss-Coray et al., 2002; Weydt and Moller, 2005). The

detailed mechanisms underlying the shift from neuroprotective effects of microglial activation to its detrimental consequences are under study.

Relationship between microglia and Aβ

Consistently observed phenomena in the brains of AD patients are the prominent activation of inflammatory processes and the innate immune response (Akiyama et al., 2000; Wyss-Coray et al., 2002). Activation of inflammatory pathways in very early stages of the disease may be beneficiary to limit the disease progression (Wyss-Coray et al., 2002; El Khoury et al., 2007). Activated microglia may play an important role in clearing Aβ *in vivo* by binding and/or releasing proteases to degrade the Aβ assemblies (Bard et al., 2000; Rogers et al., 2002; Nicoll et al., 2003; Akiyama and McGeer, 2004). Very recent dynamic confocal microscopy indicates that within 1-2 days after Aβ plaques form, microglia are activated (Meyer-Luehmann et al., 2008). Despite numerous studies in the past showing effects of soluble and fibrillar Aβ on microglia (Floden and Combs, 2006) and microglial uptake and degradation of soluble and fibrillar Aβ (Chung et al., 1999), the important question of whether there are differential effects of Aβ dimers vs. monomers on microglia still needs to be investigated, especially in light of the recent establishment of soluble low-n Aβ oligomers as the earliest potent synaptotoxins (McLean et al., 1999; Klyubin et al., 2008; Shankar et al., 2008a; Li et al., 2009; Mc Donald et al., 2010; O'Nuallain et al.,

2010; Jin et al., 2011; Li et al., 2011). How do microglia affect the local pool of soluble Aβ? Do microglia react to the synaptotoxic soluble Aβ oligomers (but not to the apparently innocuous monomers) before amyloid plaques build up and neuronal cell death is observed? Interestingly, cell-secreted, soluble low *n* oligomers, but not monomers, are resistant to degradation by the microglial-released protease, insulin-degrading enzyme (IDE) (Qiu et al., 1997). Does the inability of IDE to degrade dimers and trimers lead to extracellular accumulation of the synaptotoxic Aβ oligomeric species? Answers to these questions will provide important insights into the interplay between the various Aβ assemblies and microglia.

Furthermore, microglial activation has been suggested to be a necessary mediator for Aβ's ability to inhibit long-term potentiation (LTP) (Wang et al., 2004). Upon application of minocycline, a potent (however, widely nonspecific) inhibitor of microglial activation, Aβ no longer inhibited the NMDAR-dependent LTP induction. The notorious role of Aβ as the prime synaptotoxic offender has been extensively researched (see Chapter 1). Previously thought to be neuronal events, such as synaptogenesis, modulation of synaptic functions and synaptic pruning, are now being found to include glia as active players (Slezak and Pfrieger, 2003; Tremblay et al., 2011). What role, if any, does microglia play in Aβ mediating its synaptotoxic effects?

An attractive candidate to mediate neuron-glia interaction is the glial-secreted tumor necrosis factor-alpha (TNF-α). Several reports have suggested

that TNF-α may influence synaptic function (Tancredi et al., 1992; Cunningham et al., 1996; Albensi and Mattson, 2000), synapse maturation (Beattie et al., 2002), and synaptic scaling (Stellwagen and Malenka, 2006). Soluble Aβ has been found to bind potently to TNF type I receptor (TNFRI) (Li et al., 2004), and activated microglia and astrocytes are the major sources of TNF-α in the CNS (Hanisch, 2002). However, whether glial-released TNF-α mediates the inhibitory effect of Aβ in NMDAR-dependent LTP induction has yet to be revealed. Other candidates that might mediate the interplay between Aβ and microglia in synaptic function are the immune proteins in the CNS that have recently been found to play important roles in regulating synaptic function, in particular, C1q (Fonseca, 2004; Stevens et al., 2007) and the major histocompatibility complex class I (MHC-I) (Huh et al., 2000; Goddard et al., 2007). It will be interesting to see whether Aβ regulates the expression of these molecules and/or the secretion of these molecules impacts Aβ production and accumulation, thereby inducing alterations in synaptic function.

Results

Here, we used a cell culture line of microglia (the N9 cells) to determine whether the soluble Aβ dimers affect microglia *in vitro* differently than the monomers do. The Aβ monomers and oligomers were from two sources: a conditioned media of Chinese hamster ovary (CHO) cells that have mutated

human APP (the *APP* V717F) stably transfected in them and thus secrete an abundant amount of Aβ species (the 7PA2 cells) (Podlisny et al., 1998; Walsh et al., 2000) and the saline extracts of AD human brain homogenates (the AD TBS ext), which has been found to carry an ample amount of Aβ monomers and dimers (Shankar et al., 2008b). The 7PA2 cells were conditioned for 48 hours in DMEM, upon which the conditioned media (termed 7PA2CM herein) was collected and concentrated. Non-transfected CHO-cells were also conditioned in the same manner as negative control (termed CHO-CM). For the AD TBS ext, grey matter from a frozen cortical tissue from an AD human patient was isolated from the white matter, then homogenized in TBS buffer 1:4 brain tissue weight:TBS volume. Then, the homogenate was ultracentrifugated at 75,000 g for 30 min at 4 °C. The supernatant (termed the AD TBS ext) was then either loaded onto a Superdex 75 column or immunoprecipitated for Aβ using a monoclonal anti-Aβ antibody 3D6 or polyclonal anti-Aβ antibody AW8. The concentrated 7PA2CM, AD TBS ext, or the Aβ immunoprecipitate (IP) of AD TBS ext were loaded onto the Superdex 75 SEC column and materials were eluted off the column by non-denaturing size exclusion chromatography (SEC) at 0.5 ml/min in 50 mM ammonium acetate, pH 8.5. The resulting SEC fractions were promptly lyophilized upon fractionation. The separation of the Aβ monomers from the LMW oligomers (i.e., dimers and trimers) were identified by Western blotting. The fractions which were identified to be enriched with Aβ monomers (termed monomer fraction) or dimers (termed dimer fraction) (Figure A3.1) were

then brought up in macrophage serum free media (MSFM) and applied onto the N9 microglia cells (kind gift of J. El Khoury, MGH).

The N9 microglia cells were passaged in DMEM with 10% serum, then plated onto a 96-well poly-D-lysine-coated plate at 5,000 cells per well. The plated cells were serum-starved for 24 h, then treated with either the Aβ monomer or dimer fraction (Figure A3.2: treated with fractions from the 7PA2CM; Figure A3.3: treated with SEC fractions from two different huAD brains (void volume fraction, dimer fraction or monomer fraction); and Figure A3.4: treated with Aβ dimers isolated by IP/SEC method from huAD TBS ext). Lipopolysaccharide (LPS) with interferon-γ (IFNγ) were applied at 100 ng/ml and 10 U/ml, respectively, as positive controls, and the fractions from the conditioned media of the non-transfected CHO cells that correspond to the dimer-containing fractions in 7PA2CM were used as negative controls. 24 hours upon application of the different fractions, the activation properties of the N9 cells were determined by measuring the number of metabolically active cells (using the WST-1 assay), cytotoxicity (using the lactate dehydrogenase (LDH) assay), and nitric oxide (NO) secretion (using the Griess assay).

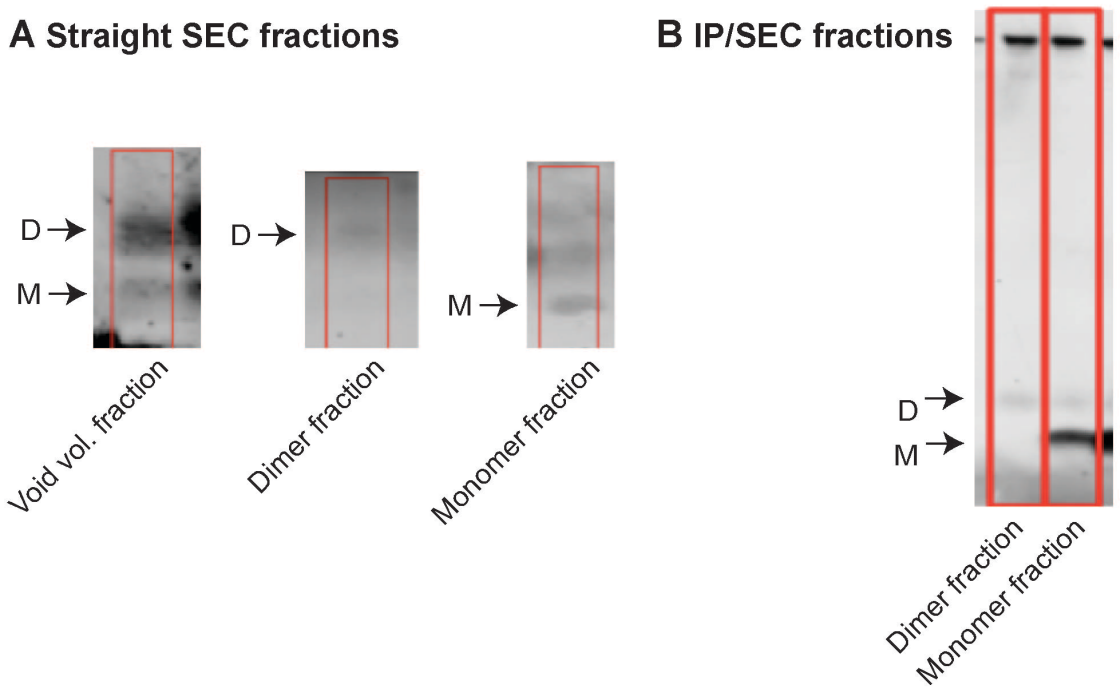

Figure A3.1. Separation of soluble Aβ monomers and dimers from human AD by SEC.

(A) Human AD TBS ext. was straight-loaded onto the Superdex 75 SEC column. The material that eluted at the void volume of the SEC column carried Aβ that separated into Aβ dimers and monomers by denaturing SDS-PAGE. The dimer fraction contained mostly Aβ species that ran as dimers on SDS-PAGE and the monomer fraction contained mostly Aβ species that ran as monomers on SDS-PAGE. (B) Human AD TBS ext. was IP'ed with 3D6 anti-Aβ antibody and the immunoprecipitated was straight-loaded onto the Superdex 75 SEC column. WB: 2G3 and 21F12 antibodies (directed against $A\beta_{31\text{-}40}$ and $A\beta_{33\text{-}42}$, respectively; gift of Elan, plc.). D: Aβ Dimers, M: Aβ Monomers.

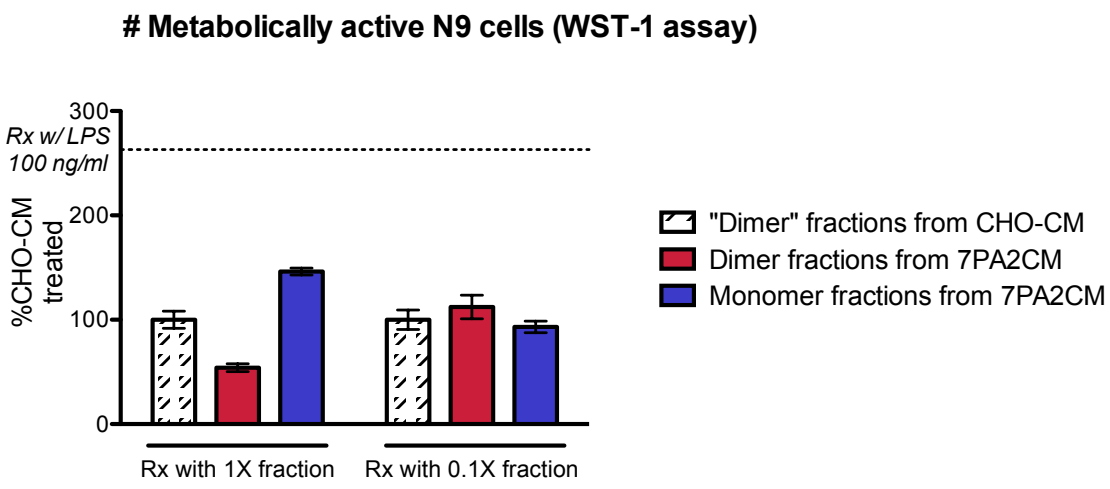

Figure A3.2. Aβ oligomers from 7PA2 cells reduced number of metabolically active cells, whereas Aβ monomers appeared to induce cell proliferation.

The N9 cells were treated for 24 hours with fractions that contain mostly Aβ low *n* oligomers or mostly Aβ monomers from 7PA2CM at two doses (1X corresponding to 1-ml fraction, 0.1X corresponding to 0.1-ml fraction). As a negative control, the SEC fraction from CHO-CM that corresponds to the dimer fraction of 7PA2CM was also applied onto the N9 cells. 24 hours later, the number of metabolically active cells was quantified using the WST-1 assay. Aβ oligomers from 7PA2 cells reduced the number of metabolically active cells, whereas Aβ monomers appeared to induce cell proliferation. N=2 experiments (in triplicates per experiment).

Figure A3.3. Soluble Aβ dimers from two human AD brains induce microglial proliferation and LDH release.

The N9 cells were treated with Aβ dimer-containing fraction (dimer fxn), Aβ monomer-containing (monomer fxn), and the SEC fraction that eluted in the void volume which contained mostly Aβ dimers and monomers (void volume fxn). 24 hours later, the number of metabolically active cells was quantified using the WST-1 assay and LDH release was measured in the conditioned media of the treated cells. The cell proliferative effect and the stimulated LDH release were greatest and most consistent in the treatment with "free-floating" Aβ dimers, i.e., the dimer fxn, despite there being very little Aβ present (see Figure A3.1). Interestingly, Aβ monomers and dimers from the void volume fraction also induced cell proliferation, albeit in a much less concentration than the "free-floating" dimers. N=3 experiments for huAD TBS ext. #1; N=1 experiment for huAD TBS ext. #2; triplicates per experiment.

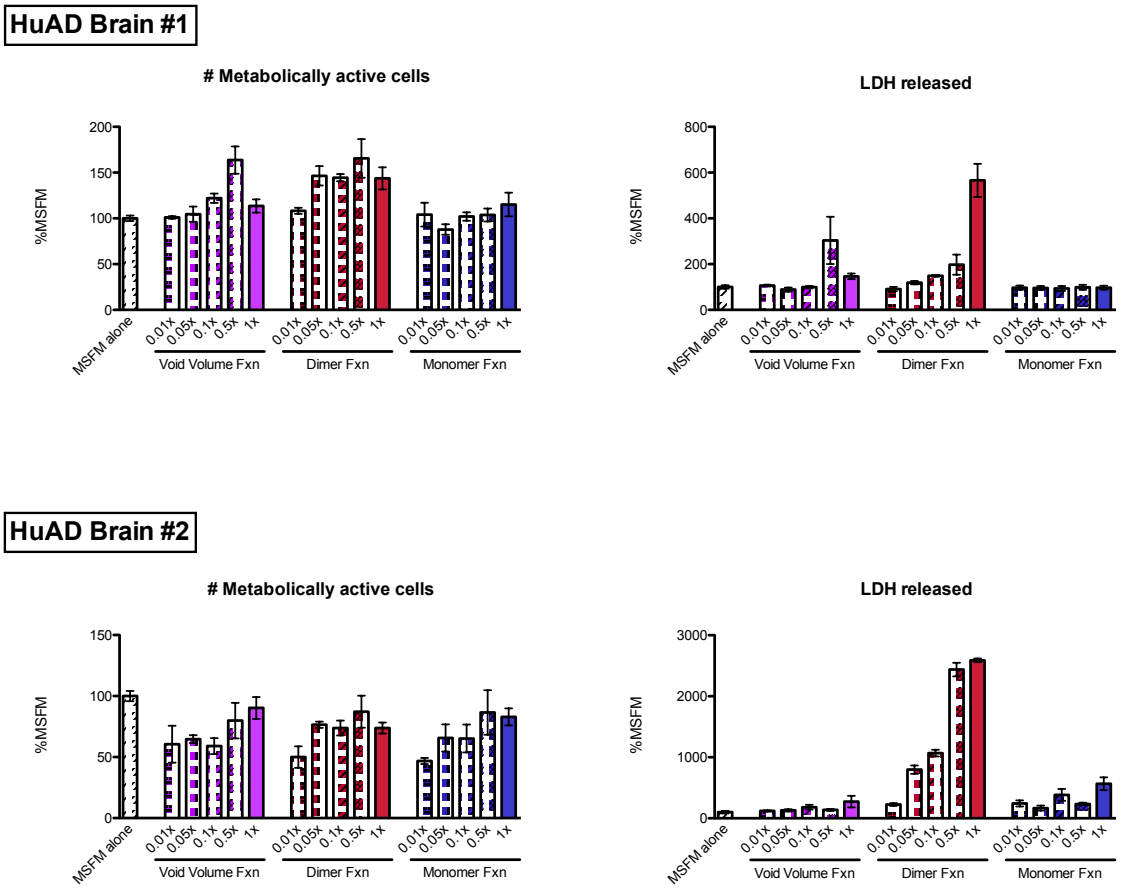

Figure A3.3 (Continued). Soluble Aβ dimers from two human AD brains induce microglial proliferation and LDH release.

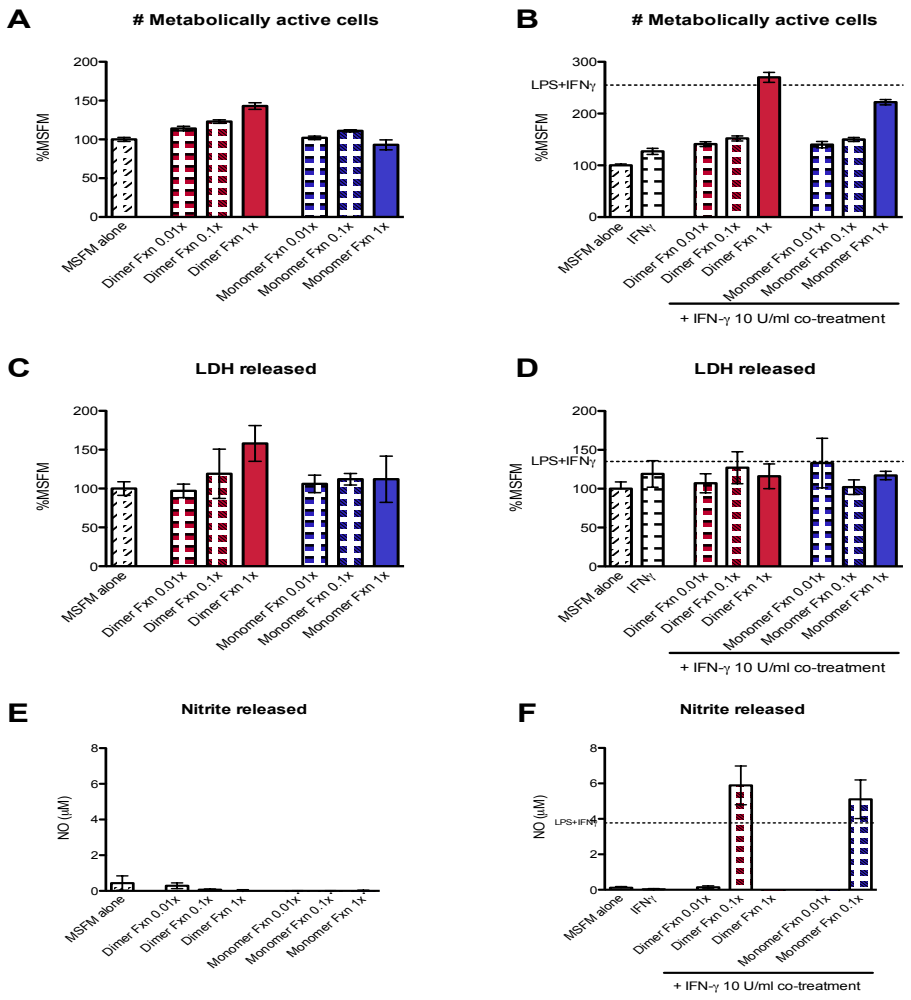

Figure A3.4. Soluble Aβ dimers isolated from human AD brain by IP/SEC induce microglial activation and this effect is exacerbated when cells are primed with IFNγ.

Only the Aβ dimers (isolated using IP/SEC) induced cell proliferative effect (A) and LDH release (C) from the N9 cells, whereas the monomers did not. Interestingly, they did not induce nitrite release (E), unless co-stimulated with IFNγ (F). The Aβ monomers failed to induce any effect, unless cells were already primed with IFNγ. N=2 experiments (in triplicates per experiment).

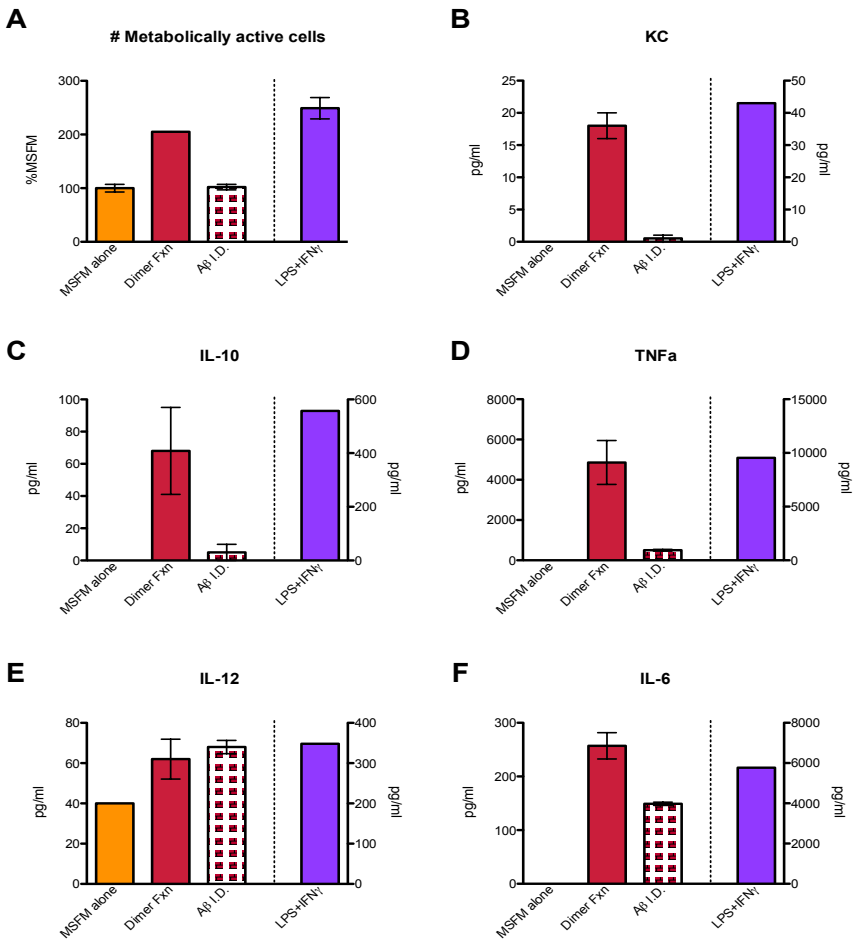

Figure A3.5. Human AD brain-derived soluble Aβ dimers induce cell proliferation and several cytokines, and these effects are abolished upon Aβ immunodepletion.

N9 cells treated for 24 hours with Aβ dimers from huAD TBS ext. (IP/SEC; IP'ed with AW8; ~5 pM) were quantified using the WST-1 and their conditioned media were assayed for various cytokines using the MesoScale 7-plex cytokine ELISA. Both the proliferative effect and induction of certain cytokines were abolished upon Aβ-immunodepletion (using the AW7 antibody). The secretion of IL-12 seem to be non Aβ-specific, and to some degree, IL-6 as well. N=1 experiment.

Discussion

In summary, the preliminary experiments suggest the following: (1) Aβ low *n* oligomers from 7PA2CM affect cell viability, whereas Aβ monomers induce cell proliferation; (2) soluble Aβ dimers alone induce microglial proliferation and LDH release, whereas monomers do not, and the proliferative effect is abolished upon Aβ-immunodepletion; and (3) the soluble Aβ by themselves do not induce nitrite release, unless primed with IFN-γ. Furthermore, several cytokines also seem to be induced specifically with the soluble Aβ dimers derived from human AD brain (note, these are results from only one experiment). We have attempted to repeat the findings multiple times with the human brain AD material; however, we have failed to do so. One likely explanation for the failure to repeat the above findings is the heterogeneous level of purity of the Aβ dimers obtained with the IP/SEC technique from the huAD brains (with the additive variability coming from the human brain materials themselves) (Figure A3.6 shows silver stains of the 5 different preparations and Table A3.1 summarizes the experimental results obtained from some of these preparations). Another likely explanation is the contamination of the samples with endotoxin, which are known to robustly induce microglial activity (Weinstein et al., 2005), and therefore endotoxin could be masking the effects of Aβ in the fractions. A removal of endotoxin contamination or attempt at its neutralization (for e..g, with polymyxin B) in the fractions may be necessary.

In conclusion, to date, I was unable to repeat the preliminary findings.

Nonetheless, I think the question, i.e., “Do microglia react different to natural Aβ dimers versus monomers at physiological concentrations?” is still an interesting one that remains unanswered in the AD field (especially as the field is limited in obtaining natural Aβ). However, before the question can be pursued in an *in vitro* setting such as that attempted here, a considerable amount of work should be focused in obtaining relatively pure, homogenous and endotoxin-free Aβ samples from the human brain homogenates. Even then, data obtained should be carefully evaluated in the most rigorous manner, as microglia are responsive to many agents that may be present in post-mortem tissue.

#1-#4: different IP/SEC preparations

#1 huAD brain ID#296; Prep date 11/24/10; IP'ed with 3D6
#2 huAD brain ID#A94-155; Prep date 9/25/10; IP'ed with AW8
#3: huAD brain ID#A94-153; Prep date 12/15/10; IP'ed with 3D6
#4: huAD brain ID#A94-153; Prep date 12/30/10; IP'ed with 3D6
#5: non-AD Control brain; Prep date 7/21/10; IP'ed with 3D6

A-F: Silver stains

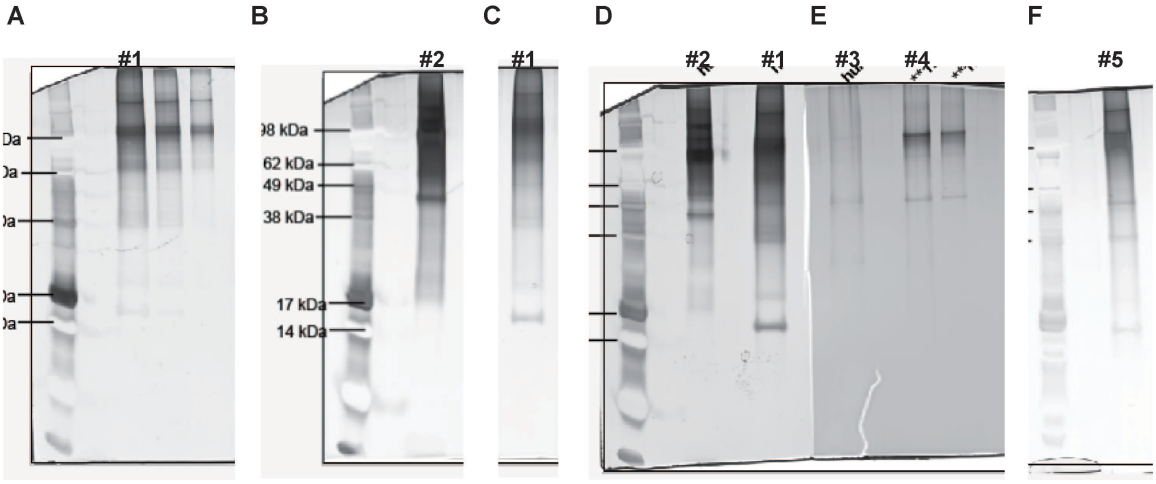

Figure A3.6. Heterogeneity in the IP/SEC fractions prepared from 5 different human brain materials (#1-5) shown by silver stain (A-F).

Table A3.1. Heterogeneity in the experimental results obtained from different IP/SEC fractions.

IP/SEC Prep	WST-1 results	# experiments
Prep #2	No difference between monomer and dimer fractions	2
Prep #3	Inconsistent	4
Prep #4	No difference between monomers and dimers	2

References

Adames N, Blundell K, Ashby MN, Boone C (1995) Role of yeast insulin-degrading enzyme homologs in propheromone processing and bud site selection. Science 270:464-467.

Akiyama H, McGeer PL (2004) Specificity of mechanisms for plaque removal after A beta immunotherapy for Alzheimer disease. Nat Med 10:117-118; author reply 118-119.

Akiyama H et al. (2000) Inflammation and Alzheimer's disease. Neurobiol Aging 21:383-421.

Albensi BC, Mattson MP (2000) Evidence for the involvement of TNF and NF-kappaB in hippocampal synaptic plasticity. Synapse 35:151-159.

Bard F et al. (2000) Peripherally administered antibodies against amyloid beta-peptide enter the central nervous system and reduce pathology in a mouse model of Alzheimer disease. Nat Med 6:916-919.

Beattie EC, Stellwagen D, Morishita W, Bresnahan JC, Ha BK, Von Zastrow M, Beattie MS, Malenka RC (2002) Control of synaptic strength by glial TNFalpha. Science 295:2282-2285.

Carson MJ (2002) Microglia as liaisons between the immune and central nervous systems: functional implications for multiple sclerosis. Glia 40:218-231.

Chung H, Brazil MI, Soe TT, Maxfield FR (1999) Uptake, degradation, and release of fibrillar and soluble forms of Alzheimer's amyloid beta-peptide by microglial cells. J Biol Chem 274:32301-32308.

Cunningham AJ, Murray CA, O'Neill LA, Lynch MA, O'Connor JJ (1996) Interleukin-1 beta (IL-1 beta) and tumour necrosis factor (TNF) inhibit long-term potentiation in the rat dentate gyrus in vitro. Neurosci Lett 203:17-20.

Davalos D, Grutzendler J, Yang G, Kim JV, Zuo Y, Jung S, Littman DR, Dustin ML, Gan W-B (2005) ATP mediates rapid microglial response to local brain injury in vivo. Nat Neurosci 8:752-758.

El Khoury J, Toft M, Hickman SE, Means TK, Terada K, Geula C, Luster AD (2007) Ccr2 deficiency impairs microglial accumulation and accelerates progression of Alzheimer-like disease. Nat Med 13:432-438.

Floden AM, Combs CK (2006) Beta-amyloid stimulates murine postnatal and adult microglia cultures in a unique manner. J Neurosci 26:4644-4648.

Fonseca MI (2004) Absence of C1q Leads to Less Neuropathology in Transgenic Mouse Models of Alzheimer's Disease. Journal of Neuroscience 24:6457-6465.

Goddard CA, Butts DA, Shatz CJ (2007) Regulation of CNS synapses by neuronal MHC class I. Proc Natl Acad Sci U S A 104:6828-6833.

Hanisch U-K (2002) Microglia as a source and target of cytokines. Glia 40:140-155.

Huh GS, Boulanger LM, Du H, Riquelme PA, Brotz TM, Shatz CJ (2000) Functional requirement for class I MHC in CNS development and plasticity. Science 290:2155-2159.

Jin M, Shepardson N, Yang T, Chen G, Walsh D, Selkoe DJ (2011) Soluble amyloid beta-protein dimers isolated from Alzheimer cortex directly induce Tau hyperphosphorylation and neuritic degeneration. Proc Natl Acad Sci U S A 108:5819-5824.

Klyubin I, Betts V, Welzel AT, Blennow K, Zetterberg H, Wallin A, Lemere CA, Cullen WK, Peng Y, Wisniewski T, Selkoe DJ, Anwyl R, Walsh DM, Rowan MJ (2008) Amyloid beta protein dimer-containing human CSF disrupts synaptic plasticity: prevention by systemic passive immunization. Journal of Neuroscience 28:4231-4237.

Li R, Yang L, Lindholm K, Konishi Y, Yue X, Hampel H, Zhang D, Shen Y (2004) Tumor necrosis factor death receptor signaling cascade is required for amyloid-beta protein-induced neuron death. J Neurosci 24:1760-1771.

Li S, Hong S, Shepardson NE, Walsh DM, Shankar GM, Selkoe D (2009) Soluble oligomers of amyloid Beta protein facilitate hippocampal long-term depression by disrupting neuronal glutamate uptake. Neuron 62:788-801.

Li S, Jin M, Koeglsperger T, Shepardson NE, Shankar GM, Selkoe DJ (2011) Soluble Aβ oligomers inhibit long-term potentiation through a mechanism involving excessive activation of extrasynaptic NR2B-containing NMDA receptors. Journal of Neuroscience 31:6627-6638.

Mc Donald JM, Savva GM, Brayne C, Welzel AT, Forster G, Shankar GM, Selkoe DJ, Ince PG, Walsh DM (2010) The presence of sodium dodecyl sulphate-stable A dimers is strongly associated with Alzheimer-type dementia. Brain 133:1328-1341.

McLean C, Cherny R, Fraser F, Fuller S, Smith M, Vbeyreuther K, Bush A, Masters C (1999) Soluble pool of Aβ amyloid as a determinant of severity of neurodegeneration in Alzheimer's disease. Annals of Neurology 46:860-866.

Meyer-Luehmann M, Spires-Jones TL, Prada C, Garcia-Alloza M, De Calignon A, Rozkalne A, Koenigsknecht-Talboo J, Holtzman DM, Bacskai BJ, Hyman BT (2008) Rapid appearance and local toxicity of amyloid-β plaques in a mouse model of Alzheimer's disease. Nature 451:720-724.

Nicoll JA, Wilkinson D, Holmes C, Steart P, Markham H, Weller RO (2003) Neuropathology of human Alzheimer disease after immunization with amyloid-beta peptide: a case report. Nat Med 9:448-452.

Nimmerjahn A, Kirchhoff F, Helmchen F (2005) Resting microglial cells are highly dynamic surveillants of brain parenchyma in vivo. Science 308:1314-1318.

O'Nuallain B, Freir DB, Nicoll AJ, Risse E, Ferguson N, Herron CE, Collinge J, Walsh DM (2010) Amyloid beta-protein dimers rapidly form stable synaptotoxic protofibrils. Journal of Neuroscience 30:14411-14419.

Podlisny MB, Walsh DM, Amarante P, Ostaszewski BL, Stimson ER, Maggio JE, Teplow DB, Selkoe DJ (1998) Oligomerization of endogenous and synthetic amyloid β-protein at nanomolar levels in cell culture and stabilization of monomer by Congo red. Biochem 37:3602-3611.

Qiu WQ, Ye Z, Kholodenko D, Seubert P, Selkoe DJ (1997) Degradation of amyloid beta-protein by a metalloprotease secreted by microglia and other neural and non-neural cells. J Biol Chem 272:6641-6646.

Rogers J, Strohmeyer R, Kovelowski CJ, Li R (2002) Microglia and inflammatory mechanisms in the clearance of amyloid beta peptide. Glia 40:260-269.

Shankar GM, Li S, Mehta TH, Garcia-Munoz A, Shepardson NE, Smith I, Brett FM, Farrell MA, Rowan MJ, Lemere CA, Regan CM, Walsh DM, Sabatini BL, Selkoe DJ (2008a) Amyloid-l[beta]l protein dimers isolated directly from Alzheimer's brains impair synaptic plasticity and memory. Nature Medicine 14:837.

Shankar GM, Li S, Mehta TH, Garcia-Munoz A, Shepardson NE, Smith I, Brett FM, Farrell MA, Rowan MJ, Lemere CA, Regan CM, Walsh DM, Sabatini BL, Selkoe DJ (2008b) Amyloid-β protein dimers isolated directly from Alzheimer's brains impair synaptic plasticity and memory. Nat Med 14:837-842.

Slezak M, Pfrieger FW (2003) New roles for astrocytes: regulation of CNS synaptogenesis. Trends Neurosci 26:531-535.

Stellwagen D, Malenka RC (2006) Synaptic scaling mediated by glial TNF-α. Nature 440:1054-1059.

Stevens B, Allen NJ, Vazquez LE, Howell GR, Christopherson KS, Nouri N, Micheva KD, Mehalow AK, Huberman AD, Stafford B, Sher A, Litke AM, Lambris JD, Smith SJ, John SWM, Barres BA (2007) The classical complement cascade mediates CNS synapse elimination. Cell 131:1164-1178.

Streit WJ (2002) Microglia as neuroprotective, immunocompetent cells of the CNS. Glia 40:133-139.

Streit WJ, Kincaid-Colton CA (1995) The brain's immune system. Scientific American 273:54-55, 58-61.

Tancredi V, D'Arcangelo G, Grassi F, Tarroni P, Palmieri G, Santoni A, Eusebi F (1992) Tumor necrosis factor alters synaptic transmission in rat hippocampal slices. Neurosci Lett 146:176-178.

Tremblay ME, Stevens B, Sierra A, Wake H, Bessis A, Nimmerjahn A (2011) The Role of Microglia in the Healthy Brain. Journal of Neuroscience 31:16064-16069.

van Rossum D, Hanisch UK (2004) Microglia. Metabolic brain disease 19:393-411.

Walsh DM, Tseng BP, Rydel RE, Podlisny MB, Selkoe DJ (2000) The oligomerization of amyloid beta-protein begins intracellularly in cells derived from human brain. Biochemistry 39:10831-10839.

Wang Q, Rowan MJ, Anwyl R (2004) Beta-amyloid-mediated inhibition of NMDA receptor-dependent long-term potentiation induction involves activation of microglia and stimulation of inducible nitric oxide synthase and superoxide. Journal of Neuroscience 24:6049-6056.

Weinstein JR, Hong S, Kulman JD, Bishop C, Kuniyoshi J, Andersen H, Ransom BR, Hanisch U-K, Möller T (2005) Unraveling thrombin's true microglia-activating potential: markedly disparate profiles of pharmaceutical-grade and commercial-grade thrombin preparations. Journal of Neurochemistry 95:1177-1187.

Weydt P, Moller T (2005) Neuroinflammation in the pathogenesis of amyotrophic lateral sclerosis. Neuroreport 16:527-531.

Wyss-Coray T, Yan F, Lin AH, Lambris JD, Alexander JJ, Quigg RJ, Masliah E (2002) Prominent neurodegeneration and increased plaque formation in complement-inhibited Alzheimer's mice. Proc Natl Acad Sci U S A 99:10837-10842.

Appendix 4

Development of an electrophoretic system for a better separation of proteins with molecular masses of 3-14 kDa

Contributions to this Appendix:

Experiments were designed by John Maggio, Dennis Selkoe and Soyon Hong.

All experiments were performed by Soyon Hong.

Aim: To create an electrophoretic system for a better separation of proteins with molecular masses of 3-14 kDa while retaining a high resolving power.

Variables considered/tested:

(1) Gel composition: Tricine, Bis-Tris
(2) Detergent: 2% LiDS, 2% AOT, 2% SDS
(3) Running buffer: 0.1% SDS MES, 0.25% SDS MES, 0.1% AOT
(4) % Acrylamide: 4-12, 12, 16, 20
(5) % Cross-linker: 3.3, 5, 6
(6) Gel length: Mini-gel, 20 cm
(7) Gel thickness: 0.75, 1 mm
(8) 10% "Spacer" gel: Considerably sharpens the bands for proteins and peptides of 1-5 kDa (Schägger, 2006)
(9) 10% glycine in separating gel: Increased the density of solutions and facilitate gel casting, but had no obvious effect on protein separation.
(10) Urea 6M: For unknown reasons, urea seems to alter SDS-binding to proteins and while reducing the electrophoretic mobility of proteins in general, it enhances the resolution of very small proteins (to the peptide level) (Klafki et al., 1996).

Results:

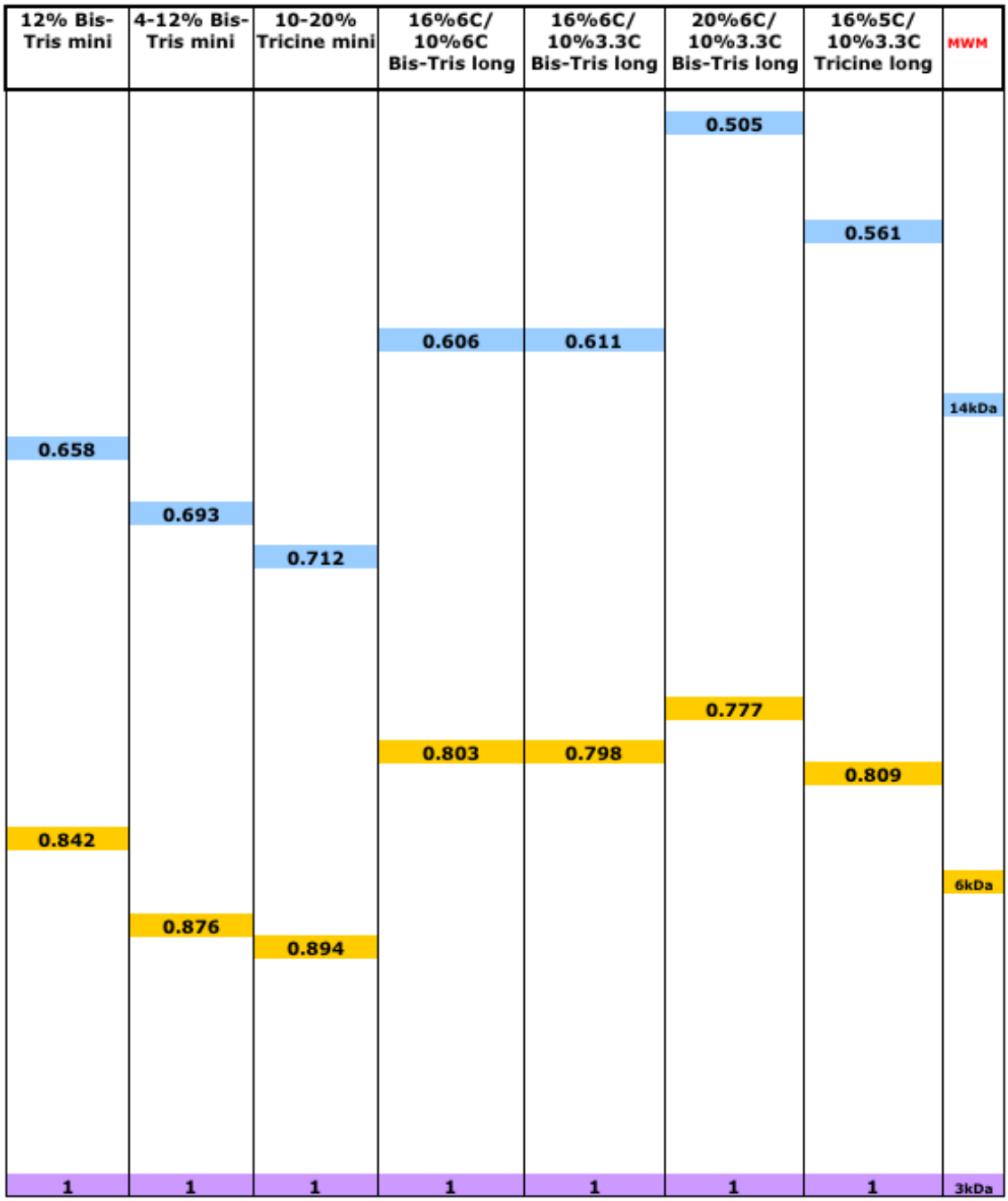

Figure A4.1. Migration table of the 3-14 kDa molecular weight markers in the different gels tested, in relation to the 3 kDa (1.0).

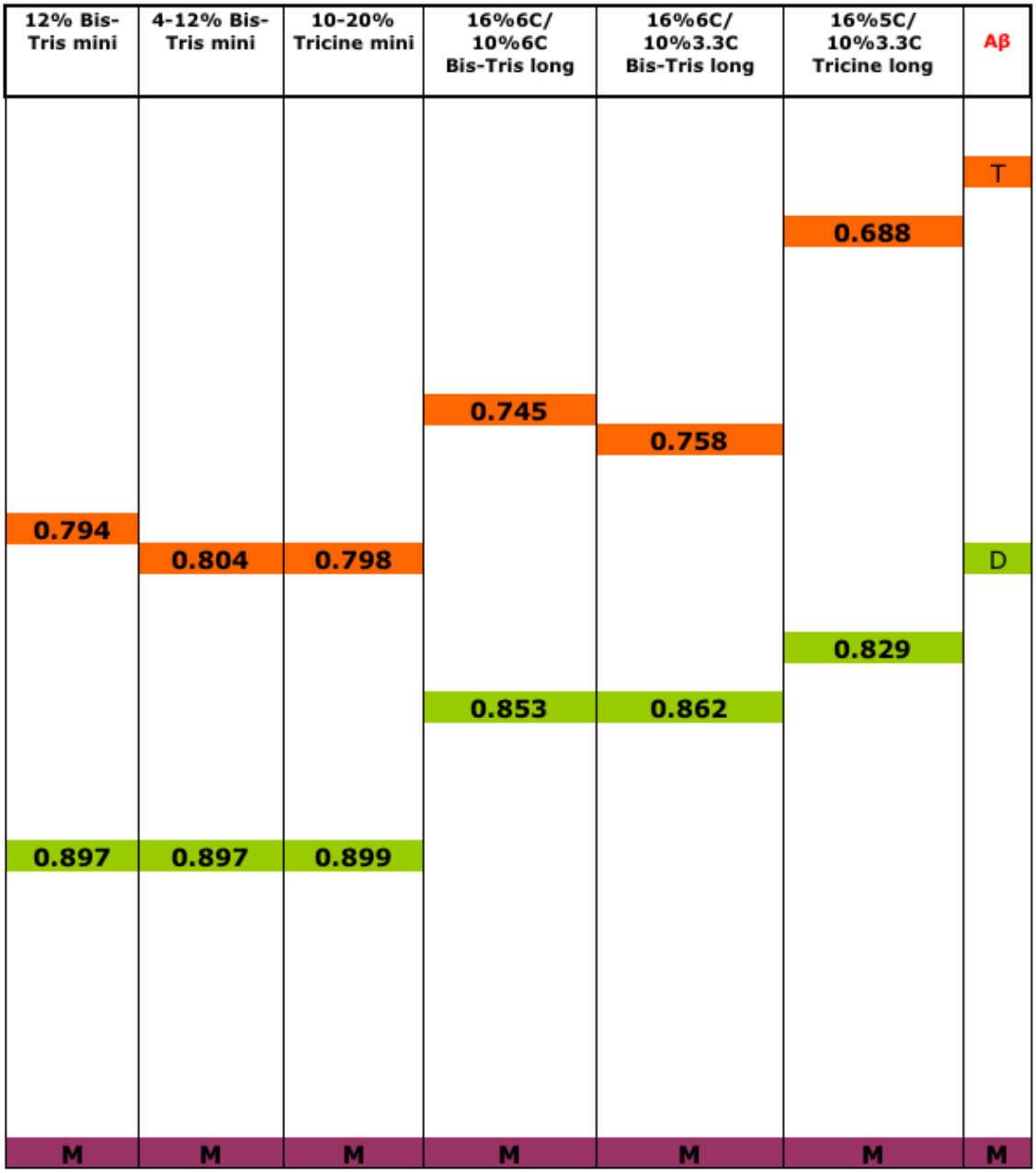

Figure A4.2. Separation of Aβ dimers and trimers, in relation to the monomers (1.0).

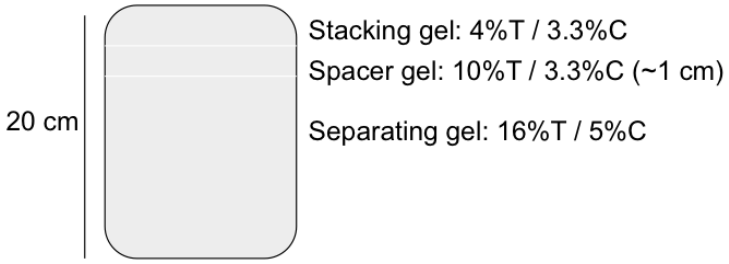

Figure A4.3. Gel composition for the 20-cm long 16% Tricine gel with 1-cm spacer gel, which provides optimal separation of Aβ monomers and dimers.

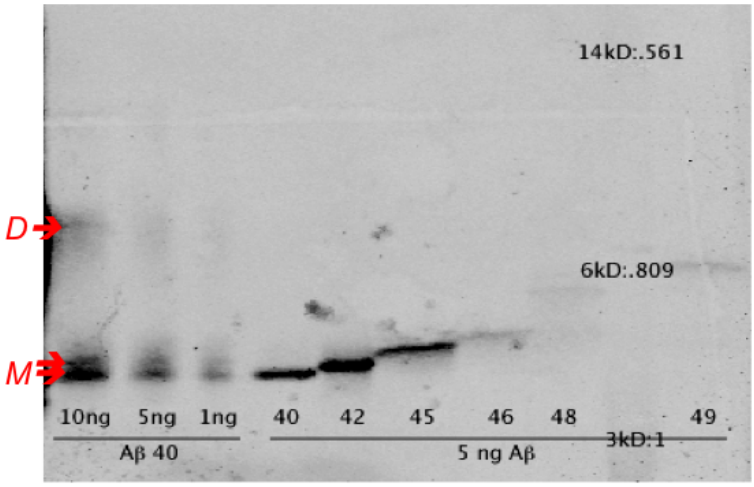

Figure A4.4. Optimal separation of Aβ by the 20-cm 16% Tricine gel. It also resolves Aβ monomer peptides, the $Aβ_{40}$ and $Aβ_{42}$ from the longer Aβ species. WB: 6E10. D: Aβ Dimers, M: Aβ Monomers.

(A)

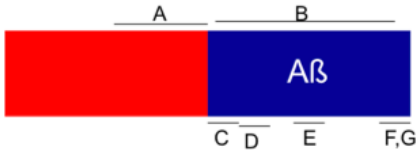

Antibodies & their recognition sites

A. R1872: APP(577-596), i.e. -20 to -1 rel. Aß; a.k.a. pre-ß
B. R1282: APP(597-636)
C. 3D6: Aß(1-5), requires intact N-terminus
D. 6E10: Aß(5-9)
E. 4G8: Aß(17-24)
F. 2G3: Aß(31-40), requires intact C-terminus
G. 21F12: Aß(33-42), requires intact C-terminus

(B)

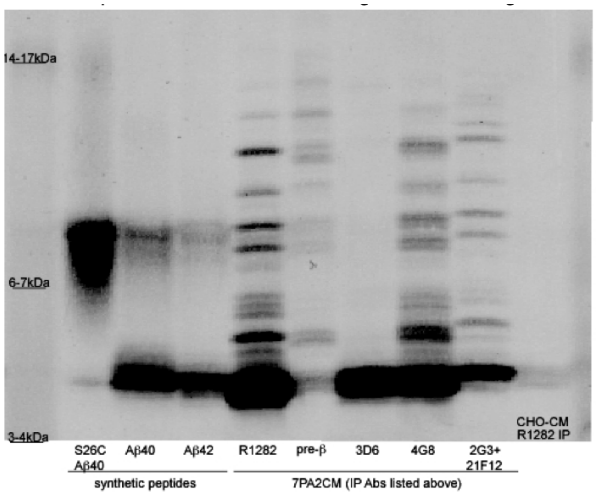

(C)

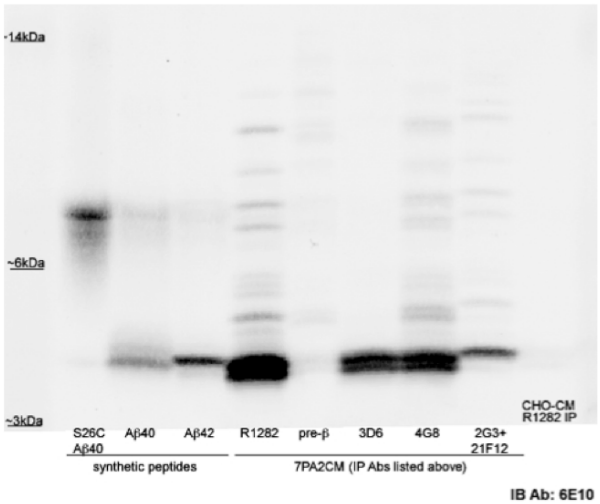

Figure A4.5. The powerful separation of the gel allowed a better distinction between the different APP cleavage products in the conditioned media of the 7PA2 cells.

(A) Antibodies used in the immunoprecipitation (IP) panel study.

(B, C) The different Aβ peptides present in the conditioned media of 7PA2 cells as recognized by the respective antibodies. WB: 6E10.

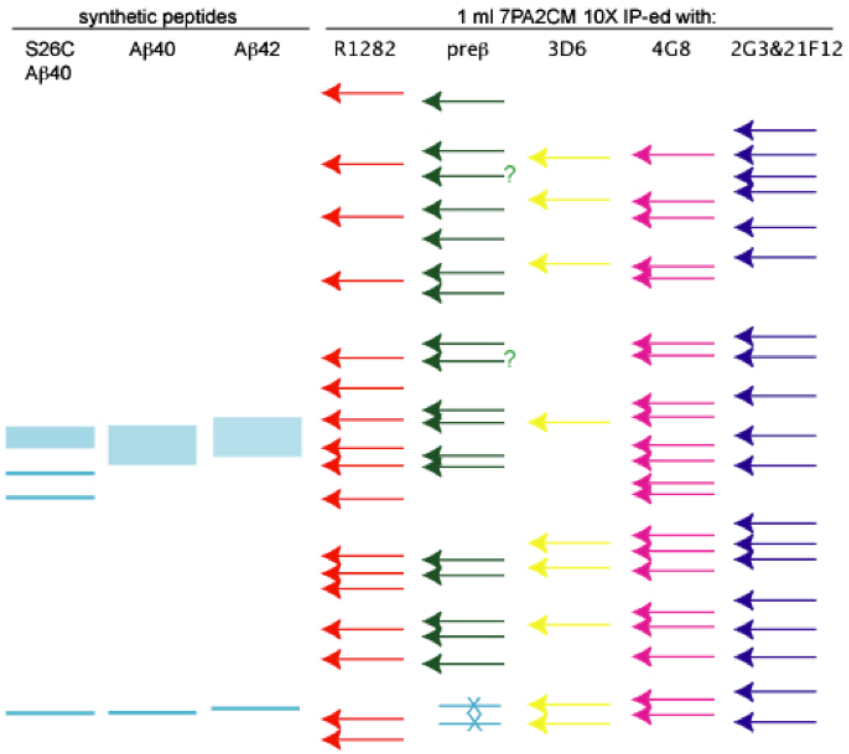

Figure A4.6. The heterogeneous pattern as recognized by the respective antibodies in the IP panel.

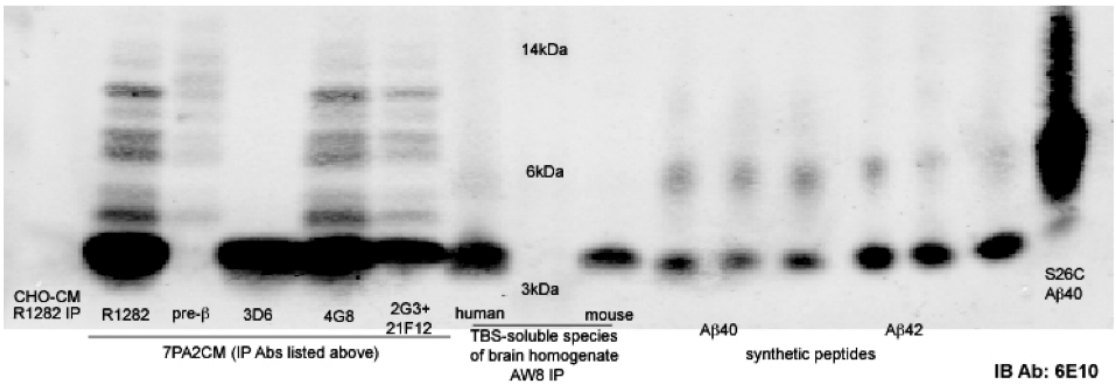

Figure A4.7. The same materials in the IP panel as Figure A4.5 now run on a mini 12% Bis-Tris gel (Invitrogen Novex).

Conclusion

The 20-cm long 16% tricine gel with 1-cm spacer gel provided optimal resolution between Aβ monomers and low *n* oligomers; furthermore, it allowed separation between the Aβ monomer peptides available. This gel may be a useful tool in studying the heterogeneity of APP processing, as shown in Figure A4.5, where it allowed for a better distinction between the different Aβ peptides present (as compared to Figure A4.7).

Reference

Klafki HW, Wiltfang J, Staufenbiel M (1996) Electrophoretic separation of betaA4 peptides (1-40) and (1-42). Analytical Biochemistry 237:24-29.

Schägger H (2006) Tricine-SDS-PAGE. Nat Protoc 1:16-22.

Appendix 5

LRP promotes endocytosis and degradation, but not transcytosis, of the amyloid-beta peptide in a blood-brain barrier in vitro model

Babak Nazer, Soyon Hong, and Dennis J. Selkoe

Contributions to this Appendix:

Babak Nazer performed all experiments, except for the WB in Figure 4C which Soyon Hong performed. This manuscript was published in Neurobiology of Disease, Volume 30, Issue 1, pp 94-102 and is reproduced here in that form.

ELSEVIER

Neurobiology of Disease

www.elsevier.com/locate/ynbdi
Neurobiology of Disease 30 (2008) 94–102

LRP promotes endocytosis and degradation, but not transcytosis, of the amyloid-β peptide in a blood–brain barrier *in vitro* model

Babak Nazer,[a,b] Soyon Hong,[a] and Dennis J. Selkoe[a,*]

[a]*Center for Neurologic Diseases, Brigham and Women's Hospital and Harvard Medical School, Boston, MA 02115, USA*
[b]*Howard Hughes Medical Institute, Chevy Chase, MD 20815, USA*

Received 3 July 2007; revised 12 December 2007; accepted 23 December 2007
Available online 5 January 2008

The pathogenesis of Alzheimer's disease is characterized by aggregation of the amyloid-β protein (Aβ) into neurotoxic plaques. Recent *in vivo* studies have suggested the non-proteolytic clearance of Aβ via receptor-mediated transport across the blood–brain barrier (BBB). The aim of this study was to investigate the role of P-glycoprotein (Pgp) and the low-density lipoprotein receptor-related protein (LRP) in Aβ efflux across the BBB. We developed an in vitro BBB-like model using Madin–Darby Canine Kidney (MDCK) cells seeded on filters separating apical (blood) and basolateral (brain) compartments. MDCK cells were stably transfected with Pgp or mLRP4, an LRP mini-receptor. When compared to empty vector-transfected cells, MDCK-Pgp cells did not transcytose radiolabeled Aβ in the basolateral-to-apical direction. MDCK-mLRP4 cells were found to endocytose and degrade, but not to trasncytose intact radiolabeled Aβ. These results implicate LRP as a mediator of Aβ degradation, but indicate that overexpression of LRP or Pgp alone is insufficient for non-proteolytic transcytosis of intact Aβ.

Keywords: Alzheimer's disease; Amyloid-β protein; Blood–brain barrier; Low-density lipoprotein receptor-related protein; MDCK cells; P-glycoprotein

Introduction

Alzheimer's disease (AD) is the most common cause of dementia, with over 30 million people affected world-wide. A key neuropathological lesion in AD, the neuritic plaque, consists of extracellular deposits of the amyloid-β protein (Aβ). Accumulation of Aβ is believed to initiate AD when there is an imbalance between its production and clearance, leading to its aggregation into oligomers and neuritic plaques (Hardy and Selkoe, 2002).

Research into therapeutic avenues to lower cerebral Aβ levels has largely centered on decreasing its production by inhibiting the proteases that generate Aβ (Selkoe and Schenk, 2003), increasing its clearance through immunotherapy (Weiner and Frenkel, 2006), or promoting its degradation by proteases such as insulin-degrading enzyme and neprilysin (Tanzi et al., 2004). In addition, non-proteolytic clearance by receptor-mediated transport of Aβ out of the CNS has been investigated as another potential mechanism for decreasing cerebral Aβ load. Two pathways for Aβ transport out of the CNS exist: bulk flow (Silverberg et al., 2003) of interstitial fluid (ISF) into the blood via the cerebrospinal fluid (CSF), and transcytosis of Aβ across the blood–brain barrier (BBB). It has been reported that CSF-mediated bulk flow accounts for no more than 10–15% of non-proteolytic transport of Aβ out of the CNS *in vivo* (Shibata et al., 2000), leaving the BBB as the main route of efflux. The BBB is distinct from other cell barriers by its increased tight junction density, lower rates of non-selective pinocytosis, lack of fenestrations, and unique cell surface receptor expression profile (Rubin and Staddon, 1999). A few such receptors for Aβ transport have been described (Zlokovic, 2004).

Low-density lipoprotein receptor-related protein (LRP) is a ~600 kDa multi-ligand cell surface receptor that is highly expressed in brain and contains four extracellular ligand-binding domains (designated I–IV). Over 30 different ligands for LRP have been reported and include the classes: lipoproteins, coagulation factors, growth factors, extracellular matrix proteins, chaperones, and bacterial/viral proteins. The majority of LRP ligands bind to domains II and IV with equal affinity (Cam and Bu, 2006). Investigation into LRP's role in AD was stimulated by genetic evidence linking the LRP gene to late-onset AD (Kang et al., 1997). Zlokovic and colleagues first reported LRP's effects on Aβ efflux, showing that the *in vivo* clearance of radiolabeled Aβ peptides injected into the brains of mice was inhibited by co-injection with the endogenous inhibitor receptor-associated peptide (RAP) and by an anti-LRP antibody (Shibata et al., 2000). *In vivo* studies of LRP's potential for effluxing Aβ are promising, but they do not identify the biochemical mechanism of the apparent transcytosis of intact Aβ across the endothelial cells of the BBB.

* Corresponding author. Harvard Institutes of Medicine Room 730, 77 Avenue Louis Pasteur, Boston, MA 02115, USA. Fax: +1 617 525 5252.
E-mail address: dselkoe@rics.bwh.harvard.edu (D.J. Selkoe).
Available online on ScienceDirect (www.sciencedirect.com).

0969-9961/$ - see front matter © 2008 Elsevier Inc. All rights reserved.
doi:10.1016/j.nbd.2007.12.005

Moreover, as a member of the LDL receptor family, LRP is primarily an endocytic receptor and is not generally known to transcytose its ligands, most of which are degraded in lysosomes after endocytosis (Krieger and Herz, 1994).

P-glycoprotein (Pgp) is a 170 kDa single-transmembrane protein known for its role in resistance to chemotherapeutic drugs (Sharom, 1997). *In vivo* work has shown that PGP-null mice clear microinjected [^{125}I]Aβ out of the CNS at half the rate of wt mice and that Aβ increases within brain ISF after treatment with a Pgp inhibitor (Cirrito et al., 2005). As with LRP, the mechanism of Pgp-mediated Aβ efflux is unknown and has not been studied in controlled culture models of the BBB. All known substrates of Pgp are small molecules and cytosolic, whereas Aβ is a peptide and is not known to exist in the cytosol. While *in vivo* work has thus generated much excitement with regard to the potential of LRP and Pgp to efflux cortical Aβ, elucidating the molecular mechanisms of these effects through well-controlled in vitro models should help to promote rational therapeutic design.

Madin–Darby canine kidney (MDCK) cells are routinely used as a model of polarized protein sorting and trafficking (Irvine et al., 1999), and have been used previously to investigate polarization of amyloid-β precursor protein (APP) and its proteolytic products, Aβ and the secreted ectodomain, APPs (Haass et al., 1994). An *in vitro* model of a polarized epithelial barrier having tight intercellular junctions can be created by plating MDCK cells onto a porous polycarbonate filter, separating apical (AP) and basolateral (BL) compartments of medium, representing the brain and blood compartments, respectively, of a BBB-like barrier. MDCK monolayers plated in this manner have been used to investigate transcytosis of cell-surface proteins (Brandli et al., 1990), as well as antibody-antigen complexes (Hunziker and Mellman, 1989). MDCK monolayers have been used to simulate transport across the BBB (Garberg et al., 2005; Gumbleton and Audus, 2001). Despite its epithelial origin, this polarized, immortalized and impermeable system provides a manipulable model for investigating the effects of Pgp and LRP on Aβ BBB transport.

Materials and methods

Cell culture

MDCK wt cells (ATCC, Manassas, VA) were grown in DMEM with 10% FBS, 2 mM L-glutamine, 100 U/ml penicillin, 100 μg/ml streptomycin and 20 mM HEPES buffer. MDCK cells stably transfected with Pgp (MDCK-Pgp) or empty vector (MDCK-Parental) were the generous gift of Dr. P. Borst (Bakos et al., 1998). MDCK-Pgp cells were grown in the same media as MDCK wt cells and replaced with frozen stocks after one month of passage. MDCK cells stably transfected with mLRP4 (MDCK-mLRP4), an LRP-minireceptor which contains the native C-terminus and transmembrane domain, a N-terminal hemagglutinin (HA) tag, but only one (IV) of its four ligand-binding domains (Obermoeller-McCormick et al., 2001), were the generous gift of Dr. M. Marzolo (Marzolo et al., 2003). MDCK-mLRP4 cells were grown in the same media as MDCK cells, with the addition of 200 μg/ml G418. An immortalized human brain endothelial cell line, HCMEC/D3 (Weksler et al., 2005), was generously provided by Dr. B. Weksler, and grown in EGM-2 endothelial cell media (Lonza Group, Basel, Switzerland) on dishes coated with 50 μg/ml rat tail collagen I (BD Biosciences, Franklin Lakes, NJ).

In vitro transwell MDCK model

MDCK cells were plated onto 6.5 mm diameter Transwell filters (Corning Life Sciences, Acton, MA) with 0.4 μm pores at a seeding density of 1×10^5 cells per filter. Media was changed daily, with 100 μl in the apical (AP) compartment and 600 μl in the basolateral (BL) compartment. Trans-epithelial electrical resistance (TEER) was measured using an EVOM epithelial volt-ohmmeter with STX2 electrodes (World Precision Instruments, Sarasota, FL). Background resistance across a non-seeded filter was subtracted from the TEER measurements. Models were used for Aβ transport experiments on day 5. [^{125}I]Aβ$_{40}$, [^{14}C]Inulin or [^{3}H]Verapamil (GE Healthcare Bio-sciences, Piscataway, NJ) were added to the media in the BL side of the Transwell filters at concentrations of 1 nM, 0.5 μCi/ml and 1 μCi/ml, respectively. For inhibition of Pgp, 25 μg/ml RU-486 (Biomol International, Plymouth Meeting, PA) was added to AP and BL media immediately before transport experiments. At each timepoint, 10 μl samples of AP and BL medias were counted on a Cobra II Auto-Gamma scintillation counter (Packard Biosciences, Shelton, CT) for ^{125}I, or on a Beckman-Coulter LS6500 scintillation counter (Beckman-Coulter, Fullerton, CA) for ^{14}C or ^{3}H. To determine the amount of intact radiolabeled peptide, 50 μl of 15% trichloroacetic acid was added to a 50 μl sample of media and centrifuged at 10,000×*g* for 10 min. Supernatant (degraded peptide) and pellet (intact peptide) were counted separately for [^{125}I].

Transport of each compound across the monolayers was calculated as the percentage of the total counts per minute that were detected in the AP compartment. For Aβ transport, to control for paracellular leak in each Transwell monolayer, both [^{14}C]inulin and [^{125}I]Aβ were added to BL compartments, and an Aβ clearance quotient (Aβ CQ) was calculated as below:

$$\text{A}\beta\ \text{CQ} = \frac{\left[^{125}\text{I}\right]_{\text{AP}}/\left(\left[^{125}\text{I}\right]_{\text{AP}} + \left[^{125}\text{I}\right]_{\text{BL}}\right)}{\left[^{14}\text{C}\right]_{\text{AP}}/\left(\left[^{14}\text{C}\right]_{\text{AP}} + \left[^{14}\text{C}\right]_{\text{BL}}\right)}$$

Polarized cell surface biotinylation and gel electrophoresis

MDCK wt or MDCK-mLRP4 cells were plated onto 24 mm diameter Transwell filters with 0.4 μm pores at a seeding density of 1×10^6 cells per filter and grown for five days with 1.5 ml AP and 2.5 ml BL media. Monolayers were washed on both sides with cold PBS with Ca^{2+} and Mg^{2+} (PBS^{++}) four times. EZ-link Sulfo-NHS-SS-biotin (Pierce Biotechnology, Rockford, IL) was dissolved to 1 mg/ml in cold HBSS and 1 ml was added to either AP or BL compartments. One ml PBS^{++} was added to the non-biotinylated side. Monolayers were rocked for 1 h at 4 °C, and 50 μl quenching solution (Pierce) was added to the biotinylated side. Cells were scraped and lysed in 1% NP40 lysis buffer with protease inhibitors. After normalizing for total protein concentrations using a bicinchoninic assay (Pierce), the cell lysate was precipitated with 1 ml immobilized NeutrAvidin gel (Pierce) per 3 mg total protein overnight with mixing at 4 °C. Immobilized Neutravidin gel was centrifuged at 2500×*g* for 2 min. Biotinylated proteins were eluted with SDS-PAGE sample buffer with 50 mM DTT.

Samples were electrophoresed on an 8% Tris–Glycine gel (Invitrogen, Carlsbad, CA) and immunoblotted with 3F10 rat monoclonal anti-HA antibody (Roche, Basel, Switzerland) for detection of mLRP2, or C219 monoclonal mouse anti-Pgp antibody (ID Labs, London, Ontario).

Detection and immunoprecipitation of LRP in cell lysates

For detection of LRP, HCMEC/D3, HUVEC, MDCK wt and MDCK-mLRP4 cells were cultured to 80% confluency on 150-mm plates. Cells were washed three times with cold PBS with Ca^{2+} and Mg^{2+}, and were lysed in 300 µl of 1% Triton X-100 (Sigma) lysis buffer with 1 mM PMSF and protease inhibitors (Roche). Total protein was quantified using bicinchoninic acid protein assay (Pierce). 20 µg of cell lysates were boiled at 100 °C for 5 min in a 4x lithium dodecyl sulfate (LDS) sample buffer containing 50 mM DTT, then were electrophoresed at 200 V on a 9-well 4–12% Bis–Tris gel for 35 min in a MES SDS running buffer (Invitrogen). Proteins were transferred onto 0.2 µm nitrocellulose membranes, probed with MMMM, a rabbit polyclonal anti-LRP tail antibody (kindly provided by Dr. G. Bu), and detected using the LiCor Odyssey Infrared Imaging System.

For immunoprecipitation of LRP, lysates of HCMEC/D3 cells from 150-mm plates were prepared in 1 ml non-denaturing lysis buffer (20 mM Tris HCl pH 8 containing 137 mM NaCl, 10% glycerol, 1% Nonidet P-40 (NP-40) and 2 mM EDTA) with protease inhibitors (Roche). 300 µl of lysate was pre-cleared with 20 µl protein A-coupled sepharose (PAS) beads (Sigma) and 20 µl protein G-coupled agarose (PGA) beads (Roche) for 1 h under rotary agitation at 4 °C. Non-specifically bound proteins to beads were removed by centrifugation and supernatants were incubated with 5A6, an anti-LRP light-chain mouse monoclonal antibody (Calbiochem) and 15 µl each of PAS and PGA beads at 4 °C under rotary agitation overnight. Beads were then centrifuged and washed in lysis buffer three times. After the final wash, pellet was boiled at 100 °C for 5 min in 2X LDS sample buffer containing 50 mM DTT (Invitrogen) to denature and reduce the protein, and to separate it from the beads. The samples were centrifuged, and supernatants were electrophoresed to detect LRP via WB as described above.

FACS-based Aβ endocytosis assay

HCMEC/D3, MDCK wt or MDCK-mLRP4 cells were plated onto 6-well dishes at a seeding density of 1×10^5 cells per well and allowed to grow overnight. 500 nM RAP (Oxford Biomedical Research, Oxford, MI) was added to inhibit LRP activity in some wells. At this concentration, RAP is most selective for inhibition of LRP, while minimizing cross-inhibition of receptors in the same family, VLDL-R and LDL-R (Holtzman, personal communication). 100 nM fluorescently-labeled HiLyte Fluor 555-$A\beta_{1-40}$ or HiLyte Fluor 488-$A\beta_{1-42}$ (AnaSpec, San Jose, CA) were added at various timepoints, and cells were washed twice with PBS and then removed from the plate using 0.25% trypsin/EDTA solution. Cells were centrifuged at 800×*g* for 5 min, and resuspended in 100 µl PBS with 10% BSA. Five µl 7-amino-actinomycin D (7-AAD; BD Biosciences) was added for 10 min prior to analysis to control for cell viability. 1×10^5 cells from each sample were analyzed for fluorescence on a BD FACSCalibur machine (BD Biosciences). Unstained cells without any exposure to fluorescently-labeled Aβ were used as a control for background fluorescence, and Aβ uptake was quantified as the percentage of non-7-AAD-containing cells in each sample above the background level of fluorescence.

Radioactivity-based Aβ endocytosis assay

HCMEC/D3, MDCK wt or MDCK-mLRP4 cells were plated as in the FACS-based assay above. 1 nM [^{125}I]Aβ was added to each well at various timepoints, and cells were removed as in the FACS-based assay. Cell pellets were lysed in 100 µl of 1% NP40 lysis buffer with protease inhibitors. 10 µl samples of the lysate were analyzed for [^{125}I] counts, and 50 µl was precipitated with 50 µl TCA as described above for analysis of peptide degradation.

Statistical analysis

Data was analyzed using a one-way ANOVA with Tukey's post hoc comparison or a two-way ANOVA with Bonferroni post hoc comparison, where appropriate. Calculated comparisons of $p<0.05$ were considered significant.

Results

Assessment of Transwell MDCK model of the BBB

In order to simulate the integrity of the BBB, an *in vitro* model must demonstrate adequate tight junction formation as well as impermeability to macromolecules. To assess the former, the trans-epithelial electrical resistance (TEER) of Transwell MDCK monolayers was measured daily after plating, reaching an average of 85.8±0.60 Ω*cm^2 (mean±SD; $n=22$) after 5 days (Fig. 1A). As with most in vitro BBB models, this value falls far short of

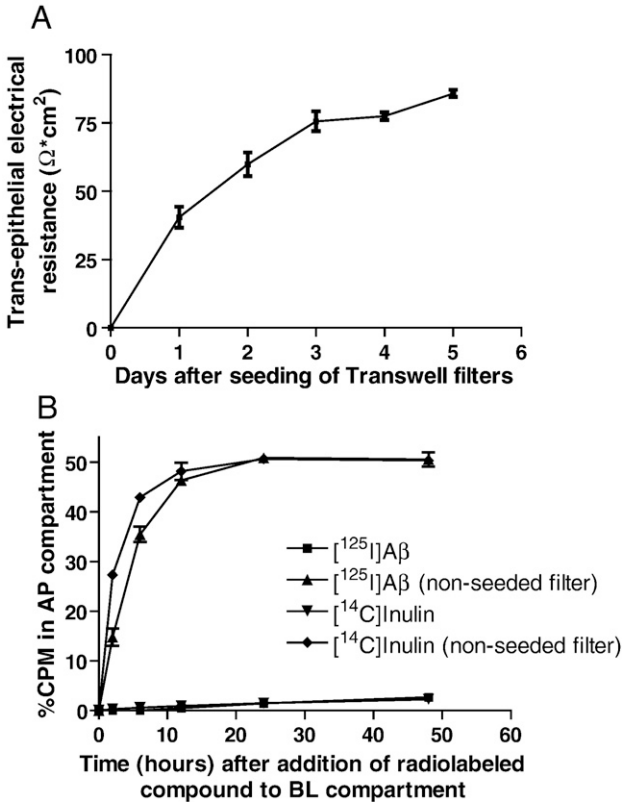

Fig. 1. BBB-like characteristics of the MDCK Transwell model. A, Trans-epithelial electrical resistance. TEER increases daily with monolayer growth. Data are mean±SEM ($n=22$ independent Transwell filters). B, [^{14}C]Inulin and [^{125}I]Aβ permeabilities. Both radiolabeled compounds freely diffuse across non-seeded Transwell filters such that half of the BL-added CPM are found in the AP compartment by 12 h. In contrast, less than 3% of each molecule is able to cross MDCK monolayers after 48 h. Data shown are mean± SD ($n=3$ at each time point).

recorded values for the *in vivo* BBB of 1870±639 Ω*cm^2 (mean± SD; n=40) (Crone and Olesen, 1982), but it is greater than achieved in most endothelial cell *in vitro* models (Garberg et al., 2005). TEER of MDCK cells transfected with Pgp or mLRP4 was not significantly different from that of MDCK wt cells (data not shown).

The inert polysaccharide, inulin (1.7 kDa) is routinely used as a control for paracellular leak in models of epithelial and endothelial barriers given its lack of active, receptor-mediated transport. [^{14}C] Inulin was added to the BL side of MDCK cell-seeded and non-seeded control Transwell filters, and radioactivity of media on both sides was counted at 2, 6, 12, 24 and 48 h. At 48 h, MDCK cell-seeded BBB models remained quite impermeable to inulin, with only 2.3% of [^{14}C]inulin counts crossing to the AP compartment compared to 50.3% that freely diffuses across non-seeded filters (Fig. 1B). To determine the ability of MDCK wt cells to transport Aβ, the same experiment was performed with [^{125}I]Aβ$_{40}$, with 2.7% crossing MDCK cell-seeded filters compared to 49.1% across non-seeded controls (Fig. 1B). The high TEER values and low [^{14}C]inulin permeability across MDCK wt cells indicates that MDCK Transwell monolayers provide a BBB-like model with low paracellular leak for the investigation of macromolecular transport. Furthermore, because permeability of MDCK wt monolayers to inulin and Aβ was similar, these cells represent a manipulable model in which transfection with LRP, Pgp, or other potential Aβ transporters can be shown to promote Aβ transport across the BBB, elucidating its mechanism.

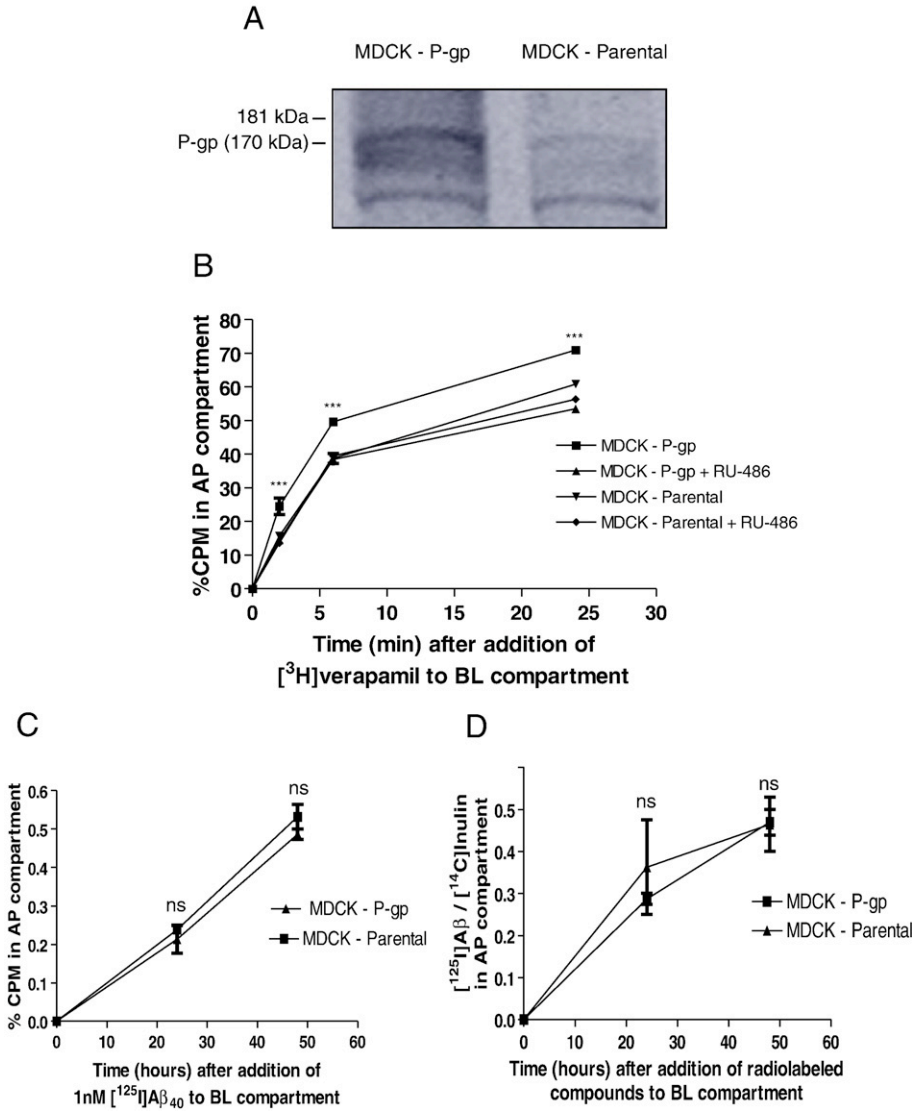

Fig. 2. Pgp upregulation does not promote Aβ transcytosis. A, Western blot of Pgp from whole cell lysatses of MDCK-Pgp and MDCK-Parental cells showing increased Pgp expression the former. B, Transport of [^{3}H]verapamil across MDCK-Pgp and MDCK-Parental Transwell monolayers. MDCK-Pgp cells express functional Pgp as evidenced by increased BL-to-AP transport of [^{3}H]verapamil across their monolayers compared to that of MDCK-Parental cells (p<0.001 at 2, 6 and 24 h). RU-486, a pharmacological Pgp inhibitor, eliminated this difference when added to MDCK-Pgp monolayers (p<0.001 at 2, 6 and 24 h). C, Transport of [^{125}I]Aβ across MDCK-Pgp and MDCK-Parental monolayers. MDCK-Pgp monolayers do not exhibit greater BL-to-AP transport of [^{125}I]Aβ than MDCK-Parental monolayers. (p>0.05 at each timepoint). D, Aβ clearance quotient, which controls for paracellular leak by dividing Aβ transport by inulin transport, is not significantly different between MDCK-Pgp and MDCK-Parental monolayers (p>0.05 at each timepoint). Data shown are mean±SEM (n=3 at each time point).

MDCK-Pgp BBB models

Expression of Pgp by MDCK-Pgp cells was verified by Western blotting. Pgp expression was significantly greater in the MDCK-Pgp cell line, although some expression was seen in the empty vector-transfected (MDCK-Parental) line (Fig. 2A). This was likely due to cross-reacting endogenous expression of canine ABC-family transporters including Pgp, as seen previously (Lalloo et al., 2004).

Verapamil, a known substrate for Pgp that is preferentially effluxed across the BBB by this transporter, was used to determine functional expression of Pgp in the cells. [^{3}H]Verapamil was added to the BL compartment of Transwell filters of MDCK-Pgp and MDCK-Parental monolayers. After 6 h, 60.0% of [^{3}H]verapamil had been transported to the AP compartment of MDCK-Pgp monolayers, as compared with 47.4% for MDCK-Parental monolayers. When RU-486, a pharmacological inhibitor of Pgp, was added to MDCK-Pgp monolayers, the 6 h transport was rescued to

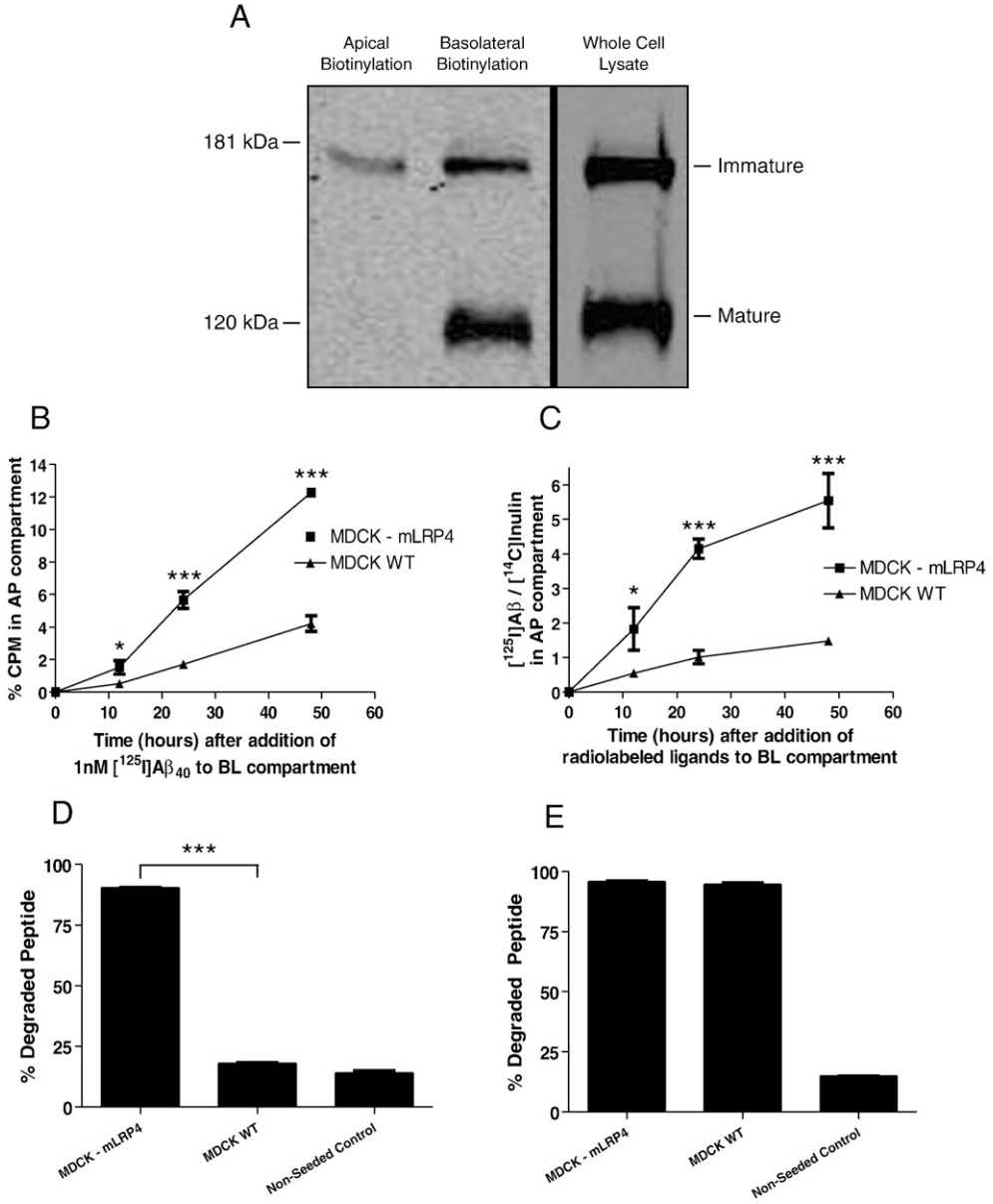

Fig. 3. mLRP4 expression promotes Aβ uptake and intracellular degradation, but not transcytosis. A, Western blot of mLRP4 in whole cell lysates, and in apically and basolaterally biotinylated of MDCK-mLRP4 cells on Transwell filters after precipitation with immobilized neutravidin. MDCK-mLRP4 cells express both mature and immature forms of the minireceptor on the BL surface, but only the immature, unprocessed form on the AP surface. B, Transport of [^{125}I] Aβ across MDCK-mLRP4 and MDCK wt monolayers. MDCK-mLRP4 monolayers exhibit greater BL-to-AP transport of [^{125}I] counts than MDCK wt monolayers ($p<0.05$ at 12 h, $p<0.001$ at 24 and 48 h). C, Aβ clearance quotient is significantly higher for MDCK-mLRP4 than for MDCK wt monolayers ($p<0.05$ at 12 h, $p<0.001$ at 24 and 48 h). D, TCA precipitation of BL media. MDCK-mLRP4 monolayers degraded significantly more of the [^{125}I]Aβ that was added to the BL compartment than MDCK wt monolayers ($p<0.001$ at 48 h), accounting for the increased transport of [^{125}I] counts seen in (B) and (C). E, TCA precipitation of AP media. 48 h after adding 1 nM [^{125}I]Aβ to the BL compartments, nearly all [^{125}I] counts that crossed MDCK-mLRP4 or MDCK wt monolayers were due to degraded peptide fragments. Data shown are mean ± SEM ($n=3$ at each time point). Error bars in D and E are present, but too small to be seen.

45.3%, near that of MDCK-Parental control cells (Fig. 2B). These results indicate functional expression of Pgp in the MDCK-Pgp cell line. The high background level of [^{3}H]verapamil transport in MDCK-Parental cells and after RU-486 treatment of MDCK-Pgp cells is presumably due to passive paracellular and transcellular leak of the small molecule, as well as to activity of other endogenous ABC-family transporters, many of which are not inhibited by RU-486.

To determine the ability of Pgp to transcytose Aβ, 1 nm [^{125}I]Aβ was added to the BL compartment of MDCK-Pgp and MDCK-Parental control Transwell monolayers. After 48 h, there was very little transport of [^{125}I] counts from the BL to AP compartment in both the MDCK-Pgp and MDCK-Parental monolayers (0.56% vs 0.47%, $p>0.05$) (Fig. 2C). There was also no significant difference in the Aβ clearance quotient (Fig. 2D), indicating that all of the apically-localized Aβ was due to paracellular leak and that up-regulation of Pgp alone is insufficient to promote Aβ transcytosis across this *in vitro* BBB model.

MDCK–mLRP4 BBB models

MDCK cells stably expressing the LRP minireceptor, mLRP4, or non-transfected controls (MDCK wt) were plated on Transwell filters. To determine expression and polarity of mLRP4, the AP and BL sides of the monolayers were biotinylated separately, and plasma membrane proteins were precipitated with neutravidin and analyzed by Western blotting. LRP and its minireceptors are known to be cleaved by furin to yield the mature, functional version of the receptor (Obermoeller-McCormick et al., 2001). Both immature and mature forms were expressed on the BL surface of our Transwell BBB model, but only the immature form was expressed on the AP surface (Fig. 3A).

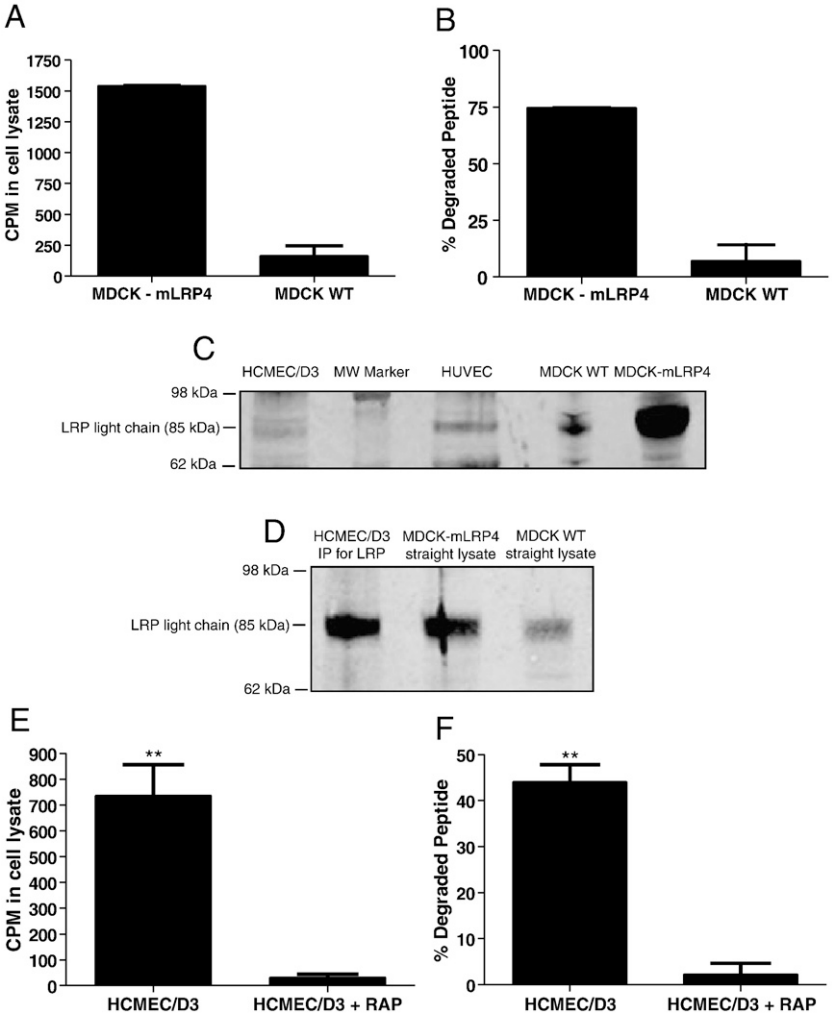

Fig. 4. LRP mediates Aβ endocytosis and intracellular degradation. A, [^{125}I] CPM in MDCK-mLRP4 and MDCK wt cell lysates after 24 h exposure to 1 nM [^{125}I]Aβ. Significantly more [^{125}I]Aβ was endocytosed by MDCK-mLRP4 cells than by MDCK wt cells ($p<0.01$). B, TCA precipitation of MDCK-mLRP4 and MDCK wt cell lysates after 24 h exposure to 1 nM [^{125}I]Aβ. Significantly more intracellular degradation occurred in MDCK-mLRP4 cells than in MDCK wt cells ($p<0.01$). C, Western blot of LRP light chain in whole cell lysates (20 μg total protein) of HCMEC/D3, HUVEC, MDCK wt, and MDCK-mLRP4 cells. D, Western blot of MMMM-immunoprecipitated LRP light chain from HCMEC/D3 cell lysates (100 μg total protein), and non-precipitated LRP light chain from whole cell lysates (20 μg total protein) of MDCK-mLRP4 and MDCK wt cells. E, [^{125}I] CPM in HCMEC/D3 endothelial cell lysates after 24 h of exposure to 1 nM [^{125}I]Aβ in the presence or absence of 500 nM RAP. [^{125}I]Aβ endocytosis was significantly inhibited by inhibition of LRP activity by RAP ($p<0.01$). F, TCA precipitation of HCMEC/D3 cell lysates after 24 h exposure to 1 nM [^{125}I]Aβ in the presence or absence of 500 nM RAP. [^{125}I]Aβ degradation was significantly inhibited by RAP ($p<0.01$) Data are mean±SEM ($n=3$).

To determine the ability of LRP to transcytose Aβ, 1 nm [^{125}I]Aβ was added to the BL compartment of MDCK-mLRP4 and MDCK wt Transwell monolayers. After 48 h, 11.8% of total [^{125}I] counts in MDCK-mLRP4 Transwell monolayers were found in the AP compartment, compared to 4.0% in MDCK wt monolayers (Fig. 3B). The Aβ clearance quotient was significantly higher for MDCK-mLRP4 monolayers than for MDCK wt monolayers (Fig. 3C), indicating a selective transport of [^{125}I]Aβ. However, when AP and BL media were precipitated with TCA to quantify the intact Aβ peptide, we found that 81.9% of the [^{125}I]Aβ in the BL compartment of MDCK wt monolayers at 48 h was still intact, whereas only 9.6% remained intact at 48 h in the BL compartment of the MDCK-mLRP4 monolayers (Fig. 3D). In the AP compartments, virtually all of the [^{125}I] counts that reached this compartment represented degraded peptide in both the MDCK wt and MDCK-mLRP4 monolayers (Fig. 3E), suggesting that only fragments of Aβ efficiently cross the in vitro barrier from the BL to AP side. These findings suggest that the overexpression of LRP on the BL plasma membrane promotes Aβ degradation, but alone is insufficient to promote the transcytosis of the intact peptide, as would be required for non-proteolytic efflux of Aβ across the barrier.

LRP-mediated Aβ endocytosis and degradation

The reported role of LRP for all studied ligands besides Aβ is to bind, endocytose and facilitate their degradation. In accord with these data, expressing mLRP4 on the BL plasma membrane in our MDCK monolayer resulted in no LRP-mediated transport of intact [^{125}I]Aβ, but rather transport of [^{125}I]-bearing cleaved peptide fragments. To directly address this process, MDCK wt and MDCK-mLRP4 cells were grown in conventional cultures and exposed to 1 nM [^{125}I]Aβ. At 24 h, the cells were washed to remove surface peptide, lysed and samples of the lysate counted for internalized [^{125}I]. We found that [^{125}I]Aβ uptake was markedly greater in MDCK-mLRP4 than MDCK wt cells (1543 vs 166 CPM; Fig. 4A). Samples of the lysate (Fig. 4B) were then precipitated with TCA to determine the percentage of intact Aβ. In MDCK-mLRP4 cultures, significantly more intracellular Aβ had been degraded by 24 h compared with MDCK wt cultures (74.7 vs 7.1%) (Fig. 4B).

While the MDCK monolayer presents a polarized, impermeable and manipulable system for the investigation of LRP's effects on Aβ transcytosis, it is not of endothelial origin. To determine the effects of LRP on Aβ endocytosis and degradation in an endothelial cell culture, immortalized HCMEC/D3 cells, which are of human brain endothelial origin, were used in a similar experiment. First, we determined LRP expression in HCMEC/D3 cells, as well in the positive controls human umbilical vein endothelial cells (HUVEC) and MDCK-mLRP4 cells by western blotting with MMMM rabbit polyclonal anti-LRP light chain antibody. A faint 85 kDa band was seen in the HCMEC/D3 lane (Fig. 4C), consistent with expression of the LRP light chain. This expression was verified by immunoprecipitation of the LRP light chain with MMMM, and western blotting with 5AG, a mouse monoclonal anti-LRP light chain (Fig. 4D).

HCMEC/D3 cells were incubated with 1 nM [^{125}I]Aβ in the presence or absence of 500 nM RAP to inhibit endogenous LRP activity. [^{125}I]Aβ uptake (33 vs 737 CPM) (Fig. 4E) and degradation (2.3 vs 44.2%) (Fig. 4F) were decreased in the presence of RAP. As with primary endothelial cells and other immortalized endothelial lines, when these cells were seeded onto Transwell filters, they failed to achieve adequate TEER or inulin impermeability to allow investigation of Aβ transcytosis (data not shown).

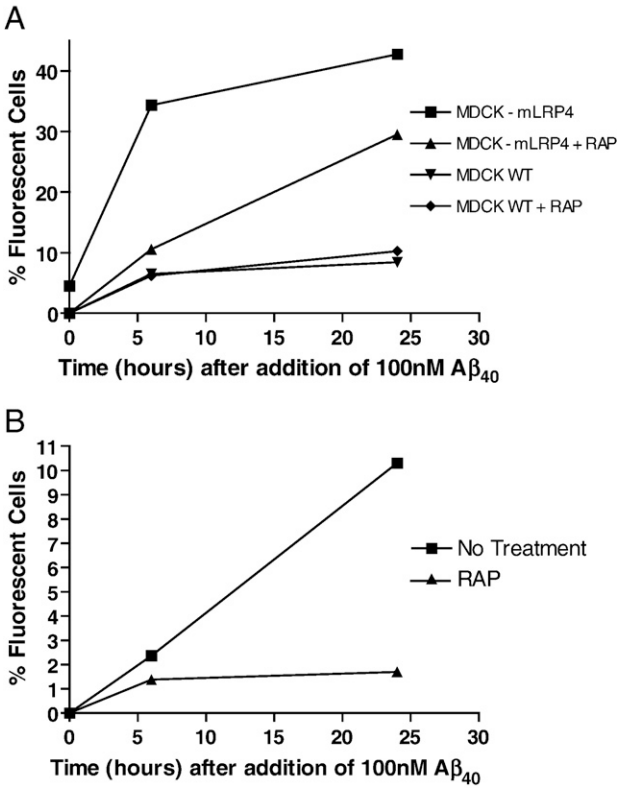

Fig. 5. FACS-based analysis of fluorescently-labeled $A\beta_{40}$ uptake. A, MDCK-mLRP4 cells exhibit greater time-dependent uptake of fluorescent Aβ than do MDCK WT cells. This effect of LRP activity was partially reversed by the addition of 500 nM RAP. B, HCMEC/D3 cells also exhibit time-dependent Aβ uptake that is inhibited by co-administering 500 nM RAP. 1×10^5 cells from each cell population were counted.

Theoretically, a radiolabel could alter the physiologic function or activity of a peptide. To further confirm the ability of LRP to promote Aβ endocytosis by using a different label on the peptide, fluorescently-labeled Aβ was added to MDCK-mLRP4 and MDCK wt cells in culture at various time points, and the fluorescent cells that had endocytosed Aβ were counted using FACS. As with the radiolabeled Aβ, the uptake of HiLyte Fluor 555-$A\beta_{1-40}$ was time-dependent and significantly greater with MDCK-mLRP4 cells than with MDCK wt cells (42.7% vs 8.41% at 24 h) (Fig. 5A). Addition of RAP significantly decreased Aβ uptake by MDCK-mLRP4 cells down to 29.5% at 24 h (Fig. 5A). Similar results were obtained for uptake of fluorescently-labeled $A\beta_{42}$ (data not shown).

Finally, HCMEC/D3 cells were used in the same FACS-based Aβ uptake assay. Their $A\beta_{40}$ uptake was also time-dependent and significantly inhibited by RAP (Fig. 5B).

Discussion

As the Aβ hypothesis has gained increasing acceptance as the apparent mechanism of AD pathogenesis, investigation surrounding potential strategies to chronically decrease cortical Aβ levels has intensified. Of several such approaches, the non-proteolytic clearance of Aβ by efflux across the BBB is perhaps the least studied, and the biochemical basis for this phenomenon is unclear. The promising *in vivo* work identifying Pgp and LRP as potential Aβ efflux pumps needs to be followed up using controlled *in vitro*

models to help elucidate the molecular basis for the apparent transport of Aβ across cell barriers by these proteins.

The MDCK in vitro model we principally used here, while of epithelial rather than endothelial origin, is a useful tool for the mechanistic investigation of potential Aβ transporters across tight monolayer barriers. These cells readily form monolayers that are polarized and impermeable to macromolecules—two properties that are vital to investigation of Aβ transcytosis, and that have not been readily reproduced in many endothelial BBB models. Furthermore, MDCK cells can be transfected with Pgp, LRP minireceptors, or other gene products that may be implicated in the process of Aβ efflux across the BBB.

In our study, MDCK cells stably overexpressing Pgp did not exhibit any increased transport of [^{125}I]Aβ across their monolayers when compared with MDCK cells transfected with empty vector and cultured identically. Although they functionally expressed Pgp, as evidenced by the efficient efflux of [^{3}H]verapamil that was inhibited by RU-486, the upregulation of Pgp alone was not sufficient to promote Aβ transcytosis as has been suggested by *in vivo* experiments in which Pgp-null mice clear CNS-injected Aβ at a lower rate than did wt mice, and in which administration of a Pgp inhibitor increased Aβ levels in the brain ISF within hours (Cirrito et al., 2005). Because Pgp is a transporter whose ligands are almost exclusively small molecules (no peptide substrates of Pgp have been identified), it is not surprising that the pump itself is unable to transport a 4 kDa peptide such as Aβ. It is possible that Pgp functions in conjunction with another transporter or requires an as-yet-unidentified cofactor for Aβ transcytosis such that its inhibition or deletion *in vivo* inhibited Aβ clearance and increased cortical Aβ levels but its upregulation failed to promote Aβ efflux in our cellular model.

In our MDCK-mLRP4 model, LRP activity led to the uptake and degradation of [^{125}I]Aβ from the BL compartment, but not to transcytosis of the intact peptide in its intact form, as has been suggested by the results of *in vivo* experiments (Shibata et al., 2000). As with Pgp, the effects of LRP seen in our study are more congruent with its accepted biological mechanism—as an endocytic receptor that usually leads to degradation of its ligands. Any role it may have in transcytosing intact Aβ across the BBB, as in the case with Pgp, may require a co-transporter, or a downstream molecule. Nevertheless, our results clearly implicate LRP as a means of promoting Aβ degradation and help to explain the apparent relationship between down-regulation of LRP and progression of AD pathology in humans (Deane et al., 2004). Although it has been shown that complexes of Aβ and its binding partner α2-macroglobulin can be endocytosed by LRP (Kang et al., 2000), we demonstrate the ability of LRP to not only endocytose, but also lead to the degradation of the pathologic peptide.

There currently exists a disconnect between the accepted biological mechanisms of Pgp and LRP, with which our *in vitro* experiments are consistent, and the *in vivo* findings regarding LRP- and Pgp-mediated Aβ efflux across the BBB in rodents. More *in vitro* work on these two transporters and others that may serve as co-transporters in Aβ efflux may help to reconcile these differences. A compelling in vitro BBB model is invaluable to such efforts. While current endothelial monolayer systems need to be improved to create more impermeable and physiologic BBB models, the MDCK Transwell model described here is an impermeable, polarized and biochemically readily manipulable system for such invenstigations.

Acknowledgments

We would like to thank Drs. Piet Borst, Guojun Bu, María Paz Marzolo and Babette Weksler for their generous contribution of cell lines used in this study. We would also like to thank Drs. David Holtzman and Berislav Zlokovic for their advice regarding experimental design, and Drs. Joseph El Khoury and Danny Frenkel for their training on the methods used in this study. We would like to thank Matthew Hemming for his critical review of this manuscript. Babak Nazer is a Howard Hughes Medical Institute Research Training Fellow.

References

Bakos, E., et al., 1998. Functional multidrug resistance protein (MRP1) lacking the N-terminal transmembrane domain. J. Biol. Chem. 273, 32167–32175.

Brandli, A.W., et al., 1990. Transcytosis in MDCK cells: identification of glycoproteins transported bidirectionally between both plasma membrane domains. J. Cell Biol. 111, 2909–2921.

Cam, J.A., Bu, G., 2006. Modulation of beta-amyloid precursor protein trafficking and processing by the low density lipoprotein receptor family. Mol. Neurodegener. 1, 8.

Cirrito, J.R., et al., 2005. P-glycoprotein deficiency at the blood–brain barrier increases amyloid-beta deposition in an Alzheimer disease mouse model. J. Clin. Invest. 115, 3285–3290.

Crone, C., Olesen, S.P., 1982. Electrical resistance of brain microvascular endothelium. Brain Res. 241, 49–55.

Deane, R., et al., 2004. LRP/amyloid beta-peptide interaction mediates differential brain efflux of Abeta isoforms. Neuron 43, 333–344.

Garberg, P., et al., 2005. In vitro models for the blood–brain barrier. Toxicol. In Vitro 19, 299–334.

Gumbleton, M., Audus, K.L., 2001. Progress and limitations in the use of in vitro cell cultures to serve as a permeability screen for the blood–brain barrier. J. Pharm. Sci. 90, 1681–1698.

Haass, C., et al., 1994. Polarized secretion of beta-amyloid precursor protein and amyloid beta-peptide in MDCK cells. Proc. Natl. Acad. Sci. U. S. A. 91, 1564–1568.

Hardy, J., Selkoe, D.J., 2002. The amyloid hypothesis of Alzheimer's disease: progress and problems on the road to therapeutics. Science 297, 353–356.

Hunziker, W., Mellman, I., 1989. Expression of macrophage-lymphocyte Fc receptors in Madin–Darby canine kidney cells: polarity and transcytosis differ for isoforms with or without coated pit localization domains. J. Cell Biol. 109, 3291–3302.

Irvine, J.D., et al., 1999. MDCK (Madin–Darby canine kidney) cells: a tool for membrane permeability screening. J. Pharm. Sci. 88, 28–33.

Kang, D.E., et al., 1997. Genetic association of the low-density lipoprotein receptor-related protein gene (LRP), an apolipoprotein E receptor, with late-onset Alzheimer's disease. Neurology 49, 56–61.

Kang, D.E., et al., 2000. Modulation of amyloid beta-protein clearance and Alzheimer's disease susceptibility by the LDL receptor-related protein pathway. J. Clin. Invest. 106, 1159–1166.

Krieger, M., Herz, J., 1994. Structures and functions of multiligand lipoprotein receptors: macrophage scavenger receptors and LDL receptor-related protein (LRP). Annu. Rev. Biochem. 63, 601–637.

Lalloo, A.K., et al., 2004. Membrane transport of camptothecin: facilitation by human P-glycoprotein (ABCB1) and multidrug resistance protein 2 (ABCC2). BMC Med. 2, 16.

Marzolo, M.P., et al., 2003. Differential distribution of low-density lipoprotein-receptor-related protein (LRP) and megalin in polarized epithelial cells is determined by their cytoplasmic domains. Traffic 4, 273–288.

Obermoeller-McCormick, L.M., et al., 2001. Dissection of receptor folding and ligand-binding property with functional minireceptors of LDL receptor-related protein. J. Cell Sci. 114, 899–908.

Rubin, L.L., Staddon, J.M., 1999. The cell biology of the blood–brain barrier. Annu. Rev. Neurosci. 22, 11–28.

Selkoe, D.J., Schenk, D., 2003. Alzheimer's disease: molecular understanding predicts amyloid-based therapeutics. Annu. Rev. Pharmacol. Toxicol. 43, 545–584.

Sharom, F.J., 1997. The P-glycoprotein efflux pump: how does it transport drugs? J. Membr. Biol. 160, 161–175.

Shibata, M., et al., 2000. Clearance of Alzheimer's amyloid-ss(1–40) peptide from brain by LDL receptor-related protein-1 at the blood–brain barrier. J. Clin. Invest. 106, 1489–1499.

Silverberg, G.D., et al., 2003. Alzheimer's disease, normal-pressure hydrocephalus, and senescent changes in CSF circulatory physiology: a hypothesis. Lancet Neurol. 2, 506–511.

Tanzi, R.E., et al., 2004. Clearance of Alzheimer's Abeta peptide: the many roads to perdition. Neuron 43, 605–608.

Weiner, H.L., Frenkel, D., 2006. Immunology and immunotherapy of Alzheimer's disease. Nat. Rev. Immunol. 6, 404–416.

Weksler, B.B., et al., 2005. Blood–brain barrier-specific properties of a human adult brain endothelial cell line. Faseb J. 19, 1872–1874.

Zlokovic, B.V., 2004. Clearing amyloid through the blood–brain barrier. J. Neurochem. 89, 807–811.

Appendix 6

Soluble oligomers of amyloid β protein facilitate hippocampal long-term depression by disrupting neuronal glutamate uptake

Shaomin Li, Soyon Hong, Nina E. Shepardson, Dominic M. Walsh, Ganesh M. Shankar, and Dennis J. Selkoe

Contributions to this Appendix: S. Li performed all electrophysiology experiments, S. Hong performed and analyzed the glutamate uptake assay in isolated synaptosomes for Figures 4G and H and also performed some IP/WB experiments for Figure 1A, and N. Sherpardson performed the SEC/WB for Figure 1A. This manuscript was published in Neuron, Volume 62, Issue 6, pp 788-801 and is reproduced here in that form.

Neuron
Article

Soluble Oligomers of Amyloid β Protein Facilitate Hippocampal Long-Term Depression by Disrupting Neuronal Glutamate Uptake

Shaomin Li,[1] Soyon Hong,[1] Nina E. Shepardson,[1] Dominic M. Walsh,[2] Ganesh M. Shankar,[1] and Dennis Selkoe[1,*]
[1]Center for Neurologic Diseases, Brigham and Women's Hospital, Harvard Medical School, Boston, MA 02115, USA
[2]Laboratory for Neurodegenerative Research, University College Dublin, Dublin 4, Ireland
*Correspondence: dselkoe@rics.bwh.harvard.edu
DOI 10.1016/j.neuron.2009.05.012

SUMMARY

In Alzheimer's disease (AD), the impairment of declarative memory coincides with the accumulation of extracellular amyloid-β protein (Aβ) and intraneuronal tau aggregates. Dementia severity correlates with decreased synapse density in hippocampus and cortex. Although numerous studies show that soluble Aβ oligomers inhibit hippocampal long-term potentiation, their role in long-term synaptic depression (LTD) remains unclear. Here, we report that soluble Aβ oligomers from several sources (synthetic, cell culture, human brain extracts) facilitated electrically evoked LTD in the CA1 region. Aβ-enhanced LTD was mediated by mGluR or NMDAR activity. Both forms of LTD were prevented by an extracellular glutamate scavenger system. Aβ-facilitated LTD was mimicked by the glutamate reuptake inhibitor TBOA, including a shared dependence on extracellular calcium levels and activation of PP2B and GSK-3 signaling. In accord, synaptic glutamate uptake was significantly decreased by soluble Aβ. We conclude that soluble Aβ oligomers perturb synaptic plasticity by altering glutamate recycling at the synapse and promoting synapse depression.

INTRODUCTION

Alzheimer's disease (AD), the most common neurodegenerative disorder, is characterized by progressive memory and cognitive impairment and cerebral accumulation of extracellular amyloid plaques and intraneuronal neurofibrillary tangles. Although the specific molecular initiators of AD remain unknown in most patients, extensive research suggests that the amyloid β protein (Aβ) plays an early and essential pathogenic role. Of note, dementia severity in AD correlates more strongly with cortical levels of soluble Aβ species than with insoluble amyloid plaque burden (Lue et al., 1999; McLean et al., 1999). Experimentally, soluble Aβ oligomers have been specifically shown to block hippocampal long-term potentiation (LTP), an electrophysiological correlate of learning and memory (e.g., Lambert et al., 1998; Walsh et al., 2002; Wang et al., 2002; Townsend et al., 2006; Shankar et al., 2008). In accord, impairment of synaptic plasticity can be detected in vivo before the formation of insoluble Aβ deposits in APP transgenic mouse models (e.g., Hsia et al., 1999; Mucke et al., 2000). Synthetic Aβ aggregates have been reported to inhibit N-methyl-D-aspartate receptor (NMDAR)-dependent LTP, but not NMDAR-independent LTP (Chen et al., 2002; Wang et al., 2004a; but see Raymond et al., 2003). This finding is consistent with evidence that Aβ can affect surface expression of NMDARs (Snyder et al., 2005; Dewachter et al., 2009) and may increase (Molnár et al., 2004; Wu et al., 1995) or decrease (Chen et al., 2002; Raymond et al., 2003) NMDAR conductance.

A principal neuropathological finding in AD subjects is cortical atrophy associated with degeneration of neurites, decreased dendritic spine density, and frank neuronal loss (Terry et al., 1991; Knobloch and Mansuy, 2008). Anatomical studies in normal rodents suggest that the induction of LTP is associated with spine formation and increased spine volume, whereas the induction of long-term synaptic depression (LTD) results in decreased spine volume and spine elimination (Matsuzaki et al., 2004; Nägerl et al., 2004; Zhou et al., 2004; Bastrikova et al., 2008). Similar to LTP, the induction of LTD in the CA1 region of hippocampus requires activation of NMDAR and/or metabotropic glutamate receptors (mGluR), depending on the stimulation protocol and recording conditions (Kemp and Bashir, 2001; Anwyl, 2006; Citri and Malenka, 2008). Mechanistically, synapse potentiation versus depression may ultimately depend on alterations in cytosolic Ca^{2+} concentration and the differential activation of certain kinases and phosphatases, including p38 mitogen-activated protein kinase (MAPK) and calcineurin (protein phosphatase 2B [PP2B]) (reviewed in Kemp and Bashir, 2001; Citri and Malenka, 2008).

Although numerous reports describe the effects of soluble Aβ species on LTP, only a few studies have examined LTD induction, and they have yielded inconsistent results. For example, synthetic Aβ peptides were reported to facilitate LTD induction in an NMDAR-dependent manner in vivo (Kim et al., 2001), whereas other studies found no effect on LTD in slices (Raymond et al., 2003; Wang et al., 2002, 2004a). We recently extracted buffer-soluble Aβ directly from the brains of typical AD patients and showed that this extract, which contains soluble Aβ dimers and trimers, facilitated LTD induction in the CA1 region of mouse hippocampus by an mGluR-dependent mechanism (Shankar et al., 2008). Given that both NMDAR and mGluR activation have been implicated in the effects of Aβ on LTD, we asked

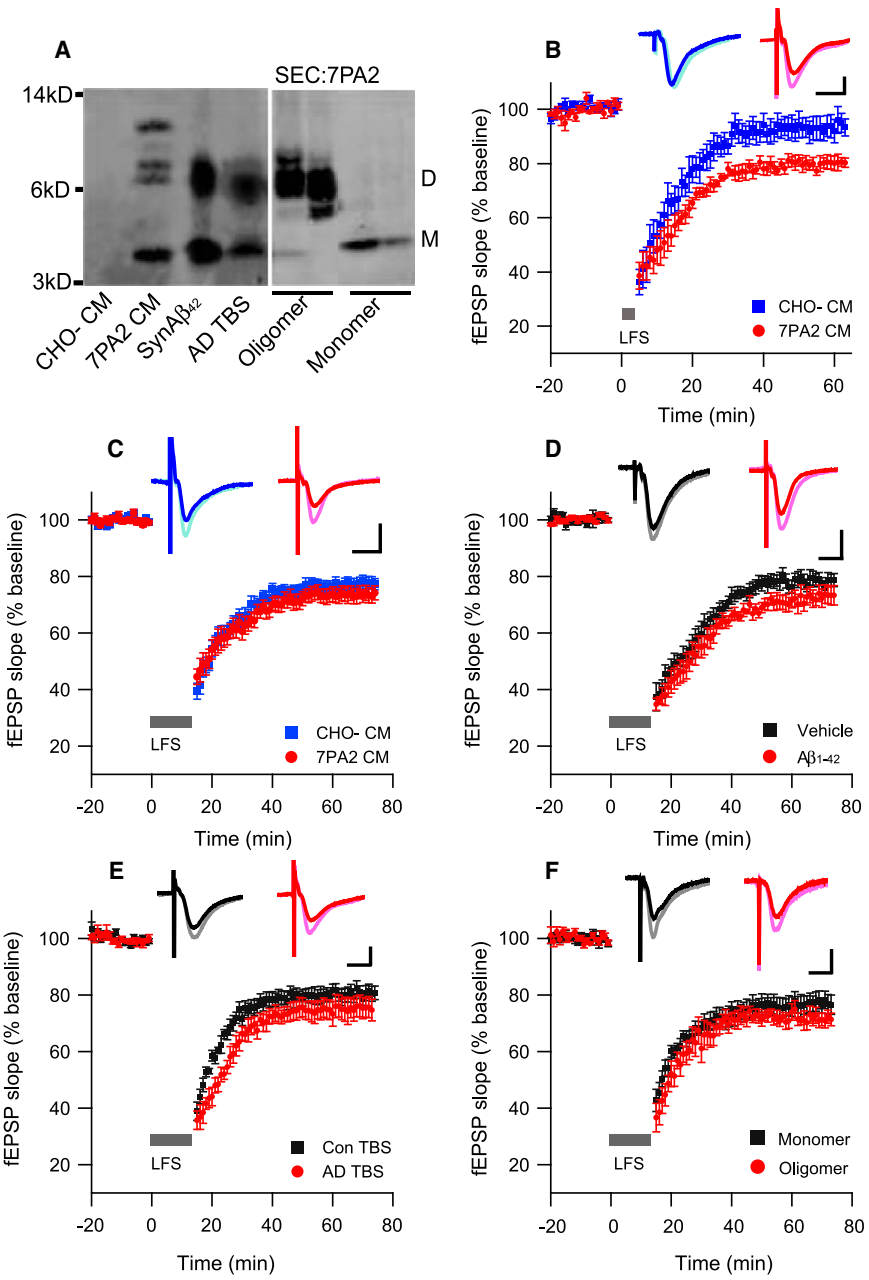

Figure 1. Soluble Aβ Facilitates Long-Term Depression in the CA1 Region of Hippocampal Slices

(A) Western blot of the three sources of soluble Aβ used for LTD experiments in this study. All three contain an SDS-stable band at ~8 kDa, and this has been confirmed previously as an Aβ dimer by mass spectrometry (Shankar et al., 2008). 7PA2 CM also contains a higher, apparent trimer species. CHO- CM is devoid of these human Aβ species, as expected, and serves as a negative control throughout these studies. All samples were immunoprecipitated with polyclonal Aβ antibody AW8 and blotted with combined Aβ monoclonal antibodies 2G3 ($Aβ_{40}$) and 21F12 ($Aβ_{42}$). SEC: fractions rich in oligomers (left) or monomers (right) separated by SEC of 7PA2 CM.

(B) A train of 300 single pulses at 1 Hz (5 min; small gray bar) did not induce LTD in acute mouse hippocampal slices in the presence of CHO- CM (blue squares, n = 6) but induced a significant LTD in the presence of 7PA2 CM (red circles, n = 7).

(C–F) A standard LTD protocol of 900 single pulses at 1 Hz (15 min; long gray bar) was applied to slices treated with 7PA2 CM (C), synthetic $Aβ_{1-42}$ (D), AD brain TBS extract (E), or SEC fractions from 7PA2 CM (F). All are not significantly different from their respective controls.

Insets in (B)–(F) represent typical field excitatory postsynaptic potentials (fEPSPs) recorded before (light) and 50 min after (dark) LFS. Horizontal calibration bar, 10 ms; vertical bar, 0.5 mV.

RESULTS

Soluble Human Aβ from Several Sources Facilitates Hippocampal LTD

Small, soluble Aβ assemblies have been obtained from a variety of sources, including synthetic peptides, cell culture medium, and human brain extracts (Lambert et al., 1998; Podlisny et al., 1995; McLean et al., 1999; Shankar et al., 2008). A common feature among the soluble Aβ preparations used in the current study is the presence of low-n assembly forms, i.e., Aβ oligomers that are slightly larger than the monomer but much smaller than amyloid fibrils. When examined on denaturing gels, these oligomers run principally as SDS-stable dimers and trimers (Figure 1A). We recently reported that soluble oligomers extracted directly from human (AD) cortex facilitate LTD induction through activation of mGluR when a subthreshold (300 pulses, 1 Hz) stimulation is applied to hippocampal slices (Shankar et al., 2008). To investigate the mechanisms underlying the enhancement of LTD by soluble human Aβ, we first used cell-secreted Aβ species obtained from a CHO cell line that stably expresses hAPP with the V717F amyloidogenic AD mutation (7PA2 cells). These cells release readily detectable levels of monomeric and oligomeric Aβ species into the medium in the

whether glutamate clearance mechanisms are perturbed by Aβ. In addition to affecting synaptic plasticity, excitotoxic effects of glutamate are believed to contribute to progressive neuronal loss in AD (Pomara et al., 1992; Harkany et al., 2000). Furthermore, gene expression and protein levels of excitatory amino acid transporters (EAAT1 and EAAT2) are altered in the hippocampus and frontal cortex of AD subjects (Jacob et al., 2007). Here, we provide evidence that small, soluble Aβ assemblies from several sources enhance synaptic depression through a mechanism involving altered glutamate uptake at hippocampal synapses. Our results have both mechanistic and therapeutic implications for the initiation of hippocampal synaptic failure in AD and in more subtle forms of age-related Aβ accumulation.

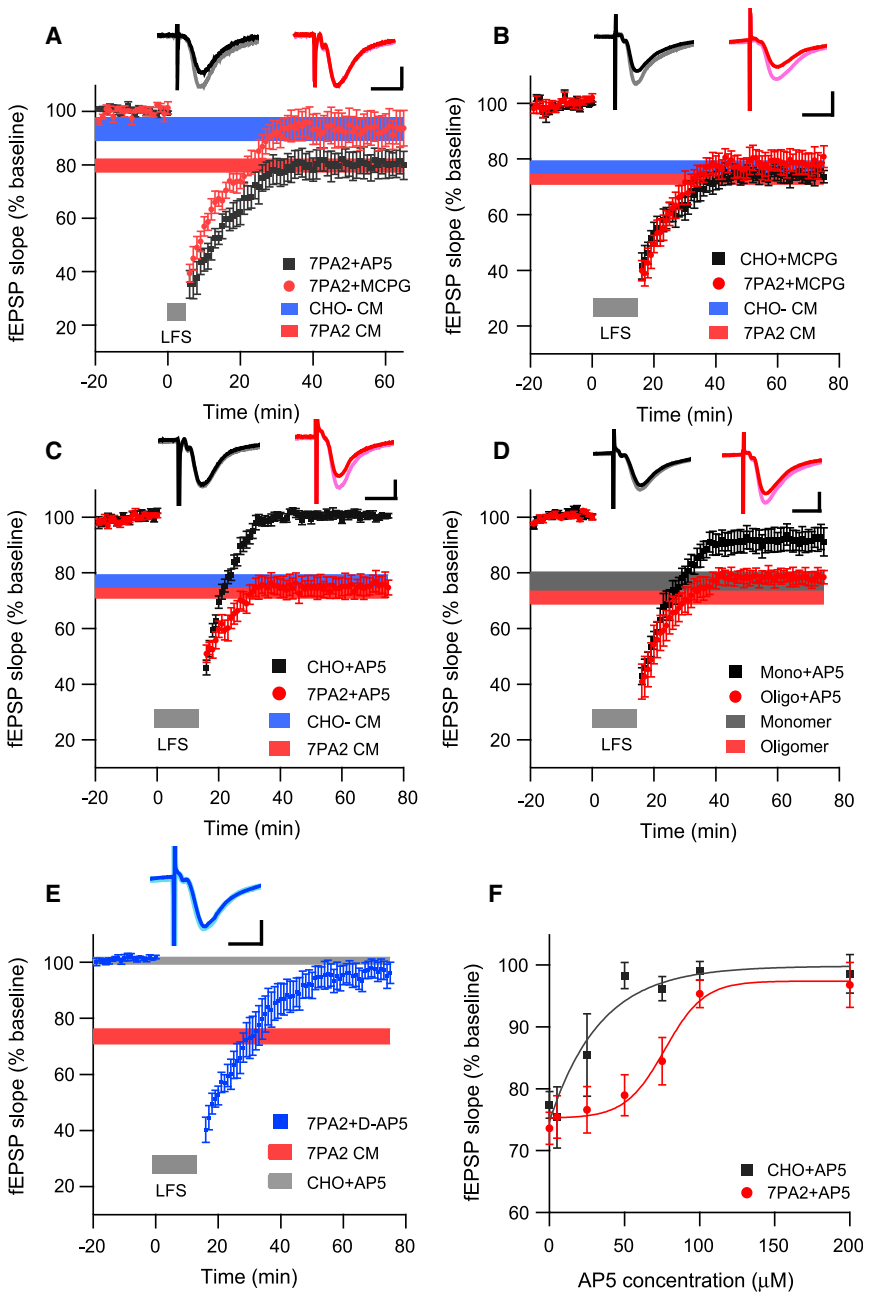

Figure 2. Soluble Aβ Enhances Hippocampal LTD through mGluR or NMDAR, Depending on the Stimulation Protocol

(A) LTD induced by the 300-pulse protocol (gray bar) in the presence of 7PA2 CM was blocked upon coadministration of the nonselective group I/II mGluR antagonist, MCPG (500 μM, red circles, n = 6), but not the NMDAR antagonist, AP5 (50 μM, black squares, n = 5). Horizontal colored bars represent the corresponding means ± SEMs from data shown in Figure 1B.

(B) LTD induced by the 900-pulse protocol (gray bar) is independent of mGluR activation. Horizontal colored bars represent the corresponding means ± SEMs from data shown in Figure 1C.

(C) The 900-pulse LTD induced in slices in CHO-CM was blocked by coadministering the NMDAR antagonist, AP5 (50 μM, black squares, n = 8), whereas LTD in slices in 7PA2 CM was unaltered (red circles, n = 6). Horizontal colored bars from data in Figure 1C.

(D) 900-pulse LTD in Aβ monomer-treated slices was blocked upon coperfusing AP5 (50 μM, black squares, n = 5), whereas the LTD in oligomer-treated slices was not (red circles, n = 6). Horizontal colored bars represent the corresponding means ± SEMs from Figure 1F.

(E) 7PA2 CM enhanced LTD was blocked by treatment with D-AP5 at 100 μM (n = 5). Horizontal colored bars represent the corresponding means ± SEMs from Figure 2C.

(F) Dose-response curves of LTD blockade by AP5 in either CHO- CM (black squares) or 7PA2 CM (red circles). Data are means ± SEMs.

Insets in (A)–(E) represent typical fEPSPs recorded before (light) and 50 min after (dark) the LFS. Horizontal calibration bar, 10 ms; vertical bar, 0.5 mV.

absence of insoluble aggregates (Podlisny et al., 1995; Walsh et al., 2002). In accord with our recent work using soluble Aβ extracted from human cortex, we found that 7PA2 CM (but not the CM of untransfected [CHO-] cells) facilitated the induction of hippocampal LTD following a subthreshold, low-frequency stimulus (LFS) (300 pulses at 1 Hz) that otherwise does not induce LTD (79.7% ± 2.4%, n = 6, versus 93.4% ± 4.2%, n = 7, of baseline fEPSP slope; $p < 0.05$) (Figure 1B). We next sought to establish the effects of soluble Aβ on the expression of LTD using a standard LTD-inducing protocol known to be NMDAR dependent (Kemp and Bashir, 2001), namely, 900 pulses at 1 Hz. This form of LTD was equally inducible in slices perfused with artificial cerebrospinal fluid (ACSF) supplemented with 7PA2 CM or CHO- CM (73.6% ± 2.6%, n = 9, versus 77.1% ± 2.1%, n = 9; $p > 0.05$) (Figure 1C). Similar results were observed using synthetic $Aβ_{1-42}$ (Figure 1D), soluble extracts of human AD cortex containing Aβ oligomers (Figure 1E), or size-exclusion chromatography (SEC) fractions of 7PA2 CM enriched in either oligomers or monomers (Figures 1A, right panel, and Figure 1F). These data are consistent with previous reports that synthetic Aβ does not significantly change the magnitude of NMDAR-dependent (i.e., 900-pulse) LTD achieved in vitro (Raymond et al., 2003; Wang et al., 2002, 2004a).

To probe the mechanism of Aβ-facilitated LTD, we used the nonselective group I/II mGluR antagonist MCPG (500 μM) and the NMDAR antagonist AP5 (50 μM). In agreement with our previous finding using soluble Aβ from AD cortex (Shankar et al., 2008), the facilitation of 300-pulse LTD by 7PA2 CM was dependent on activation of mGluR but not NMDAR, as the LTD was MCPG sensitive and AP5 resistant (93.2% ± 6.1%, n = 6, versus 80.4% ± 4.8%, n = 5; $p < 0.05$) (Figure 2A). Unlike the 300-pulse LTD, 900-pulse LTD induced in the presence of

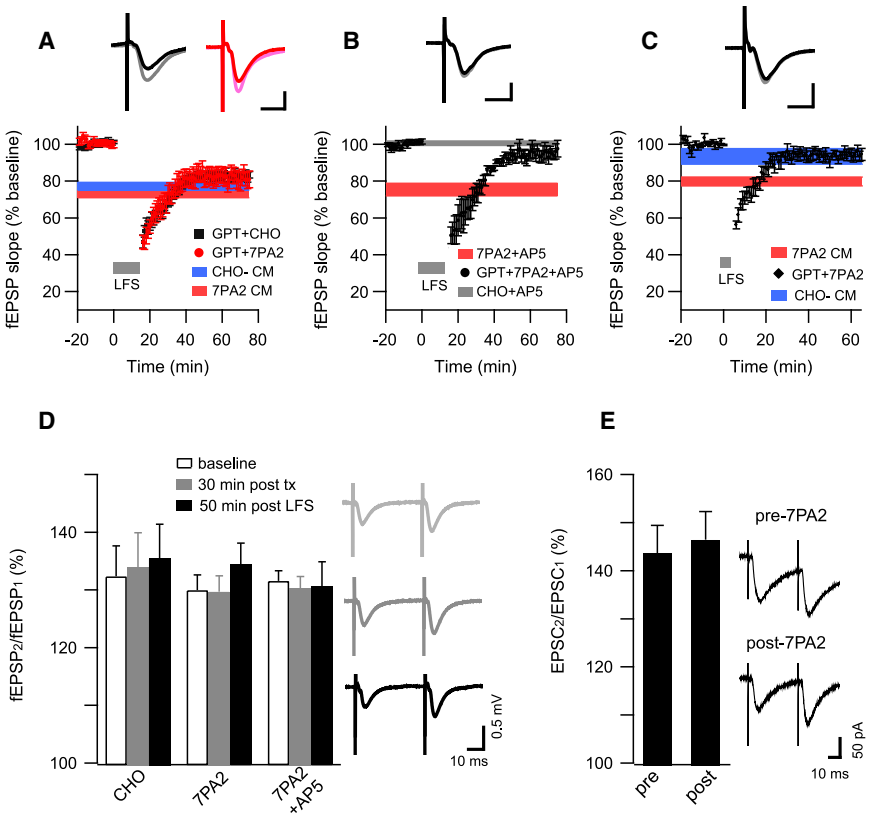

Figure 3. Selective Metabolism of Extracellular Glutamate Prevents Soluble Aβ-Facilitated LTD

(A) A glutamate scavenger system (glutamic pyruvic transaminase [GPT, 5 unit/ml] + pyruvate [2 mM]) has no significant effect on the fEPSP baseline and 900-pulse LTD in CHO- or 7PA2 CM treated slices. Horizontal colored bars represent the corresponding means ± SEMs from Figure 1C. Insets in (A)–(C) represent typical fEPSPs recorded before (light) and 50 min after (dark) LFS; horizontal calibration bar, 10 ms; vertical bar, 0.5 mV.

(B) 900-pulse LTD (gray bar) was blocked by AP5 (50 μM) in slices exposed to GPT + pyruvate for 15 min prior to 7PA2 CM (n = 6). Red horizontal bar shows the LTD resistant to the same dose of AP5 in the absence of exposure to scavengers.

(C) 300-pulse LTD (gray bar) was significantly prevented by coadministering glutamate scavengers with the 7PA2 CM. Horizontal colored bars represent the corresponding means ± SEMs from Figure 1B.

(D) Paired-pulse facilitation in slices exposed to 7PA2 CM, CHO- CM, or 7PA2 CM + AP5 (50 μM) measured before (white) or 30 min after (gray) adding these media or else measured 50 min after (black) a 900-pulse induction of LTD. At right are typical traces of these field recordings from the 7PA2 group.

(E) Similar paired-pulse facilitation recorded by whole-cell voltage clamping at −70 mV in CA1 pyramid cells before and 30 min after 7PA2 CM exposure. At right are typical traces. Data are means ± SEMs.

7PA2 CM was not prevented by MCPG (78.5% ± 4.1%, n = 6, versus 73.6% ± 2.6%, n = 9; $p > 0.05$) (Figure 2B). Interestingly, 50 μM AP5 fully blocked 900-pulse LTD in slices exposed to CHO- CM but had no significant effect on the 900-pulse LTD in slices exposed to the Aβ-rich 7PA2 CM (100.6% ± 1.4%, n = 8, versus 75.4% ± 3.4%, n = 6; $p < 0.01$) (Figure 2C). This AP5 resistance noted with 7PA2 CM was also observed with soluble synthetic $Aβ_{1-42}$ (see Figure S1A available online) and soluble extracts of AD cortex containing Aβ oligomers (Supp. Figure 1B; data quantified in Supp. Figure 1C). Furthermore, application of SEC fractions of 7PA2 CM revealed that the induction of AP5-resistant 900-pulse LTD was specific to Aβ oligomers, not monomers (Figures 2D and S1C). These results using three distinct sources of soluble low-n oligomers suggest that the LTD facilitated by Aβ oligomers is mechanistically different from conventional NMDAR-dependent LTD that is sensitive to 50 μM AP5. Because the 900-LFS protocol for inducing LTD in the CA1 region is well known to be NMDAR dependent (see Kemp and Bashir, 2001, and all control data in Figures 2C, 2D, and S1C), the resistance to AP5 of the LTD induced in the presence of the various soluble Aβ preparations was unexpected. It has been reported that synthetic Aβ can increase NMDAR activity by acting as an agonist or coagonist of NMDARs (Cowburn et al., 1997) and increasing NMDA conductance (Wu et al., 1995). Consequently, 50 μM AP5 may not have been sufficient to completely block an enhanced NMDAR activation mediated by Aβ oligomers. When we used a more potent isoform of AP5, D-AP5, and increased the concentration to 100 μM, the soluble Aβ-facilitated LTD was now significantly prevented (96.5% ± 3.4%, n = 5) (Figure 2E). Indeed, the block of Aβ-facilitated LTD was dependent on AP5 dose (Figure 2F). Rescuing LTD expression in the presence of 7PA2 CM required much higher AP5 concentrations than those needed to rescue LTD in the presence of CHO- CM (IC_{50}: 17.4 versus 72.5 μM; $p < 0.001$), supporting the conclusion that active NMDARs are involved in LTD facilitation by soluble Aβ.

An Extracellular Glutamate Scavenger Restores Soluble Aβ-Enhanced LTD to Normal Levels

Because Aβ oligomers enhanced LTD through activation of glutamate receptors, we asked whether this activity of soluble Aβ was dependent on extracellular glutamate concentration. To this end, we used an enzymatic glutamate scavenger system (glutamic-pyruvic transaminase [GPT] + pyruvate) to reduce extracellular glutamate levels (Overstreet et al., 1997; Min et al., 1998). Exposure of hippocampal slices to GPT alone (5 units/ml) had no effect on baseline synaptic activity (data not shown). GPT + pyruvate (2 mM) treatment 15 min prior to the application of CHO- CM or 7PA2 CM affected neither baseline activity nor the magnitude of LTD induced by 900-LFS (CHO-: 82.6% ± 2.1%, n = 5; 7PA2: 81.8% ± 4.5%, n = 5) (Figure 3A); however, the LTD induced in the presence of Aβ and GPT could now be blocked by 50 μM AP5 (95.1% ± 3.6%, n = 5) (Figure 3B). This result suggests that elevated extracellular glutamate concentrations contribute to the enhancement of LTD by soluble Aβ. Similarly, treatment

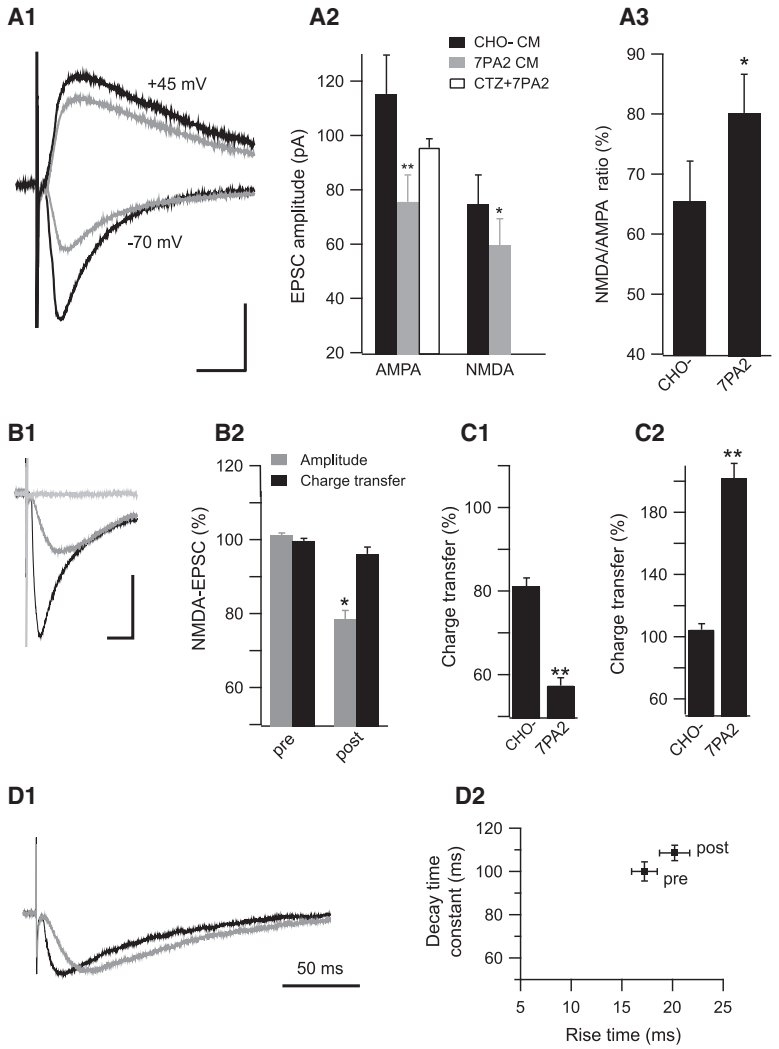

Figure 4. Soluble Aβ Oligomers Alter NMDAR-Mediated EPSCs in Whole-Cell Voltage-Clamp Recordings

(A1) Isolated AMPA-EPSC and NMDA-EPSC were recorded from −70 mV and +45 mV holding potentials, respectively, plus pharmacological blockers. Black traces, CHO- CM treated cells; gray traces, 7PA2 CM treated cells. (A2) Summary data for CHO- CM (black) and 7PA2 CM (gray) groups and for pretreatment with cyclothiazide (CTZ, 100 μM) prior to 7PA2 CM (white). (A3) NMDA/AMPA EPSC ratios are different in CHO- CM and 7PA2 CM.

(B1) Typical traces from CA1 pyramidal cells held at −70 mV (black), isolated NMDA-EPSC in low Mg^{2+} with NBQX (10 μM) and bicuculline (20 μM) at −70 mV (gray), and full blockage of the NMDA current by AP5 (50 μM) (light gray). (B2) Summary data for the isolated NMDA-EPSC before (pre) and 20–30 min after 7PA2 CM exposure. Peak amplitudes (gray) and total charge transfers (black) are expressed as means ± SEMs.

(C1) The selective NR2B inhibitor, ifenprodil (3 μM), modestly reduces NMDA charge transfers in control but markedly reduces it in 7PA2 CM. (C2) 7PA2 CM significantly increases the extrasynaptic response when synaptic NMDAR are first blocked by MK-801.

(D) NMDA-mediated EPSC kinetic analysis: (D1) representative scaled traces before (black) versus after (gray) 7PA2 CM exposure; (D2) summary data of rise time plotted versus decay time before (pre) and after (post)7PA2 CM exposure. Data are means ± SEMs.

with the GPT + pyruvate also prevented the 300-LFS Aβ-induced LTD (94.4% ± 2.8%, n = 5) (Figure 3C). We conclude that the enhancement of LTD by soluble Aβ in both mGluR-dependent and NMDAR-dependent conditions involves elevated extracellular glutamate levels.

Paired-pulse facilitation (PPF) reveals whether alterations of synaptic transmission are presynaptic. To assess whether soluble Aβ oligomers increase extracellular glutamate levels by affecting presynaptic release probability, we measured PPF in slices exposed to CHO- CM, 7PA2 CM, or 7PA2 CM + AP5 (50 μM) at baseline, 30 min after these exposures, and then 50 min after a 900-pulse LTD induction. PPF was not significantly different between these three conditions (Figure 3D). To establish further that soluble Aβ does not alter presynaptic release, we performed whole-cell recordings of pyramidal cells and found that PPF ratios before and 30 min after 7PA2 CM exposure were not significantly different (Figure 3E). The experiments described so far suggest that the facilitation of LTD by soluble oligomeric Aβ involves elevated levels of extracellular glutamate, but not by altering presynaptic release probability.

The Aβ-Mediated Increase in Synaptic Glutamate Concentration Alters Properties of Excitatory Transmission

We next sought to determine more precisely the basis of soluble Aβ-mediated alterations in glutamatergic transmission through whole-cell recordings. AMPAR-mediated currents (AMPA-EPSC) and NMDAR-mediated currents (NMDA-EPSC) were recorded from pyramidal neurons in slices treated with CHO- CM or 7PA2 CM (Figure 4A1). Both currents were significantly reduced by the soluble Aβ-rich 7PA2 CM compared to the CHO- CM (AMPA 67% ± 4%, n = 18, $p < 0.001$; NMDA 79% ± 3%, n = 13, $p < 0.01$) (Figure 4A2). This result was unexpected, as the increased extracellular glutamate concentrations observed above should increase AMPA and/or NMDA currents. However, the result could be explained if the Aβ-mediated rise in glutamate levels leads to receptor desensitization. To address this possibility, we applied a well-characterized inhibitor of AMPAR desensitization, cyclothiazide (CTZ, 100 μM), to the slices before exposure to 7PA2 CM; the AMPA EPSC was no longer significantly decreased (CHO- CM: 115 ± 14 pA versus 7PA2 CM + CTZ: 96 ± 3 pA, n = 10; $p > 0.05$) (Figure 4A2). Interestingly, we observed spiking activity escaping voltage clamp in 6/10 cells recorded in the 7PA2 CM + CTZ condition (Figures S2A and S2B) but not in the CTZ-only condition (three cells; data not shown), further suggesting alterations in excitatory transmission due to supraphysiologic levels of extracellular glutamate in the presence of soluble Aβ. To assess whether AMPAR desensitization is involved in the induction of LTD by soluble Aβ, CTZ was applied to brain slices, and 900-pulse

LTD was induced; the LTDs were not significantly different in CHO- versus 7PA2 CM (Figure S2C), suggesting that AMPAR desensitization is not required for the LTD induction.

To preserve the neuronal glutamate uptake expected under normal physiological function, we repeated the single-cell recordings at −70 mV rather than at positive potentials (Grewer and Rauen, 2005). NMDA-EPSC was isolated in low Mg^{2+} (0.1 mM) and with pharmacological blockade of AMPAR (with NBQX, 10 μM) and GABA-R (with BIC, 20 μM) (Figure 4B1). Under these conditions, the NMDAR-EPSC was again found to be decreased by 7PA2 CM (78% ± 3%, n = 10; $p < 0.01$) (Figure 4B2). The NMDA-EPSC reduction could be due to NMDAR desensitization in the presence of increased extracellular glutamate levels (Sarantis et al., 1993). To better understand the NMDA current changes, we quantified charge transfers, calculated as the area under the curve of the NMDA-EPSC. In contrast to the reduction in peak amplitude, the total charge transfer was not decreased by the Aβ-rich 7PA2 CM (96% ± 2% of pretreatment values, n = 11; $p > 0.05$) (Figure 4B2). Because NR2B receptors have a 2- to 3-fold higher sensitivity for glutamate than do NR2A receptors (Kutsuwada et al., 1992), we asked whether NR2B receptors played the principal role in the Aβ-mediated effect on NMDA currents. The selective NR2B receptor inhibitor, ifenprodil (3 μM), modestly inhibited the NMDA-EPSC total charge transfer under control (CHO- CM) conditions (81% ± 2%, n = 8) (Figure 4C1). However, ifenprodil strongly and significantly inhibited the NMDA-EPSC charge transfer in the presence of 7PA2 CM (55% ± 2%, n = 9; $p < 0.05$) (Figure 4C1), suggesting enhanced activation of NR2B-subunit-containing NMDA receptors. The NR2B subunit is considered to be predominantly present in extrasynaptic NMDA receptors (Tovar and Westbrook, 1999). We selectively blocked synaptic NMDAR with MK-801, an irreversible, use-dependent NMDA channel blocker, washed it out, and perfused with 7PA2 CM under the above NMDA-EPSC isolating conditions. The NMDA-EPSCs were markedly increased (202% ± 10% of the CHO- CM level, n = 5; $p < 0.01$) (Figure 4C2). Taken together, the above results suggest that soluble Aβ oligomers increase NR2B-mediated NMDAR activity and enhance extrasynaptic responses.

Spillover of increased extracellular glutamate remained as the most parsimonious explanation for the relative increases in NMDA currents, activation of NR2B receptors, and extrasynaptic responses in the presence of Aβ oligomers. To further support this interpretation, we analyzed the NMDA EPSC kinetics, i.e., the 10%–90% rise time and the decay time constant. While the peak amplitude decreased slightly after 7PA2 CM treatment, the rise time (16 ms versus 20 ms for pre- versus postexposure; $p < 0.05$) and decay time (100 ms versus 109 ms for pre- versus postexposure; $p < 0.05$) were significantly prolonged (Figure 4D), suggesting increased diffusion distance and dwelling times, i.e., that neurotransmitter spillover is enhanced upon exposure to soluble Aβ oligomers.

Soluble Aβ Enhances LTD through Inhibition of Glutamate Uptake

Our findings above that soluble Aβ-enhanced LTD may activate a larger population of NMDARs can be considered in terms of Aβ interrupting glutamate reuptake (Harkany et al., 2000; Gu et al., 2004). To investigate this possibility, we examined the effects of a well-characterized glutamate uptake inhibitor, TBOA. Soluble Aβ extracted from AD brain or present in 7PA2 CM (Figure 1B) facilitates LTD in CA1 after a 300-LFS protocol, whereas this low stimulus induces weak or no LTD in control-treated slices. To test whether inhibiting glutamate uptake itself facilitates LTD, the 300-LFS protocol was applied after a 30 min TBOA treatment (15 μM). Closely similar to our results with soluble Aβ treatment in this 300-LFS mode (Figure 1B), we found that TBOA alone induced LTD in an NMDAR-independent but mGluR-dependent manner (TBOA alone: 74% ± 4.5%, n = 5; TBOA + AP5: 78.1% ± 3.5%, n = 5; TBOA + MCPG: 91% ± 4.6%, n = 6) (Figure 5A). Similar to the 900-pulse LTD induced in the presence of soluble Aβ (Figure 2), the 900-pulse LTD induced in the presence of TBOA was also resistant to 50 μM AP5 but was prevented by 100 μM D-AP5 (TBOA: 73.5% ± 3.4%, n = 5; TBOA + AP5: 76.9% ± 5.6%, n = 5; TBOA + D-AP5: 94.2% ± 2.8%, n = 5; $p < 0.01$ compared to TBOA + AP5) (Figure 5B).

To assess whether TBOA-enhanced LTD has mechanistic similarity with soluble Aβ, we recorded the TBOA-induced LTD in a repetitive 900-LFS paradigm to saturate the LTD response, then washed out the TBOA and replaced it with 7PA2 CM (Figure 5C). When 900-LFS was then performed, there was no further increase in LTD (96.1% ± 9.1% of renormalized baseline measured 40 min after LFS, n = 5; $p > 0.05$) (Figures 5C and 5D). This occlusion experiment suggests that these two forms of LTD share similar mechanisms. Interestingly, if we first applied 7PA2 CM and saturated the LTD, then the usual dose (15 μM) of TBOA significantly reduced baseline neurotransmission (to 78% of the renormalized baseline at 30 min) (Figure S3A), and this effect was similar to that of a higher dose of TBOA alone (50 μM) on the baseline (81% at 30 min) (Figure S3B). The latter results further substantiate a shared mechanism between TBOA and soluble Aβ on perturbation of neurotransmission. We also examined DHK (500 μM), an inhibitor of glial glutamate transporter (GLT-1), but the 900-pulse LTD observed in the presence of this agent was largely prevented by the standard 50 μM AP5 dose (89.2% ± 3.2%, n = 6, versus 77.5% ± 2.9%, n = 6, $p < 0.05$, Figure S3C), suggesting specificity for neuronal, not glial, glutamate transporters in the enhancement of the 900-pulse LTD.

The effects of soluble Aβ in inhibiting HFS-induced LTP have been well established using several types of Aβ preparations, and we confirmed this here using soluble Aβ-rich 7PA2 CM (CHO- CM: 144.7% ± 5.4%, n = 7, versus 7PA2 CM: 108.1% ± 6.6%, n = 7; $p < 0.001$) (Figure 5E). TBOA similarly inhibited HFS-induced LTP (vehicle: 151.3% ± 4.8%, n = 6, versus TBOA: 112.2% ± 3.1%, n = 6; $p < 0.001$) (Figure 5F). These results support our conclusion that the effects of soluble Aβ on synaptic plasticity mimic those observed with the blockade of neuronal glutamate uptake.

To assess directly whether soluble Aβ inhibits glutamate uptake as all of the above data suggest, we measured the uptake of radiolabeled glutamate by isolated synaptosomes (see Experimental Procedures). As a positive control, TBOA decreased glutamate uptake in the synaptosomal preparation in a dose-dependent manner (IC_{50} = 73.9 μM) (Figure 5G). Synthetic $Aβ_{1-42}$ significantly decreased glutamate uptake into synaptosomes (69% ± 6% of vehicle treatment, n = 15; $p < 0.01$), similar to the effects of TBOA (41% ± 4% at 50 μM, n = 5; $p < 0.01$)

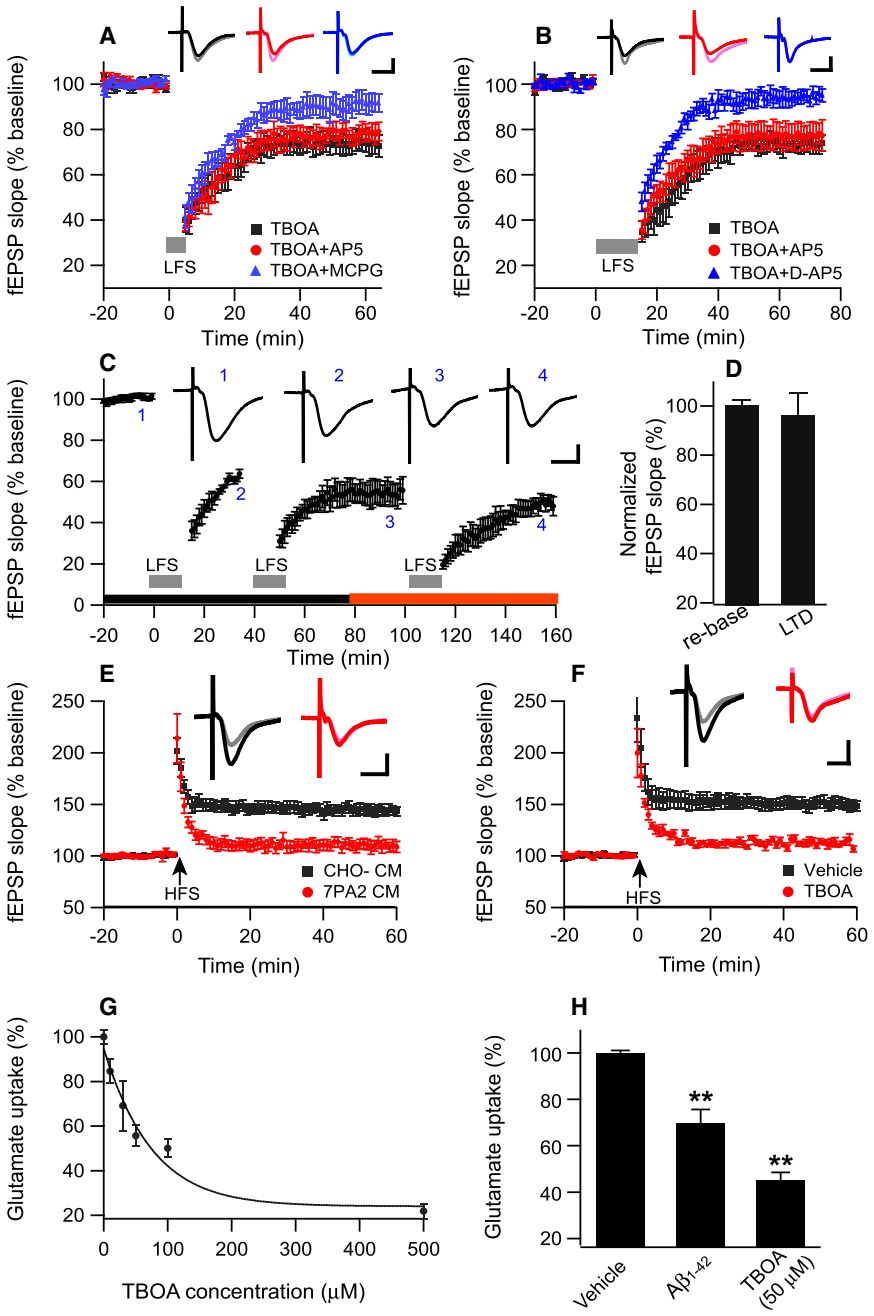

Figure 5. Soluble Aβ-Enhanced LTD Involves Impaired Glutamate Reuptake

(A) LTD was induced by 300 pulses (gray bar) when just the glutamate uptake inhibitor, TBOA (15 μM), was perfused (black squares, n = 5). This TBOA-mediated LTD was prevented by mGluR antagonist MCPG (500 μM, blue triangles, n = 6) but not by NMDAR antagonist AP5 (50 μM, red circles, n = 6).

Insets in (A)–(F) represent fEPSPs recorded before (light) and 50 min after (dark) either LFS (in A–C) or HFS (in E and F). Horizontal calibration bars, 10 ms; vertical bars, 0.5 mV.

(B) A 900-pulse LTD facilitated by TBOA was resistant to a standard dose of AP5 (50 μM, red circles, n = 6), but it could be blocked by D-AP5 (100 μM, blue triangles, n = 6).

(C) Saturation of 900-pulse LTD occurring in the presence of TBOA (black horizontal bar) occludes further LTD in the presence of 7PA2 CM (red horizontal bar).

(D) Summary data from occlusion experiments as in (C): left bar, evoked fEPSP was renormalized to baseline values (i.e., point 3 in C) before addition of 7PA2 CM to the perfusate and an additional LFS (right bar).

(E) LTP induced by high-frequency stimulation (HFS) was prevented in slices in 7PA2 CM (red circles) but unaffected in slices in CHO- CM (black squares).

(F) HFS-induced LTP was similarly prevented by TBOA.

(G) Dose-dependent inhibition of glutamate uptake by TBOA in hippocampal synaptosomes.

(H) Pretreatment with soluble synthetic Aβ1-42 impaired glutamate uptake in hippocampal synaptosomes in a fashion similar to TBOA treatment at 50 μM. Data are means ± SEMs as percentage of vehicle alone; **p < 0.01.

(Figure 5H). This biochemical evidence further supports our hypothesis that soluble Aβ impairs neuronal glutamate uptake and can thereby increase extracellular glutamate concentration and subsequent NMDAR activation.

Extracellular Calcium Influx, Not Intracellular Stores, Contributes to Soluble Aβ-Facilitated LTD

To assess whether alterations in calcium influx through NMDARs mediate the facilitation of LTD by soluble Aβ, the ACSF calcium concentration was reduced to 0.5 mM prior to the application of soluble Aβ and 900-LFS to the brain slices. This reduction of extracellular calcium concentration prevented LTD induction in the presence of either 7PA2 or CHO- CM (Figure 6A). To test whether extracellular calcium is required for the NMDAR-mediated enhancement of LTD by soluble Aβ, we applied 50 μM AP5 and varied the extracellular Ca^{2+} concentration between 0.5 mM and 6 mM (Figure 6A). The LTD induced by 900-LFS in the presence of AP5 + CHO- CM was fully blocked when the Ca^{2+} concentration was 1 mM or 2.5 mM, and only a small AP5-resistant LTD (86.4% ± 4.5%, n = 6) occurred at the highest Ca^{2+} concentration (6 mM). In contrast, LTD induced in presence of 7PA2 CM was significantly prevented by 50 μM AP5 at low (1 mM) Ca^{2+} concentration (7PA2 CM: 80% ± 4.2%, n = 5, versus 7PA2 CM + AP5: 93.2% ± 3.4%, n = 6; $p < 0.05$) but not at normal (2.5 mM: 75.4% ± 3.4%, n = 6) or high (6 mM: 70.4% ± 3.4%, n = 5) Ca^{2+} concentrations. These results indicate that Aβ-enhanced LTD is dependent on extracellular calcium concentration.

To assess whether intracellular calcium stores also regulate Aβ-mediated LTD, as they have been reported to do for Aβ neurotoxicity (Demuro et al., 2005), we tested two compounds that

inhibit the release of intracellular Ca^{2+} stores, ryanodine and U73122. Although ryanodine (20 μM) and U73122 (10 μM) each prevented 900-LFS LTD induction in slices treated with CHO-CM, they did not alter the LTD facilitation by 7PA2 CM (87% ± 2.7%, n = 5, versus 76% ± 3.2%, n = 5, for ryanodine, $p < 0.05$) (Figure 6B) (96.2% ± 3.4%, n = 4, versus 74.6% ± 4.6%, n = 6, for U73122, $p < 0.01$) (Figure 6C). This suggests that soluble Aβ-facilitated LTD requires extracellular calcium influx but not intracellular calcium release.

Activation of Calcineurin and GSK-3, but Not p38 MAPK, Is Required for Aβ-Mediated LTD

When cytosolic calcium reaches critical concentrations, certain LTD-related signaling pathways are activated (Kemp and Bashir, 2001). For example, NMDAR-dependent LTD in the CA1 region recruits calcineurin (PP2B) and p38 MAPK cascades (Mulkey et al., 1994; Bolshakov et al., 2000; Li et al., 2006). We examined these two signaling pathways using their respective inhibitors, FK506 (20 μM) and SB203580 (5 μM). Whereas blocking p38 MAPK activation with SB203580 prevented conventional 900-pulse LTD induction (i.e., in CHO- CM), it did not significantly affect the LTD induced in the presence of soluble Aβ-rich 7PA2 CM (94.6% ± 2.5%, n = 7, versus 73.9% ± 4%, n = 6; $p < 0.01$) (Figure 6D). In contrast, PP2B function was required for LTD induced both in the absence and presence of soluble Aβ (Figure 6E). Glycogen synthase kinase-3 (GSK3)-mediated signaling was recently reported to play an important role in LFS-induced LTD (Peineau et al., 2007), and it has also been implicated in Aβ-mediated neurotoxicity in cultured hippocampal slices (Nassif et al., 2007). Accordingly, we treated slices with the GSK-3β inhibitor, SB415286 (10 μM), for 30 min prior to applying either CHO- CM or 7PA2 CM and then performed 900-LFS. LTD could not be induced in either condition (94.3% ± 4.7%, n = 6, versus 98.4% ± 2.6%, n = 6) (Figure 6F), suggesting that GSK-3β activity is required for both conventional and soluble Aβ-mediated LTD. To further verify that glutamate uptake inhibition shares similar mechanisms with soluble Aβ as regards LTD induction, ryanodine, SB203580, and FK506 were each applied to the slices prior to treatment with TBOA. Entirely consistent with the results for Aβ-mediated LTD, both intracellular Ca^{2+} release and p38 MAPK activation were not required for the TBOA-mediated LTD, whereas PP2B activity was (Figures 6G–6I).

To provide further information about the receptor mechanisms of LTD facilitation by soluble Aβ, we took advantage of Ras-guanine nucleotide-releasing factor 1 (Ras-GRF1) knockout mice, which are deficient in the ability to mount an LTD response (Li et al., 2006). Ras-GRF proteins are best known for their ability to activate Ras/Erk through their CDC25-GEF domains and activate the Rac/p38 cascade through their DH-GEF domains, which act as calcium sensors for different classes of NMDARs and drive the activation of distinct MAP kinase family members. As expected, hippocampal slices from these *Ras-GRF1*$^{-/-}$ mice did not express LTD when 900-LFS was administered in the presence of CHO- CM. In contrast, LTD was elicited in the presence of the oligomer-rich 7PA2 CM (99.4% ± 2.9%, n = 6, versus 75.1% ± 2.9%, n = 7; $p < 0.01$) (Figure S4A). This soluble Aβ-facilitated LTD in the *Ras-GRF1*$^{-/-}$ mice was not blocked by 500 μM MCPG (Figure S4B) nor by 50 μM AP5 (Figure S4C), but it was significantly decreased by 100 μM AP5 (91.6% ± 3.1%, n = 5, $p < 0.05$) (Figure S4C). Furthermore, the p38 MAPK inhibitor (SB203508) had no effect on the Aβ-facilitated LTD (80.2% ± 4.8%, n = 5) (data not shown), whereas pretreatment with either the calcineurin inhibitor (FK506) or the GSK-3β inhibitor (SB415286) significantly prevented the LTD associated with 7PA2 CM (95.6% ± 4.8%, n = 6, and 88.4% ± 4.7%, n = 6, respectively) (Figure S4D). Therefore, soluble Aβ bypassed the nonfunctional LTD induction pathway in *Ras-GRF1*$^{-/-}$ mice, a pathway that is normally sensitive to 50 μM AP5 in wild-type mice.

DISCUSSION

Given the mounting evidence that soluble Aβ oligomers mediate synaptic impairment in AD, elucidating the precise molecular pathways by which this occurs has important implications for treating and preventing the disease. Here, we demonstrate that soluble Aβ oligomers facilitate LTD in the hippocampus through a mechanism that appears to involve the inhibition of glutamate uptake. With a weak (300-pulse) LFS, Aβ-mediated LTD was prevented by MCPG but not AP5, and with a conventional (900-pulse) LFS, the LTD was prevented only by a high (100 μM), not a standard (50 μM), dose of AP5. Extracellular glutamate scavengers effectively prevented Aβ-enhanced LTD. Mechanistically, soluble Aβ oligomers caused glutamate spillover, and their ability to facilitate LTD required an influx of extracellular calcium but did not detectably require Ca^{2+} release from intracellular stores. Once Ca^{2+} enters the neuron, it is known to trigger PP2B and GSK3 signaling pathways, and we implicated these in the Aβ-facilitated LTD induction.

Importantly, Aβ facilitation of LTD was closely mimicked by pharmacologically inhibiting neuronal (but not glial) glutamate uptake, consistent with the rescue of Aβ-LTD by the glutamate scavenger. In accord, we found that Aβ significantly impaired glutamate uptake by synaptosomes, suggesting that Aβ facilitates LTD in part by altering synaptic glutamate recycling. These results support the hypothesis that excess synaptic glutamate caused by Aβ mechanistically alters LTD induction in hippocampus. It should be emphasized that the effects of soluble Aβ we describe in this study are attributable to soluble oligomers (Figure 1A), as no larger assemblies (protofibrils, fibrils) were present, and SEC-isolated oligomers but not monomers conferred the effects on LTD (Figure 2D). A summary mechanism incorporating all of our findings is proposed in Figure 7.

We focused on the NMDAR-dependent induction of LTD, a widely used protocol for LTD studies. There have been contradictory findings among the few studies of the effects of Aβ on LTD (Kim et al., 2001; Wang et al., 2002; Raymond et al., 2003; Wang et al., 2004a). Hsieh et al. (2006) showed that Aβ secreted by neurons in hippocampal slices transfected with mutant human APP could induce LTD via an mGluR-dependent mechanism involving AMPAR internalization. Moreover, Chang et al. (2006) reported that aged APP/Presenilin-1 double knockin mice having reduced AMPAR mEPSCs were resistant to LTD induction, suggesting a floor effect for synapse depression following prolonged exposure to Aβ. Our new data indicate that soluble Aβ oligomers can induce hippocampal LTD, although the mechanisms do not follow canonical p38 MAPK pathways.

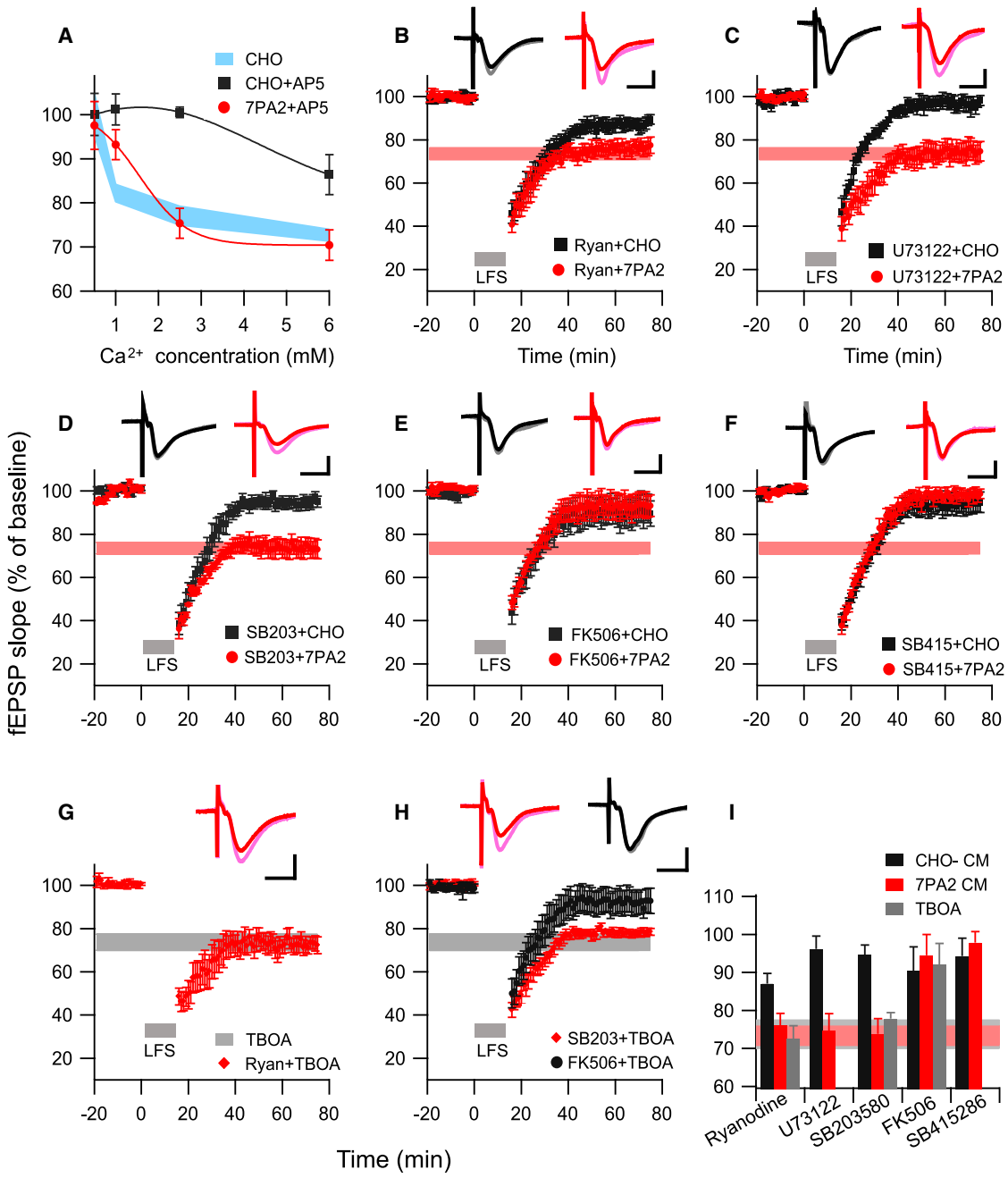

Figure 6. LTD Facilitated by Soluble Aβ or TBOA Share Similar Signaling Pathways

(A) Conventional LTD (in CHO- CM, black squares) and Aβ-enhanced LTD (in 7PA2 CM, red circles) induced by the 900-pulse LFS in the presence of AP5 (50 μM) were plotted as a function of increasing extracellular calcium concentrations in the perfusate. Light blue area represents the LTD obtained in the CHO- CM alone (without AP5). Data are means ± SEMs.

(B) Ryanodine (20 μM) given 30 min prior to 900 pulses partially blocked the LTD in CHO CM (black squares, n = 5) but produced no block of the 7PA2-facilitated LTD (red circles, n = 6).

(C) U73122 (10 μM) (applied 45 min prior to 900 pulses) fully blocked LTD in the presence of CHO- CM (black squares, n = 6) but had no effect in the presence of 7PA2 CM (red circles, n = 6).

(D) 900-pulse LTD was blocked by p38 MAPK inhibitor, SB203580 (5 μM), in CHO- CM (black squares, n = 7) but not in 7PA2 CM (red circles, n = 7).

(E) Calcineurin inhibitor, FK-506 (20 μM) perfused 40 min prior to 900 pulses prevented LTD in both CHO- CM (black squares, n = 5) and 7PA2 CM (red circles, n = 6).

(F) GSK-3β inhibitor, SB415286 (10 μM) perfused 60 min prior to 900 pulses prevented LTD in both CHO- CM (black squares, n = 6) and 7PA2 CM (red circles, n = 7).

(G) LTD enhanced by TBOA (15 μM) was likewise resistant to ryanodine (n = 5).

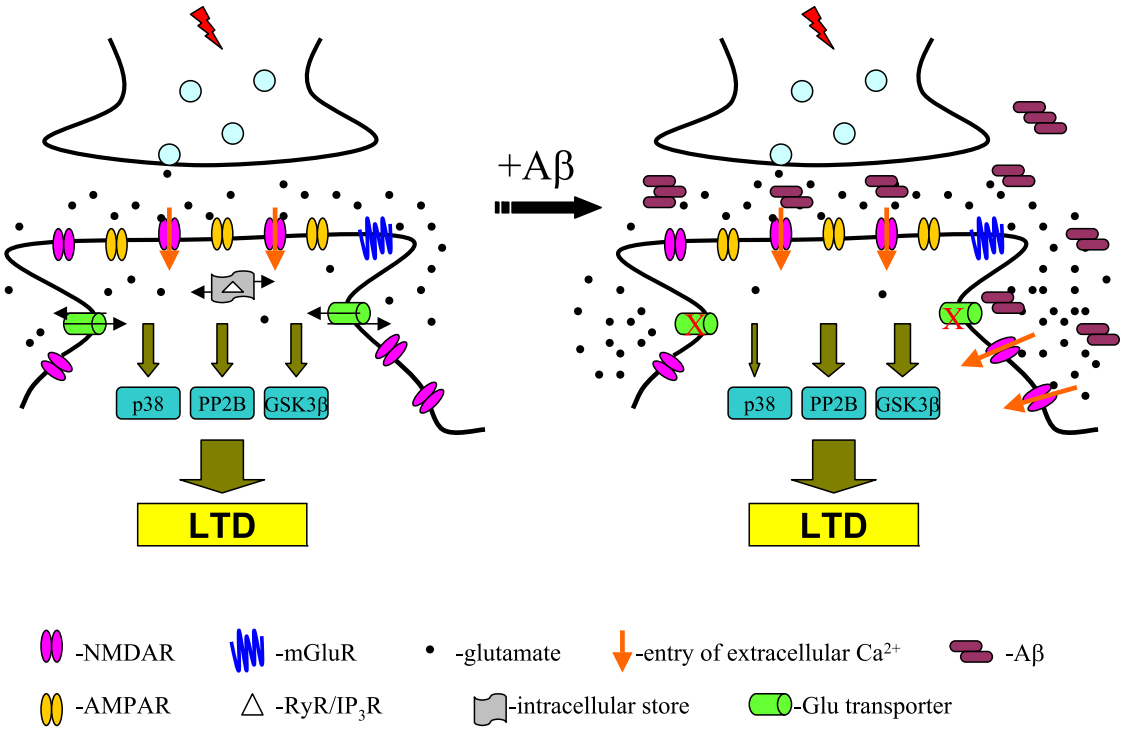

Figure 7. Schematic of the Principal Pathways Implicated by This Study in Conventional LTD and in LTD Facilitated by Soluble Aβ Oligomers
(Left panel) Conventional LTD requires NMDAR-mediated influx of extracellular calcium and liberation of intracellular calcium stores. This ultimately activates PP2B, GSK-3β, or p38 MAPK signaling pathways that induce LTD. (Right panel) Soluble Aβ oligomers lead to activation of more NMDAR, leading to extracellular calcium influx and activation of PP2B and GSK-3β pathways to facilitate LTD. Our data suggest that Aβ oligomers decrease glutamate uptake by neuronal transporters (red x's), resulting in the enhanced activation of NMDARs and thus facilitation of LTD-inducing pathways.

Synthetic Aβ has been shown to increase NMDAR-mediated currents in rat dentate gyrus (Wu et al., 1995) or enhance NMDA response in the hippocampus after a 15 min exposure in vivo (Molnár et al., 2004). Our current results show that soluble Aβ oligomers depressed AMPAR currents (Figures 4A and 4B), but this was likely due to desensitization. Earlier work has suggested that NR2B-containing NMDARs play a major role in normal LTD induction (Liu et al., 2004), although some recent evidence is not in agreement (Morishita et al., 2007). Our study suggests that soluble Aβ oligomers can significantly increase NR2B receptor activation, as demonstrated by an increased ifenprodil-sensitive component of the NMDAR-EPSC following exposure to soluble Aβ. NR2B receptors are specifically coupled to SynGAP (Kim et al., 2005), and their activation would thus inhibit the Ras-Erk signaling pathway known to be required for LTP, instead favoring LTD induction. Although some studies have colocalized Aβ with NMDAR at synapses (Dewachter et al., 2009; Lacor et al., 2007), it remains unclear whether these are a direct target of the peptide, and other studies have suggested Aβ interactions with voltage-dependent calcium channels (VDCCs) (Ueda et al., 1997), mGluRs (Wang et al., 2004b), nicotinic receptors (Dineley et al., 2001; Snyder et al., 2005), or insulin receptors (Townsend et al., 2007), all of which could modulate NMDAR activity. It remains plausible that the hydrophobic Aβ oligomers actually interact with lipid and/or protein targets upstream of these various receptors, perturbing their function secondarily.

Extrasynaptic glutamate spillover is a phenomenon that has been implicated in cross-talk among hippocampal synapses (Asztely et al., 1997; Min et al., 1998; Scimemi et al., 2004). Inhibition of glutamate uptake at the synapse (e.g., by soluble Aβ) can significantly increase the extracellular glutamate concentration and thereby enhance glutamate spillover to neighboring synapses. Electrophysiologically, NMDA currents will be increased and their rise and decay time courses significantly prolonged, due to the increased distance between the glutamate release site and the target receptors. In addition, extrasynaptic NMDAR activity will be increased by synaptic glutamate accumulation. Our present results do not fully meet these criteria, as we found that soluble Aβ depressed peak NMDAR currents. We hypothesize that Aβ oligomers depress NMDA currents as a result of desensitization of the receptors. It is of related interest that several glutamate uptake

(H) TBOA-enhanced LTD was prevented by the calcineurin inhibitor (FK 506, black circles, n = 5) but not by the p38 MAPK inhibitor (SB203580, red diamonds, n = 5).
(I) Summary data for actions of the signaling pathway modulators on Aβ- and TBOA-enhanced LTD. The horizontal gray bar represents mean LTD in TBOA alone (Figure 5B), and the horizontal light orange bar represents mean LTD in 7PA2 CM alone (Figure 1C). Data are means ± SEMs.

inhibitors have been shown to depress NMDA currents (Sarantis et al., 1993; Maki et al., 1994; Asztely et al., 1997), as we show for soluble Aβ oligomers here. Thus, Aβ-mediated decreases in glutamate uptake and consequent accumulation of extracellular glutamate could induce NMDAR desensitization and/or activation of presynaptic mGluRs, thereby reducing the peak amplitudes of the NMDA currents.

Glutamate excitotoxicity has been hypothesized to have a role in AD pathogenesis. Dysfunction of glutamate transporters has been implicated in this pathway (Masliah et al., 1996; Jacob et al., 2007). Synthetic Aβ has been shown to inhibit glutamate uptake in cultured astrocytes (Harris et al., 1996; Harkany et al., 2000; but see Ikegaya et al., 2002) and oocytes (Gu et al., 2004). Extracellular glutamate concentration is tightly controlled in the brain by a family of membrane transporters, predominantly expressed by perisynaptic astrocytes (Danbolt, 2001). Their role is to regulate the glutamate released at synapses and to prevent spillover of the transmitter to extrasynaptic receptors. Our results showing that soluble Aβ facilitates LTD through both mGluR (300-LFS protocol) and NMDAR (900-LFS protocol) pathways is supported by our concomitant finding that a common upstream element, the glutamate transporter, is also regulated by soluble Aβ. In vivo microdialysis recently revealed that microinjection of the soluble Aβ-rich 7PA2 CM can significantly increase the interstitial fluid levels of glutamate—but not GABA or aspartate—in hippocampus (O'Shea et al., 2008). Inhibition of glutamate uptake by TBOA has been shown to increase spontaneous epileptiform discharges, and this increased excitability can be blocked by AP5 (Campbell and Hablitz, 2004). Interestingly, Aβ has also been found to significantly increase spontaneous nonconvulsive seizure activity in cortical and hippocampal networks in APP-transgenic mice (Palop et al., 2007). The precise mechanism by which soluble Aβ oligomers interfere with glutamate transporters at the synapse remains to be determined. Given the numerous distinct receptors and channel proteins reported to be altered by Aβ to date, we speculate that the hydrophobic Aβ oligomers bind principally to membrane lipids and thereby secondarily interrupt the structure and function of synaptic transmembrane transporters and channels, leading to changes in the transduction of intracellular signaling cascades. Such a mechanism would be consistent with the direct effect of soluble Aβ on glutamate uptake by isolated synaptosomes in vitro (Figure 5H).

Calcium is a second messenger that controls many cellular processes, including neuronal excitability, synaptic plasticity, and neuronal death. The increase in postsynaptic calcium that results in LTD can arise from a number of sources. For example, extracellular Ca^{2+} influx can occur through NMDARs or VDCCs (Kemp and Bashir, 2001), and intracellular Ca^{2+} release can stem from activation of the ryanodine receptor (RyR) and the inositol 1,4,5-trisphosphate receptor (IP3R). Our data (Figures 6A–6C) show that conventional hippocampal LTD requires extracellular Ca^{2+} influx through NMDARs and recruits intracellular stores from IP3R and possibly RyR, in line with previous studies on hippocampal LTD (Kemp and Bashir, 2001). However, among these possible calcium sources, Aβ-facilitated LTD only required NMDAR activation and enhanced extracellular calcium entry. An increase in cytosolic calcium can trigger signaling cascades involved in LTD induction, including PP2B, p38 MAPK, and GSK3 (Mulkey et al., 1994; Bolshakov et al., 2000; Li et al., 2006; Peineau et al., 2007). The differences between our study and previous reports implicating Aβ in the activation of p38 MAPK (Hsieh et al., 2006; Origlia et al., 2008) could lie in the experimental conditions, for example, acute slices versus dissociated neuronal cultures or field versus whole-cell recordings.

In conclusion, the findings described here suggest that soluble Aβ oligomers facilitate LTD through both NMDARs and mGluRs by interfering with glutamate recycling at the synapse (Figure 7). Our study also suggests that additional mechanisms may underlie LTD in AD pathological states beyond those described previously through the NMDAR-p38/MAPK pathway. The receptors and signaling molecules activated by Aβ as described in this study could represent additional therapeutic targets in Alzheimer's disease.

EXPERIMENTAL PROCEDURES

Aβ Preparations

Secreted human Aβ peptides were collected and prepared from the conditioned medium (CM) of a CHO cell line (7PA2) that stably expresses human APP751 containing the V717F AD mutation (Podlisny et al., 1995). Cells were grown in Dulbecco's modified Eagle's medium (DMEM) containing 10% fetal bovine serum, 1% penicillin/streptomycin, 2 mM L-glutamine, and 200 mg/ml G418 for selection. Upon reaching ~95% confluency, the cells were washed and cultured overnight (~15 hr) in serum-free medium. CM was collected, spun at 1500 × g to remove dead cells and debris, and stored at 4°C. The CM was concentrated 10-fold with a YM-3 Centricon filter (Walsh et al., 2005). Aliquots of concentrated 7PA2 CM were stored at −80°C. Synthetic $A\beta_{1-42}$ (Biopolymer Lab., Dept. of Neurology, UCLA) was dissolved in water and incubated at 37°C for 10 days, then aliquoted (50 μl) and stored at −80°C.

Hippocampal Slice Electrophysiology

The procedures for the hippocampal slice preparation and field excitatory postsynaptic potentials (fEPSPs) recordings in the CA1 region of mouse hippocampus were described previously (Li et al., 2006; Shankar et al., 2008). A bipolar stimulating electrode (FHC Inc., Bowdoin, ME) was placed in the Schaffer collaterals to deliver test and conditioning stimuli. A borosilicate glass recording electrode filled with artificial cerebrospinal fluid was positioned in stratum radiatum of CA1. Test responses were recorded for 30–60 min prior to beginning the experiment to ensure stable responses. The field potentials were amplified 100× using an Axon Instruments 200B amplifier and digitized with Digidata 1322A. Traces were obtained by pClamp 9.2 and analyzed using the Clampfit 9.2 program. To induce LTD, either 300 or 900 pulses at low frequency (1 Hz) stimulation (LFS) were applied to the slices. LTP was induced by two sequential high-frequency stimulations (HFS: 100 Hz for 1 s, then repeated after 20 s). All LTD/LTP values represent fEPSP slopes measured 50 min after the conditioning stimulus unless stated otherwise. Two-tailed Student's t test and one-way analysis of variance (ANOVA) were used to determine statistical significance.

Whole-cell recordings were made from the soma of visually identified pyramidal neurons located in CA1 of the hippocampus. Patch pipettes (5~7 MΩ) were filled with an internal solution containing (in mM) 110 Cs-gluconate, 20 CsCl, 10 HEPES, 4 NaCl, 0.5 EGTA, 2 $MgCl_2$, 2 Na_2ATP, and 0.25 NaGTP, titrated with CsOH to pH 7.4. The excitatory postsynaptic currents (EPSCs) were recorded following stimulation of Schaffer collaterals ~150 μm from the CA1 cell body with a bipolar electrode. AMPA-mediated EPSCs were recorded at a holding potential of −70 mV in the presence of 10 μM bicuculline (BIC) and 50 μM AP5. NMDA-mediated EPSCs were recorded at +45 mV in ACSF containing 20 μM BIC and 10 μM NBQX, or else at −70 mV in 0.1 mM Mg^{2+} ACSF containing BIC and NBQX. Series resistance was kept 15~30 MΩ and

monitored throughout each recording. Cells were excluded from data analysis if the series resistance changed by >20% during the course of the experiment. All patch-clamp experiments were performed at 24°C.

Glutamate Uptake Assay

Preparation of crude synaptosomal fractions and glutamate uptake assay were performed as described by Yang et al. (2005) with minor modifications. Briefly, hippocampal slices were treated for 2 hr with soluble Aβ, TBOA, or DMSO, then homogenized in 0.32 M sucrose, 1 mM EDTA, 4 mM Tris, and 10 mM glucose (pH 7.4) on ice. Homogenates were centrifuged at 1000 × g for 10 min, and subsequent supernatants were spun at 9000 × g for 10 min. Final pellets were resuspended in HEPES buffer solution to yield a protein concentration of 0.25 mg/ml. To avoid treatment washout, crude synaptosomes were treated with the same respective agents for 45 min at 37°C. Then, they were incubated with 10 nM [^{3}H]glutamate (20–60 Ci/mmol; Perkin Elmer, Boston, MA) and 30 μM unlabeled glutamate for 5 min. The uptake was stopped by placing the samples on ice and spinning at 15,000 rpm for 10 min at 4°C. Pellets were washed and resuspended in ice-cold PBS. Glutamate uptake was counted on an LS6500 multipurpose scintillation counter. The absolute number of counts taken up varied from 500 to 40,000 counts per minute (cpm), with a background of 20 cpm.

Drug Treatments

Paired control and experimental hippocampal slices from a single mouse were maintained together in a single chamber, except during individual drug treatments. The following antagonists were purchased from Tocris (Ellisville, MO): DL-2-amino-5-phosphonopentanoic acid (AP5), MK-801, MCPG, cyclothiazide, NBQX, (-)-bicuculline methiodide, SB203580, SB415286, Ryanodine, U73122, DL-threo-β-benzyloxyaspartic acid (TBOA) and dihydrokainic acid (DHK). Glutamic-pyruvic transaminase, pyruvic acid, Ifenprodil, and FK506 were purchased from Sigma (St Louis, MO).

SUPPLEMENTAL DATA

Supplemental Data include four figures and their legends and can be found with this article online at http://www.cell.com/neuron/supplemental/S0896-6273(09)00387-0.

ACKNOWLEDGMENTS

Supported by NIH grant AG027443 (D.S.). We thank Dr. L. Feig (Tufts University) for providing Ras-GRF1 knockout mice and Drs. M.J. Rowan (Trinity College) and B.L. Sabatini (Harvard Medical School) for helpful discussions.

Accepted: May 6, 2009
Published: June 24, 2009

REFERENCES

Anwyl, R. (2006). Induction and expression mechanisms of postsynaptic NMDA receptor-independent homosynaptic long-term depression. Prog. Neurobiol. *78*, 17–37.

Asztely, F., Erdemli, G., and Kullmann, D.M. (1997). Extrasynaptic glutamate spillover in the hippocampus: dependence on temperature and the role of active glutamate uptake. Neuron *18*, 281–293.

Bastrikova, N., Gardner, G.A., Reece, J.M., Jeromin, A., and Dudek, S.M. (2008). Synapse elimination accompanies functional plasticity in hippocampal neurons. Proc. Natl. Acad. Sci. USA *105*, 3123–3127.

Bolshakov, V.Y., Carboni, L., Cobb, M.H., Siegelbaum, S.A., and Belardetti, F. (2000). Dual MAP kinase pathways mediate opposing forms of long-term plasticity at CA3-CA1 synapses. Nat. Neurosci. *3*, 1107–1112.

Campbell, S.L., and Hablitz, J.J. (2004). Glutamate transporters regulate excitability in local networks in rat neocortex. Neuroscience *127*, 625–635.

Chang, E.H., Savage, M.J., Flood, D.G., Thomas, J.M., Levy, R.B., Mahadomrongkul, V., Shirao, T., Aoki, C., and Huerta, P.T. (2006). AMPA receptor downscaling at the onset of Alzheimer's disease pathology in double knockin mice. Proc. Natl. Acad. Sci. USA *103*, 3410–3415.

Chen, Q.S., Wei, W.Z., Shimahara, T., and Xie, C.W. (2002). Alzheimer amyloid beta-peptide inhibits the late phase of long-term potentiation through calcineurin-dependent mechanisms in the hippocampal dentate gyrus. Neurobiol. Learn. Mem. *77*, 354–371.

Citri, A., and Malenka, R.C. (2008). Synaptic plasticity: multiple forms, functions, and mechanisms. Neuropsychopharmacology *33*, 18–41.

Cowburn, R.F., Wiehager, B., Trief, E., Li-Li, M., and Sundström, E. (1997). Effects of beta-amyloid-(25-35) peptides on radioligand binding to excitatory amino acid receptors and voltage-dependent calcium channels: evidence for a selective affinity for the glutamate and glycine recognition sites of the NMDA receptor. Neurochem. Res. *22*, 1437–1442.

Danbolt, N.C. (2001). Glutamate uptake. Prog. Neurobiol. *65*, 1–105.

Demuro, A., Mina, E., Kayed, R., Milton, S.C., Parker, I., and Glabe, C.G. (2005). Calcium dysregulation and membrane disruption as a ubiquitous neurotoxic mechanism of soluble amyloid oligomers. J. Biol. Chem. *280*, 17294–17300.

Dewachter, I., Filipkowski, R.K., Priller, C., Ris, L., Neyton, J., Croes, S., Terwel, D., Gysemans, M., Devijver, H., Borghgraef, P., et al. (2009). Deregulation of NMDA-receptor function and down-stream signaling in APP[V717I] transgenic mice. Neurobiol. Aging *30*, 241–256.

Dineley, K.T., Westerman, M., Bui, D., Bell, K., Ashe, K.H., and Sweatt, J.D. (2001). Beta-amyloid activates the mitogen-activated protein kinase cascade via hippocampal alpha7 nicotinic acetylcholine receptors: In vitro and in vivo mechanisms related to Alzheimer's disease. J. Neurosci. *21*, 4125–4133.

Grewer, C., and Rauen, T. (2005). Electrogenic glutamate transporters in the CNS: molecular mechanism, pre-steady-state kinetics, and their impact on synaptic signaling. J. Membr. Biol. *203*, 1–20.

Gu, Q.B., Zhao, J.X., Fei, J., and Schwarz, W. (2004). Modulation of Na(+),K(+) pumping and neurotransmitter uptake by beta-amyloid. Neuroscience *126*, 61–67.

Harkany, T., Abrahám, I., Timmerman, W., Laskay, G., Tóth, B., Sasvári, M., Kónya, C., Sebens, J.B., Korf, J., Nyakas, C., et al. (2000). beta-amyloid neurotoxicity is mediated by a glutamate-triggered excitotoxic cascade in rat nucleus basalis. Eur. J. Neurosci. *12*, 2735–2745.

Harris, M.E., Wang, Y., Pedigo, N.W., Jr., Hensley, K., Butterfield, D.A., and Carney, J.M. (1996). Amyloid beta peptide (25-35) inhibits Na+-dependent glutamate uptake in rat hippocampal astrocyte cultures. J. Neurochem. *67*, 277–286.

Hsia, A.Y., Masliah, E., McConlogue, L., Yu, G.Q., Tatsuno, G., Hu, K., Kholodenko, D., Malenka, R.C., Nicoll, R.A., and Mucke, L. (1999). Plaque-independent disruption of neural circuits in Alzheimer's disease mouse models. Proc. Natl. Acad. Sci. USA *96*, 3228–3233.

Hsieh, H., Boehm, J., Sato, C., Iwatsubo, T., Tomita, T., Sisodia, S., and Malinow, R. (2006). AMPAR removal underlies Abeta-induced synaptic depression and dendritic spine loss. Neuron *52*, 831–843.

Ikegaya, Y., Matsuura, S., Ueno, S., Baba, A., Yamada, M.K., Nishiyama, N., and Matsuki, N. (2002). Beta-amyloid enhances glial glutamate uptake activity and attenuates synaptic efficacy. J. Biol. Chem. *277*, 32180–32186.

Jacob, C.P., Koutsilieri, E., Bartl, J., Neuen-Jacob, E., Arzberger, T., Zander, N., Ravid, R., Roggendorf, W., Riederer, P., and Grünblatt, E. (2007). Alterations in expression of glutamatergic transporters and receptors in sporadic Alzheimer's disease. J. Alzheimers Dis. *11*, 97–116.

Kemp, N., and Bashir, Z.I. (2001). Long-term depression: a cascade of induction and expression mechanisms. Prog. Neurobiol. *65*, 339–365.

Kim, J.H., Anwyl, R., Suh, Y.H., Djamgoz, M.B., and Rowan, M.J. (2001). Use-dependent effects of amyloidogenic fragments of (beta)-amyloid precursor protein on synaptic plasticity in rat hippocampus in vivo. J. Neurosci. *21*, 1327–1333.

Kim, M.J., Dunah, A.W., Wang, Y.T., and Sheng, M. (2005). Differential roles of NR2A- and NR2B-containing NMDA receptors in Ras-ERK signaling and AMPA receptor trafficking. Neuron *46*, 745–760.

Knobloch, M., and Mansuy, I.M. (2008). Dendritic spine loss and synaptic alterations in Alzheimer's disease. Mol. Neurobiol. *37*, 73–82.

Kutsuwada, T., Kashiwabuchi, N., Mori, H., Sakimura, K., Kushiya, E., Araki, K., Meguro, H., Masaki, H., Kumanishi, T., Arakawa, M., et al. (1992). Molecular diversity of the NMDA receptor channel. Nature *358*, 36–41.

Lacor, P.N., Buniel, M.C., Furlow, P.W., Clemente, A.S., Velasco, P.T., Wood, M., Viola, K.L., and Klein, W.L. (2007). Abeta oligomer-induced aberrations in synapse composition, shape, and density provide a molecular basis for loss of connectivity in Alzheimer's disease. J. Neurosci. *27*, 796–807.

Lambert, M.P., Barlow, A.K., Chromy, B.A., Edwards, C., Freed, R., Liosatos, M., Morgan, T.E., Rozovsky, I., Trommer, B., Viola, K.L., et al. (1998). Diffusible, nonfibrillar ligands derived from Abeta1-42 are potent central nervous system neurotoxins. Proc. Natl. Acad. Sci. USA *95*, 6448–6453.

Li, S., Tian, X., Hartley, D.M., and Feig, L.A. (2006). Distinct roles for Ras-guanine nucleotide-releasing factor 1 (Ras-GRF1) and Ras-GRF2 in the induction of long-term potentiation and long-term depression. J. Neurosci. *26*, 1721–1729.

Liu, L., Wong, T.P., Pozza, M.F., Lingenhoehl, K., Wang, Y., Sheng, M., Auberson, Y.P., and Wang, Y.T. (2004). Role of NMDA receptor subtypes in governing the direction of hippocampal synaptic plasticity. Science *304*, 1021–1024.

Lue, L.F., Kuo, Y.M., Roher, A.E., Brachova, L., Shen, Y., Sue, L., Beach, T., Kurth, J.H., Rydel, R.E., and Rogers, J. (1999). Soluble amyloid beta peptide concentration as a predictor of synaptic change in Alzheimer's disease. Am. J. Pathol. *155*, 853–862.

Maki, R., Robinson, M.B., and Dichter, M.A. (1994). The glutamate uptake inhibitor L-trans-pyrrolidine-2,4-dicarboxylate depresses excitatory synaptic transmission via a presynaptic mechanism in cultured hippocampal neurons. J. Neurosci. *14*, 6754–6762.

Masliah, E., Alford, M., DeTeresa, R., Mallory, M., and Hansen, L. (1996). Deficient glutamate transport is associated with neurodegeneration in Alzheimer's disease. Ann. Neurol. *40*, 759–766.

Matsuzaki, M., Honkura, N., Ellis-Davies, G.C., and Kasai, H. (2004). Structural basis of long-term potentiation in single dendritic spines. Nature *429*, 761–766.

McLean, C.A., Cherny, R.A., Fraser, F.W., Fuller, S.J., Smith, M.J., Beyreuther, K., Bush, A.I., and Masters, C.L. (1999). Soluble pool of Abeta amyloid as a determinant of severity of neurodegeneration in Alzheimer's disease. Ann. Neurol. *46*, 860–866.

Min, M.Y., Rusakov, D.A., and Kullmann, D.M. (1998). Activation of AMPA, kainate, and metabotropic receptors at hippocampal mossy fiber synapses: role of glutamate diffusion. Neuron *21*, 561–570.

Molnár, Z., Soós, K., Lengyel, I., Penke, B., Szegedi, V., and Budai, D. (2004). Enhancement of NMDA responses by beta-amyloid peptides in the hippocampus in vivo. Neuroreport *15*, 1649–1652.

Morishita, W., Lu, W., Smith, G.B., Nicoll, R.A., Bear, M.F., and Malenka, R.C. (2007). Activation of NR2B-containing NMDA receptors is not required for NMDA receptor-dependent long-term depression. Neuropharmacology *52*, 71–76.

Mucke, L., Masliah, E., Yu, G.Q., Mallory, M., Rockenstein, E.M., Tatsuno, G., Hu, K., Kholodenko, D., Johnson-Wood, K., and McConlogue, L. (2000). High-level neuronal expression of abeta 1-42 in wild-type human amyloid protein precursor transgenic mice: synaptotoxicity without plaque formation. J. Neurosci. *20*, 4050–4058.

Mulkey, R.M., Endo, S., Shenolikar, S., and Malenka, R.C. (1994). Involvement of a calcineurin/inhibitor-1 phosphatase cascade in hippocampal long-term depression. Nature *369*, 486–488.

Nägerl, U.V., Eberhorn, N., Cambridge, S.B., and Bonhoeffer, T. (2004). Bidirectional activity-dependent morphological plasticity in hippocampal neurons. Neuron *44*, 759–767.

Nassif, M., Hoppe, J., Santin, K., Frozza, R., Zamin, L.L., Simão, F., Horn, A.P., and Salbego, C. (2007). Beta-amyloid peptide toxicity in organotypic hippocampal slice culture involves Akt/PKB, GSK-3beta, and PTEN. Neurochem. Int. *50*, 229–235.

O'Shea, S.D., Smith, I.M., McCabe, O.M., Cronin, M.M., Walsh, D.M., and O'Connor, W.T. (2008). Intracerebroventricular administration of amyloid b-protein oligomers selectively increases dorsal hippocampal dialysate glutamate levels in the awake rat. Sensors *8*, 7428–7437.

Origlia, N., Righi, M., Capsoni, S., Cattaneo, A., Fang, F., Stern, D.M., Chen, J.X., Schmidt, A.M., Arancio, O., Yan, S.D., and Domenici, L. (2008). Receptor for advanced glycation end product-dependent activation of p38 mitogen-activated protein kinase contributes to amyloid-beta-mediated cortical synaptic dysfunction. J. Neurosci. *28*, 3521–3530.

Overstreet, L.S., Pasternak, J.F., Colley, P.A., Slater, N.T., and Trommer, B.L. (1997). Metabotropic glutamate receptor mediated long-term depression in developing hippocampus. Neuropharmacology *36*, 831–844.

Palop, J.J., Chin, J., Roberson, E.D., Wang, J., Thwin, M.T., Bien-Ly, N., Yoo, J., Ho, K.O., Yu, G.Q., Kreitzer, A., et al. (2007). Aberrant excitatory neuronal activity and compensatory remodeling of inhibitory hippocampal circuits in mouse models of Alzheimer's disease. Neuron *55*, 697–711.

Peineau, S., Taghibiglou, C., Bradley, C., Wong, T.P., Liu, L., Lu, J., Lo, E., Wu, D., Saule, E., Bouschet, T., et al. (2007). LTP inhibits LTD in the hippocampus via regulation of GSK3beta. Neuron *53*, 703–717.

Podlisny, M.B., Ostaszewski, B.L., Squazzo, S.L., Koo, E.H., Rydell, R.E., Teplow, D.B., and Selkoe, D.J. (1995). Aggregation of secreted amyloid beta-protein into sodium dodecyl sulfate-stable oligomers in cell culture. J. Biol. Chem. *270*, 9564–9570.

Pomara, N., Singh, R., Deptula, D., Chou, J.C., Schwartz, M.B., and LeWitt, P.A. (1992). Glutamate and other CSF amino acids in Alzheimer's disease. Am. J. Psychiatry *149*, 251–254.

Raymond, C.R., Ireland, D.R., and Abraham, W.C. (2003). NMDA receptor regulation by amyloid-beta does not account for its inhibition of LTP in rat hippocampus. Brain Res. *968*, 263–272.

Sarantis, M., Ballerini, L., Miller, B., Silver, R.A., Edwards, M., and Attwell, D. (1993). Glutamate uptake from the synaptic cleft does not shape the decay of the non-NMDA component of the synaptic current. Neuron *11*, 541–549.

Scimemi, A., Fine, A., Kullmann, D.M., and Rusakov, D.A. (2004). NR2B-containing receptors mediate cross talk among hippocampal synapses. J. Neurosci. *24*, 4767–4777.

Shankar, G.M., Li, S., Mehta, T.H., Garcia-Munoz, A., Shepardson, N., Smith, I., Brett, F.M., Farrell, M.A., Rowan, M.J., Lemere, C.A., et al. (2008). Soluble amyloid β-protein dimers isolated directly from Alzheimer disease patients potently impair synaptic plasticity and memory. Nat. Med. *14*, 837–842.

Snyder, E.M., Nong, Y., Almeida, C.G., Paul, S., Moran, T., Choi, E.Y., Nairn, A.C., Salter, M.W., Lombroso, P.J., Gouras, G.K., and Greengard, P. (2005). Regulation of NMDA receptor trafficking by amyloid-beta. Nat. Neurosci. *8*, 1051–1058.

Terry, R.D., Masliah, E., Salmon, D.P., Butters, N., DeTeresa, R., Hill, R., Hansen, L.A., and Katzman, R. (1991). Physical basis of cognitive alterations in Alzheimer's disease: synapse loss is the major correlate of cognitive impairment. Ann. Neurol. *30*, 572–580.

Tovar, K.R., and Westbrook, G.L. (1999). The incorporation of NMDA receptors with a distinct subunit composition at nascent hippocampal synapses in vitro. J. Neurosci. *19*, 4180–4188.

Townsend, M., Shankar, G.M., Mehta, T., Walsh, D.M., and Selkoe, D.J. (2006). Effects of secreted oligomers of amyloid beta-protein on hippocampal synaptic plasticity: a potent role for trimers. J. Physiol. *572*, 477–492.

Townsend, M., Mehta, T., and Selkoe, D.J. (2007). Soluble Abeta inhibits specific signal transduction cascades common to the insulin receptor pathway. J. Biol. Chem. *282*, 33305–33312.

Ueda, K., Shinohara, S., Yagami, T., Asakura, K., and Kawasaki, K. (1997). Amyloid beta protein potentiates Ca2+ influx through L-type voltage-sensitive Ca2+ channels: a possible involvement of free radicals. J. Neurochem. *68*, 265–271.

Walsh, D.M., Klyubin, I., Fadeeva, J.V., Cullen, W.K., Anwyl, R., Wolfe, M.S., Rowan, M.J., and Selkoe, D.J. (2002). Naturally secreted oligomers of amyloid

beta protein potently inhibit hippocampal long-term potentiation in vivo. Nature *416*, 535–539.

Walsh, D.M., Townsend, M., Podlisny, M.B., Shankar, G.M., Fadeeva, J.V., El Agnaf, O., Hartley, D.M., and Selkoe, D.J. (2005). Certain inhibitors of synthetic amyloid beta-peptide (Abeta) fibrillogenesis block oligomerization of natural Abeta and thereby rescue long-term potentiation. J. Neurosci. *25*, 2455–2462.

Wang, H.W., Pasternak, J.F., Kuo, H., Ristic, H., Lambert, M.P., Chromy, B., Viola, K.L., Klein, W.L., Stine, W.B., Krafft, G.A., and Trommer, B.L. (2002). Soluble oligomers of beta amyloid (1-42) inhibit long-term potentiation but not long-term depression in rat dentate gyrus. Brain Res. *924*, 133–140.

Wang, Q., Rowan, M.J., and Anwyl, R. (2004a). Beta-amyloid-mediated inhibition of NMDA receptor-dependent long-term potentiation induction involves activation of microglia and stimulation of inducible nitric oxide synthase and superoxide. J. Neurosci. *24*, 6049–6056.

Wang, Q., Walsh, D.M., Rowan, M.J., Selkoe, D.J., and Anwyl, R. (2004b). Block of long-term potentiation by naturally secreted and synthetic amyloid beta-peptide in hippocampal slices is mediated via activation of the kinases c-Jun N-terminal kinase, cyclin-dependent kinase 5, and p38 mitogen-activated protein kinase as well as metabotropic glutamate receptor type 5. J. Neurosci. *24*, 3370–3378.

Wu, J., Anwyl, R., and Rowan, M.J. (1995). beta-Amyloid selectively augments NMDA receptor-mediated synaptic transmission in rat hippocampus. Neuroreport *6*, 2409–2413.

Yang, C.H., Huang, C.C., and Hsu, K.S. (2005). Behavioral stress enhances hippocampal CA1 long-term depression through the blockade of the glutamate uptake. J. Neurosci. *25*, 4288–4293.

Zhou, Q., Homma, K.J., and Poo, M.M. (2004). Shrinkage of dendritic spines associated with long-term depression of hippocampal synapses. Neuron *44*, 749–757.